Enlightening the primordial dark ages

Iarygina, O.

Enlightening the Primordial Dark Ages

Proefschrift

ter verkrijging van
de graad van doctor aan de Universiteit Leiden,
op gezag van rector magnificus prof.dr.ir. H. Bijl,
volgens besluit van het college voor promoties
te verdedigen op woensdag 3 november 2021
klokke 13:45 uur

door

Oksana Iarygina
geboren te Kyiv (Oekraïne)
in 1992

Promotor:	Prof. dr. A. Achúcarro	
Co-promotor:	Dr. E. I. Sfakianakis	(IFAE, Barcelona, Spain)
Promotiecommissie:	Prof. dr. E. J. Copeland	(University of Nottingham, UK)
	Prof. dr. S. I. Vilchinskiy	(Shevchenko U., Kyiv, Ukraine)
	Dr. F. Bezrukov	(University of Manchester, UK)
	Dr. A. Maleknejad	(CERN, Switzerland)
	Prof. dr. J. Aarts	
	Prof. dr. K. E. Schalm	

Casimir PhD series, Delft-Leiden 2021-29
ISBN: 978-90-8593-495-0
An electronic version of this thesis can be found at
`https://openaccess.leidenuniv.nl`.

The work in this thesis is funded by the Gravity program of the Netherlands Organization for Scientific Research (NWO) and the Ministry of Education, Culture and Science (OCW).

The cover shows the spotlight that illuminates four pieces of a puzzle that represent chapters of this thesis (clockwise): the potential of shift-symmetric orbital inflation (Chapter 2), the three-dimensional plot of inflationary and reheating trajectories on the two-field α-attractor potential (Chapter 4), the three-dimensional Floquet chart with resonance bands (Chapter 5), tachyonic growth of the left-polarized gauge field mode function around the time of horizon crossing (Chapter 3). However, many pieces of the primordial dark ages puzzle are still unknown. It is a challenge for modern cosmology to discover and put them together.

To my family

Contents

1 Introduction

"I... a universe of atoms, an atom in the universe."

Richard P. Feynman

1.1 The very early universe cosmology

Since ancient times people have been observing the sky and asking philosophical and theological questions: "Where do we come from?", "How was our world created?". From those times science has made a huge progress and nowadays, with the help of precision measurements and observations within the theoretical approaches of modern cosmology, humanity has learned a lot about space-time and our Universe. Below we briefly outline the most important stages of this development, based mainly on Refs. [1–3]. Throughout the introduction we use natural units $\hbar = c = 1$ and the reduced Planck mass defined by $M_{\text{pl}} = (8\pi G)^{-1/2}$.

1.1.1 Cosmological ideas prior to inflation

The breakthrough in modern cosmology started from Albert Einstein with the appearance of the Theory of General Relativity in 1915 [5]. It merged the geometry of space-time and the energy-momentum tensor of matter into a single equation, providing an accurate description of gravitation that has been tested and confirmed by many experiments to date. Despite the fact that matter changes the geometry of the space-time, on the very large scales our Universe appears to be flat, homogeneous and isotropic. The most general solution for such universe was found independently by Friedmann, Lemaître, Robertson, Walker (FLRW) [6–10] in the 1920s and 1930s, that is given by the metric

$$ds^2 = -dt^2 + a(t)^2 \left(dr^2 + r^2(d\theta^2 + \sin^2\theta d\phi^2) \right) , \tag{1.1}$$

where $a(t)$ is the scale factor which describes the expansion or contraction of the universe. In particular, the expansion rate is parametrised by the Hubble parameter $H(t) \equiv \frac{\dot{a}(t)}{a(t)}$. Historically, Lemaître was the first who in 1927 suggested that the universe could be traced back in time to an originating single point, which he called the "primeval atom". The first attempt to observe the expansion of the universe was done by Slipher [11] in 1912, who noticed the shift of spectral lines of galaxies. However, he did not relate this to the actual expansion of the universe, but rather with "island universes" outside our Milky Way. Much later, Hubble and Humason [12, 13] combined their own galaxy distance measurements with Slipher's measurements of redshifts and found that galaxies are moving away at speeds proportional to their distance. Lemaître understood that this is caused by the expansion of spacetime. Nowadays this velocity-distance relation is called as *the*

Hubble–Lemaître law

$$v \simeq Hd, \tag{1.2}$$

which established the expansion of the universe as a commonly accepted scientific fact.

Now, for the FLRW metric the energy-momentum tensor is of the form of the energy-momentum tensor of a perfect fluid, with a pressure p and energy density ρ. From Einstein equations Friedmann derived the evolution equations for the homogeneous and isotropic case, that are of the following form

$$3M_{\rm pl}^2 H^2 = \rho, \tag{1.3}$$

$$M_{\rm pl}^2 \dot{H} = -\frac{1}{2}\left(\rho + p\right), \tag{1.4}$$

and called *Friedmann equations*. With known p and ρ it is possible to find the corresponding scale factor, which allows us to trace back the expansion history of the universe. Extrapolating the cosmic expansion backwards in time leads to the idea that the Universe had a finite age and started from a hot and dense state, that gave rise to *the hot Big Bang theory*.

In 1948 Gamov [14] suggested that light elements (namely deuterium, helium, and lithium) were produced at the times when the Universe was hot enough for nucleosynthesis, that is now called Big Bang Nucleosynthesis (BBN). As the Universe cooled down due to its expansion, protons and electrons combined to form neutral hydrogen atoms, initiating the recombination epoch. Since Thomson scattering of photons on free electrons was not efficient any more, the universe became transparent to photons and they could travel freely, i.e. decoupled. This thought led Gamov to the realization that some relic radiation should be present since those times, which we call now the cosmic microwave background (CMB). In the same year [15] Alpher and Herman estimated the present day temperature of the relic radiation to be $T \sim 5K$. Remarkably, that CMB was first detected by accident, by Penzias and Wilson [16] in 1965, during radiometer calibrations that they used for satellite communication experiments at Bell Telephone Laboratories. This was a sensational discovery of radiation, that was emitted about thirteen and a half billion years ago, only a few hundred thousand years after the Big Bang, long before stars or galaxies ever formed. In 1978 they received the Nobel Prize in Physics for this discovery.

The formation of galaxies remained an open question. Already in 1946 Lifshitz [17] calculated that the amplitude of density perturbations grows too slowly. To form galaxies, the right level of primordial density inhomogeneities was required: too small leads to the absence of galaxies, too large means having different structure than the observed one. Later, in 1967 Sachs and Wolfe [18] showed that the inhomogeneities may be potentially visible as small variations in the temperature of CMB in different directions on the sky. In 1992 the Cosmic Background Explorer (COBE) satellite confirmed this prediction with the detection of the CMB background radiation [19, 20] with an average temperature of $T \sim 2.7K$ and temperature variations of order 10^{-5}, that reflect the presence of small density inhomogeneities required for structure formation.

Despite the stunning successes of the hot Big Bang theory, supported by measurements of the CMB and observations of Hubble's Law together with predictions for the relative abundances of light elements during BBN [21–23], several problems remained unsolved. The first one is the *horizon problem*. Within the Big Bang cosmology, distinct patches of the CMB were not in causal contact at recombination. However, the observations show the isotropy in the CMB temperature across the entire sky and it is unclear why the causally-disconnected patches share similar physical properties. In addition to that, from the CMB data the geomety of the universe appears to be nearly flat. To satisfy within the Big Bang theory today's observed values, extremely flat initial conditions would be required. This fine-tuning forms the *flatness problem*. Finally, the *origin of primordial fluctuations* that seed all the structure remains unknown. In Section 1.2 we will show how the framework of cosmic inflation deals with the aforementioned problems.

1.2 Inflation

The main idea of the inflationary scenario is that the very early universe could be in an *unstable vacuum-like state* with high energy density and equation of state $p = -\rho$ that drives extremely rapid exponential expansion prior to the standard Big Bang evolution. After inflation ends, the vacuum energy is transformed into thermal energy in the form of the Standard Model particles, initiating the radiation dominated phase of the Universe. The transition from the phase of accelerated expansion to the thermal universe is called *reheating*, and will be described in detail in Sec. 1.3. Because of the exponential expansion, distant points on the CMB become causally connected and any initial curvature stretches to be nearly flat. That solves both the horizon and flatness problems. In addition to that, inflation also explains the origin of structure in the universe, producing quantum density fluctuations that expanded during inflation, forming the higher density regions that condensed over the next several hundred million years into stars, galaxies and us.

Historically, the space that expands exponentially with a scale factor $a(t) \sim a_0\, e^{Ht}$, with H being the Hubble parameter, was first described in 1917 by de Sitter in [24, 25], even before Friedmann's solutions. However, for a long time its physical meaning remained unclear and it was used mostly for developing quantum field theory in curved space. The possibility of an exponential expansion during the early stages of the universe's evolution, although for superdense baryonic matter, was first considered by Gliner in [26]

In 1980 Guth [27] for the first time proposed a solution to the horizon and flatness problems by introducing the exponential expansion (inflation) of the universe trapped in a supercooled metastable vacuum state $\phi = 0$. Inflation was associated with the phase transition to a stable state $\phi_0 \neq 0$, and was accompanied by bubble nucleation via quantum tunneling. Bubble-wall collisions were responsible for reheating the universe, however collisions of the very large bubbles were destroying the homogeneity and isotropy after the end of inflation. This scenario was subsequently named as "old inflation".

The solution to this problem was introduced by Linde and independently by Albrecht and Steinhardt in [28, 29] and called the "new inflation" or "slow-roll inflation" scenario. In the new approach the supercooled state and tunneling out of a false vacuum state was not required any more, but instead inflation occurred when a scalar field ϕ was slowly rolling down its potential $V(\phi)$. The reheating era this time happens not because of bubble wall collisions, but via creation of elementary particles by damped oscillations of the classical field near the minimum of its potential.

1.2.1 Slow-roll inflation

The idea that inflation may be driven by a scalar field has revolutionized the whole cosmological community. Since inflationary dynamics is highly dependent on the underlying inflationary potential $V(\phi)$, a big variety of models have been already developed to date [1]. It is a challenge of the present-day cosmology to distinguish and falsify among all of them. Below we will describe the conditions on the potential that would enable inflation

[1] This may also be an effective description of some ultraviolet complete theory.

to happen.

Before we proceed, let us first outline the general conditions required for inflation to occur. To start with, the accelerated expansion $\ddot{a} > 0$ requires

$$\frac{\ddot{a}}{a} = H^2(1 - \epsilon_H) > 0, \tag{1.5}$$

where the parameter ϵ_H is called *the first Hubble slow-roll parameter* and defined as

$$\epsilon_H \equiv -\frac{\dot{H}}{H^2}. \tag{1.6}$$

The inequality (1.5) implies that to ensure the accelerated expansion, ϵ_H should be in the range $0 < \epsilon_H < 1$. In the limit $\epsilon_H \to 0$ the Hubble parameter $H = const$ and hence the space-time becomes de Sitter space $ds^2 = -dt^2 + e^{2Ht}dx^2$. In order for inflation to end, the space-time has to deviate from a perfect de Sitter space. However, for small and finite $\epsilon_H \ll 1$ de Sitter space remains a good approximation, that's why slow-roll inflation is often called a quasi-de Sitter period. To sum up, inflation requires $\epsilon_H < 1$, while the slow-roll inflation $\epsilon_H \ll 1$.

To solve the horizon and flatness problems, inflation has to last long enough. The current estimate is between 50 and 60 e-folds [2]. This condition is ensured by introducing *the second Hubble slow-roll parameter* [3]

$$\eta_H \equiv \frac{\dot{\epsilon}}{\epsilon H} \tag{1.7}$$

and the requirement $|\eta_H| \ll 1$. The above condition guarantees that the change of ϵ_H per Hubble time is small and therefore inflation can persist.

Finally, we can discuss what microscopic physics can lead to the conditions $\epsilon_H \ll 1$ and $|\eta_H| \ll 1$. We start from the general form of the action for the inflaton field $\phi(t, x)$ with a canonical kinetic term and a potential $V(\phi)$, minimally coupled to gravity, that is given by

$$S = \int d^4x\sqrt{-g}\left[\frac{M_{\rm pl}^2}{2}R - \frac{1}{2}\partial_\mu\phi\partial^\mu\phi - V(\phi)\right], \tag{1.8}$$

[2]Both problems are solved when the observable universe was smaller than the comoving Hubble radius at the beginning of inflation $(a_0H_0)^{-1} < (a_iH_i)^{-1}$. This restricts the number of e-folds of inflation to $N_{\rm tot} = \ln(a_e/a_i) > 64 + \ln(T_R/10^{15}{\rm Gev})$, with T_R being the reheating temperature. The number $N_{\rm tot}$ is smaller for the lower reheating temperature.

[3]Alternatively it may be defined as $\eta_H = -\frac{1}{2}\frac{\ddot{H}}{\dot{H}H}$.

where R is the Ricci scalar curvature of the space-time. The homogeneity and isotropy of the background implies the inflaton field depends only on time, i.e. $\phi = \phi(t)$. For the FLRW space-time its dynamics is governed by equations of motion

$$\ddot{\phi} + 3H\dot{\phi} + V_\phi = 0, \tag{1.9}$$

with $V_\phi = \frac{dV}{d\phi}$, together with two Friedmann equations

$$3M_{\rm pl}^2 H^2 = \frac{1}{2}\dot{\phi}^2 + V, \tag{1.10}$$

$$\dot{H} = -\frac{\dot{\phi}^2}{2M_{\rm pl}^2}. \tag{1.11}$$

With the above equations, the slow-roll parameters may be written in terms of the scalar field and its potential as

$$\epsilon_H = \frac{\frac{3}{2}\dot{\phi}^2}{\frac{1}{2}\dot{\phi}^2 + V}, \quad \eta_H = 2\frac{\ddot{\phi}}{H\dot{\phi}} + 2\epsilon_H. \tag{1.12}$$

To satisfy $\epsilon_H \ll 1$ and $|\eta_H| \ll 1$, one may see that the kinetic energy of the inflaton field has to be negligible in comparison to the potential one, as well as the field acceleration has to be small. This explains the name *slow-roll approximation*, which is defined as

$$\dot{\phi}^2 \ll V, \quad \ddot{\phi} \ll H\dot{\phi}. \tag{1.13}$$

The left inequality in (1.13) ensures that the Hubble parameter is nearly constant $\dot{H} \ll H^2$, leading to the quasi-exponential expansion with $a \sim e^{Ht}$. The right inequality allows one to neglect the acceleration term in (1.9) that assures long enough inflation. Slow-roll inflation is an attractor in the phase space $(\phi, \dot{\phi})$, which means that non-slow roll initial trajectories will very quickly converge to those that follow (1.13), as shown in Figure 1.1. For the review see for instance Ref. [30–32].

Comparing (1.10) - (1.11) with Friedmann equations (1.3) - (1.4), one may immediately find the energy density $\rho = \frac{1}{2}\dot{\phi}^2 + V(\phi)$ and pressure $p = \frac{1}{2}\dot{\phi}^2 - V(\phi)$ expressed in terms of the scalar field and its potential. In the slow-roll approximation this leads to the equation of state $w = p/\rho \approx -1$.

Alternatively, slow-roll conditions may be written in terms of the potential as

$$\epsilon_V \equiv \frac{M_{\rm pl}^2}{2}\left(\frac{\partial_\phi V}{V}\right)^2 \ll 1, \quad |\eta_V| \equiv M_{\rm pl}^2 \frac{|\partial^2_{\phi\phi} V|}{V} \ll 1, \tag{1.14}$$

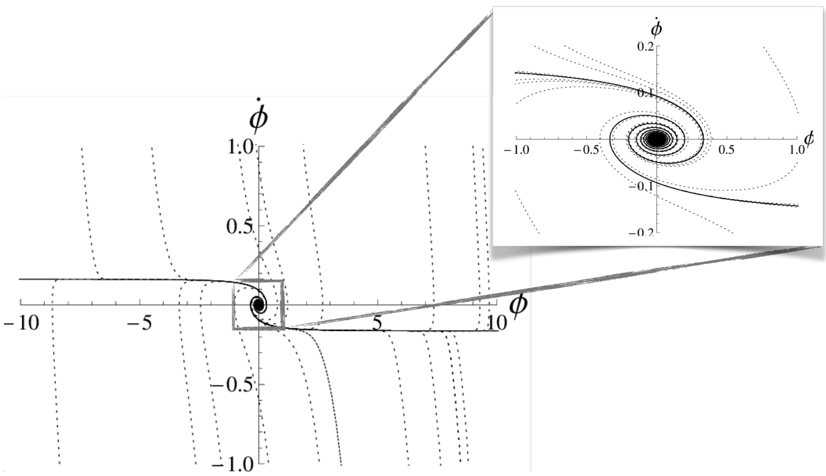

Figure 1.1: Attractor solutions for $m^2\phi^2$ potential with $m = 0.2M_{\rm pl}$ in $\phi - \dot\phi$ plane in units of $M_{\rm pl} = 1$. Solid curves are attractor solutions, that at large field values asymptote to $\dot\phi = \pm\sqrt{2/3}m$ and at small field values converge to the origin. Dotted curves show numerical solutions for random initial values. The top right plot is a zoom-in into the area around the origin. This figure is an adaptation of the one, presented in [31].

which are called *potential slow-roll parameters*. For single field models of inflation and in the slow-roll regime, the potential and the Hubble slow-roll parameters are related as

$$\epsilon_V \approx \epsilon_H, \quad \eta_V = 2\epsilon_H - \frac{1}{2}\eta_H. \tag{1.15}$$

However, in a broader class of models, including multi-field inflation, when the inflationary trajectory does not follow the gradient flow of the potential, their relation is much more involved, if possible at all [4].

1.2.2 Inflation beyond single-field approximation

Single field inflation is the leading framework for the early universe physics that sets the initial conditions and primordial density fluctuations in accordance with observations. However, the energy scale of the very early universe may be as high as 10^{15} GeV [5] and could contain multiple scalar fields that may participate in inflationary dynamics. Moreover, UV-complete theories typically lead to effective field theory descriptions with many distinct

[4]In multi-field inflation there is no good definition of η_V.

[5]The precise magnitude is unknown and this number should be taken as a reference value only.

fields, in flat as well as curved field-space geometries. This motivates the multi-field description of inflation, that we will outline below based on the covariant formalism described by van Tent et al in Refs. [33–37].

The general form of the action for multi-field inflation is given by

$$S = \int d^4x\sqrt{-g}\left[\frac{M_{\rm pl}^2}{2}R - \frac{1}{2}\mathcal{G}_{IJ}(\phi)g^{\mu\nu}\partial_\mu\phi^I\partial_\nu\phi^J - V(\phi)\right], \tag{1.16}$$

where $\mathcal{G}_{IJ}(\phi)$ is the field-space metric and $V(\phi)$ is a multi-field potential for scalar fields ϕ^I, with $I = 1\ldots n$, with n being the number of fields. The background solution $\phi_0^I(t)$ may be found from the following equations of motion

$$\mathcal{D}_t\dot\phi_0^I + 3H\dot\phi_0^I + \mathcal{G}^{IJ}V_{,J} = 0, \quad 3H^2 = \frac{1}{2}\dot\phi_0^2 + V, \tag{1.17}$$

where $\dot\phi_0 = \sqrt{\mathcal{G}_{IJ}\dot\phi_0^I\dot\phi_0^J}$ is the proper field velocity and $\mathcal{D}_t$ is a covariant derivative whose action on an arbitrary vector A^I is defined as $\mathcal{D}_tA^I \equiv \dot A^I + \Gamma^I_{JK}\dot\phi^JA^K$. Here Γ^I_{JK} are the Christoffel symbols associated with the metric $\mathcal{G}_{IJ}(\phi)$. In the multi-filed case the inflationary trajectory is a line in multi-dimensional space, non-geodesic in general. At each point along the trajectory unit vectors tangent and normal to the trajectory may be defined as

$$T^I \equiv \frac{\dot\phi^I}{\dot\phi_0}, \quad N_I \equiv -\frac{1}{|\mathcal{D}_tT|}\mathcal{D}_tT^I. \tag{1.18}$$

Next, the rate of turning (or simply, the angular velocity) of the inflationary trajectory is defined as

$$\Omega \equiv -N_I\mathcal{D}_tT^I. \tag{1.19}$$

The background equations of motion can be now projected into the tangent and normal directions and written in the following form

$$\ddot\phi_0 + 3H\dot\phi_0 + V_T = 0, \quad V_N = \dot\phi_0\Omega, \tag{1.20}$$

with $V_T = T^IV_I$ and $V_N = N^IV_I$, such that the gradient of the potential is written as $V_I = T_IV_T + N_IV_N$. For $\Omega = 0$ the field dynamics reduces to the single field description and the background motion is geodesic. In general, however, $\Omega \neq 0$, which may bring potentially observable physical signatures, such as features in the primordial power spectra [36], that can also lead to generation of primordial black holes and gravitational waves, see recent works on this topic [38–40] and references therein.

Non-zero turn rate also distinguishes the potential and Hubble slow roll parameters in the multi-field case. The potential first slow-roll parameter in the multiple-field case may be defined as [41]

$$\epsilon_V \equiv \frac{1}{2}\frac{V^I V_I}{V^2}. \tag{1.21}$$

It follows [41, 42] that two alternative definitions of first slow-roll parameters in multi-field inflation now are related as

$$\epsilon_V = \epsilon_H \left(1 + \frac{\Omega^2}{9H^2}\right), \tag{1.22}$$

which clearly shows how different ϵ_V and ϵ_H are in case of a non-zero turn rate.

1.2.2.1 Muti-field inflation vs Swampland conjectures

The discussion regarding ultraviolet (UV) complete theories may lead to the absolutely legitimate question: can inflation be embedded into a full quantum theory of gravity? There are two ways to talk about this problem. The first one is the so-called *top-down approach*, which takes some UV complete theory, like string M- or F-theory in higher dimensional space and via compactification to four-dimensional space-time conclude which common features do the effective field theories (EFT) share. The second way is to follow *the bottom-up approach*, the essence of which is to start with a four-dimensional EFT coupled to gravity and identify the consistency criteria that quantum gravity sets. Recently, Vafa in [43] introduced consistency criteria named *swampland conjectures*. Before this work there were other studies in this direction, however they have not gained so much attention. For the recent reviews on the subject see Refs. [44–47]. The swampland represents the space of quantum field theories which are incompatible with quantum gravity, opposite to the landscape, which includes compatible EFTs with possible UV completions. The two conjectures directly question the possibility of a UV embedding for single-field inflation [48]. We will briefly discuss them below [6], taking into account also the recent investigations mentioned above.

Two necessary conditions that low energy four dimensional EFT, obtained from string theory compactifications, conjectured to satisfy are:

[6] This is an active research direction nowadays and we present here the state of the art of 2021.

- *Swampland distance conjecture.* Quantum gravity effects sets a maximum distance in field space beyond which the low energy description is not valid any more

$$\Delta\phi < M_{\rm pl}\Delta, \tag{1.23}$$

where $\Delta \sim \mathcal{O}(1)$.

- *Swampland de Sitter conjecture.* The potential of the four-dimensional EFT should be steep enough to satisfy

$$M_{\rm pl}\frac{|\nabla V|}{V} \geqslant c \quad \text{or} \quad \min(\nabla_i\nabla_j V) \leqslant \frac{-c'V}{M_{\rm pl}^2} \tag{1.24}$$

where $c, c' \sim \mathcal{O}(1)$.

While the swampland distance conjecture is in a mild tension with single-field inflation, the de Sitter conjecture has far more dramatic implications. As we have seen in Sec. 1.2.1, the first slow-roll parameters should satisfy $\epsilon_H \simeq \epsilon_V \ll 1$, which automatically constrains the inflationary potential to be flat, in order for slow-roll inflation to happen. This is in tension with the requirement (1.24) and satisfying simultaneously $\Delta \sim \mathcal{O}(1)$, $c, c' \sim \mathcal{O}(1)$. Hence, if the criteria are true, this questions the existence of flat directions in the potential or de Sitter minima, and therefore all single field inflation models.

However, this is not the case for multi-field inflation. As was shown in [41], when the inflationary trajectory is non-geodesic and has a non-zero turning rate, it is possible to simultaneously satisfy both aforementioned swampland conjectures. Because of the relation (1.22), it is possible to have successful inflation with both $\epsilon_H \ll 1$ and $\epsilon_V \sim \mathcal{O}(1)$ when $\Omega^2/H^2 \gg 1$. In addition to that, there is a lower bound on the turning rate Ω to satisfy the second conjecture and agree with CMB observations.

It is worth mentioning, that the rigorousness of swampland conjectures is still debated in the scientific community. Despite this, it is an important step towards a better understanding of the UV completion of inflationary cosmology and EFTs in general.

1.2.2.2 Inflation in curved field-space

Besides discussions about the shape of the inflationary potential $V(\phi)$, for multi-field inflation there is also a freedom in the choice of the field-space metric $\mathcal{G}_{IJ}(\phi)$ that is defined in the action (1.16).

A revival of interest in curved field-space geometries was initiated by Kallosh and Linde, with the development of their inflationary *α-attractor model* [49–52]. Following the top-down approach discussed in the previous section, this class of models originate from supergravity theories with a special choice of the Kähler potential and superpotential. The hyperbolic geometry, that is inherited by the theory, provides the exponential stretching for the inflationary potentials, creating flat plateaus ideal for slow-roll inflation. Because any initial potential is stretched exponentially, the α-attractor model provides universal predictions for the scalar spectral index and tensor-to-scalar ratio, that so far are in the very good agreement with the latest observational constraints [53]. It is remarkable that, because of the UV nature, this model is intrinsically a multi-field model of inflation. In Chapter 4 we will present a comprehensive analysis of the reheating process for the two-field α-attractors and demonstrate the significance of the curved field-space geometry for efficient transition to the radiation-dominated state of the universe.

A number of research works has followed after the appearance of α-attractors. In particular, it was shown that the negative curvature of the field space manifold may lead to tachyonic instabilities that destabilize inflationary trajectories. This phenomenon was called *the geometrical destabilization* of inflation [54–58]. Such instability may be catastrophic for inflation, since huge instabilities may terminate it too early, however is beneficial for reheating as will be discussed in more detail in the Part II of the thesis. Another possible evolution scenario with a non-trivial field-space manifold where the inflaton field orbits to the bottom of its potential, was introduced in [59] and called *hyperinflation*. It has drawn a lot of attention and was followed by various developments in the context of non-trivial field-space geometries and multi-field inflation [60–68].

One particular class of multi-field inflationary models was developed in [69–73] and is called *the ultra-light isocurvature scenario*. In these models, the perturbations orthogonal to the inflationary trajectory are massless, but efficiently coupled to the inflaton. They freeze on superhorizon scales and source the tangential (curvature) perturbation, that results in the primordial observables at the end of inflation having a similar phenomenology as in the single-field case. The first exact realization of the ultra-light isocurvature scenario is called *shift-symmetric orbital inflation* and will be discussed in Chapter 2.

1.2.3 Gauge fields during inflation

Gauge fields are unavoidable ingredients of any realistic field theory. For instance, in the Standard Model the strong, electromagnetic, and weak interactions are described by a non-Abelian gauge theory with the symmetry group $U(1)\times SU(2)\times SU(3)$, with the total amount of twelve gauge bosons that include the photon, three weak boson and eight gluons.

Typically, scalar fields are the main characters of inflationary frameworks, however gauge fields can also drive isotropic inflation [7]. In [74, 75] it was shown that gauge fields minimally coupled to gravity with a Lagrangian of the form

$$\mathcal{L}=\mathcal{L}\left(g_{\mu\nu},F_{\mu\nu}\right)=\frac{M_{\rm Pl}^2}{2}R+\mathcal{L}_G\left(F_{\mu\nu}\right), \tag{1.25}$$

may lead to inflationary solutions. Here $F^A_{\mu\nu}=\partial_\mu A^A_\nu-\partial_\nu A^A_\mu-gf^{ABC}A^B_\mu A^C_\nu$ is the field strength of the gauge field, g is the gauge coupling and f^{ABC} are structure constants with gauge indices $A=1,2,\dots,dimG$ of the gauge group G. The generators are denoted as T^A with the standard normalization $[T^A,T^B]=if^{ABC}T^C$ and $Tr(T^AT^B)=\frac{1}{2}\delta^{AB}$. Above $\mathcal{L}_G\left(F_{\mu\nu}\right)$ is a general diffeomorphism- and gauge-invariant Lagrangian that may contain powers of $F_{\mu\nu}$, where the space-time indices are summed up via the metric $g_{\mu\nu}$ or the Levi-Civita tensor $\epsilon^{\mu\nu\rho\sigma}$, and gauge indices are summed by taking the trace. The change under the local gauge transformation with $U\in G$ is defined as

$$A_\mu \quad\longrightarrow\quad A'_\mu=-\frac{i}{g}U^{-1}\partial_\mu U+U^{-1}A_\mu U, \tag{1.26}$$

$$F_{\mu\nu} \quad\longrightarrow\quad F'_{\mu\nu}=U^{-1}F_{\mu\nu}U. \tag{1.27}$$

In this set-up the choice of the non-Abelian gauge group is crucial. In the Abelian case, in order to preserve the rotational symmetry of the flat FLRW background, only the time-component of a vector gauge field may be non-zero and depend solely on time due to homogeneity. Hoverer, such a choice leads to a pure gauge configuration, since it implies the vanishing field strength of the gauge field. By contrast, the choice of non-Abelian gauge group allows us to keep spatial components A_i non-zero and at the same time preserve rotational symmetry. To understand this, first let us note that the time component A_0 may be always set to zero by fixing a gauge to a temporal gauge, i.e. there is always $U=U(t)$ such that $A'_\mu=0$.

[7]This section in mainly based on [76].

This fixes the gauge freedom up to space-time independent global gauge transformations. The remaining global gauge transformations may be used to preserve the rotational invariance, since due to gauge transformations (1.26) two fields are related as $(A_i)_G = U^{-1}A_\mu U \equiv_G A_i$, with constant $U \in G$. It is known that upon spatial rotations $A \to (A_i)_R = R_{ij}A_j$. Hence, the rotational symmetry is preserved if the background configuration is chosen such that $A_R = A_G$. Since any non-Abelian gauge group has an $SU(2)$ subgroup, the gauge group G may be chosen to be $SU(2)$ or $SO(3)$ without loss of generality.

To sum up, a rotationally invariant and homogeneous background is achieved via the ansatz

$$A_0^a = 0, \tag{1.28}$$

$$A_i^a = \delta_i^a a(t)Q(t), \tag{1.29}$$

where $a(t)$ is a scale factor and $Q(t)$ is a vacuum expectation value (VEV) of the gauge field. In this ansatz the gauge group G is chosen to be $SU(2)$ and, hence, $A \equiv a = 1, 2, 3$.

Now let us come back to (1.25) and see that together with (1.28),(1.29) it may indeed lead to inflationary solutions, i.e. to achieve simultaneously $\rho + 3p < 0$ and $\rho > 0$. The simplest possible choice for $\mathcal{L}_G\left(F_{\mu\nu}\right)$ would be the Yang-Mills lagrangian, i.e. $\mathcal{L}_G\left(F_{\mu\nu}\right) = -\frac{1}{4}F^a_{\mu\nu}F^{a\,\mu\nu}$. However, in the Yang-Mills theory $\rho + 3p = 2\rho > 0$, which have the equation of state of radiation. Another choice is to consider higher terms in $F^a_{\mu\nu}F^{b\mu\nu}$, but the conditions to obtain accelerated expansion are not easily satisfied there [77–84]. The way out is to involve terms with $\epsilon^{\mu\nu\rho\sigma}$. The first possibility would be $F \wedge F \propto \epsilon^{\mu\nu\rho\sigma}F^a_{\mu\nu}F^a_{\rho\sigma}$, which is a total derivative and does not contribute to the energy momentum tensor. Hence, the simplest non-trivial choice appears to be $(F \wedge F)^2 = \frac{1}{4}(\epsilon^{\mu\nu\rho\sigma}F^a_{\mu\nu}F^a_{\rho\sigma})^2$, which leads to $p = -\rho$ and hence satisfies the desired criteria.

Taking into account the aforementioned arguments, Refs. [74, 75] proposed the Gauge-flation action of the form

$$S = \int d^4x\sqrt{-\det(g_{\mu\nu})}\left[\frac{M_{\rm Pl}^2}{2}R - \frac{1}{4}F^a_{\mu\nu}F^{a\,\mu\nu} + \frac{\kappa}{384}\left(\epsilon^{\mu\nu\rho\sigma}F^a_{\mu\nu}F^a_{\rho\sigma}\right)^2\right], \tag{1.30}$$

where $\kappa > 0$ is a parameter of the theory with dimension $M_{\rm pl}^{-4}$. The energy-momentum tensor is given by

$$T_{\mu\nu} \equiv \frac{-2}{\sqrt{-\det(g_{\mu\nu})}}\frac{\delta\left(\sqrt{-\det(g_{\mu\nu})}\mathcal{L}\right)}{\delta g^{\mu\nu}} = 2\frac{\delta\mathcal{L}}{\delta F^a{}_\sigma{}^\mu}F^a{}_{\sigma\nu} + g_{\mu\nu}\mathcal{L}, \tag{1.31}$$

which for a homogeneous and isotropic configuration takes the form of the energy-momentum tensor of a perfect fluid. From the above action it follows that

$$\rho = \rho_{\rm YM} + \rho_\kappa, \quad p = \frac{1}{3}\rho_{\rm YM} - \rho_\kappa, \tag{1.32}$$

where $\rho_{\rm YM}$ stands for the energy density contribution from the Yang-Mills part of the action and ρ_κ from the $(F \wedge F)^2$. When $\rho_\kappa \gg \rho_{\rm YM}$, the equation of state $w \approx -1$ which indicates the desired phase of accelerated expansion.

In [74–76, 85] it was shown that the action (1.30) indeed leads to an attractor solution and the isotropic background is stable with regard to the initial anisotropies and choice of initial conditions.

Despite of the beautiful idea of incorporating gauge fields as inflatons, the Gauge-flation model does not match the observational constraints. It turns out that it is impossible to satisfy simultaneously the bounds for the tensor-to-scalar ratio and scalar spectral tilt. However, the search for alternative gravitational wave production mechanisms initiated renewal of interest in models that involve gauge fields. These, based on [86], will be discussed in more detail in Chapter 3.

1.2.4 Observations

To extract observables from the inflationary epoch, in 1980-1990s Bardeen, Kodama, Sasaki, Mukhanov et al [87–91] developed *the cosmological perturbation theory*. We will briefly outline how quantum perturbations that originate during inflation generate the temperature anisotropies in the CMB as well as produce gravitational waves.

1.2.4.1 Perturbation theory

The small perturbations of the metric and the energy-momentum tensor may be written as [8]

$$\begin{aligned} g_{\mu\nu}(t,x) &= \bar{g}_{\mu\nu}(t) + \delta g_{\mu\nu}(t,x), \\ T_{\mu\nu}(t,x) &= \bar{T}_{\mu\nu}(t) + \delta T_{\mu\nu}(t,x), \end{aligned} \tag{1.33}$$

where $\bar{g}_{\mu\nu}$ is the background flat FLRW metric (1.1) and $\bar{T}_{\mu\nu}(t)$ the homogeneous and isotropic energy-momentum tensor. Here $\mu = 0,1,2,3$ denote the space-time indices. It is convenient to perform a scalar-vector-tensor

[8] This Section is based mainly on [4].

(SVT) decomposition of the perturbations, then the perturbed space-time metric takes the form

$$ds^2 = -(1+2A)dt^2 - 2a(t)B_i dx^i dt + a^2(t)(\delta_{ij} + h_{ij})dx^i dx^j, \qquad (1.34)$$

where $i, j = 1, 2, 3$ label the spatial directions. Here the 3-vector B_i may be written as a combination of the gradient of a scalar and a divergenceless vector $B_i = \partial_i B + \hat{B}_i$ with $\partial^i \hat{B}_i = 0$, and the rank-2 symmetric tensor h_{ij} may de decomposed into a scalar, vector and tensor as $h_{ij} = 2C\delta_{ij} + 2\partial_{\langle i}\partial_{j\rangle}E + 2\partial_{(i}\hat{E}_{j)} + \hat{E}_{ij}$ with divergenceless vector $\hat{E}_i$ that satisfy $\partial^i \hat{E}_i = 0$ and a divergenceless and traceless tensor perturbation $\hat{E}_{ij}$ with $\partial^i \hat{E}_{ij} = 0$, $\hat{E}^i_i = 0$ and

$$\begin{aligned} \partial_{\langle i}\partial_{j\rangle}E &\equiv \left(\partial_i\partial_j - \frac{1}{3}\delta_{ij}\nabla^2\right)E, \\ \partial_{(i}\hat{E}_{j)} &\equiv \frac{1}{2}\left(\partial_i\hat{E}_j + \partial_j\hat{E}_i\right). \end{aligned} \qquad (1.35)$$

Hence, perturbations decompose into scalars: A, B, C, E; vectors: $\hat{B}_i, \hat{E}_i$; tensors: $\hat{E}_{ij}$, which have 4+4+2 degrees of freedom (d.o.f.) respectively. Invariance of the theory under the coordinate transformations removes 4 more d.o.f., leading to only 6 physical d.o.f. At linear order the Einstein equations for scalars, vectors and tensors do not mix and hence can be studied separately. This is why the SVT decomposition is useful. Vector perturbations quickly decay with the expansion of the universe and not produced at all in standard single-field inflationary models. Therefore, we will focus only on the description of scalar and tensor perturbations in the forthcoming sections.

Before we proceed further, let us note that the metric perturbations in (1.34) depend on the choice of coordinate system, i.e. are gauge dependent, and hence are not uniquely defined. This problem was resolved by Bardeen [87], who introduced special combinations of metric perturbations that do not change under coordinate transformations. Gauge invariant variables are called *the Bardeen variables* and defined as

$$\begin{aligned} \Psi &\equiv A + \mathcal{H}(B - E') + (B - E')', & \hat{\Phi}_i &\equiv \hat{B}_i - \hat{E}'_i, \\ \Phi &\equiv -C + \frac{1}{3}\nabla^2 E - \mathcal{H}(B - E'), & &\hat{E}_{ij}, \end{aligned} \qquad (1.36)$$

which for convenience are written in conformal time $d\tau \equiv dt/a(t)$ with the conformal Hubble rate $\mathcal{H} = a'/a$. These variables cannot be removed by a gauge transformation. Two more gauge-invariant quantities that combine metric and matter perturbations are called *curvature perturbations*

$$\begin{aligned}\zeta &= -C + \frac{1}{3}\nabla^2 E + \mathcal{H}\frac{\delta\rho}{\bar{\rho}'},\\ \mathcal{R} &= -C + \frac{1}{3}\nabla^2 E - \mathcal{H}(v+B),\end{aligned} \tag{1.37}$$

where $v_i = \partial_i v$ is the bulk velocity, that appears from the perturbed energy-momentum tensor, in particular $T^i{}_0 = (\bar{\rho} + \bar{p})v_i$. In case of the adiabatic fluctuations, ζ and $\mathcal{R}$ become constant and coincide with each other on the scales where the physical wavelength is larger than the comoving horizon. As we will see in the next section, they play a major role in describing scalar perturbations from inflation.

Another possibility to deal with the gauge-dependence is to fix the gauge, i.e. set two of the four scalar metric perturbations to zero: $B = E = 0$ in *the Newtonian gauge*, $C = E = 0$ in *the spatially-flat gauge* and $A = B = 0$ in *synchronous gauge*.

1.2.4.2 Scalar perturbations in single field-inflation

Let us start by describing [9] the scalar fluctuations for the single field inflationary action (1.8) by perturbing the matter inflaton field as

$$\phi(t,x) = \bar{\phi}(t) + \delta\phi(t,x), \tag{1.38}$$

where $\bar{\phi}(t)$ is a solution to the background equations of motion. The coupling of the inflaton perturbations $\delta\phi$ to the metric depends on the gauge choice. We fix the gauge to the spatially flat one, meaning that A and B are related to the inflaton fluctuations through the Einstein equations. Solving the Einstein equations together with the equations of motion of the perturbed field, leads to the linear equation of motion for the gauge-invariant perturbations. Introducing variables $f \equiv a\,\delta\phi$ and $z \equiv \frac{a\bar{\phi}'}{\mathcal{H}}$ and going to Fourier space results in *the Mukhanov-Sasaki equation* for the mode functions

$$f_k'' + \left(k^2 - \frac{z''}{z}\right) f_k = 0. \tag{1.39}$$

This is the master equation for inflationary perturbations. It is valid on all scales, exact (does not assume the slow-roll approximation) and contains the coupling between matter and metric fluctuations. This equation has the

[9] More detailed analysis may be found for instance in Refs. [3, 4, 92].

form of the harmonic oscillator equation with a time-dependent frequency $\omega^2(k,\tau) = k^2 - \frac{z''}{z}$. With the knowledge of the second order action for the Fourier components of the inflaton perturbations, the quantization of the theory is performed in complete analogy with the quantum harmonic oscillator problem. The quantisation of the field f is implemented as

$$\hat{f}(\tau,x) = \frac{1}{(2\pi)^3}\int d^3k \left[f_k(\tau)\hat{a}_k(t)e^{-i\mathbf{kx}} + f_k(\tau)^*\hat{a}_k^\dagger e^{i\mathbf{kx}}\right], \tag{1.40}$$

where $\hat{a}_k^\dagger, \hat{a}_k$ are creation and annihilation operators that satisfy the canonical commutation relations.

Next we can get back to the analysis of solutions of the Mukhanov-Sasaki equation. For $k \gg |z''/z|$, the frequency is constant and proportional to the wave number k, which leads to the oscillating solutions that match *the Bunch-Davies vacuum* in the asymptotic past $\lim_{\tau\to-\infty} f_k = \frac{e^{-ik\tau}}{\sqrt{2k}}$. Since $\frac{z''}{z} \approx 2\mathcal{H}^2$ during slow-roll, it is a measure of the comoving horizon $\mathcal{H}^{-1}$. Therefore, the regime above corresponds to $k \gg \mathcal{H}$, which denotes *the sub-Hubble* scales. With time the comoving Hubble scale shrinks, and modes at some moment in time cross and exit it. The relation $k \ll \mathcal{H}$ distinguishes *the super-Hubble* scales, on which the frequency $\omega(k,\tau)$ becomes imaginary. In this regime there is a growing $f_k \propto z$ and a decaying solution $f_k \propto z^{-2}$ for perturbation modes. The growing solution is the relevant one for observations [10]. It implies that the gauge-invariant curvature perturbation defined in (1.37) is conserved on super-Hubble scales, specifically

$$\mathcal{R}_k = -\frac{\mathcal{H}}{\bar{\phi}'}\delta\phi_k = -\frac{f_k}{z} = const. \tag{1.41}$$

In particular, in the slow-roll approximation the solution of (1.39) is given by

$$f_k(\tau) = \frac{\sqrt{\pi}}{2}\sqrt{-\tau}H_\nu^{(1)}(-k\tau), \quad \text{with} \quad \nu \equiv \frac{3}{2} + \epsilon_H + \frac{1}{2}\eta_H. \tag{1.42}$$

where $H_\nu^{(1)}$ is the Hankel function of the first kind.

The next step is to find the quantum statistics for the operator $\hat{f}$. The expectation value of it is zero $\langle 0|\hat{f}|0\rangle = 0$, but the variance is not and is given by

$$\langle|\hat{f}|^2\rangle \equiv \langle|\hat{f}(\tau,0)\hat{f}(\tau,0)|0\rangle = \int d\ln k \frac{k^3}{2\pi^2}|f_k(\tau)|^2. \tag{1.43}$$

[10] Decaying mode can be relevant in some multi-field set-ups.

The dimensionless power spectra for mode functions is defined as

$$\Delta_f^2(k,\tau) \equiv \frac{k^3}{2\pi^2}|f_k(\tau)|^2, \tag{1.44}$$

which leads to the power spectra for $\delta\phi$ fluctuations

$$\Delta_{\delta\phi}^2(k,\tau) = \frac{\Delta_f^2(k,\tau)}{a^2(\tau)} \approx \left(\frac{H(t)}{2\pi}\right)^2 \bigg|_{k=aH}. \tag{1.45}$$

Finally, we have all the necessary ingredients to relate the fluctuations in the inflaton field to observable fluctuations after inflation. Since the curvature perturbation freezes on super-Hubble scales, it is a perfect quantity to provide this link. The dimensionless power spectrum $\Delta_\mathcal{R}^2(k)$ is defined by

$$\langle \mathcal{R}_k \mathcal{R}_{k'} \rangle = (2\pi)^3 \delta^{(3)}(k+k') P_\mathcal{R}(k), \quad \Delta_\mathcal{R}^2(k) = \frac{k^3}{2\pi^2} P_\mathcal{R}(k). \tag{1.46}$$

Therefore, the power spectrum of $\mathcal{R}$ can be computed via the power spectrum of $\delta\phi$, evaluated at the horizon crossing $k = aH$, which results into

$$\Delta_\mathcal{R}^2(k) = \left(\frac{H}{\dot{\phi}}\right)^2 \Delta_{\delta\phi}^2 = \frac{1}{8\pi^2 \epsilon_H} \frac{H^2}{M_\mathrm{pl}^2}\bigg|_{k=aH}. \tag{1.47}$$

Even though during the slow-roll inflation both $\epsilon_H(t)$ and $H(t)$ depend on time very mildly, they have different values when different modes cross the horizon. This introduces a source of scale dependence, which is captured by the parameter named as *the scalar spectral index* and defined as

$$n_s - 1 \equiv \frac{d \ln \Delta_\mathcal{R}^2(k)}{d \ln k}, \quad \Delta_\mathcal{R}^2(k) = A_s(k_*) \left(\frac{k}{k_*}\right)^{n_s - 1}, \tag{1.48}$$

where $A_s(k_*)$ is the amplitude of the scalar power spectrum at *the pivot scale* k_*, at which the reference scale exit the horizon. The scalar spectral index may be written in terms of the slow-roll parameters as

$$n_s = 1 - 2\epsilon_H - \eta_H. \tag{1.49}$$

Currently the observations show deviation from scale-invariance at 5.6σ confidence level [53] with values $n_s = 0.9603 \pm 0.0073$ for $k_* = 0.05\mathrm{Mpc}^{-1}$, which is a direct measurement of time dependence during the inflationary dynamics [11].

[11] Assuming inflation is the right explanation.

The higher order correlation functions reflect non-Gaussian initial conditions (IC's) that are associated with *primordial non-Gaussianity.* Here IC's refer to those created by inflation, that will be subsequently stretched to macroscopic scales, become classical and provide seeds for the cosmic structure. Within linear perturbation theory, an initial Gaussian probability distribution will not change throughout the evolution, meaning that the amplitude of perturbations will have Gaussian shape around the mean value. Higher order correlations then test the deviations from the Gaussian distribution of the IC's of perturbations. Whereas the two-point correlation function probes a free theory, the three-point function is associated with non-linear interactions and hence encodes the particle content and the interactions during inflation. The primordial bispectrum is the Fourier transform of the three-point correlation function of curvature perturbation, defined as

$$\langle \mathcal{R}_{k_1}\mathcal{R}_{k_2}\mathcal{R}_{k_3}\rangle = (2\pi)^3\delta^{(3)}(k_1+k_2+k_3)\frac{(2\pi^2)^2}{(k_1k_2k_3)^2}B_{\mathcal{R}}(k_1,k_2,k_3). \quad (1.50)$$

Because of the homogeneity of the background, the momentum three-vectors add up to zero and hence form a triangle. Depending on the shape of this triangle, the signal will also change. Typically, the most commonly studied are equilateral, local and folded shapes. The amplitude of the non-Gaussianity is defined in equilateral configuration ($k_1 = k_2 = k_3$) as

$$f_{\rm NL}(k) \equiv \frac{5}{18}\frac{B_{\mathcal{R}}(k,k,k)}{\Delta^4_{\mathcal{R}}(k)}, \quad (1.51)$$

which allows one to express the bispectrum as

$$B_{\mathcal{R}}(k_1,k_2,k_3) \equiv \frac{18}{5}f_{\rm NL}\times S(x_2,x_3)\times \Delta^4_{\mathcal{R}}(k), \quad (1.52)$$

where $x_2 \equiv k_2/k_1$, $x_3 \equiv k_3/k_1$ and $S(x_2,x_3)$ is the shape function. The current constraint from CMB observations on the amplitude of local non-Gaussianity is $f_{\rm NL}^{\rm local} = -0.9 \pm 5.1$.

1.2.4.3 Scalar perturbations with multiple fields

Similarly as in the single-field case, the perturbations $\delta\phi^I(x^\mu)$ to the background field trajectories $\varphi^I(t) \equiv \phi^I_0(t)$ may be written as

$$\phi^I(x^\mu) = \varphi^I(t) + \delta\phi^I(x^\mu), \quad (1.53)$$

where I runs through the number of fields in the underlying theory. The perturbations may be combined into the gauge-invariant Mukhanov-Sasaki variable [88, 91, 93, 94]

$$Q^I \equiv \delta\phi^I + \frac{\dot{\phi}^I}{H}\psi. \tag{1.54}$$

Then, from the background equations of motion (1.17), one finds the equation of motion for perturbations Q^I in the form

$$\mathcal{D}_t^2 Q^I + 3H\mathcal{D}_t Q^I + \left[\frac{k^2}{a^2}\delta^I{}_J + \mathcal{M}^I{}_J\right] Q^J = 0, \tag{1.55}$$

with the mass-squared matrix defined by

$$\mathcal{M}^I{}_J \equiv \mathcal{G}^{IK}\left(\mathcal{D}_J\mathcal{D}_K V\right) - \mathcal{R}^I{}_{LMJ}\dot{\varphi}^L\dot{\varphi}^M - \frac{1}{M_{\rm pl}^2 a^3}\mathcal{D}_t\left(\frac{a^3}{H}\dot{\varphi}^I\dot{\varphi}_J\right). \tag{1.56}$$

Here the first term is the analogue of the Hessian of the potential, calculated in a curved field space defined by the field metric $\mathcal{G}^{IJ}(\varphi^K)$. The second contribution resembles the right-hand side of the geodesic deviation equation, where $\mathcal{R}^I{}_{LMJ}$ is the Riemann tensor calculated from the field-space metric $\mathcal{G}_{IJ}(\varphi^K)$. Hence it indicates how two distinct trajectories in field space approach or recede from each other. This term is a unique consequence of the non-trivial field geometry and is identically zero in single-field models or models with canonical kinetic terms. Finally, the third term encodes the kinematic effects, such as turns in the field trajectory.

In the case with multiple fields it is convenient to classify the scalar perturbations in two types: the adiabatic (curvature) perturbations that are tangential to the inflationary trajectory and the isocurvature perturbations, that are orthogonal to it. Let us focus on the case with two fields and project the perturbations along the tangent T^I and normal directions N^I, defined in Section 1.2.2. Then the second order action for curvature $\mathcal{R}$ and isocurvature σ perturbations is given by [69]

$$S_2 = \int d^4x a^3\left[\epsilon_H\left(\dot{\mathcal{R}} - \frac{2\Omega}{\sqrt{2\epsilon_H}}\sigma\right)^2 - \frac{\epsilon_H}{a^2}(\partial_i\mathcal{R})^2 + \frac{1}{2}\left(\dot{\sigma}^2 - \frac{1}{a^2}(\partial_i\sigma)^2\right) - \frac{1}{2}\mu^2\sigma^2\right], \tag{1.57}$$

where Ω is the turning rate of the trajectory defined in (1.19) and μ is the mass of the isocurvature mode that can be written as

$$\mu^2 = V_{NN} + \epsilon_H\mathbb{R}H^2 + 3\Omega^2. \tag{1.58}$$

Here $V_{NN} = N^I N^J \nabla_I \nabla_J V$ is the analogue of the Hessian of the potential and $\mathbb{R}$ is the Ricci scalar computed from the field-space metric $\mathcal{G}_{IJ}$. From (1.57) one can see that if the turn rate Ω is non-zero, the curvature and isocurvature perturbations get coupled. This is an important property of multi-field inflationary models. Depending on the magnitude of μ with regard to the Hubble scale H, multi-field models may be divided into three different cases. The case when $\mu \gg H$ corresponds to the regime with heavy fields. They may be integrated out that leads to the effective single-field theory with a reduced sound speed [36, 95–98]. Another regime with $\mu \sim \mathcal{O}(H)$ corresponds to the quasi-single field regime and was studied in [99–101]. The regime $\mu \ll H$ corresponds to the case with light isocurvature fields, that was extensively studied within the curvaton scenario [102, 103].

The case with $\mu^2 = 0$, however, is special. In this case the above action is invariant under the shift of both $\dot{\mathcal{R}}$ and σ. This ensures that σ behaves as a massless perturbation on super-Hubble scales and acts as a constant source for the curvature perturbation. Such situation will be discussed in detail in Chapter 2 of the thesis. We will also get back to the general discussion of multi-field perturbations in Part II of the thesis in Section 1.3.3, with further focus on the reheating era.

1.2.4.4 Tensor modes

After 100 years from the discovery of Einstein's General Relativity theory, the LIGO/VIRGO collaboration [104–109] announced the direct observation of gravitational waves (GW), which opened the era of GW astronomy. In addition to astronomical observations, GW interferometers allow us to directly probe the physics of the early Universe via the stochastic gravitational wave background (SGWB). The latter differs considerably from the gravitational waves coming from binary inspirals and burst events or continuous periodic gravitational waves that originate from pulsars. The signal from such events is coming from a specific direction, whereas the SGWB, similarly to the CMB, is uniform in all directions. Remarkably, its potential observation (as well as the absence of this observation) would give unique information about the physics of the early Universe, in particular the energy scale of inflation which is encoded in the Hubble parameter.

The GWs originate from tensor perturbations of the FRW metric (1.34)

$$ds^2 = -dt^2 + a(t)^2 \left(\delta_{ij} + h_{ij}\right) dx^i dx^j, \tag{1.59}$$

where the perturbation h_{ij} is symmetric, trace-free and transverse.

From the perturbed Einstein equations

$$\bar{G}_{\mu\nu} + \delta G_{\mu\nu} = 8\pi G \left(\bar{T}_{\mu\nu} + \delta T_{\mu\nu}\right), \tag{1.60}$$

it follows that the equation of motion for tensor perturbation in Fourier space appears in the form (see for instance [110, 111])

$$\ddot{h}_{ij} + 3H\dot{h}_{ij} + k^2 h_{ij} = 16\pi G \Pi_{ij}^{TT}, \tag{1.61}$$

where Π_{ij}^{TT} is the transverse-traceless part of the anisotropic stress tensor. In standard slow-roll single field inflationary models the anisotropic stress tensor is identically zero and amplification of the tensor vacuum metric fluctuations occurs because of the exponential expansion during inflation. It is convenient to align the z-axis with the momentum of the mode $\vec{k} = (0, 0, k)$ and write h_{ij} in terms of the two polarization modes of the gravitational wave

$$\frac{M_{\rm pl}}{2} a h_{ij} \equiv \frac{1}{\sqrt{2}} \begin{pmatrix} f_+ & f_\times & 0 \\ f_\times & -f_+ & 0 \\ 0 & 0 & 0 \end{pmatrix}. \tag{1.62}$$

Such parametrization reduces the equation of motion (1.61) to two copies of the equation of motion (1.39) with $\frac{z''}{z} = \frac{a''}{a}$ for massless scalar fields f_+ and $f_\times$. Hence, for each mode $f_+, f_\times$ the computation is performed exactly in the same way as for the case of scalar perturbations. The tensor power spectrum is then simply a rescaling of (1.45) by a factor $2 \times \left(\frac{2}{M_{\rm pl}}\right)^2$ that accounts for the sum of two polarizations and the normalization in (1.62) respectively. Hence, the tensor power spectrum results in

$$\Delta_t^2(k) = \left.\frac{2H^2}{\pi^2 M_{\rm pl}^2}\right|_{k=aH}. \tag{1.63}$$

As before the scale dependence is captured via *the tensor spectral index* that is defined as

$$n_t \equiv \frac{d \ln \Delta_t^2(k)}{d \ln k}, \quad \Delta_t^2(k) = A_t(k_*) \left(\frac{k}{k_*}\right)^{n_t}, \tag{1.64}$$

and may be written in terms of the slow roll parameters as

$$n_t = -2\epsilon_H. \tag{1.65}$$

Therefore, the tensor tilt is a direct measure of ϵ_H. Observational constraints on the amplitude of tensor perturbations are usually expressed in terms of *the tensor-to-scalar ratio*

$$r \equiv \frac{A_t}{A_s}, \tag{1.66}$$

which via the slow-roll parameter is written as $r = 16\epsilon_H$. It in turn provides the consistency relation for single field inflation models $r = -8n_t$. Its violation would be a signal of physics beyond the standard single-field approach. Currently n_t is constrained to be slightly red tilted and $r < 0.056$ at 95% confidence level by Planck 2018 results [53].

Therefore, inflation provides an irreducible SGWB. Observational constraints, however, lead to a very small amplitude of the GW power spectra. Denoting by $\Omega_{\rm GW}$ to be today's GW fractional energy density per logarithmic wave-number interval, its amplitude at CMB scales is of order at most $\Omega_{\rm GW} \sim 10^{-15}$. So small values are potentially detectable only for the next-to-next-generation of space-based observatories, for instance Big Bang Observatory (BBO) [112] or Deci-hertz Interferometer Gravitational wave Observatory (DECIGO) [113], as well as large surveys of stars such as Gaia [114, 115] and the upgrade THEIA (Telescope for Habitable Exoplanets and Interstellar/Intergalactic Astronomy)[116], see Figure 1.2. That is why there is a broad interest in alternative or complementary scenarios that could produce the stochastic GWs background at different levels, that are more likely to be detected during the next two decades.

One possibility to significantly enhance GW production within the inflationary framework, is the presence of a non-zero source term. In the early universe there are several possible sources for Π_{ij}^{TT}, coming from

- gauge fields,
- scalar field gradients,
- bulk fluid motion,
- gradients of second order scalar perturbations,

as well as other possibilities not listed here.

Another option is to break the space-time symmetries during inflation, the so-called space-reparametrization. In this case the graviton can acquire a mass which leads to the enhancement of tensor spectra at small scales, implying a blue tensor tilt. In addition to that, the brief but strong violation

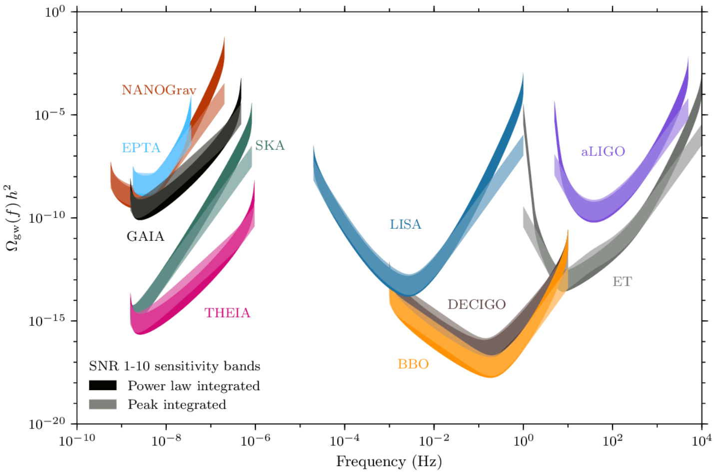

Figure 1.2: The sensitivity curves for different gravitational wave detectors, taken from [117].

of the slow-roll conditions may lead to a bump in the power spectra of scalar fluctuations, which imprints on $\Omega_{\rm GW}$. If the bump is big enough (at least 10^7 larger than its CMB value), this can also lead to the formation of primordial black holes. Besides inflation, the SGWB may be generated during (p)reheating. The non-perturbative particle production together with the non-linear-dynamics produce the GW background, which is unlike the one coming from inflation and has a peaked power-spectrum at very high-frequencies $f \sim 10^{10}$Hz [118]. Another possible cosmological origin for the SGWB may be cosmic strings, first order phase transitions and pre Big Bang models. From the astrophysical side, the SGWB may be generated for instance by binary black holes, binary neutron stars, other binary star systems, pulsars, magnetars and supernovae. For comprehensive reviews on cosmological backgrounds of gravitational waves and discussions of possible astrophysical sources see Ref. [119, 120] and references therein.

Now, the question arises: how to distinguish the cosmological origin of GWs from the astrophysical one? There are several "smoking guns" for the cosmological origin of SGWB, such as a non-Gaussian signal (the signal from astrophysical origin is Gaussian), chirality, anisotropy (intrinsic or induced) and a rich profile of GW power spectrum.

In Chapter 3 we will discuss the theoretical limitations on the chiral gravitational wave production sourced by spectator non-Abelian gauge fields during inflation, that can significantly enhance the tensor-to scalar ratio r while keeping the scalar spectral index n_s within the observational bounds.

1.2.5 Upcoming experiments

One of the main goals in observational cosmology nowadays is to detect the primordial tensor fluctuations. Possible direction is polarization measurement of CMB. At the level of a few micro Kelvin the CMB is linearly polarized due to Thomson scattering of photons off free electrons just before decoupling. It was first observed by the Degree Angular Scale Interferometer (DASI) in 2002 [121] and was confirmed by many other experiments. The main idea of upcoming experiments is that scalar perturbations can only create polarization patterns of a particular type, parallel or perpendicular to the wave vector $\vec{k}$, that are called E-modes. If, in addition to that, a gravitational wave background is present, it would create an extra stretching of spacetime, which induces a polarization pattern that is rotated by a 45-degree angle and is called the B-mode polarization. Such polarization pattern cannot be produced by scalar fluctuations and hence, provides a unique signature of primordial gravitational waves. In addition to that, in some models with parity breaking, like Gauge-flation and Chromo-Natural inflation, gauge field tensor modes experience a transient growth in one of their polarizations, hence leading to production of chiral GWs. They could be potentially distinguishable from the standard vacuum fluctuations in future experiments, like CMB Stage-4 [122] and LiteBIRD [123], which aim to probe the tensor sector to values $r \simeq 0.001$.

Furthermore, CMB spectral distortions experiments like PIXIE, SuperPIXIE, Voyage 2050, 10×Voyage 2050 (see [124] for a recent review and references therein) aim to probe 10 e-folds of inflation further, that are not visible for CMB anisotropy measurements. Spectral distortions of the CMB spectrum occur because of dissipation of density perturbations through photon diffusion in the early universe, which is also called Silk damping. Such measurements will provide a unique test for departures from scale-invariance that, depending on the outcome, would support or disfavour a simple single-field inflationary scenario.

1.2.6 Open problems

Inflation nowadays is the leading framework for the early universe cosmology, that solves the horizon and flatness problems, and can produce density fluctuations that match the latest observational constraints. However, there are still some theoretical challenges that we outline below.

Since there is no UV complete theory of the early universe yet, inflation is an effective description that is valid until some cut-off scale $\Lambda < M_{\rm pl}$. Then the question should be asked: can the physics above this cut-off affect the low-energy dynamics during inflation? It turns out that corrections may affect the flatness of the potential. In particular, important corrections are of the form [125, 126] $\sum_n c_n V(\phi)\frac{\phi^{2n}}{\Lambda^{2n}}$, where c_n are dimensionless Wilson coefficients of order one. The major effect from these corrections is coming from the dimension-six operator $\Delta V = c_1 V(\phi)\frac{\phi^2}{\Lambda^2}$. When the inflaton value is smaller than the cut-off scale $\phi \ll \Lambda$, the correction is small $\Delta V \ll V$, however the second slow-roll parameter $\eta_V \ll 1$ gets significantly altered by this correction

$$\Delta\eta_V = \frac{M_{\rm pl}^2}{V}(\Delta V)'' \approx 2c_1\left(\frac{M_{\rm pl}}{\Lambda}\right)^2 > 1, \tag{1.67}$$

for $c_1 \sim 1$ and $\Lambda \lesssim M_{\rm pl}$. This issue is called *the eta problem*, that is present in most slow-roll models of inflation. One possible resolution is the presence of a shift symmetry for the inflaton field $\phi \to \phi + c$, which is the case in natural inflation [127].

The second problem is the problem of *initial conditions* for inflation, since it requires some fine-tuning of initial values for selected dynamics, see Ref. [128]. It includes *the overshoot problem*, meaning that for big initial velocities of the inflaton field, the flat region of the potential where inflation should happen may be overshot. It typically happens in small-field inflationary models, where field excursions $\Delta\phi$ are small in comparison to $M_{\rm pl}$. There the Hubble friction is not strong enough to decelerate the inflaton field. This is not the case for large-field models, where the Hubble friction is strong and leads to inflationary attractor solutions.

In addition to that, it was shown that inflation is past-geodesically incomplete [129–131], therefore some other physics is required to describe the past boundary of the inflating region of space-time, that is also called the singularity problem. This is resolved in alternatives to cosmological inflation, the so-called Bouncing cosmologies. In such models the universe never reaches a singularity, but instead undergoes a phase of contraction, that is followed by a bounce and a further expansion, that may repeat several times, see [132] for a review. Bouncing cosmologies have other problems, which, however, we will not pursue here.

Coming back to the inflationary framework and summing up its open problems, the legitimate questions arise: what happened before inflation has started or did inflation start at the top of the potential or somewhere else? This questions are challenging and we hope that they will be answered in the forthcoming theoretical explorations.

1.3 Reheating

After the universe expanded at least e^{55} times, inflation has to end. Because of the enormous exponential expansion, the temperature of the universe also dropped considerably. However, in order for BBN to happen and meet the observable abundances of light elements, the universe has to be in a radiation-dominated state. This is the first and foremost motivation to assume, that between inflation and BBN, there was one more transition period that is called *reheating*. Below we outline the physics of this era, based mainly on Refs. [118, 133–136].

1.3.1 Reheating vs preheating

The necessity of the reheating mechanism was already clear after the first appearance of Guth's theory of inflation [27], which however lacked a "graceful exit", since collision of bubble walls does not lead to a thermal, homogeneous and isotropic universe. This was naturally resolved in the new inflation scenario proposed by Linde [28], where the reheating process was happening via the background oscillations of the inflaton field near the minimum of its potential. Historically, it was first described in 1982 *perturbatively* in works by Dolgov & Linde [137] and Abbott, Fahri & Wise [138] for the new inflation scenario. Soon after that new works devoted to reheating for various inflationary scenarios [139–142] started to appear.

The evolution of the inflaton field during the period of oscillations after inflation, see Figure 1.3, was described through the phenomenological equation

$$\ddot{\phi} + 3H(t)\dot{\phi} + \Gamma_{\rm tot}\,\dot{\phi} + V_\phi = 0, \tag{1.68}$$

where $\Gamma_{\rm tot}$ is the total decay width of the inflaton to daughter fields, which is calculated via quantum field theory (QFT) methods. The solution for $\phi(t)$ approaches the oscillatory regime and may be parametrised by

$$\phi(t) = \Phi(t)\sin\left(f(t)\,t\right), \tag{1.69}$$

where $\Phi(t)$ is the decreasing amplitude and $f(t)$ is the frequency of oscillations. The amplitude decays because of particle production as well as expansion of space. It may be written in the form

$$\Phi(t) = \Phi_0 e^{-\frac{1}{2}\Gamma_{\rm tot}t} e^{-\frac{1}{2}\int 3H\,dt}, \tag{1.70}$$

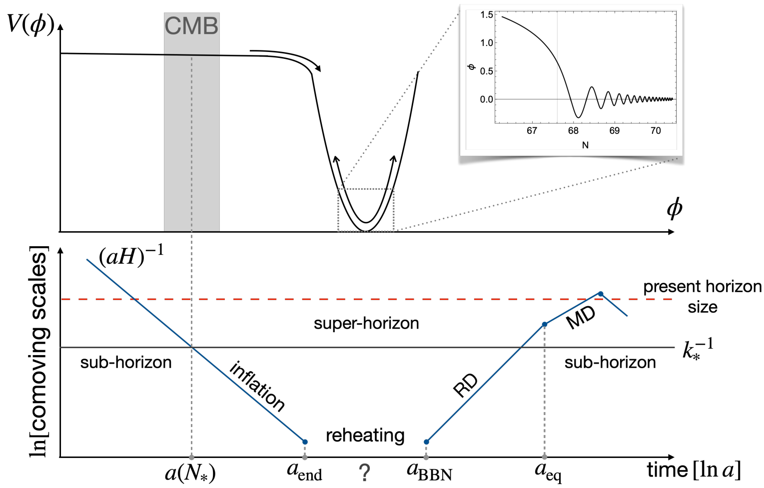

Figure 1.3: *Top panel:* The illustration of the inflation and reheating eras, as well as oscillations of the inflaton field ϕ around the minima of its potential $V(\phi)$, depending on the number of e-folds N from the start of inflation. The grey grid line in the $\phi - N$ inset corresponds to the moment of the end of inflation. The shaded grey region illustrates the perturbations during inflation that are visible in the CMB.
Bottom panel: Evolution of the Hubble radius $(aH)^{-1}$ (solid blue curve) and a representative fluctuation with comoving wave number k_* (solid grey line) in time. The red dashed line represents the present horizon size. RD and MD stand for the radiation dominated and matter dominated eras respectively. The scale factor $a(N_*)$ corresponds to the scale factor evaluated at the moment of horizon crossing of the representative mode, which happened at N_* e-folds starting from the beginning of inflation. Knowledge of N_* is crucial for the accurate determination of the CMB predictions, as will be discussed in detail in Section 1.3.4.1. Scale factors $a_{\rm end}, a_{\rm BBN}, a_{\rm eq}$ correspond to the moment of the end of inflation, start of the BBN and to the moment of matter and radiation equality respectively. The question mark symbolizes the unknown expansion history of the universe during the reheating era.

the precise values of which depend on the shape of the inflationary potential around its minimum. For instance, for a quadratic potential $V = \frac{1}{2}m^2\phi^2$ the oscillation amplitude equals $\Phi(t) \sim a^{-3/2}(t)\exp(-\Gamma_{\rm tot}t/2)$ and the frequency coincides with the inflaton mass $f(t) = m$.

In general, the equation of state of the reheating era highly depends on the shape of the potential near its origin. For polynomial behaviour $V \propto |\phi|^{2n}$, where n is not necessarily an integer number, however with the restriction $n > 1/2$ to ensure a non-singular first derivative at the minimum, the equation of state is given by [143]

$$\langle w \rangle \approx \frac{n-1}{n+1}. \tag{1.71}$$

This leads to a matter-dominated reheating era with $w = 0$ for quadratic potentials $n = 1$ and radiation-domination $w = 1/3$ for $n = 2$. The requirement $n > 1/2$ always leads to $w > -1/3$, which means that oscillations around minima of potential in any case lead to a decelerating stage of expansion. As we will see in Section 1.3.4.1, knowledge of the equation of state for the reheating era is crucial in order to provide accurate predictions for CMB observables.

However, such description appears to be incomplete. First of all, the perturbative description fails for large coupling constants which may easily emerge in the very early universe due to high energy scales. Secondly, in such description particle production becomes efficient when $H \lesssim \Gamma_{\mathrm{tot}}$, which is typically achieved only in a couple of e-folds after the end of inflation and may lead to a prolonged reheating era, that could change inflationary predictions and also affect BBN. The last and, perhaps, the most important reason is that it does not take into account the collective effects of the Bose condensate. Since the inflaton field at the end of inflation is a coherent wave, a condensate with a large occupation number of inflaton quanta that oscillate with the same phase around the minimum of its potential, the particle production should be described as a collective process. Due to large occupation numbers, the condensate itself may be treated as a classical field, however this is not the case for the decay products where a quantum description is required. Bose condensation effects may lead to exponential increase in particle production, that is impossible to capture via the perturbative analysis. This was realised by Traschen and Brandenberger in [144] and developed further in works by Dolgov & Kirilova, Shtanov and Kofman et al in [133, 145–149]. In these works it was proposed that reheating can proceed through *non-perturbative* processes, i.e. via parametric or tachyonic resonances. In the aforementioned and subsequent investigations, including lattice simulations [150], it turned out that in many inflationary models the first stages of reheating were dominated by the parametric resonance, hence in order to distinguish this stage from the slow perturbative description it was named *preheating*. Despite of this, the perturbative treatment is still used in the final stages of the reheating era, to complete the transfer of energy after the shut down of a resonance.

To better understand the essence of preheating, let us consider the static universe approximation, i.e. $H(t) = 0$. Without specifying the interaction term for now, let χ be the daughter scalar field that is produced via inflaton oscillations. As discussed above, χ should be treated as a quantum field and considered as a fluctuation to the classical oscillating inflaton background.

In the Heisenberg representation it is written as

$$\hat{\chi}(t, \mathbf{x}) = \frac{1}{(2\pi)^3} \int d^3k \left(\hat{a}_k \chi_k(t) e^{-i\mathbf{kx}} + \hat{a}_k^\dagger \chi_k^* e^{i\mathbf{kx}} \right). \tag{1.72}$$

Fluctuations start to evolve from their vacuum state, since inflation washed out all possible initial particle densities to negligible values. Then, the equation of motion for each mode k in the static universe approximation may be written in the form

$$\ddot{\chi}_k + \omega^2(k, t)\chi_k = 0, \tag{1.73}$$

which describes an oscillator with a time-dependent and periodic frequency. In particular, for the trilinear model where the interaction between the inflaton field ϕ and the daughter scalar field χ is given by $V_{\phi,\chi} = m^2\phi^2/2 + m_\chi^2\chi^2/2 + \sigma\phi\chi^2$, the frequency is equal to $\omega^2(k,t) = k^2 + m_\chi^2 + 2\sigma\phi(t)$, with m_χ being the mass of χ. The equation (1.73) for a periodic $\omega(k,t)$ is known as *Hill's equation*, which, according to the Floquet theorem [151], admits the general solution

$$\chi_k(t) = e^{\mu_k t}\mathcal{P}_{k+}(t) + e^{-\mu_k t}\mathcal{P}_{k-}(t). \tag{1.74}$$

Here $\mathcal{P}_{k\pm}(t) = \mathcal{P}_{k\pm}(t+T)$ are periodic with period T. The quantity μ_k is called *the Floquet exponent.* If the real part of the Floquet exponent is non-zero, the mode function χ_k experiences an exponential growth and parametric resonance happens. In addition to that, if $\omega(k,t)$ is a harmonic function, Hill's equation may be reduced to *the Mathieu equation*

$$\chi_k'' + (A_k - 2q\cos 2z)\chi_k = 0, \tag{1.75}$$

where the prime derivative corresponds to "a new time coordinate z". For instance, in the trilinear model $A_k = 4(k^2 + m_\chi^2)/m^2$, $q = 4\sigma\Phi(t)/m^2$, $z = mt/2$. Then the number density of created particles will be given by

$$n_k \sim |\chi_k|^2 = e^{2\mu_k z}. \tag{1.76}$$

The stability and instability regions of the Mathieu equation are very well known [152], which allows us to determine regions in parameter space where modes experience the exponential amplification that leads to the bursts in particle production, see Figure 1.4.

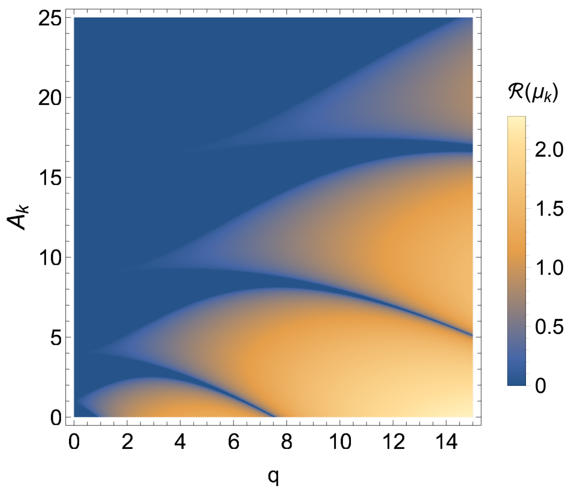

Figure 1.4: Instability chart of the Mathieu equation. Here A_k is the constant offset and q is the amplitude of oscillations in the Mathieu equation (1.75). Regions in blue correspond to the stability bands, while yellow correspond to the instability bands with values of the Floquet exponent $\mathcal{R}(\mu_k) > 0$ shown at the bar legend on the right.

1.3.2 Narrow and broad resonance

It is well known [152] that the Mathieu equation (1.75) has two different regimes of the parametric resonance: narrow and broad resonances. As could be guessed from its name, *a narrow* resonance occurs only in some narrow bands $A_k \simeq l^2$, with $l = 1, 2, \ldots$, for small oscillation amplitudes, meaning for $|q| \ll 1$ (for $A_k > 0$), see Figure 1.4. Hence, only a very narrow range of modes with corresponding wave-numbers Δk get exponentially excited, while modes with the remaining wave numbers stay in the vacuum state and can be produced through perturbative decays. Such resonance eventually stops because of two reasons. The first reason is the decay of the oscillation amplitude $\Phi(t)$ that in turn determines the behaviour of the parameter q and the Floguet exponent μ_k. According to (1.70), $\Phi(t)$ decays because of both perturbative decay as well as the expansion of space. Hence, the narrow parametric resonance will stop when the perturbative decay becomes efficient. The second reason is that the physical momenta redshift as $k_{\text{phys}} = k/a$, hence initially resonant bands Δk will very quickly redshift away and the narrow resonance will eventually finish.

A broad resonance happens when the amplitude of oscillations is large. This corresponds to the regime $|q| \gtrsim 1$. In this case a broad, continuous range of modes with wave numbers k get excited and thus the broad reso-

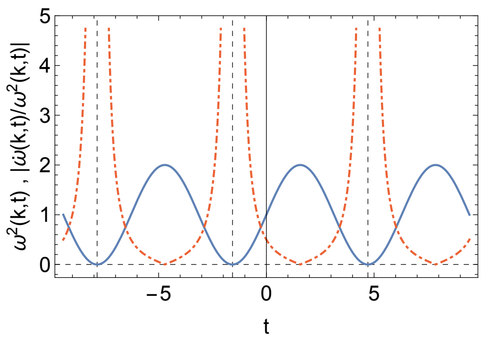

Figure 1.5: Illustration of the violation of the adiabaticity condition. The blue solid curve shows the frequency $\omega^2(k,t)$, while the red dot-dashed line illustrates the violation of the adiabaticity condition (1.77) at points with $\omega^2(k,t) = 0$.

nance is much more efficient than the narrow one. The particle production happens in bursts, at the points of maximum acceleration of the inflaton field when *the adiabaticity condition* is *violated*, i.e. when

$$\left| \frac{\dot{\omega}(k,t)}{\omega^2(k,t)} \right| \gg 1. \tag{1.77}$$

The adiabaticity condition violation (1.77) holds when the interaction term inside $\omega^2(k,t)$ vanishes, which happens twice per period, making the particle production rate to be comparable to the inflaton period of oscillations T, see Figure 1.5. Let us note that for the narrow resonance the adiabaticity condition is satisfied all the time, because the oscillation amplitude is small and hence the oscillation frequency is approximately constant $\omega^2(k,t) \approx k^2 = \text{const}$ and particle production happens continuously.

It turns out that physics of the broad parametric resonance reduces to the partial waves scattering off successive inverted parabolic potentials. To understand better why this is the case, let us write down solutions to the (1.73) when the adiabaticity condition is satisfied, i.e. in *the Wentzel–Kramers–Brillouin (WKB) approximation*

$$\chi_k(t) = \frac{\alpha_k(t)}{\sqrt{2\omega(k,t)}} e^{-i\int \omega(k,t)dt} + \frac{\beta_k(t)}{\sqrt{2\omega(k,t)}} e^{i\int \omega(k,t)dt}, \tag{1.78}$$

where $\alpha_k(0) = 1$, $\beta_k(0) = 0$ are the Bogolyubov coefficients. The occupation numbers are then expressed as

$$n_k(t) = |\beta_k(t)|^2. \tag{1.79}$$

Let us define the points t_j where the frequency $\omega^2(k,t)$ has a minimum and the adiabaticity condition is violated. We may expand the frequency of oscillations around t_j as

$$\omega^2(k,t) = \omega^2(k,t_j) + \omega^{2''}(k,t_j)(t-t_j)^2 + \cdots , \tag{1.80}$$

with $\omega^{2''}(k,t_j) = \left.\frac{d\omega^2(k,t)}{dt}\right|_{t=t_j}$. In terms of new variables that are defined as

$$\tilde{\eta} \equiv \left(2\omega^{2''}(k,t_j)\right)^{1/4}(t-t_j), \quad \tilde{\kappa}^2 \equiv \frac{\omega^2(k,t_j)}{\sqrt{2\omega^{2''}(k,t_j)}}, \tag{1.81}$$

the evolution equation for the mode functions (1.73) may be rewritten in the form

$$\frac{d^2\chi_k}{d\tilde{\eta}^2} + \left(\tilde{\kappa}^2 + \frac{\tilde{\eta}^2}{4}\right)\chi_k = 0. \tag{1.82}$$

This is the Schrödinger equation for a wave function scattering in an inverted parabolic potential with solutions being the parabolic cylinder functions $W(\tilde{\kappa}^2, \pm\tilde{\eta})$. Hence, indeed, the broad resonance problem is replaced by the partial waves scattering on inverted parabolic potentials.

Before t_j the WKB approximation is valid, hence the solution for mode functions is given by (1.78) with the Bogolyubov coefficients α_k^j, β_k^j. After the scattering at t_j has already happened, the wave $\chi_k(t)$ again takes the form of (1.78) but now with $\alpha_k^{j+1}, \beta_k^{j+1}$. The relation between ingoing and outgoing waves may be found via the relation for the Bogolyubov coefficients, that are expressed through the reflection R_k and transmission D_k coefficients as

$$\begin{pmatrix} \alpha_k^{j+1} e^{-i\theta_k^j} \\ \beta_k^{j+1} e^{+i\theta_k^j} \end{pmatrix} = \begin{pmatrix} \frac{1}{D_k} & \frac{R_k^*}{D_k^*} \\ \frac{R_k}{D_k} & \frac{1}{D_k^*} \end{pmatrix} \begin{pmatrix} \alpha_k^j e^{-i\theta_k^j} \\ \beta_k^j e^{+i\theta_k^j} \end{pmatrix}, \tag{1.83}$$

where $\theta_k^j = \int_0^{t_j} \omega(k,t)dt$ is the accumulated phase until the jth scattering. To satisfy the properties of the Bogolyubov coefficients, the reflection and transmission coefficients satisfy the usual relation $|R_k|^2 + |D_k|^2 = 1$. Assuming the daughter field χ_k was in the vacuum state at the beginning, its occupation numbers after $(j+1)$ scatterings may be written as

$$n_k^{j+1} = \left|\frac{R_k^j}{D_k^j}\right|(n_k^j + 1)\left|\frac{1}{D_k^j}\right|^2 n_k^j + 2\left|\frac{R_k^j}{D_k^j D_k^{j*}}\right|\sqrt{n_k^j(n_k^j+1)}\cos(\theta_k^j + \Delta\theta_k^j), \tag{1.84}$$

with $\Delta\theta_k^j = \arg(R_k^j \alpha_k^j \beta_k^{j*})$.

Let us briefly describe the properties of the result (1.84). As was already mentioned before, the occupation numbers grow as a step-like function of time, staying constant between successive scatterings, because there the oscillation amplitude is approximately constant. In addition to that, such behaviour of occupation numbers cannot be captured perturbatively, since (1.84) depends on the coupling as $\sim e^{-1/g}$, and hence becomes non-analytical at $g = 0$, with g being some coupling constant. For $n_k^j \gg 1$ the occupation number of created particles grows exponentially because of the effects of the Bose-Einstein statistics. In that case from (1.84) we find $n_k^{j+1} = e^{2\mu_k^j} n_k^j$ and the Floquet exponent μ_k^j may be expressed as

$$\mu_k^j = \ln \left| \frac{1 + |R_k^j| e^{i(\theta_k^j + \Delta\theta_k^j)}}{\sqrt{1 - |R_k^j|^2}} \right| . \tag{1.85}$$

Because of the presence of the accumulated phase $\theta_k^j + \Delta\theta_k^j$, the incoming and outgoing waves may add up constructively or destructively. This leads to a particular *band structure* in Floquet charts.

The analysis above was performed in the static universe approximation. In most cases the expansion of the universe may be taken into account by changing the variables to $X_k(t) = f[a(t)]\chi_k(t)$, where $f[a(t)]$ is a function of the scale factor $a(t)$, which leads to the equation of motion for the mode functions of the form

$$\ddot{X}_k + \left[\omega^2(k,t) + \Delta\right] X_k = 0, \tag{1.86}$$

where the dot derivative is taken with respect to cosmic time t. Here Δ depends on the scale factor $a(t)$ and may be interpreted as an additional phase. In some cases this phase that is coming from the expansion of the universe may exactly compensate the phase acquired in a scattering, leading to the destructive interference and decrease in the number of particles in that mode. This leads to the stochastic evolution of the particle number and is known as *stochastic preheating*. The general condition for significant particle production is the requirement that the growth rate of fluctuations is much larger than the rate of expansion, that is written as

$$\frac{|\mathrm{Re}(\mu_k)|}{H} \gg 1. \tag{1.87}$$

1.3.3 Multi-field preheating

In this section we will discuss the physics of preheating in multi-field models with non-trivial field-space manifolds. Similarly to the single-field case presented above, the primary question for investigation is the evolution of fluctuations. For multiple field case such formalism was developed and applied in [34, 35, 37, 136, 153].

1.3.3.1 Perturbations and mass scales

To start with, the perturbations $\delta\phi^I(x^\mu)$ to the background field trajectories $\varphi^I(t)$ may be written in the form of the gauge-invariant Mukhanov-Sasaki variable $Q^I \equiv \delta\phi^I + \frac{\dot{\phi}^I}{H}\psi$ that satisfies the equation of motion (1.55) with the mass-squared matrix $\mathcal{M}^I{}_J$ defined in (1.56), as was discussed in Section 1.2.4.3. The next step is the quantisation procedure and analysis of resulting perturbations, which is rather cumbersome even for the two field case. Below we will outline this procedure and focus on the case involving two scalar fields that converge to the single-field attractor along geodesic, which is the main topic of the Part II of the thesis.

To perform the quantisation, it is convenient to introduce another set of variables $Q^I(x^\mu) \to X^I(x^\mu)/a(t)$ and change cosmic time to conformal time $d\tau = dt/a(t)$. Next we need to quantize the fields X^I. In the two-field case, let us define the fields as ϕ and χ, hence the corresponding operators $\hat{X}^\phi$ and $\hat{X}^\chi$ for the general case of the field-space metric may be written as [136]

$$\hat{X}^\phi(x^\mu) = \int \frac{d^3k}{(2\pi)^{3/2}} \left[\left(v_k e_1^\phi \hat{a}_k + c_k e_2^\phi \hat{b}_k \right) e^{i\mathbf{kx}} + \left(v_k^* e_1^\phi \hat{a}_k^\dagger + c_k^* e_2^\phi \hat{b}_k^\dagger \right) e^{-i\mathbf{kx}} \right], \tag{1.88}$$

$$\hat{X}^\chi(x^\mu) = \int \frac{d^3k}{(2\pi)^{3/2}} \left[\left(y_k e_1^\chi \hat{a}_k + z_k e_2^\chi \hat{b}_k \right) e^{i\mathbf{kx}} + \left(y_k^* e_1^\chi \hat{a}_k^\dagger + z_k^* e_2^\chi \hat{b}_k^\dagger \right) e^{-i\mathbf{kx}} \right], \tag{1.89}$$

where $\hat{a}, \hat{b}_k, \hat{a}_k^\dagger, \hat{b}_k^\dagger$ are creation and annihilation operators, v_k, c_k, y_k, z_k are associated mode functions, and e_a^I with $I = \phi, \chi$, $a = 1, 2$ are components of the vielbein in the field space, defined as

$$\delta^{bc} e_b^I(\tau) e_c^J(\tau) = \mathcal{G}^{IJ}(\tau). \tag{1.90}$$

For such general case of the field-space metric, the resulting equations for the mode functions appear to be in the form of two systems of two coupled equations where v_k couples with y_k, and c_k with z_k:

$$\left(v_k'' + \omega_\phi^2(k,\tau) v_k\right) e_1^\phi = -a^2 \mathcal{M}^\phi_{\ \chi} y_k e_1^\chi, \quad \left(c_k'' + \omega_\phi^2(k,\tau) c_k\right) e_2^\phi = -a^2 \mathcal{M}^\phi_{\ \chi} z_k e_2^\chi,$$
$$\left(y_k'' + \omega_\chi^2(k,\tau) y_k\right) e_1^\chi = -a^2 \mathcal{M}^\chi_{\ \phi} v_k e_1^\phi, \quad \left(z_k'' + \omega_\chi^2(k,\tau) z_k\right) e_2^\chi = -a^2 \mathcal{M}^\chi_{\ \phi} c_k e_2^\phi. \tag{1.91}$$

Here $\mathcal{M}^I_{\ J}$ defined in (1.56) and

$$\begin{aligned} \omega_\phi^2(k,\tau) &\equiv k^2 + a^2(\mathcal{M}^\phi_{\ \phi} - \frac{1}{6}R), \\ \omega_\chi^2(k,\tau) &\equiv k^2 + a^2(\mathcal{M}^\chi_{\ \chi} - \frac{1}{6}R). \end{aligned} \tag{1.92}$$

We will focus our attention on the case where at the beginning of reheating the background motion is geodesic. Without loss of generality this assumes the attractor solution along $\chi = 0$, which may be always achieved upon rotation $\phi^I \to \phi^{I'}$, see [136] for the detailed discussion. This behaviour is common in models of inflation with non-minimal coupling to gravity that are called ξ-attractors [154, 155] and include Higgs inflation [156, 157], and models with hyperbolic field-space geometry, like α-attractors [50–52, 61]. With such a choice the cross-terms in $\mathcal{G}_{IJ}$ and $\mathcal{M}^I_{\ J}$ vanish and the field space vielbein becomes diagonal

$$e_a^I \to \begin{pmatrix} e_1^\phi & 0 \\ 0 & e_2^\chi \end{pmatrix}, \tag{1.93}$$

with $e_2^\phi \sim e_1^\chi \sim 0$, $e_1^\phi e_1^\phi \simeq \mathcal{G}^{\phi\phi}$, $e_2^\chi e_2^\chi \simeq \mathcal{G}^{\chi\chi}$ and $\mathcal{G}_{\phi\phi}\mathcal{G}^{\phi\phi} = \mathcal{G}_{\chi\chi}\mathcal{G}^{\chi\chi} = 1 + \mathcal{O}(\chi^2)$. Because $\mathcal{M}^\phi_{\ \chi} \sim \mathcal{M}^\chi_{\ \phi} \sim 0$ the source term in (1.91) is zero, that decouples mode functions v_k and z_k, while setting the remaining two to zero $c_k \sim y_k \sim 0$. Therefore, the equations for scalar mode functions reduce to the familiar case of two independent harmonic oscillator equations with time-dependent frequency

$$\begin{aligned} \partial_\tau^2 \phi_k + \omega_\phi^2(k,\tau)\phi_k \simeq 0, \quad \omega_\phi^2(k,\tau) \equiv k^2 + a^2 m^2_{\text{eff},\phi}(\tau), \\ \partial_\tau^2 \chi_k + \omega_\chi^2(k,\tau)\chi_k \simeq 0, \quad \omega_\chi^2(k,\tau) \equiv k^2 + a^2 m^2_{\text{eff},\chi}(\tau). \end{aligned} \tag{1.94}$$

Here, we have denoted mode functions as $v_k \equiv \phi_k$ and $z_k \equiv \chi_k$ to indicate the clear relation with each field perturbation. The effective masses for each fluctuation have four different contributions:

$$m^2_{\text{eff},I} = m^2_{1,I} + m^2_{2,I} + m^2_{3,I} + m^2_{4,I}, \tag{1.95}$$

with $I = \phi, \chi$. Different terms are defined as

$$
\begin{aligned}
m_{1,\phi}^2 &\equiv \mathcal{G}^{\phi K}\left(\mathcal{D}_\phi \mathcal{D}_K V\right), \\
m_{2,\phi}^2 &\equiv -\mathcal{R}^{\phi}_{\ LM\phi}\dot{\varphi}^L\dot{\varphi}^M, \\
m_{3,\phi}^2 &\equiv -\frac{1}{M_{\rm pl}^2 a^3}\delta^\phi_K \delta^J_\phi \, \mathcal{D}_t\left(\frac{a^3}{H}\dot{\varphi}^K\dot{\varphi}_J\right), \\
m_{4,\phi}^2 &\equiv -\frac{1}{6}R = (\epsilon - 2)H^2 ,
\end{aligned}
\tag{1.96}
$$

with identical contributions to $m^2_{\text{eff},\chi}$ but with $\phi \leftrightarrow \chi$. Here $m^2_{1,I}$ is the Hessian of the potential in a curved field space defined by the field metric $\mathcal{G}^{IJ}$. The second term $m^2_{2,I}$ demonstrates the geodesic deviation of the two trajectories caused by the non-trivial field-space geometry. The third term $m^2_{3,I}$ encodes turning of the trajectory and the last contribution $m^2_{4,I}$ shows the changes in the background space-time via the presence of the space-time curvature R.

For the particular choice of the two-field α-attractor model [158, 159], with the attractor solution along $\chi = 0$, effective masses simplify to

$$
m^2_{\text{eff},\phi} \simeq V_{\phi\phi}(\chi = 0) \tag{1.97}
$$

$$
m^2_{\text{eff},\chi} \simeq V_{\chi\chi}(\chi = 0) + \frac{1}{2}\mathcal{R}\dot{\phi}^2, \tag{1.98}
$$

where the field space Ricci curvature scalar $\mathcal{R}$ is parametrised by the dimensionless parameter α as $\mathcal{R} = -4/3\alpha$. From here one can see that $m^2_{\text{eff},\phi}$ is always positive, since it is determined by the Hessian of the potential near the minimum $V_{\phi\phi}(\chi = 0) > 0$. It means that the inflaton field ϕ in some regions of parameter space may preheat through the parametric resonance described in detail in Section 1.3.1. However, for χ perturbations and $m^2_{\text{eff},\chi}$, the situation is different. In the case of α-attractors, the field space is a negatively curved manifold and hence the Ricci curvature scalar always takes negative values. It means that, depending on the interplay between the potential $V_{\chi\chi}$ and curvature $\frac{1}{2}\mathcal{R}\dot{\phi}^2$ terms, the effective mass $m^2_{\text{eff},\chi}$ may take both positive and negative values. If $m^2_{\text{eff},\chi}$ becomes negative, the perturbations of the χ field rapidly experience exponential amplification caused by the tachyonic resonance and the system quickly reaches the radiation-dominated equation of state $w \simeq 1/3$, as was shown in lattice simulations [160].

Remarkably, the instability bands are easily parametrised by the one parameter α that determines the value of the field space curvature, as well as observational predictions such as the tensor-to-scalar ratio. In particular, the term $\frac{1}{2}\mathcal{R}\dot{\phi}^2 \propto -\frac{1}{\alpha}\left(\frac{\sqrt{\alpha}}{\mathcal{O}(1)}\right)^2 = -\mathcal{O}(1)$ stays almost the same and does not react to the changes in the field curvature from different values of α. However, this is not the case for the Hessian of the potential $V_{\chi\chi}$. First of all, the potential term does not scale so uniformly with α and, in addition to that, the cases with symmetric and asymmetric potentials appear to be very different. Here we refer to the symmetry/asymmetry of the potential near its minimum, that is relevant for classification of the reheating behaviour.

Let us start with describing the case with *symmetric* two-field α -attractor potential. For such a choice, for any value of $\alpha \lesssim 10^{-4}$ and the potential steepness n, the curvature term (1.98) always dominates over the Hessian of the potential. For any wave number that is smaller than a maximally amplified wave number $k_{\max}$, determined by $\omega_\chi^2(k_{\max}, \tau) = 0$, the effective frequency $\omega_\chi^2(k_{\max}, \tau)$ is negative, which leads to the tachyonic resonance.

Instead, the choice of *asymmetric* potentials distinguishes two distinct sub-cases. The first one corresponds to *massive fields*, meaning that around the global minimum at $\phi = \chi = 0$ the Hessian of the potential $V_{\chi\chi} > 0$, which happens for potentials with steepness $n = 1$. For higher potential steepness $n > 1$ the potential gradient $V_{\chi\chi} = 0$, and hence corresponds to the case with *massless fields*.

The massless field case leads to the dominance of the negative field space curvature contribution over the positive potential one in (1.98). This results in a negative effective mass square $m^2_{\text{eff},\chi} < 0$ and the outbreak of tachyonic resonance, starting at values $\alpha \approx 10^{-3}$.

By contrast, for massive fields the potential contribution always dominates over the field curvature term, making $m^2_{\text{eff},\chi} > 0$. Hence, in such case both perturbations of ϕ and χ fields may be amplified via parametric resonance, while more efficient tachyonic resonance does not happen. It turns out that for massive potentials and bigger values of α (or equivalently smaller field-space curvatures), the parametric resonance is stronger for $\delta\phi$ perturbations than for $\delta\chi$ in comparison to the case with symmetric potentials. This happens at values $\alpha \approx 10^{-3}$ where the same model with symmetric potential and any potential steepness does not reheat at all.

Therefore, the two-field α -attractor model with asymmetric potential reheats efficiently in a region of parameter space which is absolutely inefficient when the symmetric potential is chosen. This is the crucial finding, since, as will be discussed in Section 1.2.4, inefficient reheating may lead to a prolonged matter-dominated phase after inflation, change the time when

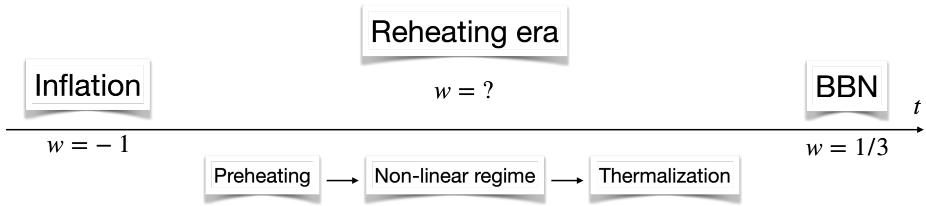

Figure 1.6: The illustration of stages of the reheating era.

CMB modes exit the horizon and thus shift CMB predictions. The complete analysis of scaling properties and their universality that determine the preheating efficiency is discussed in Chapter 4. It is followed by an extensive investigation of the symmetry properties for the two-field inflationary potentials and their implications for the duration of the reheating era, presented in Chapter 5 of the thesis.

1.3.4 Observational signatures from the reheating era

The preheating process, outlined above, does not describe the complete transition of the universe to the thermal state, as illustrated in Figure 1.6. Instead, it is followed by the non-linear regime, during which various non-trivial field configurations may be formed, such as oscillons, Q-balls, solitons and topological defects, like domain walls and metastable global cosmic strings. After the non-linear phase the turbulent scaling occurs, which is characterized by a slow transfer of energy to both ultraviolet and infrared modes, and completed by the process of thermalization, which brings all degrees of freedom into kinetic and chemical equilibrium and the spectrum to a thermal distribution.

There are several complications in extracting observational constraints for the reheating era. First of all, the details of dynamics on subhorizon scales is hidden by later, non-linear evolution of cosmic structure on short scales. Hence, it is not possible to extract the effect on the curvature perturbation from the CMB. Secondly, the thermalization process completely washes away the details of the earlier stages of the reheating era. Nevertheless, there are some very important observational implications of the reheating era, that we will outline below.

1.3.4.1 CMB predictions and reheating

The first indirect manifestation is related to the expansion history of the universe during the reheating era. As was discussed in Section 1.3.1 and, in particular, shown by the equation (1.71), there is a high uncertainty in the equation of state w during reheating. It is extremely important, since the expansion history highly influences the CMB predictions, as it changes the time of mapping of the inflationary perturbation modes from the horizon exit to its re-entry, see Figure 1.3. It was shown [161] that the number of e-folds N_* from the end of inflation to the pivot scale $k_* = a_* H_*$, where the modes cross the horizon, is related to the expansion history of the universe as follows

$$\frac{k_*}{a_0 H_0} = e^{-N_*} \frac{a_{\text{end}}}{a_{\text{reh}}} \frac{a_{\text{reh}}}{a_{\text{eq}}} \frac{H_*}{H_{\text{eq}}} \frac{a_{\text{eq}} H_{\text{eq}}}{a_0 H_0}, \tag{1.99}$$

where the subscripts "$*, \text{end}, \text{reh}, \text{eq}, 0$" denote that quantities are evaluated at the pivot scale, at the end of inflation, at the end of reheating, at the moment when radiation and matter densities are equal and at the present moment of time respectively. This relation may be further rewritten [162, 163] (see also Ref. [135] for more detailed discussion) as

$$N_* = 66.89 - \ln \frac{k_*}{a_0 H_0} + \frac{1}{4} \ln \frac{V_*^2}{M_{\text{pl}}^4 \rho_{\text{end}}} + \frac{1}{12} \ln \left[\frac{1}{g_{\text{th}}} \left(\frac{\rho_{\text{th}}}{\rho_{\text{end}}} \right)^{\frac{1-3\bar{w}_{\text{int}}}{1+\bar{w}_{\text{int}}}} \right], \tag{1.100}$$

where $\rho_{\text{th}}, g_{\text{th}}$ are the energy density and the number of relativistic degrees of freedom respectively at thermalization and V_* is the inflationary potential at the pivot point, defined by $V_* = V_*(\{q_i\}, \phi_*)$ where $\{q_i\}$ are the parameters entering the inflaton potential $V = V(\{q_i\}, \phi)$. The mean equation of state $\bar{w}_{\text{int}} > -1/3$ between the end of inflation and complete thermalization is defined as

$$\bar{w}_{\text{int}} \equiv \int_{t_{\text{end}}}^{t_{\text{th}}} \frac{w(t) dt}{t_{\text{th}} - t_{\text{end}}} . \tag{1.101}$$

One of the parameters in the potential may be fixed from the measured amplitude of scalar perturbations A_s. Hence, from (1.100), it turns out that N_* may be parametrised by the following set of parameters

$$N_* = N_* \left(\{q_i - 1\}, A_s, \rho_{\text{th}}^{\frac{1-3\bar{w}_{\text{int}}}{1+\bar{w}_{\text{int}}}} / g_{\text{th}} \right) . \tag{1.102}$$

In turn, the N_* parametrises the CMB observables as

$$n_s = n_s(N_*, \{q_i - 1\}), \quad r = r(N_*, \{q_i - 1\}). \tag{1.103}$$

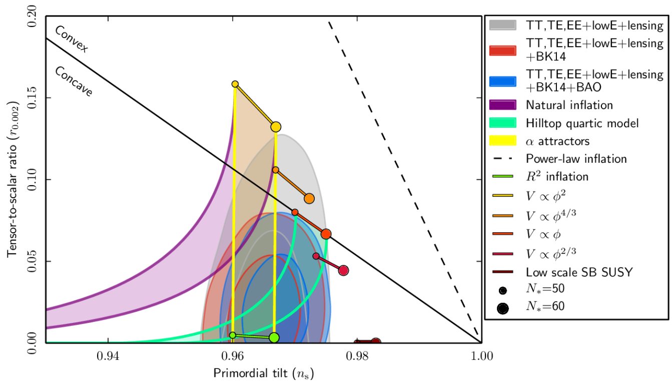

Figure 1.7: $68\,\%$ and $95\,\%$ confidence level regions for n_s and r from Planck, together with theoretical predictions of inflationary models [53].

Currently, every figure that confronts model-dependent inflationary predictions with Planck constraints for n_s and r, contains the theoretical uncertainty in N_*, since its precise value is not known and is typically set to 50 and 60 e-folds. This uncertainty is so big, that takes nearly one half of the 1σ contour in $n_s - r$ plane, see Figure 1.7. Therefore, knowledge of the equation of state $\bar{w}_{\rm int}$, as well as the energy scale $\rho_{\rm th}$ and the time of thermalization $a_{\rm th}$ which is specified by $g_{\rm th}$, are crucial for the accurate determination of N_* and correct comparison of inflationary predictions with the CMB observations.

The development of the Effective Field Theory of preheating would help to provide an easy determination of the reheating efficiency together with the number of e-folds N_*, leading to reducing the error bars in the $n_s - r$ plane. This would allow us to rule out many inflationary models that, because of huge uncertainties, still match the Planck constraints. In Chapter 4, 5 we identify the important mass scales that control the tachyonic growth of fluctuations and determine the resonance efficiency, taking a first step towards an Effective Field Theory description of preheating in hyperbolic manifolds.

1.3.4.2 Stochastic gravitational wave background from reheating

The idea that non-linear processes during the reheating era can generate a stochastic gravitational wave background was first studied in [164] and further developed in subsequent works [165–176]. The GW background coming from reheating is generated from the classical evolution of inhomogeneities on sub-horizon scales, whereas the origin of the inflationary background is purely quantum, as was discussed in Section 1.2.4.4. That is why the power spectra from reheating appear to be peaked, unlike the almost scale-invariant tensor spectra from single field inflation. The peak frequency may be determined by the scale where the inflaton condensate is substantially fragmented (or destroyed). This happens when the back-reaction effects become important. The peak frequency f_0 of the gravitational energy density $\Omega_{\rm GW}$ per logarithmic frequency interval depends on the wave number and the Hubble scale as follows $f_0 \propto \frac{k}{\sqrt{M_{\rm pl}H}}$ [167, 177]. Typically $k \propto H$, hence the peak frequency is equal to [118, 135]

$$f_0 \sim \beta^{-1}\sqrt{\frac{H_{\rm br}}{M_{\rm pl}}} \times 4 \times 10^{10}\text{Hz}, \quad \Omega_{\rm GW} \sim 10^{-6}\beta^2, \tag{1.104}$$

where $H_{\rm br}$ is the Hubble rate at back-reaction. The constant factor β is usually of the value $10^{-2} - 10^{-3}$ and is estimated from a linear analysis of the instabilities. This leads to typical frequencies $f_0 \sim 10^{10} - 10^{11}$Hz and amplitudes of the GW energy density $\Omega_{\rm GW} \sim 10^{-10} - 10^{-12}$, which is far from the observable ranges of contemporary GW detectors, that can measure frequencies at most $f_0 \sim 10^3 - 10^4$Hz, see Figure 1.2. For smaller values of $H_{\rm br}$, the peak frequency moves towards the observable range, however the smallness of the GW amplitude $\Omega_{\rm GW}$ leaves it currently inaccessible to direct detection.

1.3.4.3 Baryon asymmetry and relics

When the particle energies in the expanding universe become too small to create new pairs, almost all particles and antiparticles annihilate each other. However, a small amount of matter does not annihilate and leads to the remnant matter density that is observable today. This is the essence of *the baryon asymmetry problem.* Baryon asymmetry may be defined as the ratio between the difference of baryon n_B and antibaryon $n_{\bar{B}}$ number density to the photon number density n_γ

$$\tau \equiv \frac{n_b}{n_\gamma} \approx 6 \times 10^{-10}, \tag{1.105}$$

where $n_b = n_B - n_{\bar{B}}$ and $n_\gamma \sim n_B + n_{\bar{B}}$. This asymmetry has no explanation within the Standard Model (SM) and is one of the observational signatures of physics beyond it [178].

Hence, to explain the baryon asymmetry there should be new physics, that should meet Sakharov's conditions [179]: (i) non-conservation of the baryon number, (ii) violation of C and CP invariance; (iii) deviation from thermal equilibrium. Since during the reheating era particles are produced non-perturbatively and out of thermal equilibrium, with off-shell processes during the thermalisation stage, the reheating era is of a particular interest for a better understanding of the baryon asymmetry problem. In various studies [180–188] it was shown that indeed the non-linear dynamics during reheating can highly influence the generation of the baryon asymmetry.

In addition to that, the non-linear dynamics of reheating can lead to fragmentation of the inflaton condensate and to the formation of stable localized configurations. Some of these configurations, such as oscillons, can stay stable for millions of inflaton oscillations and as a result lead to a prolonged matter-dominated phase after inflation that may alter observational predictions and also delay BBN. In addition to that, oscillon formation may generate features in tensor power spectra at specific wavenumbers, as was discussed in [189]. Large inhomogeneities can also form primordial black holes, that would induce a matter-dominated expansion history during the reheating era. Moreover, self-interactions may lead to nongravitational dark matter structure growth resulting in compact halos, leading to several observational signatures [190]. Last but not least, the reheating era may play an important role in primordial magnetogenesis [191–194].

1.4 Work in this thesis

This thesis consists of two parts. Part I investigates inflation with multiple fields together with emerging observational consequences for scalar and tensor power spectra. Part II is focused on multi-field reheating, its efficiency and duration in curved field-space manifolds.

- **Part I. Multi-field inflation.**

  Chapter 2: introduces for the first time a model for inflation with light fields on an axion-dilaton system, with a new type of exact multi-field inflationary attractor that is true for both flat and curved field-space manifolds. Despite the fact that the inflaton trajectory is strongly turning, the isometry in the field space protects the dynamics of coupled inflationary perturbations, keeping the phenomenology to be single- field-like with negligible non-Gaussianity, as favoured by observations.

This chapter is based on [70]:
A. Achúcarro, E. J. Copeland, O. Iarygina, G. A. Palma, D. G. Wang and Y. Welling, *Shift-Symmetric Orbital Inflation: single field or multi-field?*, Phys. Rev. D **102**, no.2, 021302 (2020), [arXiv:1901.03657].

Chapter 3: investigates the viability of inflation with a spectator non-Abelian gauge field sector. We studied the theoretical restrictions for gravitational wave production dictated by the requirements for the gauge field to be in the spectator sector, as well as from the physics of the gauge sector itself. Such requirements result in the constraints for the amplitude and tensor tilt for chiral gravitational waves, and hence restrict the enhancement of the gravitational wave background with respect to the one coming from vacuum fluctuations.

This chapter is based on [86]:
O. Iarygina and E. I. Sfakianakis, *Gravitational waves from spectator Gauge-flation*, [arXiv:2105.06972].

- **Part II. Reheating in curved field spaces.**

  Chapter 4: analytically demonstrates a competition between field-space and potential contributions that change the dynamics, duration and observable predictions of reheating for the multi-field α-attractors. We find universal scaling relations that allow for an easy estimate of the preheating efficiency for highly curved field geometries. Identification of important mass scales that control the tachyonic growth of fluctuations enables our work to take a first step towards an Effective Field Theory description of preheating in hyperbolic manifolds.

  This chapter is based on [158]:
  O. Iarygina, E. I. Sfakianakis, D. G. Wang and A. Achúcarro, *Universality and scaling in multi-field α-attractor preheating*, JCAP **06**, 027 (2019), [arXiv:1810.02804].

  Chapter 5: provides an extensive study of the preheating behaviour for symmetric and asymmetric potentials about the minimum. We demonstrate the existence of a region in parameter space, where the symmetric and asymmetric multi-field α-attractors are explicitly not the same: one preheats and one does not. This leads to a different cosmic history for the two models, with one possibly exhibiting a long matter-dominated phase, and a shift in the observational predictions for n_s and r.

This chapter is based on [159]:
O. Iarygina, E. I. Sfakianakis, D. G. Wang and A. Achúcarro, *Multi-field inflation and preheating in asymmetric α-attractors*, [arXiv:2005.00528].

Part I

Multi-field inflation

2 Shift-symmetric orbital inflation

Abstract: We present a new class of two-field inflationary attractor models, known as *'shift-symmetric orbital inflation'*, whose behaviour is strongly multi-field but whose predictions are remarkably close to those of single-field inflation. In these models, the field space metric and potential are such that the inflaton trajectory is along an 'angular' isometry direction whose 'radius' is constant but *arbitrary.* As a result, the radial (isocurvature) perturbations away from the trajectory are exactly *massless* and they freeze on superhorizon scales. These models are the first exact realization of the 'ultra-light isocurvature' scenario, previously described in the literature, where a combined shift symmetry emerges between the curvature and isocurvature perturbations and results in primordial perturbation spectra that are entirely consistent with current observations. Due to the turning trajectory, the radial perturbation sources the tangential (curvature) perturbation and makes it grow linearly in time. As a result, only one degree of freedom (*i.e.* the one from isocurvature modes) is responsible for the primordial observables at the end of inflation, which yields the same phenomenology as in single-field inflation. In particular, isocurvature perturbations and local non-Gaussianity are highly suppressed here, even if the inflationary dynamics is truly multi-field. We comment on the generalization to models with more than two fields.

Keywords: multi-field inflation, cosmological perturbation theory.

Based on:

A. Achúcarro, E. J. Copeland, O. Iarygina, G. A. Palma, D. G. Wang and Y. Welling
Shift-Symmetric Orbital Inflation: single field or multi-field?
Phys. Rev. D **102**, no.2, 021302 (2020), [arXiv:1901.03657].

2.1 Introduction

Single field slow roll inflation is the leading explanation for the observations through the CMB [53] that primordial perturbations are very close to Gaussian and adiabatic, yet embedding it in an ultraviolet complete theory such as string theory is notoriously difficult. Moduli fields arising from string compactifications require stabilizing to realize single field inflation [126], and large field excursions test the validity of using four dimensional effective theories[1].

In the usual understanding, light fields during inflation may lead to isocurvature perturbations and local non-Gaussianity tightly constrained by current observations. However, it has been suggested recently that inflation with non-stabilized light fields on an axion-dilaton system can be compatible with the latest CMB data [61, 69, 95, 195–198]. In particular, it was pointed out in [69] that, when the perturbations orthogonal to the trajectory are *massless* but efficiently *coupled* to the inflaton, the isocurvature modes are dynamically suppressed. This is the "ultra-light isocurvature" scenario.

In this paper we provide for the first time a family of exact models of inflation in which the multi-field effects are significant, but the phenomenology remains similar to single field inflation. The models combine two ingredients: First, the inflaton trajectory proceeds along an isometry direction of the field space, so it is Orbital Inflation in the sense of [72, 73]. This ensures time independence of the coupling between the radial and tangential inflationary perturbations. Second, the trajectory can have an *arbitrary* radius (within some range described below), and a constant radius is proven to be a neutrally stable attractor. Hence, isocurvature perturbations become exactly massless. The two ingredients, combined, guarantee that the sourcing of the curvature perturbation is sustained over many e-folds of inflationary expansion. The action for the perturbations inherits a symmetry between background solutions that is not manifest in the potential or in the Lagrangian. We show that, at the end of inflation, only the isocurvature degree of freedom is responsible for the generation of primordial observables, but perturbations still remain adiabatic and Gaussian. We call this scenario *shift-symmetric orbital inflation*.

Crucially this scenario provides a new direction to explore inflation and

[1]The recent swampland debate highlights the importance of finding viable scenarios for inflation that are not strictly single-field. See, for instance, the discussion in [41] as compared to [48, 219]

a potential resolution to some of the problems faced by the embedding of inflation in string theory. That is, in the construction of inflationary models wherein every modulus is stabilized except for the inflaton, one could be missing less restrictive realizations of inflation compatible with current observational constraints. We set $\hbar = c = 1$ and the reduced Planck mass $M_p \equiv (8\pi G)^{-1/2} = 1$, where G is Newton's constant.

2.2 A toy model

To illustrate the idea, we first consider the following Lagrangian in flat field space with polar coordinates (illustrated in Fig. 2.1)

$$\mathcal{L} = \frac{1}{2}\left[\rho^2(\partial\theta)^2 + (\partial\rho)^2\right] - \frac{1}{2}m^2\left(\theta^2 - \frac{2}{3\rho^2}\right). \tag{2.1}$$

The potential has a monodromy in the angular coordinate, and although it is unbounded at $\rho \to 0$, inflation only takes place in the physically consistent regime where $V(\rho,\theta) > 0$. Moreover, as shown in the perturbation analysis below, our study is restricted to radii that cannot be too small. Therefore, we only care about the local form of the potential close to the inflationary trajectory, which we assume is captured well by (2.1). In general, it is difficult to solve the background equations analytically in such a system. However, this model has the following exact neutrally stable solutions at any radius

$$\rho = \rho_0, \quad \dot{\theta} = \pm\sqrt{\frac{2}{3}}\frac{m}{\rho_0^2}. \tag{2.2}$$

The Friedmann equation becomes $H^2 = m^2\theta^2/6$ on the attractor, where H is the Hubble parameter, and the first slow-roll parameter is $\epsilon \equiv -\dot{H}/H^2 = \frac{2}{\rho_0^2\theta^2}$. This trajectory is nongeodesic in field space, with turning effects that depend on the radius κ of the trajectory. Note that here $\kappa = \rho_0$ but, if the field space geometry is curved, κ will be a more general function of ρ_0.

The situation is reminiscent of circular orbits in a spherically symmetric gravitational field, where the centripetal force stabilizes the radial direction, and the inflaton can circle at any radius with the corresponding angular velocity. For the field system on the cosmological background, only the isometric circular orbits appear, and we need to break the shift symmetry of θ in the potential to overcome the Hubble friction. We can label each solution by a continuous parameter c with the corresponding map

$$\rho_c = \rho_0 + c, \quad \left(\theta_c^2\right)' = \frac{\left(\theta_0^2\right)'}{(1 + c/\kappa)^2}, \tag{2.3}$$

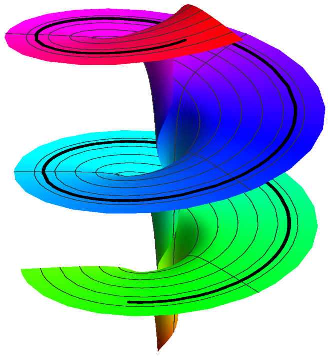

Figure 2.1: The toy model potential $V(\rho,\theta)$ given in (2.1) together with a typical inflationary trajectory indicated with the solid black line.

where the prime $'$ denotes a derivative with respect to efolds $d/dN = d/(Hdt)$. This transformation identifies all the trajectories in (2.2) and hints at the existence of a shift symmetry for the perturbations. In flat gauge, the isocurvature perturbation σ is associated with $\delta\rho$ and the curvature perturbation $\mathcal{R}$ with $\frac{\rho}{\sqrt{2\epsilon}}\delta\theta$, which equals $\frac{1}{4}\rho^2\delta\left(\theta^2\right)$ in this toy model. To find the effect of the transformation on the perturbations, we split $\rho = \rho_0 + \sigma$ and $\left(\theta^2\right)' = \left(\theta_0^2\right)'(1-\mathcal{R}')$. This allows us to determine how a small c changes σ and $\mathcal{R}'$. In the long wavelength limit every transformed set of perturbations $(\sigma_c, \mathcal{R}_c')$ provide a new solution to the equations of motion. This is because homogeneous perturbations map background solutions onto each other. Therefore, we expect the following *symmetry* for linearized perturbations

$$\sigma \to \sigma + c, \quad \mathcal{R}' \to \mathcal{R}' + \frac{2}{\kappa}c. \tag{2.4}$$

Given the shift symmetry of σ, the isocurvature perturbation is expected to be massless and freeze after horizon-exit. Meanwhile, the symmetry also indicates that $\mathcal{R}$ has a growing solution that is dictated by the constant σ on superhorizon scales.

To get an intuitive notion of the perturbations behavior, we employ the δN formalism [199–203]. From the Friedmann equation and the exact solution (2.2), the number of efolds until the end of inflation is $N = \rho^2\theta^2/4 - 1/2$. The curvature perturbation at the end of inflation is

$$\mathcal{R}(k_*) = \delta N \simeq \frac{1}{\sqrt{2\epsilon_*}}(\rho\delta\theta)_* + \frac{2N_*}{\kappa}\delta\rho_*, \tag{2.5}$$

where $(\rho\delta\theta)_*$ and $\delta\rho_*$ are field fluctuations with typical amplitude $\frac{H_*}{2\pi}$ at horizon-exit of the k_* mode. This yields the following power spectrum of curvature perturbations

$$P_{\mathcal{R}}(k_*) \simeq \frac{H_*^2}{4\pi^2}\left(\frac{1}{2\epsilon_*}+\frac{4N_*^2}{\kappa^2}\right). \tag{2.6}$$

Here the first contribution has an adiabatic origin, just like in the single-field models, and the second term corresponds to the conversion from isocurvature to curvature modes on superhorizon scales. When the radius of the trajectory is small enough, namely $8\epsilon_* \ll \kappa^2 \ll 8\epsilon_* N_*^2 \approx 4N_*$, the second term in (2.6) dominates. Then the final power spectrum becomes $P_{\mathcal{R}}(k_*) \simeq H_*^2 N_*^2/(\pi^2\kappa^2)$, which is generated by one single degree of freedom – the isocurvature mode.

2.3 Shift-symmetric orbital inflation

To construct generic models with the above properties, we begin with an axion-dilaton system in a non-trivial field manifold (θ, ρ) with kinetic term $K = -\frac{1}{2}\left(f(\rho)\partial_\mu\theta\partial^\mu\theta + \partial_\mu\rho\partial^\mu\rho\right)$. This field space, of curvature $\mathbb{R} = f_\rho^2/2f^2 - f_{\rho\rho}/f$, arises generically from UV completions of inflation in quantum gravity or from an effective field theory (EFT) viewpoint. To realize shift-symmetric orbital inflation, we assume the inflationary trajectory to be isometric, *i.e.* along the θ direction at *any* (constant) radius in field space. The potential can be derived by generalizing the Hamilton-Jacobi formalism [200, 204–206] to a two-field system (See Appendix 2A). It has the general form

$$V = 3H^2 - 2\frac{H_\theta^2}{f(\rho)}, \tag{2.7}$$

where H is a function of θ only, $H_\theta \equiv dH/d\theta$ and $f(\rho) > 0$. The model (2.1) is recovered for $H \propto \theta$ and $f(\rho) = \rho^2$, corresponding to a flat field space parametrized by polar coordinates. This non-linear system admits exact solutions

$$\dot{\theta} = -2\frac{H_\theta}{f}, \qquad \rho = \rho_0. \tag{2.8}$$

Thus the inflaton moves in an orbit of constant radius, as ensured by the Hamilton-Jacobi formalism. As in the toy model, this trajectory is not along a geodesic. Here the tangent and normal vectors to the trajectory are $\mathcal{T}^a = 1/\sqrt{f}(1,0)$ and $\mathcal{N}^a = (0,1)$, and the radius of the turning trajectory is a constant given by $\kappa = 2f/f_\rho$. It follows that all these trajectories are *neutrally stable*: a small perturbation orthogonal to a given orbital trajectory will bring us to one of the neighbouring trajectories (See Appendix 2B).

2.4 Analysis of perturbations

In flat gauge, the comoving curvature perturbation $\mathcal{R}$ is defined as the projection of the field perturbation along the inflationary trajectory $\mathcal{R} = \frac{1}{\sqrt{2\epsilon}}\mathcal{T}_a\delta\phi^a$, and the isocurvature perturbation σ corresponds to the orthogonal projection $\sigma = \mathcal{N}_a\delta\phi^a$. Then for generic multi-field models, the quadratic action of perturbations takes the following form [69]

$$S^{(2)} = \frac{1}{2}\int d^4x a^3\left[2\epsilon\left(\dot{\mathcal{R}} - \frac{2H}{\kappa}\sigma\right)^2 + \dot{\sigma}^2 - \mu^2\sigma^2 + \ldots\right], \tag{2.9}$$

where ellipses stand for the gradient terms $-(\partial_i\sigma)^2 - 2\epsilon(\partial_i\mathcal{R})^2$. The interaction between curvature and isocurvature modes is given by the term $a^3(8\epsilon H/\kappa)\dot{\mathcal{R}}\sigma$. To guarantee perturbative analysis we require that $\sqrt{8\epsilon}/\kappa \ll 1$ [69, 207]. The mass of entropy perturbations is defined as $\mu^2 \equiv V_{NN} + \epsilon H^2\left(\mathbb{R} + 6/\kappa^2\right)$, where the first term is obtained from the standard Hessian of the potential $V_{NN} \equiv \mathcal{N}^a\mathcal{N}^b\left(V_{ab} - \Gamma^c_{ab}V_c\right)$, the second and third terms correspond to the field space curvature and turning contributions respectively.

For shift-symmetric orbital inflation, we expect the isocurvature perturbations to be exactly massless, as in the toy model, and this is confirmed by using (2.8) to show $\mu^2 = 0$. This implies that the quadratic action (2.9) has the combined shift symmetry (2.4), as in the toy model. The power spectra of perturbations in the massless limit can be directly estimated from the coupled evolution of perturbations [69]. When $\mu = 0$, the linearized system simplifies in the superhorizon limit, yielding

$$\mathcal{R}'_k = \frac{2}{\kappa}\sigma_k, \qquad \sigma_k = \frac{H_*}{2\pi}, \tag{2.10}$$

where $*$ denotes evaluation at the time of horizon crossing. That is, on superhorizon scales the isocurvature perturbation quickly becomes a constant, and it sources the growth of $\mathcal{R}$. At the end of inflation, the primordial curvature perturbation can be expressed as $\mathcal{R}_k = \mathcal{R}_* + 2N_*\sigma_k/\kappa$, where the first term is the curvature perturbation amplitude at horizon-exit, and the second term comes from the isocurvature source. Thus these two contributions are uncorrelated with each other, and the dimensionless power spectrum for $\mathcal{R}$ is given by

$$P_{\mathcal{R}} = \frac{H_*^2}{8\pi^2\epsilon_*}\left(1+\mathcal{C}\right), \tag{2.11}$$

where $\mathcal{C} = 8\epsilon_* N_*^2/\kappa^2$ represents the contribution from isocurvature modes. This result agrees with the δN calculation for the toy model given in (2.6). The full calculation via the in-in formalism gives the same answer up to subleading corrections [69]. Note that the power spectrum is completely determined by the isocurvature perturbations if $\mathcal{C} \gg 1$, which corresponds to trajectories with a small radius κ or, equivalently, significant turning effects with $8\epsilon_* \ll \kappa^2 \ll 8\epsilon_* N_*^2$. Thus at the end of inflation, curvature perturbations are highly enhanced compared to the ones at horizon-exit. Meanwhile, the isocurvature power spectrum for $\mathcal{S} \equiv \sigma/\sqrt{2\epsilon}$ remains unchanged as $P_{\mathcal{S}} = \frac{H_*^2}{8\pi^2\epsilon_*}$. Therefore, the amplitude of the isocurvature perturbation is dynamically suppressed, *i.e.* $P_{\mathcal{S}}/P_{\mathcal{R}} \simeq 1/\mathcal{C} \ll 1$. The details of how $P_{\mathcal{S}} \neq 0$ can generate isocurvature components in the CMB are rather model-dependent, and one cannot automatically claim that a suppressed ratio $P_{\mathcal{S}}/P_{\mathcal{R}}$ is compatible with observations. However, if $\mathcal{R}$ and $\mathcal{S}$ contributed similarly to the curvature and isocurvature components in the CMB, the result is compatible with current constraints.

2.5 Phenomenology

We now turn to the observational predictions of shift-symmetric orbital inflation. For any positive $\mathcal{C}$, from (2.11), the tensor-to-scalar ratio can be expressed as $r = 16\epsilon_*/(1+\mathcal{C})$, and the scalar spectral index is $n_s - 1 \equiv \frac{d\ln P_{\mathcal{R}}}{d\ln k} = -2\epsilon_* - \eta_* + (d\mathcal{C}/dN)/(1+\mathcal{C})$, where we used $d\ln k = dN$. Note that $\frac{\partial N_*}{\partial N} = -1$, since N_* counts the number of efolds backwards. These predictions depend on the function $H(\theta)$. As in single field inflation, this function determines how slow-roll parameters ϵ and $\eta \equiv \epsilon'/\epsilon$ scale with N_*.

For concreteness, we consider models with $H \sim \theta^p$. Solving (2.8) for $\theta(N)$ yields[2] $\epsilon_* \simeq p/(2N_*)$ and $\eta_* \simeq 1/N_*$. The predictions for n_s and r are therefore well approximated by

$$n_s - 1 \simeq -\frac{p+1}{N_*} - \frac{4p}{\kappa^2 + 4pN_*}, \quad r \simeq \frac{8p\kappa^2}{N_*\kappa^2 + 4pN_*^2}. \tag{2.12}$$

[2]We note that for $0 < p < 1$ this toy model is not well defined as $\theta \to 0$, as can be seen in (2.7). This is not a problem as the inflationary period we are interested in occurs before that point is reached. The true underlying potential would have to be completed in some way. This is similar to case with say axion monodromy.

We plot these results against the Planck 1σ and 2σ contours [53] in Fig. 2.2. N_* is taken to be between 50 and 60, and the radius κ^2 varies between 1 and 10^5. The purple region is for $p = 1$, corresponding to the toy model (2.1), and we also show the predictions for $p = 0.5$ (red region), $p = 0.2$ (yellow region) and $p = 0.1$ (green region).

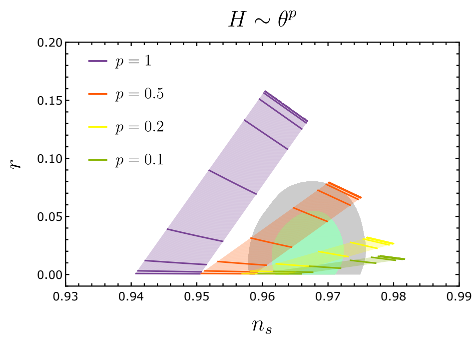

Figure 2.2: The analytical predictions (2.12) for (n_s, r) compared to the *Planck* 1σ and 2σ contours [53]. We show the predictions for wavenumbers which cross the horizon $50-60$ efolds before the end of inflation. The predictions for $n_s - r$ depend on the value of $\kappa \in [1, 1000]$, where the values $(1, 2, 4, 8, 16, 32, 64, 128, 256)$ are depicted with thick lines (from bottom to top).

Notice that n_s and r only depend on the value of κ and are therefore insensitive to the details of the field metric. When $\kappa \to \infty$ one recovers the predictions of chaotic inflation with $V \propto \phi^{2p}$. Meanwhile as κ decreases, predictions are pushed downwards and to the left in this $n_s - r$ diagram. Therefore, in the case of power-law potentials only for small p do the predictions remain within the Planck contours. The interesting regime here is still the case with significant turning (small κ or $\mathcal{C} \gg 1$), where the final power spectrum $P_{\mathcal{R}} \simeq \frac{H_*^2 N_*^2}{\pi^2 \kappa^2}$ mainly has an isocurvature origin. Then the tensor-to-scalar ratio is given by $r = 2\kappa^2/N_*^2 = 16\epsilon_*/\mathcal{C}$, which is suppressed. The spectral index reduces to $n_s - 1 = -(p+2)/N_*$ which, for small p, lies in the sweet spot $n_s = 0.9649 \pm 0.0042$.

Another important observable is primordial non-Gaussianity, which is currently bounded by Planck through $f_{\rm NL}^{\rm loc} = 0.8 \pm 5$ [208]. There are examples in the literature of how $\mathcal{O}(1)$ local non-Gaussianity can arise in multi-field models, especially when the coupling between isocurvature and curvature modes is large [99, 209–211] - see [212] for a review. There are also examples of how small levels of non-Gaussianity can arise in multi-field models [213–215]. However, in most cases a detailed analytic understanding of the size of the non-Gaussianity is lacking because the associated dynamics is non-linear and complicated. This is not the case in shift-symmetric orbital inflation, where we find that we can both easily satisfy the Planck constraint and crucially understand its origin analytically. The amplitude of local non-Gaussianity can be determined using the δN formalism. In a generic multi-field inflation model with curved field manifold, we have $f_{\rm NL}^{\rm loc} = \frac{5}{6} G^{ab} G^{cd} N_a N_c N_{bd}/(G^{ab} N_a N_b)^2$ [209, 216], where $G_{ab} = {\rm diag}\{f(\rho), 1\}$ is the field space metric, N_a and N_{ab} are derivatives of N with respect to the fields (θ, ρ). To gain some analytical understanding, here we still focus on models with $H \sim \theta^p$, where N can be expressed as $N = f(\rho)\theta^2/4p - p/2$. The amplitude of local non-Gaussianity then follows

$$f_{\rm NL}^{\rm loc} = \frac{5}{12}\eta_* \left[1 - \frac{\mathcal{C}^2}{(1+\mathcal{C})^2} \frac{\kappa^2 \mathbb{R}}{2}\right], \tag{2.13}$$

where we used the relation $\mathcal{C} = 2p^2/(\epsilon_* \kappa^2)$. When $\kappa \to \infty$, we have $\mathcal{C} \to 0$ and $\mathcal{C}^2\kappa^2 \to 0$. Thus the second term in (2.13) vanishes, which leads to the single field result $f_{\rm NL}^{\rm loc} = 5\eta_*/12$ as expected. The enhancement of non-Gaussianity is possible in the intermediate regime $\mathcal{C} \sim \mathcal{O}(1)$, where the transfer from isocurvature to adiabatic modes is inefficient. In that case, $f_{\rm NL}^{\rm loc} \sim -5p\mathbb{R}/12$ can be large if the field space is highly curved.

For the interesting regime with $\mathcal{C} \gg 1$, the δN expansion is dominated by N_ρ and $N_{\rho\rho}$. This then leads to what, at first sight, appears as the counterintuitive result that $f_{\rm NL}^{\rm loc}$ is negligible and slow-roll suppressed

$$f_{\rm NL}^{\rm loc} \simeq \frac{5}{6}\frac{N_{\rho\rho}}{N_\rho^2} = \frac{5}{12}\eta_* \left(1 - \frac{\kappa^2 \mathbb{R}}{2}\right). \tag{2.14}$$

This is the same as happened in the calculation of the power spectrum: the contribution to the curvature perturbation sourced by the isocurvature modes dominates the final result. The bispectrum is found to be slow-roll suppressed, just like in single field inflation, but there are small corrections from the field space curvature, which violates Maldacena's consistency relation [217, 218]. We have recently confirmed this result via a scaling symmetry approach in [71].

2.6 Discussions

We have proposed a class of multi-field inflationary models that demonstrate a new type of attractor trajectory along the isometry direction in field space. Here the isocurvature modes become massless and freeze on superhorizon scales. Moreover, when the turning effects become significant, the curvature perturbations keep growing after horizon-exit and thus isocurvature modes are dynamically suppressed. As a consequence, these multi-field models yield the single-field-like phenomenology favored by observations.

Additional isocurvature perturbations will either decay if they are massive or freeze if they are light. Therefore, although our computations were done in a simple two-field setting, we expect the conclusions will continue to hold in multi-field extensions with more than two fields, provided that the number of additional light isocurvature fields is not too large.

One counterintuitive result of shift-symmetric orbital inflation is the negligible amount of local non-Gaussianity. Here the isocurvature degree of freedom can be the dominant contribution to the bispectrum, but in such cases $f_{\rm NL}$ is slow-roll suppressed. This unusual result teaches us a generic lesson: that in multi-field models, even if the isocurvature-to-adiabatic conversion is very efficient, the resulting non-Gaussianity can still be suppressed. A large coupling between curvature and isocurvature modes enhances the transfer of non-Gaussianity, but for this transfer to generate large non-Gaussianity, one needs sizable self-interactions affecting the isocurvature field during horizon crossing [99, 207]. In this class of scenarios, however, the shift symmetry along the radial direction (2.4) has a role in suppressing the self-interactions of the isocurvature field (see [71]). Therefore, it is perfectly fine to study multi-field models with significant and sustained turning trajectories, without worrying about generating large non-Gaussianity.

Our model has important implications on the realization of inflation in UV-complete theories. Contrary to what is usually assumed, and as emphasized in [69], it is not always necessary to stabilize all compactification moduli, or to have a large mass hierarchy between the inflaton and other fields. The most problematic effects usually associated with multi-field effects – the generation of isocurvature perturbations and non-Gaussianity at unacceptable levels – cancel each other in the shift-symmetric orbital scenario. From an EFT point of view this can be traced back to the effect of derivative interactions among the curvature and isocurvature perturbations that are absent in single-field inflation. These are unavoidable on curved trajectories and curved field spaces and, therefore, ubiquitous in string compactifications.

2.7 Appendix 2A: Hamilton-Jacobi Formalism

Here we apply the Hamilton-Jacobi formalism [200, 204–206] to derive the potential for shift-symmetric orbital inflation, replacing the potential as an input function with the Hubble parameter $H(\phi)$ which leads directly to the inflation dynamics.

Friedmann's second equation yields

$$\dot{H} = \dot{\phi} H_\phi = -\frac{\dot{\phi}^2}{2} \longrightarrow -2H_\phi = \dot{\phi}\,. \tag{2.15}$$

leading to the Hamilton-Jacobi form of the first Friedmann equation

$$V = 3H^2 - 2H_\phi^2\,, \tag{2.16}$$

with all functions now being explicitly dependent on ϕ. Therefore, if $H(\phi)$ is known, so is $V(\phi)$.

For the multi-field case, we simply generalise, $\phi \to \phi^a$, so equations (2.15) and (2.16) become

$$\dot{H} = \dot{\phi}^a H_a = -\frac{\dot{\phi}^a \dot{\phi}^b G_{ab}}{2} \longrightarrow H_a = -\frac{G_{ab}\dot{\phi}^b}{2}\,. \tag{2.17}$$

and

$$3H^2 = V + 2H^a H_a. \tag{2.18}$$

which we use to construct the generic potentials for shift-symmetric orbital inflation. The important requirement here is that the inflaton trajectory is along the isometry direction at any radius. Thus for the field space (θ, ρ) with metric $G_{ab} = \mathrm{diag}\{f(\rho), 1\}$, the inflaton should move in the θ direction for any value of ρ. For this behaviour, equation (2.18) simplifies to $3H^2 = V + 2\frac{H_\theta^2}{f(\rho)}$. Therefore, we conclude that our two-field inflationary model has a potential of the following form

$$V = 3H(\theta)^2 - 2\frac{H_\theta^2}{f(\rho)}. \tag{2.19}$$

2.8 Appendix 2B: Stability Analysis

Here we demonstrate the neutral stability of the exact solutions. We have seen that there is a continuous set of orbital solutions parametrized by ρ_0 and that normal perturbations move us freely between these 'attractors', so the system is not stable in the usual sense. The property we need to prove is that small perturbations shift us to another inflationary solution $\dot{\rho} = 0$.

Each attractor solution

$$\dot{\theta} = -2\frac{H_\theta}{f}, \qquad \rho = \rho_0$$

corresponds to a point in the $(\dot{\rho}, \dot{\theta})$ plane. These points are all different and lie on a curve, therefore the stability of this system is non-trivial to prove analytically. If we simply perturb the field equations we will find zero eigenvalues associated with the perturbations that move us between attractors. Moreover, it is not obvious how to find variables such that the linearized system of perturbations becomes diagonal. Introducing the variables

$$x(\theta, \rho, \theta', \rho') \equiv \tfrac{fH}{H_\theta}\theta' - 2\tfrac{f}{f_\rho}\rho' + 2, \tag{2.20}$$

$$y(\theta, \rho, \theta', \rho') \equiv \tfrac{fH}{H_\theta}\theta' + 2\,, \tag{2.21}$$

$$z(\theta, \rho) \equiv \tfrac{fH^2}{H_\theta^2} - 2/3\,, \tag{2.22}$$

here a prime denotes a derivative with respect to the number of efolds $(..)' = \frac{d}{dN}(..)$. Remember that $H = H(\theta)$ and $f = f(\rho)$. Our definition of stability now amounts to the presence of a fixed point at $(x, y) = (0, 0)$.

For $H \sim \theta$ the potential in (2.19) satisfies the following scaling relation

$$\theta V_\theta - 2\frac{f}{f_\rho}V_\rho = 2V. \tag{2.23}$$

This ensures that the equations for x and y diagonalize at the linear level, and below we prove linear stability for the models $H \sim \theta$, although it applies to any power law $H \sim \theta^n$ and more general models.

Linear stability analysis

In terms of x, y, ρ and z, the field equations and second Friedmann equation become

$$x' + (3-\epsilon)x + \left(2\left(\tfrac{f}{f_\rho}\right)_\rho - g(\theta)\right)(\rho')^2 \tag{2.24}$$
$$+\tfrac{2(z+2/3)}{z} g(\theta)\left(\epsilon - \epsilon_0\right) = 0,$$
$$y' + (3-\epsilon)y + \tfrac{2}{z}\left(-\tfrac{1}{3}(\rho')^2 - \tfrac{1}{2}y^2 + 2y\right) \tag{2.25}$$
$$-g(\theta)(\rho')^2 + \tfrac{2(z+2/3)}{z} g(\theta)\left(\epsilon - \epsilon_0\right) = 0,$$
$$z' = 2(y-2)\left(1 - g(\theta)\right) + \left(\tfrac{f_\rho}{f}\right)^2 \tfrac{y-x}{2}\left(z + \tfrac{2}{3}\right), \tag{2.26}$$
$$\rho' = \tfrac{f_\rho}{f}\tfrac{y-x}{2}, \tag{2.27}$$
$$\epsilon = \tfrac{1}{2}\tfrac{(y-2)^2}{z+2/3} + \tfrac{f_\rho^2}{f^2}\tfrac{(x-y)^2}{8}, \tag{2.28}$$

where $\epsilon_0 = \frac{2}{z+2/3}$. All the terms in brackets are combined to be manifestly zero on the attractor, and we have introduced the model specific function $g(\theta) \equiv \frac{HH_{\theta\theta}}{H_\theta^2}$. Note that $g(\theta)$ is in general a function of z and ρ, but it reduces to a constant in the case when we have a power law $H(\theta) \sim \theta^n$, and it is zero for $n = 1$.

In terms of the four variables, shift-symmetric Orbital Inflation is given by $(x, y, z', \rho') = (0, 0, -4(1-g(\theta)), 0)$. To prove it is the attractor we must show $(y, \rho') = (0, 0)$ is a fixed point. Note that the friction term is very large during inflation. We can already see that without the friction the system would be unstable, so we now establish whether the friction term is in fact large enough to make the system stable.

Linearly perturbing around $(y, \rho') = (0, 0)$ with $\epsilon = \frac{2}{z+2/3}$ yields

$$\delta x' + \left(3 - \tfrac{2}{z+2/3}\right)\delta x - \tfrac{4g(\theta)}{z}\delta y = 0, \tag{2.29}$$
$$\delta y' + \left(3 - \tfrac{2}{z+2/3} + \tfrac{4(1-g(\theta))}{z}\right)\delta y = 0, \tag{2.30}$$
$$\delta z' = 2(1-g(\theta))\delta y + \left(\tfrac{f_\rho}{f}\right)^2 \tfrac{\delta y - \delta x}{2}\left(z + \tfrac{2}{3}\right), \tag{2.31}$$
$$\delta\rho' = \tfrac{f_\rho}{f}\tfrac{\delta y - \delta x}{2}. \tag{2.32}$$

For constant $g(\theta)$ below we explicitly prove stability. For a general $g(\theta)$ we express it in terms of z and ρ and integrate the equations numerically. However, we expect the system to be stable. If $(1 - g(\theta))$ takes values of order 1 and does not vary too rapidly, then z will take large values during inflation and behave smoothly as well. In that case we see from (2.29) and

(2.30) that $\delta x'$ and $\delta y'$ are dominated by the friction terms $-3\delta x$ and $-3\delta y$ respectively. Therefore, we expect both of them to decay like e^{-3N}. Finally (2.32) then implies that we quickly converge to the fixed point.

Power law inflation $H \sim \theta^n$

In the case of power law inflation with $1-g(\theta)=\frac{1}{n}$, using $z=z_0-\frac{4}{n}N$, we can solve (2.30) and (2.29) yielding

$$\begin{aligned} \delta x &= \delta x_0 \left(\tfrac{2+3z_0}{2+3z}\right)^{n/2} e^{-3N} + \delta y_0 \tfrac{4(n-1)N}{n} \left(\tfrac{2+3z_0}{2+3z}\right)^{n/2} e^{-3N}, \\ \delta y &= \delta y_0 \tfrac{z}{z_0} \left(\tfrac{2+3z_0}{2+3z}\right)^{n/2} e^{-3N}, \end{aligned} \tag{2.33}$$

which in (2.32) demonstrates that $(y,\rho')=(0,0)$ is a fixed point. This proves stability for power law inflation.

Linearized equations in the slow-roll parameters

We can write the linearized perturbation equations in terms of the slow-roll parameters ϵ and η

$$\epsilon = \frac{2H_\theta^2}{fH^2}, \quad \eta \equiv \frac{\dot{\epsilon}}{H\epsilon} = -\frac{4H_{\theta\theta}}{fH} + \frac{4}{f}\left(\frac{H_\theta}{H}\right)^2 . \tag{2.34}$$

In particular, the model specific function $g(\theta)$ becomes

$$g(\theta) = (2\epsilon-\eta)\sqrt{\frac{f}{8\epsilon}} . \tag{2.35}$$

We see that $g(\theta)$ is not necessarily positive, but it will be small if both the slow-roll approximation and the condition $\eta \ll \sqrt{\epsilon}$ hold true. The linearized equations (2.29) – (2.32) are then given by

$$\begin{aligned} \delta x' + (3-\epsilon)\,\delta x - \tfrac{2\epsilon-\eta}{1-\epsilon/3}\sqrt{\tfrac{\epsilon f}{2}}\delta y &= 0, \\ \delta y' + \left(3-\epsilon+\tfrac{1}{1-\epsilon/3}\left(2\epsilon-(2\epsilon-\eta)\sqrt{\tfrac{\epsilon f}{2}}\right)\right)\delta y &= 0, \\ \delta z' &= 2\left(1-(2\epsilon-\eta)\sqrt{\tfrac{f}{8\epsilon}}\right)\delta y + \left(\tfrac{f_\rho}{f}\right)^2 \tfrac{\delta y-\delta x}{\epsilon}, \\ \delta\rho' &= \tfrac{f_\rho}{f}\tfrac{\delta y-\delta x}{2}. \end{aligned} \tag{2.36}$$

In the slow-roll approximation δx and δy are therefore exponentially decaying

$$\delta x \approx \delta x_0 e^{-3N}, \tag{2.37}$$

$$\delta y \approx \delta y_0 e^{-3N}. \tag{2.38}$$

Looking at the equation for δz we find that a sufficient condition for stability is that e^{-3N}/ϵ goes to zero exponentially fast. This requires $\eta < 3$, which is automatically satisfied assuming the slow-roll approximation $\eta \ll 1$. In addition, ϵ cannot be arbitrarily small.

3 | Gravitational waves from spectator Gauge-flation

Abstract: We investigate the viability of inflation with a spectator sector comprised of non-Abelian gauge fields coupled through a higher order operator. We dub this model "spectator Gauge-flation". We study the predictions for the amplitude and tensor tilt of chiral gravitational waves and conclude that a slightly red-tilted tensor power spectrum is preferred with $n_T = -\mathcal{O}(0.01)$. As with related models, the enhancement of chiral gravitational waves with respect to the single-field vacuum gravitational wave background is controlled by the parameter $\gamma = g^2Q^2/H^2$, where g is the gauge coupling, H is the Hubble scale and Q is the VEV of the $SU(2)$ sector. The requirement that the $SU(2)$ is a spectator sector leads to a maximum allowed value for γ, thereby constraining the possible amplification. In order to provide concrete predictions, we use an α-attractor T-model potential for the inflaton sector. Potential observation of chiral gravitational waves with significantly tilted tensor spectra would then indicate the presence of additional couplings of the gauge fields to axions, like in the spectator axion-SU(2) model, or additional gauge field operators.

Keywords: physics of the early universe, inflation, primordial gravitational waves, gravitational waves and CMBR polarization.

Based on:

O. Iarygina and E. I. Sfakianakis
Gravitational waves from spectator Gauge-flation
arXiv:2105.06972.

3.1 Introduction

Inflation provides an elegant solution for the horizon and flatness problems, as well as a mechanism for producing density fluctuations in very good agreement with the latest observational tests. Typically, scalar fields play a major role in inflationary model-building since they do not spoil the homogeneity and isotropy of the background cosmology. However, models of particle physics generically include also gauge fields and their presence in the inflationary epoch may significantly influence cosmological predictions. Scalar perturbations that are produced during inflation are tightly constrained by observations [220], while the primordial tensor modes (generated as primordial gravitational waves) are still not detected. The primordial Stochastic Gravitational Wave Background (SGWB) is a unique test of the physics of the very early Universe, that could provide signatures of the particle content and the energy scale of inflation. Nowadays, the search for primordial gravitational waves (GWs) is mainly focused [221, 222] on the parity-odd polarization pattern in the CMB the B-modes. A correct interpretation of B-mode measurements strongly relies on understanding their production mechanism.

One intriguing scenario is GW generation by gauge fields. Gauge field tensor modes can experience a tachyonic growth in one of their polarizations, leading to production of chiral GWs. In addition to chirality, produced GWs may be significantly red or blue tilted and non-Gaussian. One of the very-well known models of inflation, where non-Abelian gauge fields generate accelerated expansion, is the Gauge-flation model that was originally proposed in Refs. [74, 75]. Gauge-flation is related to Chromo-Natural inflation [223] that contains an axion coupled to $SU(2)$ gauge fields. Gauge-flation can be formally obtained from chromo-natural inflation after integrating out an axion field near the minimum of the axion potential [76, 224–226]. The original formulation of both models is ruled out by *Planck* observations [227–230]. However, both models can be made consistent with current CMB bounds if the gauge symmetry is spontaneously broken by a Higgs sector [231, 232]. Interestingly Higgsed gauge-flation and Higgsed Chromo-natural inflation give somewhat different predictions for the shape of the produced GW spectrum.

Recent interest in potentially distinguishable signatures from the standard vacuum fluctuations by future B-mode experiments, like LiteBIRD, has led to a number of generalizations of gauge-field-driven GW models. In particular considering a spectator axion sector coupled to non-abelian gauge fields has significantly opened up the parameter space [233–237]. It was recently demonstrated [238] that Chromo-Natural inflation as a spectator sector for the scalar single-field inflation can be in agreement with the current data, while at the same time generating potentially distinguishable observable signatures for the tensor modes. In Ref. [239] it was shown that in spectator Chromo-Natural inflation, depending on the choice of the axion potential, all three possible tensor tilts may be generated: flat, red and blue. In addition to that, peaked or oscillating GW spectra are also possible for well-motivated axion potentials. Since in Gauge-flation there is much less freedom due to the absence of the axion field, a question arises: what are the possible GW spectra arising from a spectator Gauge-flation sector?

In this work we demonstrate the viability of the spectator Gauge-flation scenario, study its predictions and limitations and also provide a comparison with predictions of related models. The paper is organised as follows: In Section 3.2 we introduce the framework for non-Abelian gauge field inflation and then embed it as a spectator sector for scalar single-field inflation. In Section 3.3 we discuss the necessary conditions for the $SU(2)$ sector to be subdominant, as compared to the inflaton sector. This ensures that the scalar fluctuations will be dominated by the inflaton sector and can be made to agree with the observational constraints, for example by considering an α-attractor inflationary potential. Keeping the non-Abelian sector subdominant leads to an upper bound for the amplitude enhancement of the tensor power spectra. In Section 3.4 we discuss predictions for the primordial tensor tilt and it's dependence on the parameters of the theory. We use a well-known α-attractor model as the inflaton sector, since it can provide an arbitrarily low amount of vacuum-generated GWs (at least in principle), while at the same time obeying the constraints for the scalar fluctuations. We conclude in Section 3.5.

3.2 Framework

3.2.1 The model

In this section we describe the theory of Gauge-flation and its embedding as a spectator sector for inflation. The Gauge-flation action is given by [74, 75]

$$S = \int d^4x \sqrt{-\det(g_{\mu\nu})} \left[\frac{M_{\rm Pl}^2}{2} R - \frac{1}{4} F^a_{\mu\nu} F^{a\,\mu\nu} + \frac{\kappa}{96} \left(F^a_{\mu\nu} \tilde{F}^{a\,\mu\nu} \right)^2 \right], \quad (3.1)$$

where R is the space-time Ricci scalar, $F^a_{\mu\nu} = \partial_\mu A^a_\nu - \partial_\nu A^a_\mu - g\epsilon^{abc}A^b_\mu A^c_\nu$ is the field strength of an $SU(2)$ gauge field A^a_μ, $\tilde{F}^{a\,\mu\nu} = \epsilon^{\mu\nu\rho\sigma}F^a_{\rho\sigma}/\left(2\sqrt{-\det(g_{\mu\nu})}\right)$ its dual (where $\epsilon^{\mu\nu\alpha\beta}$ is the antisymmetric tensor and $\epsilon^{0123} = 1$), $\kappa > 0$ is a parameter with dimension $M_{\rm pl}^{-4}$ and g is the gauge field coupling.

We will work with the FLRW metric

$$ds^2 = -dt^2 + a(t)^2\delta_{ij}dx^i dx^j, \tag{3.2}$$

where i, j indicate the spatial directions. An isotropic solution for the background is given by the following configuration of the gauge field

$$A^a_0 = 0, \tag{3.3}$$
$$A^a_i = \delta^a_i a(t)Q(t) \tag{3.4}$$

and it has been shown to be an attractor solution [75]. For this ansatz the closed system of equations for the vacuum expectation value (VEV) of the gauge field $Q(t)$ and the Hubble parameter $H(t)$ is given by

$$M_{\rm Pl}^2\dot{H} = -\left((\dot{Q}+HQ)^2 + g^2Q^4\right) \tag{3.5}$$
$$M_{\rm Pl}^2H^2 = \frac{1}{2}\left((\dot{Q}+HQ)^2 + g^2Q^4 + \kappa g^2Q^4(\dot{Q}+HQ)^2\right), \tag{3.6}$$
$$\left(1+\kappa g^2Q^4\right)\left(\ddot{Q}+3H\dot{Q}+\dot{H}Q\right) + 2g^2Q^3\left(1+\kappa\dot{Q}^2\right) + 2H^2Q = 0, \tag{3.7}$$

where an overdot denotes a derivative with respect to cosmic time t.

We now introduce a scalar field $\varphi(t)$ with a potential $V(\varphi)$ that is responsible for driving inflation and consider the Gauge-flation terms as a spectator sector, i.e.

$$S = \int d^4x\sqrt{-\det(g_{\mu\nu})}\left[\frac{M_{\rm Pl}^2}{2}R - \frac{1}{2}(\partial\varphi)^2 - V(\varphi) - \frac{1}{4}F^a_{\mu\nu}F^{a\,\mu\nu} + \frac{\kappa}{96}\left(F^a_{\mu\nu}\tilde{F}^{a\,\mu\nu}\right)^2\right]. \tag{3.8}$$

Up to gravitational interactions the dynamics of the inflaton sector is completely decoupled from the dynamics of the gauge field. This allows the inflaton field $\varphi(t)$ to be responsible for the predictions for scalar fluctuations. At the same time the gravitational waves generated by the gauge field sector can lead to observable signatures in the tensor power spectra. In this paper we will not consider scalar fluctuations and refer to Ref. [233] where scalar fluctuations were studied for a related model, where the spectator sector involved an axion coupled to an $SU(2)$ field through a Chern-Simons term (which we call spectator Chromo-natural inflation). A recent analysis of scalar fluctuations, including non-linear effects, can be found in Refs. [240, 241]. We expect that the bounds on tensor modes arising from the spectator nature of the Gauge-flation sector will result in subdominant density fluctuations from it. We will thus focus our attention solely on the tensor sector, leading to the production of GW's.

Using the ansatz of Eq. (3.4) the background system of equations in the presence of the inflaton field changes to

$$M_{\rm Pl}^2\dot{H} = -\left((\dot{Q}+HQ)^2+g^2Q^4\right)-\frac{1}{2}\dot{\varphi}^2, \tag{3.9}$$

$$M_{\rm Pl}^2H^2 = \frac{1}{3}\left(\frac{1}{2}\dot{\varphi}^2+V(\varphi)\right)+\frac{1}{2}\left((\dot{Q}+HQ)^2+g^2Q^4+\kappa g^2Q^4(\dot{Q}+HQ)^2\right), \tag{3.10}$$

$$\left(1+\kappa g^2Q^4\right)\left(\ddot{Q}+3H\dot{Q}+\dot{H}Q\right)+2g^2Q^3\left(1+\kappa\dot{Q}^2\right)+2H^2Q=0, \tag{3.11}$$

$$\ddot{\varphi}+3H\dot{\varphi}+V_\varphi(\varphi)=0, \tag{3.12}$$

where $V_\varphi(\varphi)=\partial V(\varphi)/\partial\varphi$. The standard Hubble slow roll parameters are defined as

$$\epsilon=-\frac{\dot{H}}{H^2},\quad \eta=-\frac{\ddot{H}}{2H\dot{H}}=\epsilon-\frac{\dot{\epsilon}}{2\epsilon H}. \tag{3.13}$$

The slow-roll parameter ϵ contains contributions from the scalar (inflaton) and the gauge field (spectator) sectors. The various contributions can be written as

$$\epsilon=\epsilon_\varphi+\epsilon_{Q_E}+\epsilon_{Q_B}, \tag{3.14}$$

where

$$\epsilon_\varphi=\frac{\dot{\varphi}^2}{2M_{\rm Pl}^2H^2},\quad \epsilon_{Q_E}=\frac{(\dot{Q}+HQ)^2}{M_{\rm Pl}^2H^2},\quad \epsilon_{Q_B}=\frac{g^2Q^4}{M_{\rm Pl}^2H^2}. \tag{3.15}$$

Throughout this work we assume – and check – that the inflaton field $\varphi(t)$ dominates the energy budget of the theory. This translates into the conditions $\epsilon_\varphi \gg \epsilon_Q$, where $\epsilon_Q=\epsilon_{Q_E}+\epsilon_{Q_B}$, and hence $\epsilon\simeq\epsilon_\varphi$. Despite this regime of interest, we keep the analytic part of our analysis as general as possible and clearly state the approximations wherever they are necessary for making analytical progress.

Although the inflationary era is dominated by $\varphi(t)$, in the same way as in the original Gauge-flation approach we will assume that the gauge field also slow-rolls together with the inflaton field[1]. Hence for the later analysis we define

$$\delta = -\frac{\dot{Q}}{HQ}, \quad \gamma = \frac{g^2 Q^2}{H^2}. \tag{3.16}$$

We will require $\delta \ll 1$ to ensure that the gauge field slow-rolls long enough, to secure the needed amount of e-folds for inflation. The parameter γ is a characteristic quantity of the model. It was shown in Ref. [227] that for $\gamma < 2$ the scalar perturbations are tachyonically unstable. We thus restrict our analysis to the stable region with $\gamma > 2$. For the tensor sector this parameter characterises the enhancement of one of the polarizations for the tensor perturbation with respect to the gravitational wave background coming from the inflaton sector. So far there were no theoretical upper bounds on this parameter, only the observational constraints coming from the tensor-to-scalar ratio r. As we will see in the next subsection, for spectator Gauge-flation there exists an upper bound $\gamma_{\max}$ which is determined solely from the self-consistency of the theory and the slow-roll conidtions. For a given set of parameters g, ϵ and H, the upper bound on γ allows for an estimation of the maximal enhancement for the tensor power spectra and thus a theoretical upper bound on r.

3.2.2 Background parameters

In this subsection we will collect all the expressions for the background parameters that will be relevant for the tensor power spectra computation. To start with, there are two equivalent ways to write down the first slow-roll parameter in terms of background quantities. The first one follows directly from Eqs. (3.9) and (3.13), i.e.

$$\epsilon = \frac{1}{M_{\rm Pl}^2} Q^2 \left((1-\delta)^2 + \gamma \right) + \epsilon_\varphi. \tag{3.17}$$

Another way is to use the combination $\dot{H} + 2H^2$, which through Eqs. (3.9), (3.10) leads to

$$\epsilon = 2 - \frac{\kappa g^2 Q^6}{M_{\rm Pl}^2} (1-\delta)^2 + \frac{1}{3}\epsilon_\varphi - \Upsilon\,. \tag{3.18}$$

[1]A fast-rolling spectator gauge-flation sector can also lead to GW production. However, some fine-tuning is required to bring it in the observable window. We thus do not pursue this regime further.

We have defined

$$\Upsilon = \frac{2V}{3M_{\rm Pl}^2 H^2}\,, \tag{3.19}$$

which is determined by the scalar field inflation potential and can be taken to be approximately constant for slow-roll models of inflation. From Eqs. (3.13) and (3.17) we derive the second slow-roll parameter

$$\eta = \frac{Q^2}{M_{\rm Pl}^2}\left((1-\delta)^2 + (1-\delta)\frac{\dot{\delta}}{\epsilon H} + \gamma\frac{\delta}{\epsilon}\right) + \delta - \frac{\epsilon_\varphi}{\epsilon}\left(\delta - \eta_\varphi\right), \tag{3.20}$$

with $\eta_\varphi = -\frac{\ddot{\varphi}}{H\dot{\varphi}}$. An alternative derivation follows from Eqs. (3.13) and (3.18)

$$\begin{aligned}\eta = \epsilon - (2 - \Upsilon - (\epsilon - \frac{1}{3}\epsilon_\varphi))\left(\frac{\dot{\delta}}{H\epsilon(1-\delta)} + \frac{3\delta}{\epsilon}\right) - \frac{\epsilon_\varphi}{3}\left(1 - \frac{\eta_\varphi}{\epsilon}\right) + \\ + \frac{2}{3}\left(\frac{\epsilon_\varphi V_\varphi}{\dot{\varphi}H\epsilon} + \frac{V}{H^2 M_{\rm Pl}^2}\right).\end{aligned} \tag{3.21}$$

Up to now the above equations are exact. If the inflaton is assumed to dominate the total energy budget, Eq. (3.20) leads to $\eta \simeq \frac{\epsilon_\varphi}{\epsilon}\eta_\varphi$. Substituting that into Eq. (3.21) and neglecting[2] $\frac{\dot{\delta}}{H(1-\delta)}$, we find

$$\delta \simeq \frac{\epsilon}{3(2 - \Upsilon - (\epsilon - \frac{1}{3}\epsilon_\varphi))}\left(\epsilon - \frac{2}{3}\frac{\epsilon_\varphi}{\epsilon}\eta_\varphi - \frac{\epsilon_\varphi}{3} + \Upsilon\left(1 - \frac{\epsilon_\varphi}{\epsilon}\right)\right), \tag{3.22}$$

where we have used $\epsilon_V = \frac{M_{\rm Pl}^2}{2}\left(\frac{V_\varphi}{V}\right)^2 \simeq \epsilon_\varphi$ and $\dot{\varphi} = -HM_{\rm Pl}\sqrt{2\epsilon_\varphi}$ is chosen to be negative without loss of generality.

In addition to that, Eqs. (3.16) and (3.18) we find

$$\kappa = \frac{1}{H^2\gamma Q^2}\frac{(1-\delta)^2+\gamma}{(1-\delta)^2}\frac{2 - \left(\epsilon_Q + \frac{2}{3}\epsilon_\varphi + \Upsilon\right)}{\epsilon_Q}. \tag{3.23}$$

Moreover, from Eq. (3.17) one may derive the relation that will help to eliminate $M_{\rm Pl}$ from the equations

$$M_{\rm Pl} = Q\sqrt{\frac{(1-\delta)^2+\gamma}{\epsilon_Q}}, \tag{3.24}$$

[2] The arguments for neglecting this term are discussed in Ref. [75]. We numerically checked the validity of this approximation

where ϵ_Q is the first slow-roll parameter for the gauge field sector, i.e. $\epsilon_Q = \epsilon_{Q_E} + \epsilon_{Q_B}$. The relations above with the inflaton sector set to zero coincide with relations obtained in Ref. [227], which provides a consistency check for our analysis. Eq. (3.22) was derived strictly under the assumption of a dominant inflaton sector and thus does not reduce to the gauge-flation result for $\epsilon_\phi \to 0$, which is not true for all equations before it, which are exact and hence applicable to any gauge-flation scenario, with or without a separate inflaton sector.

Finally, from Eqs. (3.16) and (3.17) we find that for $\delta \ll 1$

$$1 - \frac{\epsilon_\varphi}{\epsilon} \simeq \frac{H^2}{M_{\rm Pl}^2 g^2 \epsilon}\gamma(\gamma+1). \tag{3.25}$$

From Eq. (3.25) we obtain γ as a function of ϵ and ϵ_φ

$$\gamma \simeq -\frac{1}{2} + \frac{1}{2}\sqrt{1 + 4M_{\rm Pl}^2 \frac{g^2\epsilon}{H^2}\left(1 - \frac{\epsilon_\varphi}{\epsilon}\right)}. \tag{3.26}$$

The dependence of γ on $\epsilon_\varphi/\epsilon$ is shown in Fig. (3.1). Since $0 < \epsilon_\varphi < \epsilon$, the right hand side of Eq. (3.25) is in the range $0 < \frac{H^2}{M_{\rm Pl}^2 g^2 \epsilon}\gamma(\gamma+1) < 1$. Hence, the maximum value of the parameter γ is

$$\gamma_{\rm max} = -\frac{1}{2} + \frac{1}{2}\sqrt{1 + 4M_{\rm Pl}^2 \frac{g^2\epsilon}{H^2}}\,. \tag{3.27}$$

The result of Eq. (3.27) is obtained without the requirement $\epsilon \simeq \epsilon_\varphi$ and is rather generic. One can see that the parameter γ cannot be chosen arbitrarily high any more, but reaches its maximal value given by Eq. (3.27) due to the restrictions of the theory. The maximum value of γ is achieved when the energy budget is completely controlled by the gauge sector, i.e. when $\frac{\epsilon_\varphi}{\epsilon} \ll 1$, meaning that ϵ is dominated by ϵ_Q. In the spectator case $\epsilon \simeq \epsilon_\varphi$, and γ is limited to a smaller range of values, with a magnitude that depends only on g (with fixed H and ϵ). Interestingly enough, this allows us to find the minimum allowed value of the gauge coupling $g_{\rm min}$ for spectator Gauge-flation. Simply from the stability condition of scalar perturbations[3] $\gamma_{\rm max} > 2$ we obtain

$$g_{\rm min} > \sqrt{\frac{6}{M_{\rm Pl}\,\epsilon}}H. \tag{3.28}$$

[3]For $\gamma_{\rm max} < 2$ scalar perturbations experience a tachyonic instability, see [227] for a detailed discussion.

We can estimate the value of $g_{\rm min}$ by relating H and ϵ to the amplitude of the scalar power spectrum $P_\zeta = \frac{H^2}{8\pi^2 M_{\rm Pl}^2 \epsilon} \simeq 2.2 \times 10^{-9}$, since we assume that the scalar power spectrum is dominated by the fluctuations in the inflaton sector. This results in $g_{\rm min} \simeq 4\pi\sqrt{3P_\zeta} \simeq 0.001$. Then $\gamma_{\rm max}$ may be estimated as $\gamma_{\rm max} \simeq -\frac{1}{2} + \frac{1}{2}\sqrt{1+\frac{g^2}{2\pi^2 P_\zeta}} \simeq 15$ for $g = 6.5 \times 10^{-3}$. The dependence of $\gamma_{\rm max}$ on the value of g is shown in Fig. (3.1). A complementary method for computing the maximum allowed tensor amplification based on the back-reaction of the produced spin-2 particles was presented in Ref. [242].

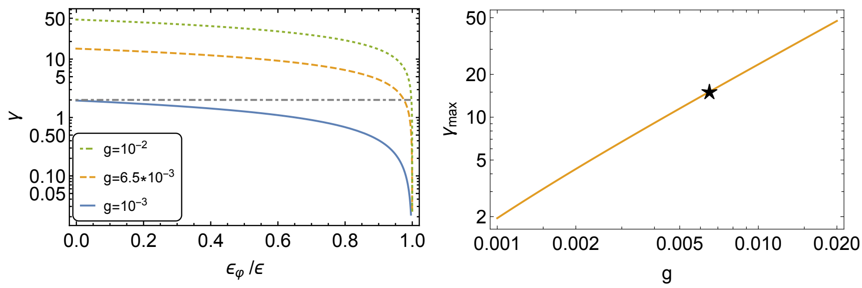

Figure 3.1: *Left:* The dependence of γ on $\epsilon_\varphi/\epsilon$ for $g = 10^{-3}, 6.5 \times 10^{-3}, 10^{-2}$ (blue-solid, orange-dashed and green-dotted lines respectively) and $H = 1.9 \times 10^{-6} M_{\rm pl}, \epsilon = 2 \times 10^{-5}$. The dot-dashed grey line shows the lower bound for the parameter, $\gamma = 2$. *Right:* The dependence of $\gamma_{\rm max}$ on the gauge coupling g for the same values of H and ϵ as on the left plot. The star represents the value of $g = 6.5 \times 10^{-3}$ that we use in our numerical simulations in the subsequent sections, unless stated otherwise.

3.3 Viability of spectator Gauge-flation

In this section we will show the viability of the spectator Gauge-flation. We will consider and discuss the most important dynamics on the example of an α-attractor potential for the inflaton field. To ensure that the gauge sector of Eq. (3.8) is a spectator sector, the energy density of the gauge fields must be subdominant to that of the inflaton

$$\rho_\varphi \gg \rho_{Q_E}, \rho_{Q_B}, \rho_{Q_\kappa}, \tag{3.29}$$

where the definitions for the energy densities are given as [74]

$$\rho_\varphi = \frac{1}{2}\dot{\varphi}^2 + V(\varphi), \tag{3.30}$$

$$\rho_{Q_E} = \frac{3}{2}(\dot{Q} + HQ)^2, \tag{3.31}$$

$$\rho_{Q_B} = \frac{3}{2}g^2 Q^4, \tag{3.32}$$

$$\rho_{Q_\kappa} = \frac{3}{2}\kappa g^2 Q^4 (\dot{Q} + HQ)^2. \tag{3.33}$$

A similar condition must hold for the first slow-roll quantity ϵ

$$\epsilon_\varphi \gg \epsilon_{Q_E}, \epsilon_{Q_B}, \tag{3.34}$$

meaning that the Hubble evolution is dominated by the rolling of the inflaton field (see eq. (3.15)). The above inequalities can be re-cast as relations between the VEVs of the inflaton and gauge fields

$$\frac{1}{2}\dot{\varphi}^2 \gg (\dot{Q} + HQ)^2, \tag{3.35}$$

$$\frac{1}{2}\dot{\varphi}^2 \gg g^2 Q^4, \tag{3.36}$$

$$\frac{1}{2}\dot{\varphi}^2 + V(\varphi) \gg \frac{3}{2}(\dot{Q} + HQ)^2 \tag{3.37}$$

$$\frac{1}{2}\dot{\varphi}^2 + V(\varphi) \gg \frac{3}{2}g^2 Q^4, \tag{3.38}$$

$$\frac{1}{2}\dot{\varphi}^2 + V(\varphi) \gg \frac{3}{2}\kappa g^2 Q^4 (\dot{Q} + HQ)^2. \tag{3.39}$$

Let us note that for spectator Chromo-natural inflation precisely the same inequalities of Eq. (3.37) and (3.38) should hold, in addition to an inequality for the axion field $\chi(t)$, i.e. $\frac{1}{2}\dot{\varphi}^2 + V(\varphi) \gg \frac{1}{2}\dot{\chi}^2 + U(\chi)$ that replaces Eq. (3.39) since the κ-term can be thought as the analogue of the axion potential in Chromo-natural inflation.

From Eqs. (3.35) – (3.39) one may see that $\epsilon_\varphi \gg \epsilon_{Q_E}, \epsilon_{Q_B}$ implies $\rho_\varphi \gg \rho_{Q_E}$, ρ_{Q_B}, as well as $\rho_\varphi \gg \rho_{Q_\kappa}$, if κ is not too large. Hence, Eqs. (3.37) and (3.38) as well as Eq. (3.39) hold automatically when Eqs. (3.35) and (3.36) are satisfied. Therefore we will focus on showing the allowed parameter ranges to satisfy $\epsilon_\varphi \gg \epsilon_{Q_E}, \epsilon_{Q_B}$, i.e. Eqs. (3.35) and (3.36), and confirm our findings with numerical simulations.

For illustrative purposes we will consider an α-attractor model for the inflaton sector [50, 243–245]. It is known that the universal predictions for the spectral index n_s and tensor-to-scalar ratio r are in agreement with the latest *Planck* data [220]. They are parametrised solely by the dimensionless coupling $\tilde{\alpha}$ and the number of e-folds N_* before the end of inflation when the CMB modes exit the horizon during inflation, i.e.

$$n_s = 1 - \frac{2}{N_*}, \quad r = \frac{12\tilde{\alpha}}{N_*^2}. \tag{3.40}$$

The α-attractor T-model potential is given by

$$V(\phi) = \tilde{\alpha}\tilde{\mu}^2 M_{\rm Pl}^2 \left((\tanh(\tilde{\beta}\phi/2))^2\right)^n, \tag{3.41}$$

where the parameters of the potential are chosen to be

$$\tilde{\beta} = \sqrt{2/3\tilde{\alpha}}, \quad n = 3/2, \quad \tilde{\alpha} = 0.1, \quad \tilde{\mu}^2 = 1.08 \times 10^{-10} M_{\rm Pl}^2, \tag{3.42}$$

and are used for numerical simulations in this section. For the gauge sector we use[4]

$$\begin{gathered} g = 6.5 \times 10^{-3}, \quad \kappa = 1.733 \times 10^{20} M_{\rm Pl}^{-4}, \\ \dot{Q}_0/M_{\rm pl}^2 = -10^{-10}, \quad Q_0/M_{\rm pl} = 7 \times 10^{-4}, 10^{-3}, 1.5 \times 10^{-3}, \end{gathered} \tag{3.43}$$

where $Q_0, \dot{Q}_0$ are initial value and initial velocity respectively for the gauge field VEV.

For given parameters one may numerically evolve the system of Eqs. (3.9) – (3.12) and find that, indeed, it is possible to satisfy the conditions of Eqs. (3.29) and (3.34). Fig. (3.2) shows the evolution of the inflaton field $\varphi(N)$ and VEV of the gauge field $Q(N)$ as a function of the number of e-folds N. Notice that $Q(N)$ evolves mildly with N and stays almost constant. The shape of the parameter $\gamma(N)$ which is defined in Eq. (3.16) mimics the behaviour of $Q(N)$ which is shown on Fig. (3.4). As we will see in Section 3.4.2, the shape of γ determines the tilt of the tensor power spectrum. Since we require that $Q(N)$ also slow-rolls during the slow-roll of $\varphi(N)$, we expect $\gamma(N)$ to be a decreasing function of time[5]. The evolution of the components of ϵ and ρ is shown on Fig. (3.3). As we have seen in our numerical simulations, for α-attractors the most restrictive condition

[4]The naturalness of the κ-term and its domination over all the other dimension eight or higher contributions coming from gauge field or fermionic loops is discussed in Ref. [76]. Also note that $\kappa^{-1/4} > H_{\rm infl.}$.

[5]The post-inflationary dynamics and the effect of parametric resonance [158–160] is left for future work.

to host a Gauge-flation sector as a spectator for inflation appears to be the condition $\epsilon_\varphi \gg \epsilon_{Q_B}$. It is known (see e.g. Refs. [50, 158]), that for α-attractors $\epsilon_\varphi \simeq \frac{3\tilde{\alpha}}{4N^2}$. Hence, with the definitions of Eqs. (3.15) and (3.16), $\epsilon_\varphi \gg \epsilon_{Q_B}$ is satisfied for

$$\frac{3\tilde{\alpha}}{4N^2} \gg \frac{\gamma Q^2}{M_{\rm Pl}^2}. \tag{3.44}$$

By fixing the parameter $\tilde{\alpha}$, the number of e-folds N and the value of $\gamma > 2$, it is easy to find the range of allowed initial values for the gauge field Q_0, in order for the non-Abelian sector to stay subdominant. One may rewrite the condition of Eq. (3.44) using Eq. (3.16) and $H^2 \simeq H_\varphi^2 \simeq \frac{\tilde{\alpha}\tilde{\mu}^2}{3}$ in the following form

$$\frac{3M_{\rm Pl}}{2\tilde{\mu}N} \gg \frac{\gamma}{g}. \tag{3.45}$$

Similarly, the condition $\epsilon_\varphi \gg \epsilon_{Q_E}$ may be written for $\delta \ll 1$ using Eqs. (3.15), (3.16) as

$$\frac{3M_{\rm Pl}}{2\tilde{\mu}N} \gg \frac{\sqrt{\gamma}}{g}. \tag{3.46}$$

Indeed, we see that the condition $\epsilon_\varphi \gg \epsilon_{Q_B}$ is more restrictive, which agrees with our numerical simulations. The left-hand side of Eqs. (3.45), (3.46) is a fixed number that is set by the number of e-folds of inflation N and the scale $\tilde{\mu}$, that does not depend on the parameters of the potential $\tilde{\alpha}$ and n, and is uniquely fixed from the amplitude of the power spectrum of the scalar density perturbations. The range for allowed values for γ and g that satisfy Eq. (3.45) is shown in Fig. 3.5.

3.4 Tensor sector

In this Section we will analyze the tensor perturbations generated by the gauge fields. We will explicitly identify restrictions in the parameter space coming from the inflaton sector on the gravitational wave production by the gauge sector.

3.4.1 Tensor perturbations

In this subsection we adopt the notation of Ref. [233] for tensor perturbations in the gauge field and the metric. The tensor sector consists of four independent perturbations that are given by

$$\begin{aligned} \delta A^1_\mu = &\quad a(0, t_+, t_\times, 0), \quad \delta A^2_\mu = a(0, t_\times, -t_+, 0), \\ \delta g_{11} = &\; -\delta g_{22} = a^2 h_+, \quad \delta g_{12} = a^2 h_\times. \end{aligned} \tag{3.47}$$

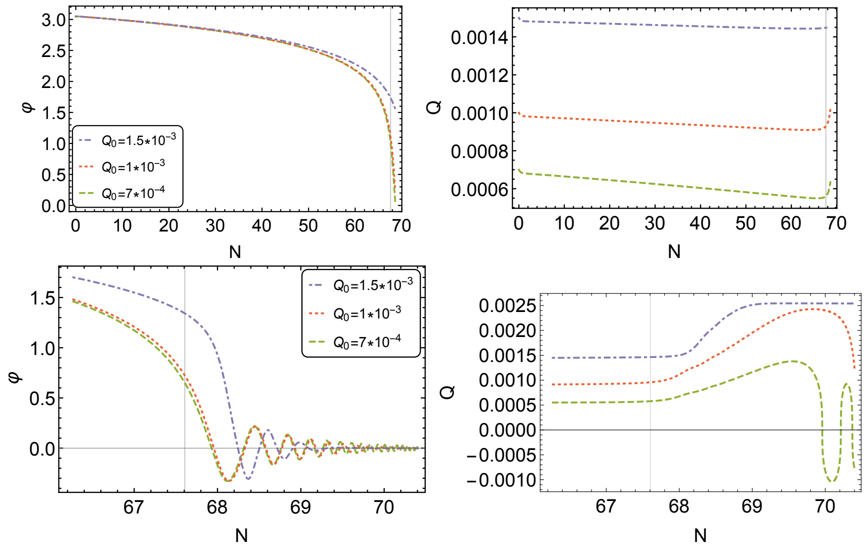

Figure 3.2: *Upper left:* The dependence of the inflaton field φ on the e-folding number N for the α-attractor T-model potential of Eq. (3.41) for $Q_0/M_{\rm pl} = 7\times10^{-4}, 1\times10^{-3}, 1.5\times10^{-3}$ (green-dashed, red-dotted and purple-dot-dashed lines respectively). The vertical grey grid line shows the end of inflation. *Upper right:* The dependence of the gauge field VEV Q on the e-folding number N for the same potential and color coding. The solid grey grid line shows the end of inflation. *Lower Left:* The evolution of the inflaton field φ after the end of inflation for the same parameters and color-coding. Lower right: The post-inflationary evolution of the gauge field VEV Q for the same parameters and color-coding.

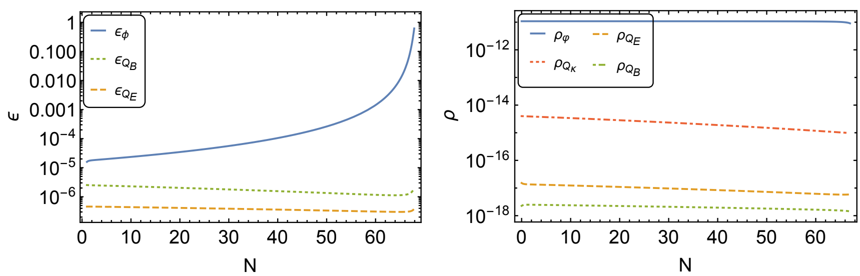

Figure 3.3: *Left:* The evolution of components of the first slow-roll parameter ϵ with the number of e-folds N for $Q_0/M_{\rm pl} = 7\times10^{-4}$. *Right:* The evolution of components of the energy-density ρ with the number of e-folds N for the same parameters.

The plus and cross polarizations are related to the left-handed and right-handed polarizations as

$$\begin{aligned} h_+ &= \frac{h_L + h_R}{\sqrt{2}}, \quad h_\times = \frac{h_L - h_R}{i\sqrt{2}}, \\ t_+ &= \frac{t_L + t_R}{\sqrt{2}}, \quad t_\times = \frac{t_L - t_R}{i\sqrt{2}}. \end{aligned} \tag{3.48}$$

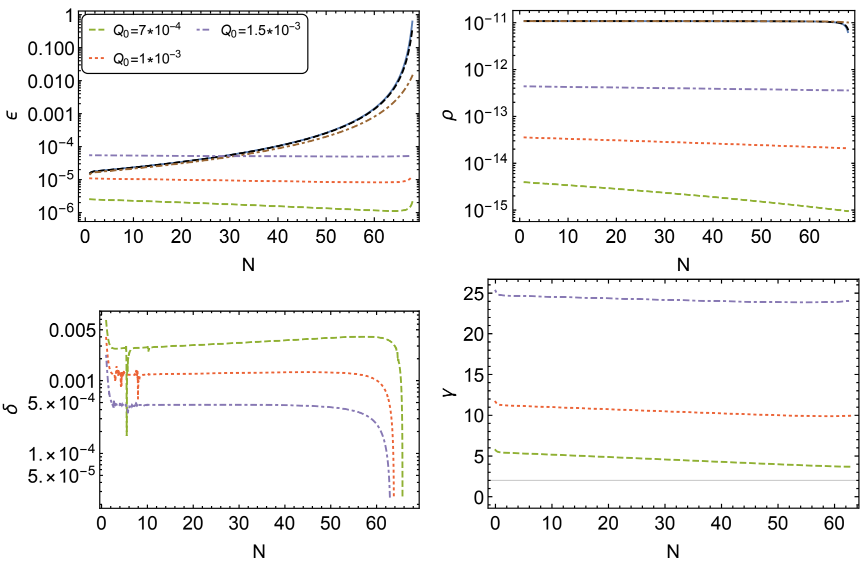

Figure 3.4: *Top left:* Components ϵ_{Q_B} as a function of the e-folding number N for $Q_0/M_{\rm pl} = 7\times 10^{-4}, 1\times 10^{-3}, 1.5\times 10^{-3}$ (green-dashed, red-dotted and purple-dot-dashed lines respectively). The blue-solid, black-dashed and brown-dot-dashed and curved correspond to ϵ_φ for $Q_0/M_{\rm pl} = 7\times 10^{-4}, 1\times 10^{-3}, 1.5\times 10^{-3}$ respectively. One can see that indeed $\gamma_{\rm max} \simeq 15$ is the maximally possible value for Gauge-flation to stay in the spectator sector for the given set of parameters. *Top right:* Components ρ_κ and their dependence on N for Q_0 and color-coding. The very top curves correspond to ρ_φ and are practically indistinguishable. *Bottom row:* The evolution of the parameter δ (left) and γ (right) for the same parameters and color-coding. The solid grey grid line on the right panel shows the bound $\gamma = 2$, below which scalar fluctuations in the theory are unstable.

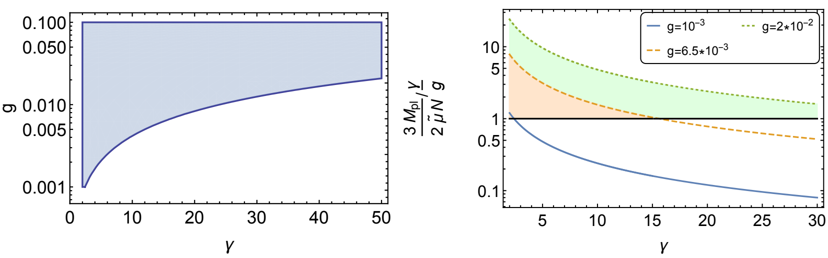

Figure 3.5: *Left:* The region plot for γ and g that satisfies Eq. (3.45) for $N = 60$. *Right:* The ratio $\frac{3M_{\rm Pl}}{2\tilde{\mu}N}/\frac{\gamma}{g}$ as a function of γ for $N = 60$ and $g = 10^{-3}, 6.5\times 10^{-3}, 2\times 10^{-2}$ (blue-solid, orange-dashed and green-dotted lines respectively). The black grid line shows when the ratio equals to 1.

We canonically normalise them by introducing

$$h_{L,R} = \frac{\sqrt{2}}{M_p a} H_{L,R}, \quad t_{L,R} = \frac{1}{\sqrt{2}a} T_{L,R}, \tag{3.49}$$

The action for canonically normalised perturbations reads

$$S_L = \frac{1}{2}\int d\tau d^3k \left[\Delta_L'^\dagger \Delta_L' + \Delta_L'^\dagger K_L \Delta_L - \Delta_L^\dagger K_L \Delta_L' - \Delta_L^\dagger \Omega_L^2 \Delta_L\right], \; \Delta_L = \begin{pmatrix} H_L \\ T_L \end{pmatrix}. \tag{3.50}$$

where the expression for the right-handed sector is identical. Prime $()'$ here denotes a derivative with respect to conformal time τ. The anti-symmetric matrix $K_{L/R}$ is defined through

$$K_{L/R,12} = \frac{1}{M_p}\left(Q' + \frac{a'}{a} Q\right), \tag{3.51}$$

and $\Omega^2_{L/R}$ is symmetric, with components

$$\Omega^2_{L/R,11} = k^2 - 2\frac{a'^2}{a^2} + \frac{3g^2a^2Q^4}{M_p^2} - \frac{(aQ)'^2}{M_p^2 a^2}, \tag{3.52}$$

$$\Omega^2_{L/R,12} = \pm k\frac{2gaQ^2}{M_p} + \frac{(aQ)'}{aM_p}\frac{a'}{a} - \frac{2\kappa g^2 Q^3}{M_p a^2}\frac{g^2a^4Q^4 + a'^2Q^2 - a^2Q'^2}{1+\kappa g^2 Q^4}, \tag{3.53}$$

$$\Omega^2_{L/R,22} = k^2 \mp 2kgaQ\left[1 + \kappa\frac{g^2a^4Q^4 + a'^2Q^2 - a^2Q'^2}{a^4(1+\kappa g^2Q^4)}\right] + \tag{3.54}$$
$$+\frac{2\kappa g^2Q^2}{a^2}\frac{g^2a^4Q^4 + a'^2Q^2 - a^2Q'^2}{1+\kappa g^2Q^4},$$

where signs refer to the left-handed or the right-handed polarization respectively, which we denote by "L/R". Now, we are going to use the background relations obtained in Section 3.2.2 to simplify the above matrix elements and expand them in slow-roll in order to identify limitations on the chiral gravitational wave production, coming from the presence of the inflaton field. It is convenient to rewrite the matrices in terms of ϵ, γ and δ. With substitutions coming from Eqs. (3.16), (3.23) and (3.24)

$$Q' \to -aQH\delta \quad , \quad a' \to a^2 H \quad , \quad \kappa \to \frac{1}{H^2\gamma Q^2}\frac{(1-\delta)^2+\gamma}{(1-\delta)^2}\frac{2 - \left(\epsilon_Q + \frac{2}{3}\epsilon_\varphi + \Upsilon\right)}{\epsilon_Q}, \tag{3.55}$$

$$M_p \to Q\sqrt{\frac{(1-\delta)^2+\gamma}{\epsilon_Q}} \quad , \quad g \to \sqrt{\gamma}\frac{H}{Q}, \tag{3.56}$$

we find exact expressions for the matrices given by

$$K_{L/R,12} = \frac{aH\sqrt{\epsilon_Q}}{\sqrt{(1-\delta)^2+\gamma}}(1-\delta), \tag{3.57}$$

$$\Omega^2_{L/R,11} = k^2 - a^2H^2\frac{(1-\delta)^2(2+\epsilon_Q)+\gamma(2-3\epsilon_Q)}{(1-\delta)^2+\gamma}, \tag{3.58}$$

$$\begin{aligned}\Omega^2_{L/R,12} = \pm aHk\frac{2\sqrt{\gamma\epsilon_Q}}{\sqrt{(1-\delta)^2+\gamma}} - a^2H^2\frac{\sqrt{\epsilon_Q}}{\sqrt{(1-\delta)^2+\gamma}}\cdot \\ \cdot\Bigg[\frac{(2\gamma^2+3\gamma(1-\delta))(2-\Upsilon-(\epsilon_Q+2/3\epsilon_\varphi))+}{(2-\Upsilon-2/3\epsilon_\varphi)(1-\delta)^2+\gamma(2-\Upsilon-(\epsilon_Q+2/3\epsilon_\varphi))}+ \\ +\frac{(1-\delta)^3(2-\Upsilon-2\epsilon_Q-2/3\epsilon_\varphi+2\delta(2-\Upsilon-(\epsilon_Q+2/3\epsilon_\varphi)))}{(2-\Upsilon-2/3\epsilon_\varphi)(1-\delta)^2+\gamma(2-\Upsilon-(\epsilon_Q+2/3\epsilon_\varphi))}\Bigg],\end{aligned} \tag{3.59}$$

$$\begin{aligned}\Omega^2_{L/R,22} = k^2 \mp 2aHk\frac{1}{\sqrt{\gamma}}\cdot \\ \cdot\Bigg[\frac{(2\gamma^2+(1-\delta)^3(1+\delta))(2-\Upsilon-(\epsilon_Q+2/3\epsilon_\varphi))}{(2-\Upsilon-2/3\epsilon_\varphi)(1-\delta)^2+\gamma(2-\Upsilon-(\epsilon_Q+2/3\epsilon_\varphi))}+ \\ +\frac{\gamma(1-\delta)(3(2-\Upsilon)-\delta(2-\Upsilon-2/3\epsilon_\varphi)-2\epsilon)}{(2-\Upsilon-2/3\epsilon_\varphi)(1-\delta)^2+\gamma(2-\Upsilon-(\epsilon_Q+2/3\epsilon_\varphi))}\Bigg]+ \\ +2a^2H^2\frac{(2-\Upsilon-(\epsilon_Q+2/3\epsilon_\varphi))(\gamma^2+2(1-\delta)\gamma+(1+\delta)(1-\delta)^3)}{(2-\Upsilon-2/3\epsilon_\varphi)(1-\delta)^2+\gamma(2-\Upsilon-(\epsilon_Q+2/3\epsilon_\varphi))}.\end{aligned} \tag{3.60}$$

Now, we substitute ϵ_Q and δ from Eq. (3.22), i.e.

$$\epsilon_Q \to \epsilon - \epsilon_\varphi \quad , \quad \delta \to \frac{\epsilon}{3(2-\Upsilon-(\epsilon-\frac{1}{3}\epsilon_\varphi))}\left(\epsilon - \frac{2}{3}\frac{\epsilon_\varphi}{\epsilon}\eta_\varphi - \frac{\epsilon_\varphi}{3} + \Upsilon\left(1-\frac{\epsilon_\varphi}{\epsilon}\right)\right) \tag{3.61}$$

and expand the matrix elements in slow roll with $\epsilon \ll 1$ and $\epsilon_\varphi \ll 1$. The lowest order in slow-roll quantities is $\sqrt{\epsilon}$, where we obtain

$$K_{L/R,12} \simeq aH\frac{\sqrt{\epsilon}}{\sqrt{1+\gamma}}C_1(\epsilon_\varphi), \tag{3.62}$$

$$\Omega^2_{L/R,11} \simeq k^2 - 2a^2H^2, \tag{3.63}$$

$$\Omega^2_{L/R,12} \simeq \left(\pm 2kaH\frac{\sqrt{\gamma\epsilon}}{\sqrt{1+\gamma}} - a^2H^2\frac{1+2\gamma}{\sqrt{1+\gamma}}\sqrt{\epsilon}\right)C_1(\epsilon_\varphi), \tag{3.64}$$

$$\Omega^2_{L/R,22} \simeq k^2 \mp 2kaH\frac{1}{\sqrt{\gamma}}\left[1+2\gamma+C_2(\epsilon_\varphi)\right] + 2a^2H^2\left[1+\gamma+C_2(\epsilon_\varphi)\right], \tag{3.65}$$

where we introduced the “correction” coefficients

$$C_1(\epsilon_\varphi) = \sqrt{1 - \frac{\epsilon_\varphi}{\epsilon}}, \tag{3.66}$$

$$C_2(\epsilon_\varphi) = -\frac{\epsilon}{2 - \Upsilon}\left(1 - \frac{\epsilon_\varphi}{\epsilon}\right) + \mathcal{O}\left(\epsilon\right). \tag{3.67}$$

Notice that when the inflaton field dominates the energy budget, Eq. (3.10) leads to $\Upsilon \sim 2$. Hence the second correction can be $\frac{\epsilon}{2-\Upsilon}\left(1 - \frac{\epsilon_\varphi}{\epsilon}\right) \sim \sqrt{\epsilon}$ and is not negligible any more. For the case $\epsilon_\varphi = 0$ and $\Upsilon = 0$, matrix elements reduce to the case of pure Gauge-flation and agree with the results obtained in Ref. [233]. The absolute value of the corrections $C_1(\epsilon_\varphi)$ and $C_2(\epsilon_\varphi)$ depend on the fraction of energy stored in the inflaton field, i.e. $\epsilon_\varphi/\epsilon$. There is an interesting “tug of war” between two different effects here.

- Since $1 - \epsilon_\varphi/\epsilon = \epsilon_Q/\epsilon$, GW production by the gauge sector requires $\epsilon_\varphi/\epsilon$ to deviate somewhat from unity.

- The requirement that the gauge-sector does not affect the dynamics of inflation and the generation of density fluctuations is encoded in $\epsilon_\varphi \gg \epsilon_Q$ or $\epsilon_Q/\epsilon \ll 1$.

Both requirements, the dominance of the inflaton sector and significant GW production by the gauge sector, can be simultaneously satisfied, but limit the available parameter space.

The equation of motion for tensor perturbations follows from Eq. (3.50) and may be written in the form

$$\Delta_L'' + 2K_L\Delta_L' + (K_L' + \Omega_L^2)\Delta_L = 0, \tag{3.68}$$

and similarly for the right-handed sector. To leading order in $\sqrt{\epsilon}$ and neglecting interactions with the gravitational wave sector, the equation of motion for the gauge field perturbation reads

$$\partial_\tau^2 T_L + \Omega_{L,22}^2 T_L = 0. \tag{3.69}$$

Substituting the matrix $\Omega_{L,22}^2$ explicitly with $\tau = -\frac{1}{aH}$ we get

$$\partial_\tau^2 T_L + \left(k^2 - \frac{2k}{-\tau}\frac{1 + 2\gamma + C_2(\epsilon_\varphi)}{\sqrt{\gamma}} + \frac{2\left(1 + \gamma + C_2(\epsilon_\varphi)\right)}{\tau^2}\right) T_L = 0. \tag{3.70}$$

Now, we may define $z = 2ik\tau$ and

$$\hat{\nu} = \frac{2\left(1 + 2\gamma + C_2(\epsilon_\varphi)\right)}{\sqrt{\gamma}} = -2i\hat{\alpha}, \tag{3.71}$$

$$\hat{\mu} = 2\left(1 + \gamma + C_2(\epsilon_\varphi)\right) = \frac{1}{4} - \hat{\beta}^2, \tag{3.72}$$

in order to rewrite Eq. (3.70) in the form of the Whittaker equation

$$\partial_z^2 T_L + \left(-\frac{1}{4} + \frac{\hat{\alpha}}{z} + \frac{\frac{1}{4} - \hat{\beta}^2}{z^2}\right) T_L = 0. \tag{3.73}$$

It can be solved with the Whittaker functions

$$T_{L,0}(k,\tau) = A_k M_{\hat{\alpha},\hat{\beta}}(2ik\tau) + B_k W_{\hat{\alpha},\hat{\beta}}(2ik\tau), \tag{3.74}$$

with $M_{\hat{\alpha},\hat{\beta}}(2ik\tau)$ and $W_{\hat{\alpha},\hat{\beta}}(2ik\tau)$ being the Whittaker M and W functions. Here the subscript 0 indicates that we neglected interactions with the gravitational wave sector. In the asymptotic past $x \equiv -k\tau \to \infty$, the solution approaches the Bunch-Davies vacuum, i.e.

$$T_{L,0}(k,\tau) \to \frac{1}{\sqrt{2k}} e^{ix}. \tag{3.75}$$

Asymptotic expansions for the Whittaker functions in this limit are also well-known, hence the constants A_k and B_k in (3.74) are given by [232]

$$A_k = \frac{1}{\sqrt{2k}} \frac{\Gamma\left(-\hat{\alpha} + \hat{\beta} + \frac{1}{2}\right)}{(2i)^{-\hat{\alpha}}\Gamma\left(2\hat{\beta} + 1\right)}, \tag{3.76}$$

$$B_k = \frac{1}{\sqrt{2k}} \frac{\Gamma\left(-\hat{\alpha} + \hat{\beta} + \frac{1}{2}\right)}{\Gamma\left(\hat{\alpha} + \hat{\beta} + \frac{1}{2}\right)} 2^{\hat{\alpha}} i^{\hat{\beta}+1} (-i)^{\hat{\alpha}-\hat{\beta}}. \tag{3.77}$$

Next, we find that metric tensor modes to leading order in $\sqrt{\epsilon}$ satisfy the following equation of motion in the x-variable

$$\partial_x^2 H_L + \left(1 - \frac{2}{x^2}\right) H_L = \frac{\sqrt{\epsilon}\, C_1(\epsilon_\varphi)}{\sqrt{1+\gamma}} \left(\frac{2}{x}\partial_x T_L + \left(\frac{2\gamma}{x^2} - \frac{2\sqrt{\gamma}}{x}\right) T_L\right). \tag{3.78}$$

Using the Born approximation, one may find the solution of Eq. (3.78) in series of $\sqrt{\epsilon}$

$$H_L = H_{L,0} + H_{L,s}, \tag{3.79}$$

where $H_{L,0}$ is the homogeneous solution of the free equation of motion, and $H_{L,\mathrm{s}}$ is inhomogeneous part that is sourced by the gauge filed perturbation T_L. The homogeneous solution matches the Bunch-Davies vacuum at asymptotic past and is given by

$$H_{L,0} = \frac{1}{\sqrt{2k}}\left(1+\frac{i}{x}\right)e^{ix}. \tag{3.80}$$

The sourced piece of the solution may be written as

$$H_{L,s} = \frac{\sqrt{\epsilon}\,C_1(\epsilon_\varphi)}{\sqrt{1+\gamma}}\int^x dx'\left(\frac{2}{x'}\partial_{x'}+\left(\frac{2\gamma}{x'^2}-\frac{2\sqrt{\gamma}}{x'}\right)\right)G(x,x')T_{L,0}(x'), \tag{3.81}$$

where $G(x,x')$ is the Green's function. We can follow the same steps as in Refs. [229, 231, 232] and find that the late-time solution for the left-handed gravitational wave is given by

$$H_L = \frac{Hx}{M_{\mathrm{Pl}}\sqrt{k^3}}u_1(x)+2\sqrt{2}\frac{H}{M_{\mathrm{Pl}}k}B_k\frac{2\sqrt{\epsilon}\,C_1(\epsilon_\varphi)}{\sqrt{1+\gamma}}\left(I_1+\sqrt{\gamma}I_2-\gamma I_3\right), \tag{3.82}$$

which contains a free and a sourced part of the solution. Here we have defined

$$u_1(x) \equiv \left(1+\frac{i}{x}\right)e^{ix}. \tag{3.83}$$

The terms I_1, I_2, I_3 are coming from the integrals in Eq. (3.81) and expressed as

$$I_1 = \frac{\left(\hat{\mu}^2-2i\hat{\mu}\hat{\nu}+2\hat{\mu}-2\hat{\nu}^2\right)\sec(\pi\hat{\beta})\sinh(-i\pi\hat{\alpha})\Gamma(\hat{\alpha})}{2\hat{\mu}(\hat{\mu}+2)} \tag{3.84}$$

$$-\frac{\pi^2\left(\hat{\mu}^2+2i\hat{\mu}\hat{\nu}+2\hat{\mu}-2\hat{\nu}^2\right)\sec(\pi\hat{\beta})\mathrm{csch}(-i\pi\hat{\alpha})}{2\hat{\mu}(\hat{\mu}+2)\Gamma(\hat{\alpha}+1)\Gamma(-\hat{\alpha}-\hat{\beta}+\frac{1}{2})\Gamma(-\hat{\alpha}+\hat{\beta}+\frac{1}{2})}, \tag{3.85}$$

$$I_2 = \frac{\pi\sec(\pi\hat{\beta})\Gamma(-\hat{\alpha})}{2\Gamma(-\hat{\alpha}-\hat{\beta}+\frac{1}{2})\Gamma(-\hat{\alpha}+\hat{\beta}+\frac{1}{2})}-\frac{\pi\sec(\pi\hat{\beta})\Gamma(1-\hat{\alpha})}{\hat{\mu}\Gamma(-\hat{\alpha}-\hat{\beta}+\frac{1}{2})\Gamma(-\hat{\alpha}+\hat{\beta}+\frac{1}{2})}$$

$$+\frac{\pi\hat{\mu}\sec(\pi\hat{\beta})-i\pi\hat{\nu}\sec(\pi\hat{\beta})}{2\hat{\mu}\Gamma(1-\hat{\alpha})}, \tag{3.86}$$

$$I_3 = \frac{\pi^2\left(\hat{\mu}+i\hat{\nu}\right)\sec(\pi\hat{\beta})\mathrm{csch}(-i\pi\hat{\alpha})}{\hat{\mu}(\hat{\mu}+2)\Gamma(\hat{\alpha})\Gamma(-\hat{\alpha}-\hat{\beta}+\frac{1}{2})\Gamma(-\hat{\alpha}+\hat{\beta}+\frac{1}{2})}+\frac{\pi\left(\hat{\nu}+i\hat{\mu}\right)\sec(\pi\hat{\beta})}{\hat{\mu}(\hat{\mu}+2)\Gamma(-\hat{\alpha})}. \tag{3.87}$$

The homogeneous solution for the gauge field perturbation $T_{L,0}$ is an excellent approximation, since it breaks down for $x \lesssim 0.1$, which does not influence gravitational wave modes which are sourced around horizon crossing $x \simeq 1$. Indeed, we see that the late-time solution of Eq. (3.82) is in a remarkable agreement with full numerical simulations, as seen on Fig. 3.6.

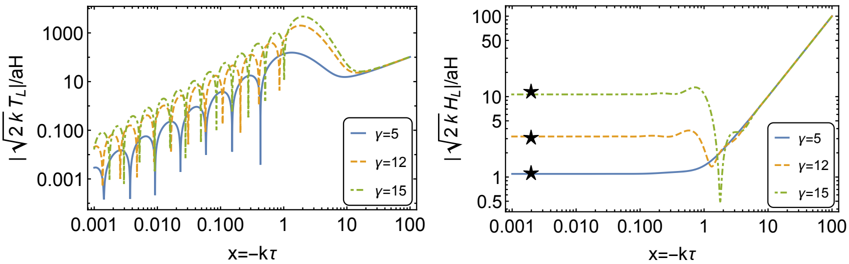

Figure 3.6: *Left:* Tachyonic growth of the left-polarized gauge field mode-function T_L around the time of horizon crossing $x = 1$ for $\gamma = 5, 12, 15$ (blue solid, orange dashed and green dot-dashed lines respectively), $H/M_{\rm pl} = 1.9 * 10^{-6}$ and $g = 6.5 * 10^{-3}$. *Right:* Enhancement of the left-polarized GW mode-function H_L, sourced by the gauge field mode-function T_L for the same parameters and color coding. Stars represent the approximate late-time solutions given by Eq. (3.82).

The right-hand polarized gravitational waves do not get enhanced and are given by the usual vacuum value

$$H_R(x) = \frac{Hx}{M_{\rm Pl}\sqrt{k^3}} u_1(x). \tag{3.88}$$

Finally, the power spectra for left-handed modes can be written as

$$P_L^2(k) = \frac{H^2}{2\pi^2 M_{\rm Pl}^2} + \frac{16kH^2}{\pi^2 M_{\rm Pl}^2} \frac{\epsilon\, C_1^2(\epsilon_\varphi)}{1+\gamma} |B_k|^2 \left| I_1 + \sqrt{\gamma} I_2 - \gamma I_3 \right|^2 . \tag{3.89}$$

The power spectra for right-handed modes is

$$P_R^2(k) = \frac{H^2}{2\pi^2 M_{\rm Pl}^2}. \tag{3.90}$$

The total tensor power spectrum is given by

$$P_T(k) = 2P_L^2(k) + 2P_R^2(k), \tag{3.91}$$

which in the limit $\epsilon \to \epsilon_\varphi$, i.e. $C_1(\epsilon_\varphi) \to 0$, reduces to the single scalar field result

$$P_{T,\varphi}(k) = \frac{2H^2}{\pi^2 M_{\rm Pl}^2}, \tag{3.92}$$

Finally, we can define the chirality parameter as

$$\Delta\chi = \frac{P_L^2 - P_R^2}{P_L^2 + P_R^2}. \tag{3.93}$$

Its behaviour is shown on Fig. 3.7. We see that sufficient enhancement of

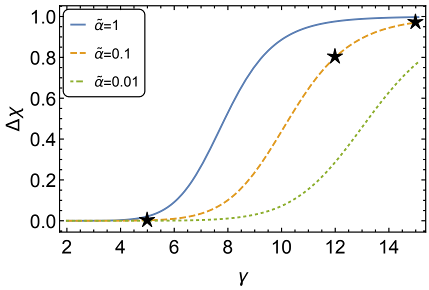

Figure 3.7: The chirality parameter $\Delta\chi$ as a function of γ for $\tilde{\alpha} = 1, 0.1, 0.01$ (blue solid, orange dashed and green dot-dashed lines respectively) for $H/M_{\rm pl} = 1.9 * 10^{-6}$, $g = 6.5 * 10^{-3}$. Stars represent $\gamma = 5, 12, 15$ used in Fig. (3.6).

one of the polarizations occurs for $\gamma \gtrsim 8$ for the given set of parameters ($H = 1.9 \times 10^{-6} M_{\rm pl}$, $\epsilon = 10^{-5}$, $g = 6.5 \times 10^{-3}$). For these parameters $\gamma_{\rm max} \simeq 15$.

3.4.2 Tensor tilt

In this subsection we will discuss the shape of the tensor power spectrum generated in the spectator Gauge-flation model, characterized by the tensor tilt n_T. In Ref. [239], it was shown that the spectator Chromo-natural inflation model, depending on the choice of the axion potential, supports both flat, red and blue tilted tensor spectra. Thus, our primary interest is to investigate if spectator Gauge-flation may generate all three possible tilts in realistic physical set-ups. The tensor tilt for Eq. (3.92) is given by $n_T = -2\epsilon_*$, where ϵ is evaluated at $t = t_*$ that defines time of horizon crossing for a mode with the wave number $k_* = a(t_*)H$. Below we will focus on the tilt for the sourced part only.

The power spectra of sourced gravitational waves from Eqs. (3.89) and (3.91) are given by

$$P_{T,s}(k) = \frac{32kH^2}{\pi^2 M_{\rm Pl}^2} \frac{\epsilon\, C_1^2(\epsilon_\varphi)}{1+\gamma} |B_k|^2 \left|I_1 + \sqrt{\gamma} I_2 - \gamma I_3\right|^2 . \tag{3.94}$$

We are going to proceed as follows: first we rewrite Eq. (3.94) in terms of $\gamma(t)$, restoring its time-dependence, and then re-express $P^2_{T,s}(k)$ in terms of $\gamma(k)$. This allows us to calculate the tensor tilt.

The time evolution of the vacuum expectation value of the gauge field $Q(t)$ may be written as

$$Q(t) = Q(t_*) + \dot{Q}(t_*)(t - t_*), \tag{3.95}$$

with t_* being the time of horizon crossing. From here it follows that

$$\frac{Q(t)}{Q(t_*)} = 1 - \delta_* H(t - t_*), \tag{3.96}$$

where $\delta_* = -\frac{\dot{Q}(t_*)}{HQ(t_*)}$. This gives the time dependence of the parameter $\gamma(t)$, i.e.

$$\gamma(t) = \gamma_* \left(\frac{Q(t)}{Q(t_*)}\right)^2 = \gamma_* \left(1 - \delta_* H(t - t_*)\right)^2 \simeq \gamma_* \left(1 + 2\frac{H(t - t_*)}{\Delta N}\right), \tag{3.97}$$

with $\gamma_* = \frac{g^2 Q^2(t_*)}{H^2}$, $\Delta N = -1/\delta_*$. Using $H(t - t_*) = \ln(k/k_*)$ we can write $\gamma(k)$ as

$$\gamma(k) \simeq \gamma_* \left(1 + 2\frac{\ln(k/k_*)}{\Delta N}\right) \simeq \gamma_* e^{\left(\frac{2\ln(k/k_*)}{\Delta N}\right)}. \tag{3.98}$$

To start with, using $|\Gamma(\frac{1}{2} + ib)|^2 = \frac{\pi}{\cosh(\pi b)}$ one can rewrite $|B_k|^2$ defined in Eq. (3.76) in terms of $\gamma(t)$ as

$$|B_k|^2 = \frac{1}{2k} e^{3\pi\left(\frac{1+2\gamma}{\sqrt{\gamma}}\right)} e^{-\pi\sqrt{7+8\gamma}} \frac{1 + e^{-\pi\left(\sqrt{7+8\gamma} + \frac{2(1+2\gamma)}{\sqrt{\gamma}}\right)}}{1 + e^{-\pi\left(\sqrt{7+8\gamma} - \frac{2(1+2\gamma)}{\sqrt{\gamma}}\right)}}. \tag{3.99}$$

Next, from Eq. (3.17) for $\delta \ll 1$ one can find

$$\epsilon\, C_1^2(\epsilon_\varphi) = \epsilon_Q \simeq \frac{H^2}{g^2 M_{\rm Pl}^2} \gamma(1 + \gamma). \tag{3.100}$$

The term γI_3 generates the main contribution in Eq. (3.94), hence we will neglect smaller contributions coming from $I_1, \sqrt{\gamma} I_2$. In terms of γ we find

$$\gamma^2 \left|I_3\right|^2 = \gamma^2 \frac{\pi\,(1 + 2\gamma)(1 + \gamma(1 + \gamma)(5 + \gamma))}{\gamma^{3/2}(1 + \gamma)^2(2 + \gamma)^2} e^{-\pi\left(\sqrt{7+8\gamma} - \frac{1+2\gamma}{\sqrt{\gamma}}\right)}. \tag{3.101}$$

Putting everything together, the sourced tensor power spectrum becomes

$$P_{T,s}(k) \simeq \frac{16H^4}{\pi^2 g^2 M_{\rm Pl}^4}\gamma\, e^{3\pi\left(\frac{1+2\gamma}{\sqrt{\gamma}}\right)} e^{-\pi\sqrt{7+8\gamma}}\, \frac{1+e^{-\pi\left(\sqrt{7+8\gamma}+\frac{2(1+2\gamma)}{\sqrt{\gamma}}\right)}}{1+e^{-\pi\left(\sqrt{7+8\gamma}-\frac{2(1+2\gamma)}{\sqrt{\gamma}}\right)}}\,|\gamma I_3|^2\,, \tag{3.102}$$

where $|\gamma I_3|^2$ is given by Eq. (3.101). Next, one may expand

$$\sqrt{7+8\gamma} = \sqrt{7+8\gamma_*} + \frac{8\gamma_*}{\sqrt{7+8\gamma_*}\Delta N}\ln\left(\frac{k}{k_*}\right) - \frac{32\gamma_*^2}{(7+8\gamma_*)^{3/2}(\Delta N)^2}\ln^2\left(\frac{k}{k_*}\right), \tag{3.103}$$

$$\frac{1+2\gamma}{\sqrt{\gamma}} = \frac{1+2\gamma_*}{\sqrt{\gamma_*}} + \frac{2\gamma_*-1}{\sqrt{\gamma_*}\Delta N}\ln\left(\frac{k}{k_*}\right) - \frac{\gamma_*-3/2}{\sqrt{\gamma_*}(\Delta N)^2}\ln^2\left(\frac{k}{k_*}\right). \tag{3.104}$$

We will not write the final expression for $P_{T,s}(k)$ in terms of γ_*, k, k_* since it is rather cumbersome, but may be easily written from the above expressions. Instead, we will focus on the tensor tilt. As usual, the tensor power spectra may be written in the form

$$P_{T,s}(k) = A_T(\gamma_*)\left(\frac{k}{k_*}\right)^{n_{T,s}}, \tag{3.105}$$

with the tensor tilt is given by

$$\begin{aligned} n_{T,s} = \frac{d\ln P_{T,s}(k)}{d\ln k} =& -\delta_*\Big[3 + 4\pi\frac{2\gamma_*-1}{\sqrt{\gamma_*}} - 16\pi\frac{\gamma_*}{\sqrt{7+8\gamma_*}} \\ & - \frac{2\gamma_*(-8-39\gamma_*-57\gamma_*^2-23\gamma_*^3+\gamma_*^4)}{(1+\gamma_*)(2+\gamma_*)(1+2\gamma_*)(1+5\gamma_*+6\gamma_*^2+\gamma_*^3)} \\ & - \pi\frac{\frac{8\gamma_*}{\sqrt{7+8\gamma_*}}+2\frac{2\gamma_*-1}{\sqrt{\gamma_*}}}{1+e^{\pi\left(\sqrt{7+8\gamma_*}+2\frac{1+2\gamma_*}{\sqrt{\gamma_*}}\right)}} + \pi\frac{\frac{8\gamma_*}{\sqrt{7+8\gamma_*}}-2\frac{2\gamma_*-1}{\sqrt{\gamma_*}}}{1+e^{\pi\left(\sqrt{7+8\gamma_*}-2\frac{1+2\gamma_*}{\sqrt{\gamma_*}}\right)}}\Big], \end{aligned} \tag{3.106}$$

where we neglected corrections $\mathcal{O}\left(\delta_*^2\right)$ and ignored the time-dependence of H. For α-attractors, as well as other plateau models, this is a very good approximation. The complicated expression above may be written via a simple fitting formula

$$n_{T,s} \simeq -\delta_*\left(3 + 1.225\pi\frac{2\gamma_*-1}{\sqrt{\gamma_*}} - 3.612\pi\frac{\gamma_*}{\sqrt{7+8\gamma_*}}\right) \simeq -\delta_*\left(2.85 + 3.68\sqrt{\gamma_*}\right). \tag{3.107}$$

Hence, we may conclude that if $Q(t)$ is a decreasing function of time, then $\delta(t)$ defined in Eq. (3.16) leads to δ_* being positive. Therefore, as follows from Eq. (3.107), a red-tilted power spectrum is generated. If, on the contrary, $Q(t)$ increases in time, $\delta(t)$ is negative, which sources a blue-tilted spectrum. We can sum up the relation of $Q(t)$ to n_T in the following table

$$\begin{array}{lllllllll} Q(t) \searrow & \Rightarrow & \dot{Q}(t) < 0 & \Rightarrow & \delta > 0 & \Rightarrow & n_T < 0 & \text{red tilt,} \\ Q(t) \nearrow & \Rightarrow & \dot{Q}(t) > 0 & \Rightarrow & \delta < 0 & \Rightarrow & n_T > 0 & \text{blue tilt.} \end{array} \tag{3.108}$$

All the results shown in Section 3.3 contain $Q(t)$ as a decreasing function of time, leading to red-tilted tensor spectra. Finally, Eq. (3.91) leads to the tensor-to-scalar ratio r

$$r = \frac{P_T}{P_\zeta}. \tag{3.109}$$

The left panel of Fig. 3.8 shows the enhancement of the tensor-to-scalar ratio r and its dependence on γ for the α-attractor potential of Eq. (3.41) with $n = 3/2$ and $\tilde{\alpha} = 10, 1, 0.1, 0.01$. We see that for small γ, we recover the single field α-attractor result $r = 16\epsilon$ with $\epsilon \to \epsilon_\varphi \simeq \frac{3\tilde{\alpha}}{4N^2}$. Further increasing r requires decreasing the gauge coupling g. However this is severely restricted by Eqs. (3.28) and (3.45), meaning that we cannot increase r significantly above what is show on Fig. 3.8. The right panel of Fig. 3.8 shows the correlation of Eq. (3.107) and r using Eq. (3.22). We see that $0 > n_T \gtrsim -0.04$ and larger r correlates with more red-tilted spectra.

Before we proceed to a brief overview of related models and comparison with our results on spectator gauge-flation, it is worth discussing the conditions for a red-tilted spectrum. It was shown in Ref. [76] that the original gauge-flation model can lead (at the background level) to both decreasing and growing functions of $Q(t)$, depending on the initial conditions. Trajectories starting close to the slow-roll attractor lead to a decreasing $Q(t)$. Trajectories that start far from the slow roll attractor in Ref. [76] were shown to undergo a brief period of $\epsilon > 1$, followed by a slow-roll inflationary phase with $Q(t)$ increasing in time. The latter behavior required different ranges of κ and g.

We were able to recover this general trend in our spectator model, at the cost of altering the parameter space of the model. In particular, to produce a growing $Q(t)$ and a correspondingly blue-tilted GW spectrum, we need to increase the value of κ. This leads to an increase in ρ_κ, which is bounded from above by the requirement $\rho_\kappa \ll \rho_\varphi$. Furthermore, γ is reduced for these trajectories, suppressing GW production by the spectator sector. In order to increase GW production, we need to increase g, which cannot be done arbitrarily. Such a realization of spectator gauge-flation is given in Appendix 3A. Our numerical tests have shown the existence of such solutions, but at the same time an increased level of parameter fine-tuning is needed to achieve them, at least in the context of an α-attractor inflationary sector. We will consider the red-tilted GW spectra as a "generic" prediction of spectator gauge-flation, keeping in mind the ability of these models to evade this prediction for proper choices of parameters and initial conditions. We leave an exhaustive parameter search for a variety of inflationary sectors for future work.

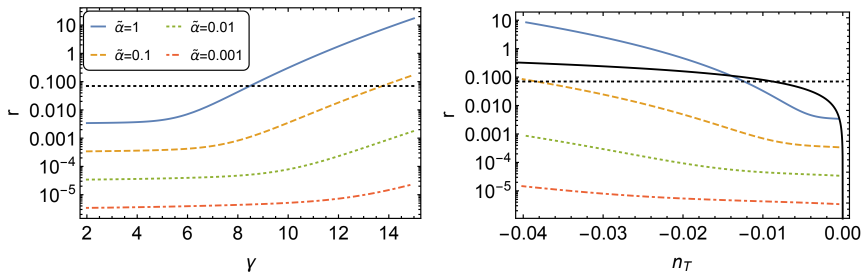

Figure 3.8: *Left:* The tensor-to-scalar ratio r as a function of γ for $g = 6.5 \times 10^{-3}$ and $\tilde{\alpha} = 1, 0.1, 0.01, 0.001$ (blue solid, orange dashed, green dotted and red dot-dashed lines respectively). The horizontal black-dotted curve shows the observational upper limit on r. *Right:* The tensor-to-scalar ratio r versus tensor tilt n_T for the same parameters and color coding. We can see the range of n_T and the clear departure from the single field consistency relation $n_T = -r/8$ (solid black curve).

3.4.3 Comparison with related models

The model presented here is part of a larger family of inflationary models, where the existence of a non-abelian sector leads to the generation of chiral GWs. We can distinguish between the original models, where the $SU(2)$ or axion$-SU(2)$ sectors are responsible for inflation and the generation of both scalar and tensor modes, and the spectator models, where the inflaton sector is decoupled from the non-abelian spectator sector. Gauge-flation and Chromo-natural inflation, along with their Higgsed variants, fit in the first category, while spectator Chromo-natural inflation and spectator Gauge-flation make up the second category.

While the original Chromo-natural inflation and Gauge-flation models are ruled out by observations, their Higgsed counterparts provide predictions compatible with CMB observations for some part of parameter space. Interesting features arise from the correlation of the resulting tensor to scalar ratio r and tensor spectral tilt n_T. For Higgsed gauge-flation, Ref. [232] showed a negative correlation between the two quantities. For $n \lesssim 0.01$ a blue-tilted spectrum is preferred. Hence Higgsed gauge-flation and spectator gauge-flation (with an α-attractor inflationary sector) tend to provide opposite predictions for the sign of n_T.

Higgsed chromo-natural inflation has an interesting space of predictions for n_T and r. For smaller values of $r < 0.01$, the correlation between r and n_T is also mostly negative. However the possible range of values for n_T is much larger, ranging between $-0.2 < n_T < 0.05$ for the parameter scan presented in Ref. [231]. This means that the possible range of values for Higgs Chromo-Natural inflation is significantly larger than that of our realization of spectator Gauge-flation (see Fig. 3.8) for red and blue tilted spectra alike.

Next, we wish to compare the present model to spectator Chromo-natural inflation, in which an axion$-SU(2)$ spectator sector is added to an otherwise dominant inflaton. The existence of an axion potential $V(\chi)$ leads for significant diversity in the form of the tensor power spectrum. Ref. [239] showed the emergence of a blue or red-tilted spectrum for monomial potential $V(\chi) \propto |\chi|^p$, where the tensor tilt scales as $n_T \propto (p-1)$. A linear potential leads to an exactly scale-invariant tensor spectrum. In principle, small deviations from $p = 1$ can lead to an arbitrarily small tensor tilt. However, this requires a rather fine-tuned axion potential. If instead we look at $p = 1/2$ and $p = 3/2$ we can see that $n_T \simeq 0.04$ and $n_T \simeq -0.07$ respectively. Concave potentials lead to blue-tilted spectra, which are generically not produced in our model of spectator Gauge-flation. On the other hand, convex potentials lead to red-tilted spectra, but for $p > 3/2$ the spectral tilt will be $n_T \lesssim \mathcal{O}(0.1)$, which is outside the predictions shown in Fig. 3.8.

Finally, Ref. [246] studied an axion-inflaton field coupled to an $SU(2)$ gauge field, where the VEV of the latter is not large enough to affect the background inflationary dynamics. Despite being subdominant, the presence of the gauge field can lead to the enhancement of GW's and the corresponding violation of the Lyth bound. The resulting tensor tilt n_T exhibits oscillations in time and asymptotes to zero at late times.

3.5 Summary and discussion

In this work we have explored the phenomenology of Gauge-flation as a spectator sector during inflation. We have uncovered significant parameter restrictions, arising both from the physics of the gauge sector as well as from the requirements that the gauge sector be subdominant to the inflationary sector. Most importantly, these requirements lead to significant constraints on the parameter γ, which controls the amount of GW enhancement.

By identifying the inflationary sector with the well-known T-model of α-attractors, we showed that a spectator gauge-flation sector can increase the tensor-to-scalar ratio by two orders of magnitude. The resulting tensor spectral index n_T is controlled by the evolution of the gauge field vacuum expectation value $Q(t)$, being red if Q is a decreasing function of time during inflation and blue otherwise. The majority of our numerical simulations resulted in red-tilted GW spectra with $-0.04 \lesssim n_T < 0$.

Our work presents an interesting generalization of gauge-flation, while opening up exciting possibilities for future work. While α-attractors provide a simple implementation of the inflationary sector, inflationary models that contain two or more distinct phases of inflation, like double inflation, side-tracked inflation and angular inflation, can help alleviate the parameter constraints of our current implementation and produce distinct GW features either at large or small scales. Furthermore, inflationary models with non-Abelian gauge fields can have interesting consequences for baryogenesis and dark matter production [247–250], leading to correlated observables.

Furthermore, the original choice of the higher-order term for gauge-flation was based on the requirement for a vacuum energy-like equation of state $w \simeq -1$, required for driving inflation. Using an $SU(2)$ sector as a spectator sector opens up the possibility of introducing more non-linear terms, since the requirement of $w \simeq -1$ is lifted. It is interesting to explore the phenomenology of gauge-flation with other non-linear terms, dictated solely by the underlying symmetries, and their possible GW signatures. We leave this exploration for future work.

3.6 Appendix 3A: Blue-tilted GW spectrum

As shown in Eq. (3.108), the dynamics of $Q(t)$ controls the sign of the tensor tilt n_T. Here we present a realization where $Q(t)$ is an increasing function of time on the example of α-attractor model, similarly as in Section 3.3, for the same parameters of Eq. (3.42) for the potential, but with $\tilde{\alpha} = 1$. The parameters we use for the gauge sector are

$$\begin{aligned} g = 1.7 \times 10^{-2}, \quad \kappa = 10^{21}\, M_{\rm pl}^{-4}, \\ \dot{Q}_0/M_{\rm pl}^2 = 10^{-10}, \quad Q_0/M_{\rm pl} = 6 \times 10^{-4}, 8 \times 10^{-4}, 1.18 \times 10^{-3}. \end{aligned} \tag{3.110}$$

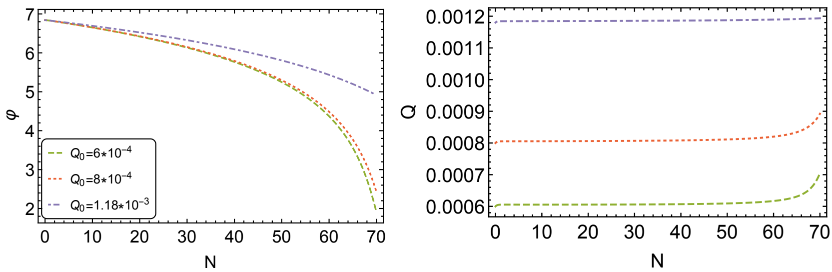

Figure 3.9: *Left:* The dependence of the inflaton field φ on the e-folding number N for the the α-attractor T-model potential of Eq. (3.41) for $Q_0/M_{\rm pl} = 6\times10^{-4}, 8\times10^{-4}, 1.18\times10^{-3}$ (green-dashed, red-dotted and purple-dot-dashed lines respectively). *Right:* The dependence of the gauge field VEV Q on the e-folding number N for the same potential and color coding.

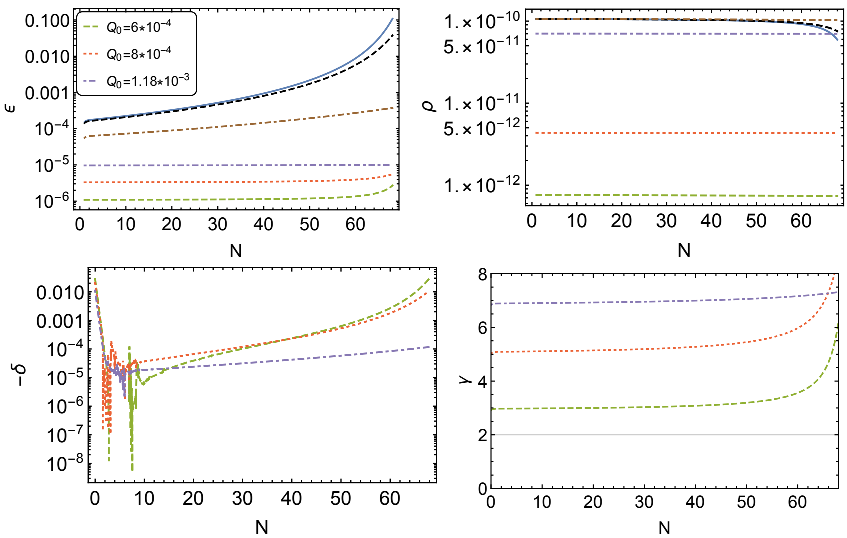

Figure 3.10: *Top left:* Components ϵ_{Q_B} as a function of the e-folding number N for $Q_0/M_{\rm pl} = 6\times10^{-4}, 8\times10^{-4}, 1.18\times10^{-3}$ (green-dashed, red-dotted and purple-dot-dashed lines respectively). The blue-solid, black-dashed and brown-dot-dashed and curved correspond to ϵ_φ for $Q_0/M_{\rm pl} = 6\times10^{-4}, 8\times10^{-4}, 1.18\times10^{-3}$ respectively. *Top right:* Components ρ_κ and their dependence on N for the same Q_0 and color-coding. The very top curves correspond to ρ_φ and are practically indistinguishable. *Bottom row:* The evolution of the parameter δ (left) and γ (right) for the same parameters and color-coding. The solid grey grid line on the right panel shows the bound $\gamma = 2$, below which scalar fluctuations in the theory are unstable.

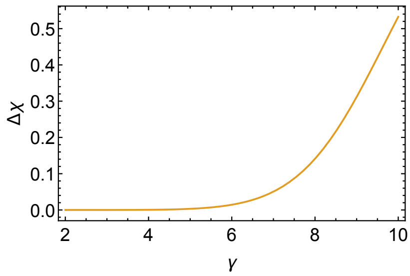

Figure 3.11: The chirality parameter $\Delta\chi$ as a function of γ for $\tilde{\alpha} = 1$, $H/M_{\rm pl} = 6 * 10^{-6}$ and $g = 1.7 * 10^{-2}$. In the allowed region $\gamma \lesssim 7$, the chirality parameter is small.

Our numerical simulations show that in order for $Q(t)$ to increase with time, one has to impose higher values of the parameter κ in comparison with those used in Section 3.3. Because of the conditions of Eqs. (3.33) and (3.39), this highly constrains the values of the allowed Q_0 and g, and hence via Eq. (3.16) limits the allowed range for the parameter γ that controls the enhancement of chiral gravitational waves.

Fig. 3.9 shows the evolution of the inflaton field φ and the vacuum expectation value of the gauge field Q with the e-folding number N, that behave similarly to those discussed in Section 3.3, but with Q being a slowly increasing function of time. In such case δ becomes negative, as shown in Fig. 3.10. However, one may see from the top right panel of the Fig. 3.10, that further increase of Q_0 will violate the condition $\rho_\varphi \gg \rho_{Q_\kappa}$. Hence for the parameters of Eq. (3.110), we compute the maximum $\gamma \simeq 7$. From Fig. 3.7 we can see that for this value the chirality parameter is only $\Delta\chi \simeq 0.05$, hence no significant production of sourced gauge fields has taken place. While this does not preclude the existence of a realization of this model, leading to significant r and $n_T > 0$, it demonstrates that this requires some level of parameter fine-tuning.

Part II

Reheating in curved field spaces

4 Universality and scaling in multi-field preheating

Abstract: We explore preheating in multi-field models of inflation in which the field-space metric is a highly curved hyperbolic manifold. One broad family of such models is called α-attractors, whose single-field regimes have been extensively studied in the context of inflation and supergravity. We focus on a simple two-field generalization of the T-model, which has received renewed attention in the literature. Krajewski et al. concluded, using lattice simulations, that multi-field effects can dramatically speed-up preheating. We recover their results and further demonstrate that significant analytical progress can be made for preheating in these models using the WKB approximation and Floquet analysis. We find a simple scaling behavior of the Floquet exponents for large values of the field-space curvature, that enables a quick estimation of the T-model reheating efficiency for any large value of the field-space curvature. In this regime we further observe and explain universal preheating features that arise for different values of the potential steepness. In general preheating is faster for larger negative values of the field-space curvature and steeper potentials. For very highly curved field-space manifolds preheating is essentially instantaneous.

Keywords: multi-field preheating, inflation.

Based on:

O. Iarygina, E. I. Sfakianakis, D. G. Wang and A. Achúcarro
Universality and scaling in multi-field α-attractor preheating.
JCAP **06**, 027 (2019), [arXiv:1810.02804].

4.1 Introduction

Inflation remains the leading paradigm for the very early universe, providing an elegant solution to the horizon and flatness problems of big bang cosmology [27, 28]. However, the biggest success of inflation is undoubtedly that it provides a framework for computing the primordial density fluctuations that can be observed as temperature variations of the Cosmic Microwave Background Radiation (CMB) and that provide the seeds for structure formation.

The recent results from the *Planck* satellite [53] are the latest in a long line of experiments, starting in 1989 with COBE, trying to constrain the characteristics of the primordial power spectrum through measuring the spectral index of scalar fluctuations (n_s). Attempts to measure the running of the spectral index α_s and the tensor to scalar ratio r have resulted so far only in placing upper bounds on both. While large-field models of inflation are tightly constrained and the simplest ones, like quadratic inflation, are practically ruled out, large families of models are still compatible with the data, providing predictions that match those of the Starobinsky model [251]

$$n_s = 1 - \frac{2}{N_*}\,, \quad r = \frac{12\alpha}{N_*^2} \tag{4.1}$$

where N_* is the time in e-folds where the CMB modes exit the horizon during inflation. The two main families of models that provide the observables of Eq. (4.1) are models with non-minimal coupling to gravity [154, 155] (sometimes called ξ-attractors[1]) and models with hyperbolic field-space geometry, also called α-attractors [50–52, 61]. Higgs inflation [156, 157] is an example of the former. For the Starobinsky model and ξ-attractors, $\alpha = 1$ in Eq. (4.1), hence the prediction for the tensor mode amplitude is fixed. For α-attractors, the parameter α corresponds to the curvature of the field-space, as we will see, hence the tensor power is suppressed for highly curved field-space manifolds [50–52]. At some level, the unifying feature of all these approaches can be attributed to a singularity in the kinetic sector [254]. We will focus only on α-attractors, drawing similarities and differences with the other observationally related models when necessary.

While a lot of theoretical and phenomenological work on inflation has focused on single-field scenarios, realistic models of high-energy particle

[1]It is worth noting that in the Palatini formulation of gravity the behavior and predictions of ξ-attractor models change significantly, as is discussed for example in Refs. [252, 253].

physics typically include many distinct scalar fields at high energies [255–259]. Furthermore, multiple fields with a curved field-space manifold (see e.g. [69, 95, 260–267]) can display a variety of effects, including non-gaussianities, isocurvature modes, imprints from heavy fields during turns in field space, curvature fluctuations from ultra-light entropy modes, as well as geometric destabilization of the inflationary trajectory [54, 55, 268, 313]. Several models that lead to the predictions of Eq. (4.1) display strong single field attractors [61, 154, 157] that persist during and after inflation. In particular, the multi-field analysis of α-attractors has become an interesting topic recently [61, 65, 66, 269–271].

During inflation, the inflaton field dominates the total energy density budget. However, the universe must be in a radiation dominated stage before Big Bang Nucleosynthesis (BBN), in order to produce the observed abundance of light elements [280–282] (see e.g. Refs. [273, 283–286] for recent reviews). The period during which the energy density locked in the inflaton condensate is transferred to radiation modes is called reheating. While inflation is tightly constrained by measurements of the CMB and Large Scale Structure [272–279], the period after inflation and before Big Bang Nucleosynthesis (BBN), provides far fewer observational handles, due to the very short length-scales involved. This is due to the fact that most dynamics during reheating takes place at sub-horizon scales, following causality arguments, hence it does not leave an imprint on larger scales, like the CMB[2]. Furthermore, the thermalization processes that have to occur before BBN wash out many of the "fingerprints" of reheating. Despite its inherent complexity, knowledge of the reheating era is essential, in order to relate inflationary predictions to present-day observations. The evolution history of the universe determines the relation between the times of horizon-crossing and re-entry of primordial fluctuations [161, 287–294]. Furthemore, preheating in multi-field models of inflation can alter the evolution of cosmological observables [93, 295–300].

The reheating era can proceed either through perturbative decay of the inflaton, or through non-perturbative processes, such as parametric and tachyonic resonance, also called preheating (see e.g. [133, 144, 149] and Ref. [118] for a review). A recent paper [160] used lattice simulations to compute the preheating behavior of a specific two-field realization of the T-model, a member of the α-attractor family [301]. In this paper we use

[2]While this is true for most models, there are well motivated cases where reheating can excite super-horizon modes and thus affect CMB observables. This does not occur for the α-attractor models that we are examining and we will not be discussing it further.

linear analysis to recover and interpret the results of Ref. [160] and examine their dependence on the potential steepness and field-space curvature. We find that the Floquet charts for a specific value of the potential steepness collapse into a single "master diagram" for small values of α when plotted against axes properly rescaled by the field-space curvature. Even for different potential parameters, the scaling behavior of the Floquet charts persists, albeit in an approximate rather than exact form. Overall we find slightly faster preheating for steeper potentials and for models with stronger field-space curvature. An important conclusion is that, in the limit of highly curved manifolds, preheating occurs almost instantaneously regardless of the exact form of the T-model potential. This is important for connecting the predictions of α-attractors to CMB observations.

The structure of the paper is as follows. In Section 4.2 we describe the model and study its background evolution, both during and after inflation. In Section 4.3 we review the formalism for computing fluctuations in multi-field models with non-trivial field-space metric. We also specify the form of the potential and analyze the resulting particle production using semi-analytic arguments, the WKB approximation and Floquet theory. Section 4.4 generalizes our results to different potentials. We conclude in Section 4.5.

4.2 Model

We consider a model consisting of two interacting scalar fields on a hyperbolic manifold of constant negative curvature. The specific Lagrangian corresponds to a two-field extension of the well-known T-model, as described in detail in Appendix 4A and Ref. [160], and can be written as

$$\mathcal{L} = -\frac{1}{2}\left(\partial_\mu\chi\partial^\mu\chi + e^{2b(\chi)}\partial_\mu\phi\partial^\mu\phi\right) - V(\phi,\chi)\,, \tag{4.2}$$

where $b(\chi) = \log\left(\cosh(\beta\chi)\right)$. The corresponding two-field potential is

$$V(\phi,\chi) = M^4\left(\frac{\cosh(\beta\phi)\cosh(\beta\chi)-1}{\cosh(\beta\phi)\cosh(\beta\chi)+1}\right)^n \left(\cosh(\beta\chi)\right)^{2/\beta^2}\,, \tag{4.3}$$

where $\beta = \sqrt{2/3\alpha}$ and $M^4 = \alpha\mu^2$[3]. For $\chi = 0$ the potential becomes

$$V(\phi,0) = M^4\left(\left(\tanh(\beta\phi/2)\right)^2\right)^n = M^4\tanh^{2n}(\beta|\phi|/2). \tag{4.4}$$

[3]In this Chapter the parameter α corresponds to $\tilde{\alpha}$ from Chapter 3.

The background equation of motion for $\phi(t)$ at $\chi(t) = 0$ is

$$\ddot{\phi} + 3H\dot{\phi} + \frac{2\sqrt{2}M^4 n}{\sqrt{3\alpha}}\mathrm{csch}\left(\sqrt{\frac{2}{3\alpha}}|\phi|\right)\tanh^{2n}\left(\frac{|\phi|}{\sqrt{6\alpha}}\right) = 0. \tag{4.5}$$

We rescale the inflaton field ϕ and the parameter α by the reduced Planck mass as $\phi = \tilde{\phi}M_{\rm Pl}$ and $\alpha = \tilde{\alpha}M_{\rm Pl}^2$. Finally, we rescale time by μ, leading to

$$\frac{d^2\tilde{\phi}}{d(\mu t)^2} + 3\frac{H}{\mu}\frac{d\tilde{\phi}}{d(\mu t)} + \frac{2\sqrt{2\tilde{\alpha}}\,n}{\sqrt{3}}\mathrm{csch}\left(\sqrt{\frac{2}{3\tilde{\alpha}}}|\tilde{\phi}|\right)\tanh^{2n}\left(\frac{|\tilde{\phi}|}{\sqrt{6\tilde{\alpha}}}\right) = 0, \tag{4.6}$$

where

$$\left(\frac{H}{\mu}\right)^2 = \frac{1}{3}\left[\frac{1}{2}\left(\frac{d\tilde{\phi}}{d(\mu t)}\right)^2 + \tilde{\alpha}\cdot\tanh^{2n}\left(\frac{|\tilde{\phi}|}{\sqrt{6\tilde{\alpha}}}\right)\right]. \tag{4.7}$$

In Ref. [160] an alternative rescaling of time was implicitly used, which we describe in Appendix 4C.

4.2.1 Single-field background motion

We start by analyzing the background motion of the ϕ and χ fields, in order to identify the regime of effectively single-field motion and describe CMB constraints on the model parameters. We initially assume that $\chi(t) = 0$ at background level, which is indeed a dynamical attractor, as we will show later. Eq. (4.6) in the slow-roll approximation and for $\tilde{\phi}/\sqrt{\tilde{\alpha}} \gg 1$, which holds during inflation, becomes

$$3H\dot{\tilde{\phi}} + \frac{4\left(\sqrt{2\alpha}n\right)}{\sqrt{3}}e^{-\sqrt{2}\tilde{\phi}/\sqrt{3\tilde{\alpha}}} \simeq 0, \tag{4.8}$$

where $H/\mu \simeq \sqrt{\tilde{\alpha}/3}$, leading to

$$\dot{\tilde{\phi}} = -\frac{4\sqrt{2}n}{3}e^{-\sqrt{2}\tilde{\phi}/\sqrt{3\tilde{\alpha}}}, \tag{4.9}$$

$$N = \frac{3\tilde{\alpha}}{8n}e^{\sqrt{\frac{2}{3\tilde{\alpha}}}\tilde{\phi}}. \tag{4.10}$$

The slow-roll parameters become

$$\epsilon \equiv -\frac{\dot{H}}{H^2} = \frac{16n^2}{3\tilde{\alpha}}e^{-2\sqrt{2}\tilde{\phi}/\sqrt{3\tilde{\alpha}}} \simeq \frac{3\tilde{\alpha}}{4N^2} \tag{4.11}$$

$$\eta \equiv \frac{\dot{\epsilon}}{\epsilon H} \simeq \frac{2}{N}. \tag{4.12}$$

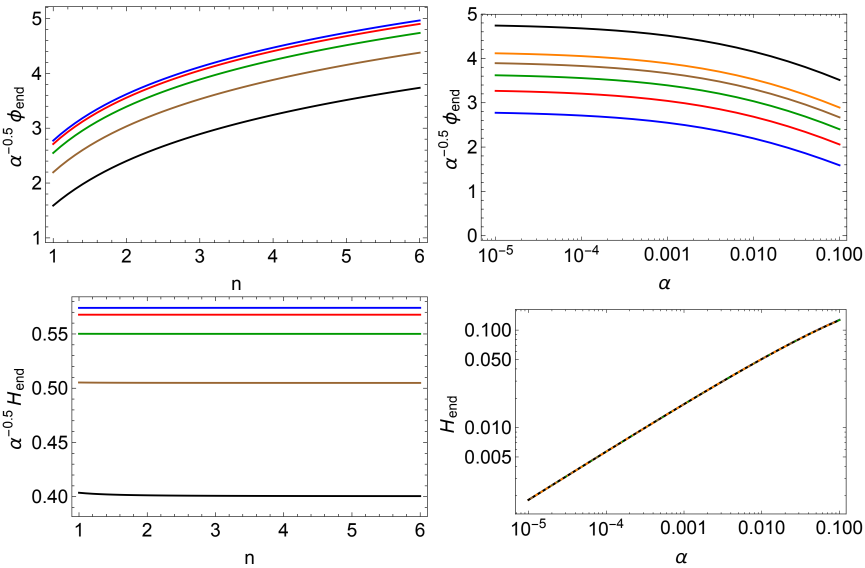

Figure 4.1: *Upper panels:* The rescaled background field at the end of inflation $\phi_{\rm end}/\sqrt{\alpha}$ as a function of n (left) and α (right). *Lower panels:* The rescaled Hubble parameter at the end of inflation $H_{\rm end}/\sqrt{\alpha}$ as a function of n (left) and α (right). The Hubble parameter is measured in units of μ. Color coding is as follows:
Left: $\alpha = 10^{-5}, 10^{-4}, 10^{-3}, 10^{-2}, 10^{-1}$ (blue, red, green, brown and black respectively).
Right: $n = 1, 1.5, 2, 2.5, 3, 5$ (blue, red, green, brown, orange and black respectively).

The end of inflation defined as $\epsilon = 1$, based on the slow-roll analysis, occurs at

$$\frac{\tilde{\phi}_{\rm end}}{\sqrt{\tilde{\alpha}}} = \frac{\sqrt{3}}{2\sqrt{2}}\left(\log\frac{16}{3} + 2\log n - \log\tilde{\alpha}\right). \tag{4.13}$$

The last term in Eq. (4.13) is subdominant for small $\tilde{\alpha}$ and can be safely ignored, leading to $\tilde{\phi}_{\rm end}/\sqrt{\tilde{\alpha}} \simeq 0.6(1.7 + 2\log n)$. Even though the slow-roll approximation fails near the end of inflation, the scaling $\tilde{\phi}_{\rm end}/\sqrt{\tilde{\alpha}} = \mathcal{O}(1)$ is valid over the whole range of potential parameters α and n that we considered, as shown in Fig. 4.1. The Hubble scale at $\epsilon = 1$ is

$$\frac{H_{\rm end}^2}{\mu^2} = \frac{1}{2}\tilde{\alpha}\cdot\tanh^{2n}\left(\frac{\tilde{\phi}_{\rm end}}{\sqrt{6\tilde{\alpha}}}\right) \sim \frac{1}{4}\tilde{\alpha}, \tag{4.14}$$

where the numerical factor in the last equality of Eq. (4.14) is fitted from the bottom right panel of Fig. 4.1.

The tensor-to-scalar ratio for single-field motion is

$$r = 16\epsilon \simeq 12\frac{\tilde{\alpha}}{N^2}. \tag{4.15}$$

In general $r = \alpha \times \mathcal{O}(10^{-3})$ for modes that exit the horizon at $N \sim 55$ e-folds before the end of inflation. The dimensionless power spectrum of the (scalar) density perturbations is measured to be

$$A_s \simeq 2 \times 10^{-9}\,. \tag{4.16}$$

Using the expression for the scalar power spectrum from single field slow-roll inflation

$$A_s = \frac{H^2}{8\pi^2 M_{\rm Pl}^2 \epsilon}, \tag{4.17}$$

and the value of the Hubble scale at the plateau of the potential $H^2 \simeq \tilde{\alpha}\mu^2/3$, it is straightforward to see that $\mu \sim 10^{-5} M_{\rm Pl}$. Hence the scale of μ fixes the amplitude of the scalar power spectrum, independent of α and n. By using μ to re-scale time, it is trivial to connect the preheating calculations performed in the present work to observational constraints on the potential parameters.

4.2.2 Initial condition dependence

It can be easily seen that the potential of Eq. (4.3) exhibits a minimum at $\chi = 0$ for all values of ϕ. However, the approach to this potential "valley" is important and could in principle leave observational signatures, if it occurs close to the time at which the CMB-relevant scales leave the horizon.

Fig. 4.2 shows the transition to the single-field trajectory for $n = 3/2$ and $\alpha = 0.001$. The initial conditions are $\phi_0 = \chi_0$, chosen such that there would be 60 e-folds of inflation for $\chi_0 = 0$. We see two distinct stages of inflation: initially $\phi(t)$ remains almost constant and $\chi(t)$ follows a slow-roll motion until it reaches the minimum $\chi = 0$. Then, after a sharp turn in field-space, the field $\phi(t)$ follows a slow-roll motion towards the global minimum of the potential, while χ stays exponentially close to zero. Hence to a good approximation, the whole inflationary era is separated into two sequential periods of distinct single-field motion.

Starting from a wide range of initial conditions $\phi_0 \equiv \phi(0)$ and $\chi_0 \equiv \chi(0)$, we see that the system generically follows the two-stage evolution shown in Fig. 4.2, proceeding along $\chi(t) = 0$ during the last stage of inflation and during the post-inflationary oscillations. Figure 4.3 shows the transition

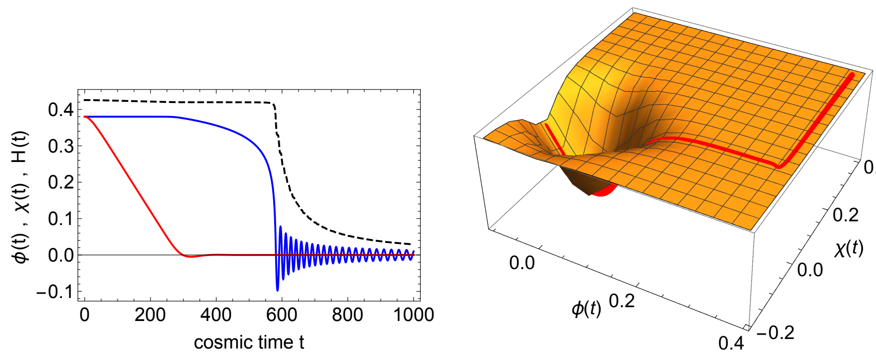

Figure 4.2: *Left:* A characteristic evolution for ϕ (blue), χ (red) and H (black-dashed) for $n = 3/2$ and $\tilde{\alpha} = 0.001$, showing the approach to $\chi(t) = 0$. The initial conditions are chosen as $\phi_0 = \chi_0$ and $\dot{\phi}_0 = \dot{\chi}_0 = 0$. *Right:* The three-dimensional plot of the trajectory on the potential. The two effectively single-field stages are easily visible: $\phi(t) \simeq const.$ followed by $\chi(t) \simeq 0$.

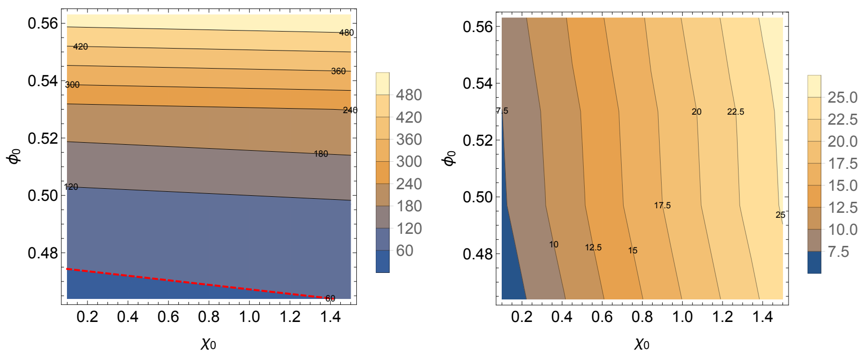

Figure 4.3: *Left:* A contour plot in the $\phi_0 \equiv \phi(0)$ and $\chi_0 \equiv \chi(0)$ plane for $n = 3/2$ and $\tilde{\alpha} = 0.001$, showing the total number of e-folds of inflation. The initial velocities are chosen as $\dot{\phi}_0 = \dot{\chi}_0 = 0$. The red-dashed line shows the initial conditions that lead to 60 e-folds of inflation. We see that the total number of e-folds are predominately controlled by ϕ_0. *Right:* A contour plot in the ϕ_0 and χ_0 plane for $n = 3/2$ and $\tilde{\alpha} = 0.001$, showing the number of e-folds from the beginning of inflation until the $\chi = 0$ attractor is reached. As expected, the number of e-folds along $\phi \simeq \phi_0$ are mostly determined by χ_0. We see that the initial stage of inflation along $\phi \simeq \phi_0$ lasts far less than the second stage of inflation along $\chi = 0$, hence it will not leave any observational imprints for non fine-tuned initial conditions.

to the single-field motion along $\chi = 0$ for broad conditions, constrained to provide more than 60 e-folds of inflation. Beyond the fact that the single field trajectory along $\chi(t) = 0$ is a dynamical attractor for the generalized two-field T-model, its predictions are robust with respect to χ_0. As shown in Fig. 4.3, the number of e-folds along the second stage $\chi(t) = 0$ is much larger than the number of e-folds along the first stage $\phi(t) = \text{const}$. The range of values $\{\phi_0, \chi_0\}$ that place the turn-rate spike (the transition between the two single-field motions) at the observable window $50 \lesssim N_* \lesssim 60$ is very narrow, requiring delicate fine-tuning. Hence the generic observational prediction of these models for the CMB is that of usual single-field α-attractors. This behavior can be understood analytically. Considering the number of e-folds along a single-field trajectory we get

$$N = \int H\, dt = \int \frac{H}{\dot{\phi}}\, d\phi \tag{4.18}$$

As a quick estimate of the number of e-folds we can use $\Delta N_1 \sim (H/|\dot{\chi}|)\Delta\chi \sim (H/|\dot{\chi}|)\chi_0$ during the first stage and $\Delta N_2 \sim (H/|\dot{\phi}|)\Delta\phi \sim (H/|\dot{\phi}|)\phi_0$ during the second stage of inflation. Assuming that the Hubble scale does not change much during inflation

$$\frac{N_1}{N_2} \sim \left|\frac{\dot{\chi}}{\dot{\phi}}\right| \frac{\chi_0}{\phi_0} \tag{4.19}$$

Fig. 4.4 shows the ratio $|\dot{\phi}/\dot{\chi}|$ as a function of ϕ for several values of χ_0. We see that for large values of ϕ_0, required to give a sufficient number of e-folds of inflation, $|\dot{\chi}| = \mathcal{O}(10)|\dot{\phi}|$, hence $N_1 = \mathcal{O}(0.1)N_2$ for typical values of $\{\phi_0, \chi_0\}$. While there is potentially interesting phenomenology from the turning trajectories, it is absent for generically chosen initial conditions. Since we are only interested in the preheating behavior of the two-field T-model, we will not pursue this subject further here.

4.2.3 Geometrical destabilization

A novel phenomenon that manifests itself in scalar field systems on a negatively curved manifold is "geometrical destabilization" [54], where the presence of a negative field-space Ricci term can turn a stable direction into an unstable one. The study of the effective mass for the ϕ and χ fluctuations will be performed in Section 4.3. In order to check the stability of the single-field trajectory, it suffices to use the effective super-horizon

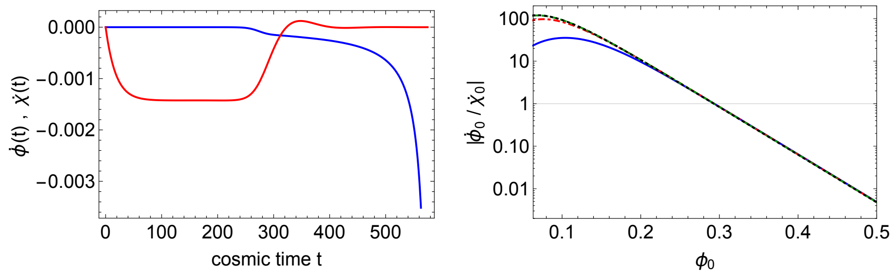

Figure 4.4: *Left:* The field velocities $\dot\phi(t)$ (blue) and $\dot\chi(t)$ (red) for the example of Fig. 4.2. We see that the initial stage of inflation along $\phi = \text{const.}$ proceeds with a much larger velocity than the one associated with α-attractors, hence it will generate fewer e-folds. *Right:* The ratio of the typical velocities $|\dot\phi/\dot\chi|$ as a function of the inflaton field ϕ_0 for different values of the field amplitude χ_0. We see that for the ϕ field values needed to generate sufficient e-folds of inflation the typical χ velocity is larger than the typical ϕ velocity.

isocurvature mass

$$
\begin{aligned}
m^2_{\chi,\text{eff}} &= V_{\chi\chi}(\chi=0) - \frac{1}{2}\frac{4}{3\alpha}\dot\phi^2 = \\
&= \frac{\left(2\tanh^{2n}\left(\frac{|\phi(t)|}{\sqrt{6}\sqrt{\alpha}}\right)\left(3\alpha + 2n\coth\left(\frac{\sqrt{\frac{2}{3}}\phi(t)}{\sqrt{\alpha}}\right)\operatorname{csch}\left(\frac{\sqrt{\frac{2}{3}}\phi(t)}{\sqrt{\alpha}}\right)\right)\right)}{3} - \frac{2\dot\phi(t)^2}{3\alpha}
\end{aligned} \tag{4.20}
$$

During inflation and using the slow-roll conditions, we get

$$
m^2_{\chi,\text{eff}} = 2\alpha\left(1 + \frac{1}{2N}\right) \tag{4.21}
$$

which is positive. However, close to the end of inflation the slow-roll approximation fails and the result cannot be trusted. Hence the model under study is safe against geometrical destabilization effects during inflation. The effective mass of isocurvature fluctuations can become negative after the end of inflation, but this falls under the scope of tachyonic preheating, as will be discussed in Section 4.3. Figure 4.5 shows the isocurvature effective mass-squared during the last e-folds of inflation, showing that it is indeed positive until very close to the end, hence no Geometrical Destabilization will occur[4]. However Fig. 4.5 shows that all computations, either

[4] Recently Ref. [65] showed the existence of yet another possible evolution for α-attractor models, angular inflation, where the background motion proceeds along the boundary of the Poincare disk. We did not see this behavior arise in the context of the two-field T-model studied here, even for highly curved manifolds.

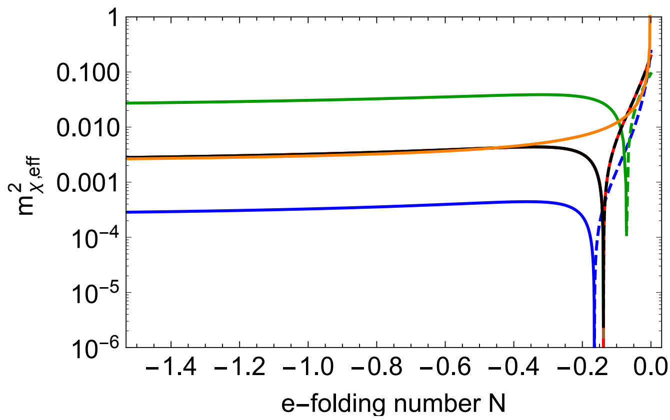

Figure 4.5: The super-horizon isocurvature effective mass-squared $m^2_{\chi,\text{eff}}$ given in Eq. (4.20) for several values of α and n. In particular $\tilde{\alpha} = 0.0001$ and $n = 3/2$ (blue), $\tilde{\alpha} = 0.001$ and $n = 3/2$ (red), $\tilde{\alpha} = 0.01$ and $n = 3/2$ (green), $\tilde{\alpha} = 0.001$ and $n = 1$ (brown), $\tilde{\alpha} = 0.001$ and $n = 10$ (black). The dotted parts show the negative part of $m^2_{\chi,\text{eff}}$. The three curves that correspond to $\tilde{\alpha} = 0.001$ are visually indistinguishable. The orange line shows the slow-roll expression of Eq. (4.21) for $\tilde{\alpha} = 0.001$. We see that the single field trajectory along $\chi = 0$ is safe against geometric destabilization effects until close to the end of inflation.

using linear analysis as the ones performed here, or full lattice simulations like in Ref. [160], must be initialized more than an e-fold before the end of inflation, where the effective isocurvature mass-squared is positive and the connection to the Bunch Davies vacuum is possible.

4.2.4 Post-inflationary background oscillations

In order to study the post-inflationary background evolution of the inflaton field $\phi(t)$, it is convenient to work in terms of the rescaled field variable $\delta \equiv \tilde{\phi}/\sqrt{\tilde{\alpha}}$ and re-write the equation of motion for the inflaton field ϕ as

$$\ddot{\delta} + 3H\dot{\delta} + \mu^2 \frac{2\sqrt{2}}{3} n \cdot \operatorname{csch}\left(\sqrt{\frac{2}{3}}|\delta|\right) \tanh^{2n}\left(\frac{1}{\sqrt{6}}|\delta|\right) = 0 \tag{4.22}$$

where

$$\left(\frac{H}{\mu}\right)^2 = \frac{\tilde{\alpha}}{3}\left[\frac{1}{2}\left(\frac{d\delta}{d(\mu t)}\right)^2 + \tanh^{2n}\left(\frac{|\delta|}{\sqrt{6}}\right)\right] \tag{4.23}$$

The field re-scaling leads to $\delta = \mathcal{O}(1)$ at the end of inflation and during preheating. We see that the evolution of δ, if one neglects the Hubble drag term, does not depend on α. This is reminiscent of non-minimally coupled

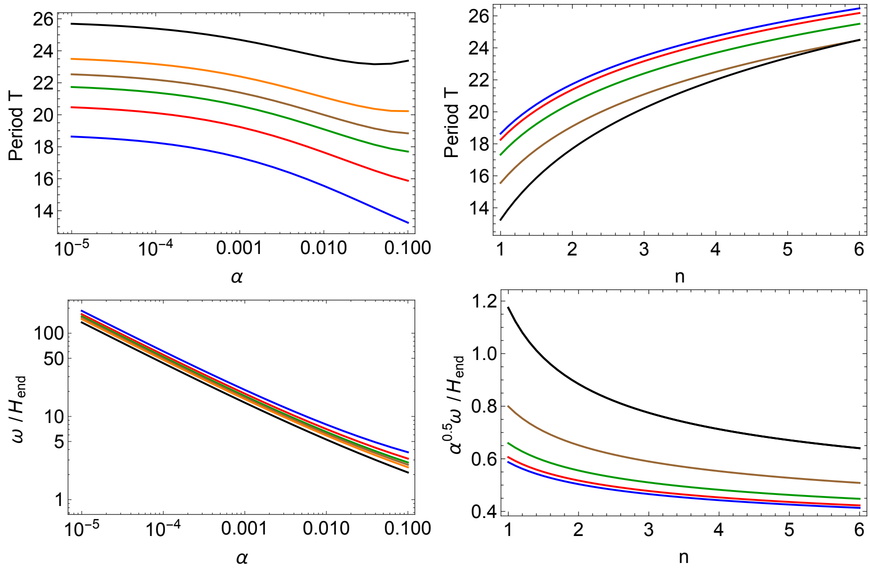

Figure 4.6: *Upper panels:* The background period T as a function of α (left) and n (right). *Lower panels:* The ratio of the background frequency $\omega = 2\pi/T$ to the Hubble scale at the end of inflation $H_{\rm end}$ as a function of α (left) and n (right). Color-coding follows Fig. 4.1, specifically:
Left: $\alpha = 10^{-5}, 10^{-4}, 10^{-3}, 10^{-2}, 10^{-1}$ (blue, red, green, brown and black respectively).
Right: $n = 1, 1.5, 2, 2.5, 3, 5$ (blue, red, green, brown, orange and black respectively)

models of inflation, where the background equation of motion approaches one "master equation", when properly normalized, and thus the background motion is self-similar for large values of the non-minimal coupling ξ. In reality the background evolution has a mild dependence on α, arising from the (very weak) dependence of $\delta_{\rm end}$ on α, which is shown in Fig. 4.1. Fig. 4.6 shows the period of background oscillations, if we neglect the Hubble drag and initialize the oscillation at $\delta_{\rm init} = \phi_{\rm end}/\sqrt{\alpha}$. We see that the period $T \sim 10$. More importantly, there is a significant separation of scales between the background oscillation frequency $\omega = 2\pi/T$ and the Hubble scale. The relation can be roughly fitted as $\omega/H_{\rm end} \sim 1/\sqrt{\tilde{\alpha}}$. This shows that there are more background oscillations per Hubble time (or per e-fold) for smaller values of $\tilde{\alpha}$, hence for highly curved field-space manifolds.

4.3 Tachyonic resonance

4.3.1 Fluctuations

The covariant formalism that must be used to study the evolution of fluctuations in models comprised of multiple scalar fields on a curved manifold has been developed and presented in Refs. [37, 266], described in detail in Ref. [136] and extensively used in Refs. [302–304] for studying preheating in multi-field inflation with non-minimal couplings to gravity. The gauge-invariant perturbations obey

$$\mathcal{D}_t^2 Q^I + 3H\mathcal{D}_t Q^I + \left[\frac{k^2}{a^2}\delta^I_{\ J} + \mathcal{M}^I_{\ J}\right] Q^J = 0, \tag{4.24}$$

where the mass-squared matrix is given by

$$\mathcal{M}^I_{\ J} \equiv \mathcal{G}^{IK}\left(\mathcal{D}_J\mathcal{D}_K V\right) - \mathcal{R}^I_{\ LMJ}\dot{\varphi}^L\dot{\varphi}^M - \frac{1}{M_{\rm pl}^2 a^3}\mathcal{D}_t\left(\frac{a^3}{H}\dot{\varphi}^I\dot{\varphi}_J\right) \tag{4.25}$$

and $\mathcal{R}^I_{\ LMJ}$ is the Riemann tensor constructed from $\mathcal{G}_{IJ}(\varphi^K)$. For the model at hand, where the background motion is restricted along the $\chi = 0$ direction, the field-space structure simplifies significantly $\mathcal{G}_{IJ}(\chi = 0) = \delta_{IJ}$ and $\Gamma^I_{JK} = 0$, hence all covariant derivatives become partial derivatives and the quantization of the fluctuations proceeds as usual. This is not the case for other parametrizations of the field-space, or other background trajectories, where $\mathcal{G}_{IJ} \neq \delta_{IJ}$, and one would have to use the field-space vielbeins to properly quantize the system, as done for example in Ref. [136].

We rescale the perturbations as $Q^I(x^\mu) \to X^I(x^\mu)/a(t)$ and work in terms of conformal time, $d\eta = dt/a(t)$. This allows us to write the quadratic action in a form that resembles Minkowski space, which makes their quantization straightforward. The quadratic action becomes

$$S_2^{(X)} = \int d^3x d\eta \left[-\frac{1}{2}\eta^{\mu\nu}\delta_{IJ}\partial_\mu X^I\partial_\nu X^J - \frac{1}{2}\mathbb{M}_{IJ}X^I X^J\right], \tag{4.26}$$

where

$$\mathbb{M}_{IJ} = a^2\left(\mathcal{M}_{IJ} - \frac{1}{6}\delta_{IJ}R\right) \tag{4.27}$$

and R is the space-time Ricci scalar. The energy density of the two fields in momentum-space becomes

$$\rho_k^{(X)} = \frac{1}{2}\delta_{IJ}\partial_\eta X_k^I\partial_\eta X_k^J + \frac{1}{2}[\omega_k^2(\eta)]_{IJ}X_k^I X_k^J = \frac{1}{2}\delta_{IJ}\left[\partial_\eta X_k^I\partial_\eta X_k^J - (\partial_\eta^2 X^I)X^J\right] \tag{4.28}$$

where we used the equation of motion for the second equality and defined the effective frequency-squared as

$$[\omega_k^2(\eta)]_{IJ} = k^2\delta_{IJ} + \mathbb{M}_{IJ} \tag{4.29}$$

We promote the fields X^I to operators $\hat{X}^I$ and expand $\hat{X}^\phi$ and $\hat{X}^\chi$ in sets of creation and annihilation operators and associated mode functions

$$\hat{X}^I = \int \frac{d^3k}{(2\pi)^{3/2}} \left[u^I(k,\eta)\hat{a}e^{ik\cdot x} + u^{I*}(k,\eta)\hat{a}^\dagger e^{-ik\cdot x}\right] . \tag{4.30}$$

and we define $u^\phi \equiv v$ and $u^\chi \equiv z$. Since the modes decouple on a single-field background with vanishing turn-rate, the equations of motion are

$$\begin{aligned} \partial_\eta^2 v_k + \omega_\phi^2(k,\eta)v_k \simeq 0\,, \quad \omega_\phi(k,\eta)^2 = k^2 + a^2 m_{\text{eff},\phi}^2\,, \\ \partial_\eta^2 z_k + \omega_\chi^2(k,\eta)z_k \simeq 0\,, \quad \omega_\chi(k,\eta)^2 = k^2 + a^2 m_{\text{eff},\chi}^2\,. \end{aligned} \tag{4.31}$$

The effective masses of the two types of fluctuations, along the background motion and perpendicular to it, consist of four distinct contributions [136]:

$$m_{\text{eff},I}^2 = m_{1,I}^2 + m_{2,I}^2 + m_{3,I}^2 + m_{4,I}^2, \tag{4.32}$$

with[5]

$$\begin{aligned} m_{1,I}^2 &\equiv \mathcal{G}^{IK}\left(\mathcal{D}_I\mathcal{D}_K V\right), \\ m_{2,I}^2 &\equiv -\mathcal{R}^I{}_{LMI}\dot{\varphi}^L\dot{\varphi}^M, \\ m_{3,I}^2 &\equiv -\frac{1}{M_{\text{pl}}^2 a^3}\delta^I_K\delta^J_I\,\mathcal{D}_t\left(\frac{a^3}{H}\dot{\varphi}^K\dot{\varphi}_J\right), \\ m_{4,I}^2 &\equiv -\frac{1}{6}R = (\epsilon-2)H^2\,. \end{aligned} \tag{4.33}$$

The various component of the effective mass-squared arises from a different source:

- $m_{1,I}^2$ is the usual effective mass term derived from the curvature of the potential around the minimum.
- $m_{2,I}^2$ comes from the geometry of field-space and has no analogue in models with a trivial field space.

[5] Note that no summation implied over the index $I = \phi, \chi$. This corrects an expression in the published paper.

- $m^2_{3,I}$ arises due to the presence of coupled metric perturbations by considering linear fluctuations in the metric as well as in the fields. This contribution vanishes in the limit of infinitely rigid space-time.

- $m^2_{4,I}$ encodes the curvature of space-time.

In general $m^2_{3,\chi} = 0 = m^2_{2,\phi}$, since the coupled metric fluctuations described by $m^2_{3,I}$ only affect the adiabatic modes $\delta\phi$, while the field-space curvature described by $m^2_{2,I}$ only affects the isocurvature modes[6] $\delta\chi$. In our case, both $m^2_{3,I}$ and $m^2_{4,I}$ are subdominant for highly curved field spaces $\tilde{\alpha} \ll 1$, as can be seen from the various scalings of the terms in Eq. (4.32)

$$\begin{aligned} m^2_{1,\phi} &\sim \mu^2 \\ m^2_{3,\phi} &\sim \mu^2\sqrt{\tilde{\alpha}} \\ m^2_{4,\phi} &= m^2_{4,\chi} \sim \mu^2\tilde{\alpha} \end{aligned} \tag{4.34}$$

The small value of $m^2_{4,I}$ is one further indication that fluctuations behave almost as if they were in flat spacetime. These scalings agree very well with numerical evaluations for a large range of $\tilde{\alpha}$, as shown in Fig. 4.7. A closer analysis of scaling relations for $m^2_{\text{eff},\chi}$, will be performed in Section 4.3.2. Meanwhile, within the single-field attractor along $\chi = 0$, the energy densities for adiabatic and isocurvature perturbations take the simple form [136]

$$\begin{aligned} \rho_k^{(\phi)} &= \frac{1}{2}\left[|v_k'|^2 + \left(k^2 + a^2 m^2_{\text{eff},\phi}\right)|v_k|^2\right], \\ \rho_k^{(\chi)} &= \frac{1}{2}\left[|z_k'|^2 + \left(k^2 + a^2 m^2_{\text{eff},\chi}\right)|z_k|^2\right], \end{aligned} \tag{4.35}$$

where we thus approximate the two effective masses as

$$m^2_{\text{eff},\phi} \simeq V_{\phi\phi}(\chi = 0) \tag{4.36}$$

$$m^2_{\text{eff},\chi} \simeq V_{\chi\chi}(\chi = 0) + \frac{1}{2}\mathcal{R}\dot{\phi}^2 \tag{4.37}$$

where $\mathcal{R} = -4/3\alpha$ is the field space Ricci curvature scalar and we dropped the subdominant terms. We must keep in mind that $Q^\phi \sim v_k/a(t)$ and $Q^\chi \sim z_k/a(t)$. We measure particle production with respect to the instantaneous adiabatic vacuum [285]. The initial conditions for preheating can be read

[6] The terms "adiabatic" and "isocurvature" refer to fluctuations along and perpendicular to the background trajectory respectively.

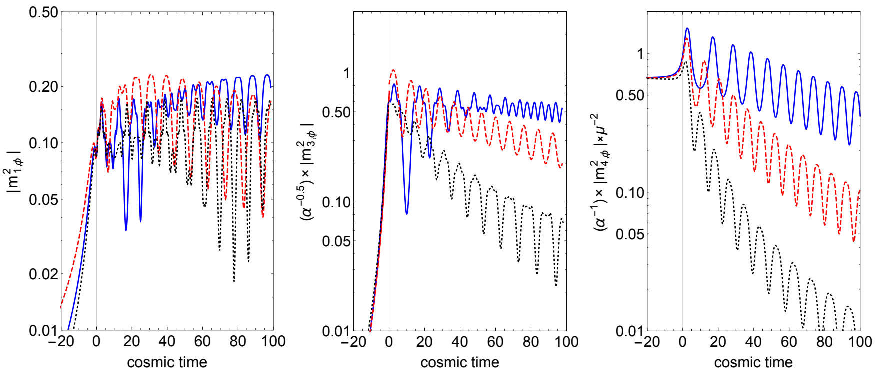

Figure 4.7: The absolute values of the non-zero components of $m^2_{\mathrm{eff},\phi}$, (left to right: $m^2_{1,\phi}$, $m^2_{2,\phi}/\sqrt{\alpha}$ and $m^2_{3,\phi}/\alpha$) properly rescaled to showcase the scalings of Eq. (4.34) for $n = 3/2$ and $\tilde{\alpha} = 10^{-2}, 10^{-3}, 10^{-4}$ (black, red and blue respectively). The fact that all curves within each panel have similar values at the end of inflation is a numerical validation of the scalings shown in Eq. (4.34). The curves on the left and middle panels for $t > 0$ are generated through using a moving average window on the values of $|m^2_{\{2,3\},\phi}|$. Without this smoothing the curves would exhibit large oscillations and hence would overlap and be very hard to distinguish. The information lost is not important, since at this point we are interested in the scaling properties of the effective mass components, not their exact form.

off from Eq. (4.31), using the WKB approximation and starting during inflation, when the effective mass is positive

$$v_k^{\mathrm{init}} = \frac{1}{\sqrt{2\omega_\phi(k,\eta)}} e^{-i\int_{\eta_0}^{\eta} \omega_\phi(k,\eta')d\eta'} \tag{4.38}$$

$$z_k^{\mathrm{init}} = \frac{1}{\sqrt{2\omega_\chi(k,\eta)}} e^{-i\int_{\eta_0}^{\eta} \omega_\chi(k,\eta')d\eta'} \tag{4.39}$$

In the far past $a(\eta) \to 0$, hence $\{\omega_\phi(k,\eta), \omega_\chi(k,\eta)\} \to k$, which makes the solutions of Eqs. (4.38) and (4.39) match to the Bunch-Davies vacuum during inflation.

Since we will be performing the computations in cosmic time, we write the equations of motion for the two types of fluctuations. The fluctuation equation for the ϕ field (adiabatic direction) is

$$\ddot{Q}_\phi + 3H\dot{Q}_\phi + \left[\frac{k^2}{a^2} + V_{\phi\phi}\right] Q_\phi = 0 \tag{4.40}$$

where we neglected the term arising from the coupled metric fluctuations, that is proportional to $M_{\rm Pl}^{-2}$. We again rescale time by μ giving us

$$\frac{d^2Q_\phi}{d(\mu t)^2}+3\frac{H}{\mu}\frac{dQ_\phi}{d(\mu t)}+\left[\frac{(k/\mu)^2}{a^2}+\frac{V_{\phi\phi}}{\mu^2}\right]Q_\phi=0 \tag{4.41}$$

where the potential-dependent term of the effective frequency is

$$\frac{V_{\phi\phi}}{\mu^2}=\sqrt{\tilde\alpha}\frac{d^2}{d\tilde\phi^2}\left[\tanh^{2n}\left(\frac{|\tilde\phi|}{\sqrt{6\tilde\alpha}}\right)\right] \tag{4.42}$$

The results for the isocurvature modes $\delta\chi$ or Q_χ are similar

$$\frac{d^2Q_\chi}{d(\mu t)^2}+3\frac{H}{m}\frac{dQ_\chi}{d(\mu t)}+\left[\frac{(k/\mu)^2}{a^2}+\frac{V_{\chi\chi}}{\mu^2}+\frac{1}{2}\left(\frac{d\phi}{d(\mu t)}\right)^2\mathcal{R}\right]Q_\chi=0 \tag{4.43}$$

The last term in the above equation is the Riemann contribution to the effective mass-squared ω_χ^2

$$m_{2,\chi}^2=-\mathcal{R}^\chi_{\phi\phi\chi}\dot\phi^2=-\frac{2}{3\alpha}\dot\phi^2=\frac{1}{2}\mathcal{R}\dot\phi^2\,. \tag{4.44}$$

Since the self-resonance of $\delta\phi$ modes in these models has been extensively studied (see for example Ref. [305]), we will focus our attention on $\delta\chi$ fluctuations, which can undergo tachyonic excitation, which is generally more efficient than parametric amplification. Also the excitation of $\delta\chi$ modes is a truly multi-field phenomenon that depends crucially on the field-space geometry.

4.3.2 Effective frequency

We examine in detail the effective frequency-squared for the $\delta\chi$ fluctuations, $\omega_\chi^2(k,t)$. For simplicity we will focus on the case of $n=3/2$, which matches the potential used in the lattice simulations presented in Ref. [160]. The generalization of our results for other potentials is discussed in Section 4.4.

In the top left panel of Fig. 4.8 we see the evolution of the background field $\phi(t)$, rescaled as $\delta(t)=\phi(t)/\sqrt{\alpha}$ after the end of inflation and we take $t=0$ as the end of inflation. We see that inflation ends at $\phi(t)/\sqrt{\alpha}\simeq 3$ for all three cases considered here, consistent with Fig. 4.1. The main difference is both the frequency of oscillation and the decay of the amplitude of the background for different values of α.

The maximum tachyonically excited wavenumber for the various cases under consideration is $k_{\rm max}\simeq 0.87\mu$ for $\tilde\alpha=10^{-2}$, $k_{\rm max}\simeq 1.04\mu$ for

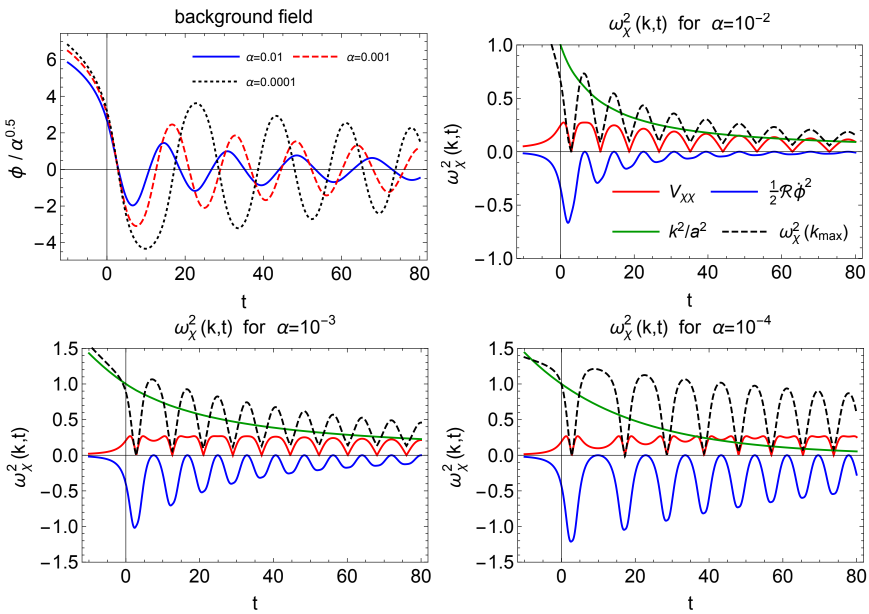

Figure 4.8: The rescaled background field (top left) $\phi/\sqrt{\alpha}$ as a function of time for $\tilde{\alpha} = 10^{-2}, 10^{-3}, 10^{-4}$ (blue, red-dashed and black-dotted respectively). The other three plots correspond to the isocurvature effective frequency-squared for the maximal marginally amplified wavenumber $k_{\rm max}$ (black-dotted), along with $(k/a)^2$ (green), the potential contribution (red) and the tachyonic Riemann term (blue).

$\tilde{\alpha} = 10^{-3}$ and $k_{\rm max} \simeq 1.11\mu$ for $\tilde{\alpha} = 10^{-4}$. So we can say[7] that $k_{\rm max} \simeq \mu$ for all values of $\tilde{\alpha} \ll 1$. Furthermore, we see that background motion corresponding to larger values of $\tilde{\alpha}$ shows greater damping. This is consistent with the observation that $H_{\rm end} \sim \sqrt{\tilde{\alpha}}$, hence the Hubble damping term is smaller for highly curved field-space manifolds.

Examining the tachyonic contribution to $\omega_\chi^2(k)$, a very simple scaling emerges

$$\frac{1}{2}\mathcal{R}\dot{\phi}^2 = -\frac{1}{2}\alpha\dot{\delta}^2\frac{4}{3\alpha} = -\frac{2}{3}\dot{\delta}^2 = \mathcal{O}(1) \tag{4.45}$$

This is again consistent with Fig. 4.8, especially as the value of $\tilde{\alpha}$ gets smaller.

Since the tachyonic contribution to the effective mass-squared is similar for models with different values of $\tilde{\alpha}$, the tachyonic amplification of the relevant mode-functions after each oscillation will be also similar. Fig. 4.9 shows the evolution of $\omega^2_{\rm min}$ and $k_{\rm max}$ for each subsequent tachyonic region. It is worth emphasizing that $\omega^2_{\rm min}$ is determined solely by the corresponding minimum (maximum negative) value of $m^2_{2,\chi}$. The maximum negative value of $m^2_{2,\chi}$ occurs when $|\dot{\phi}|$ is maximized, or equivalently when $\phi = 0$. At this point, the potential can be Taylor-expanded as

$$V(\phi = 0, \chi) \approx \frac{M^4}{4^n}\beta^{2n}|\chi|^{2n}\,. \tag{4.46}$$

For $n > 1$ the effective mass component vanishes for $\chi = 0$. In particular for $n = 3/2$ the effective mass component becomes $\partial_\chi^2 V(\phi = 0, \chi) \sim |\chi|$, as shown in Fig. 4.8. The case of $n = 1$ is different and we consider it in Section 4.4. We see that both the maximum (negative) contribution of $m^2_{2,\chi}$, as well as the range of tachyonically excited wavenumbers decrease faster for larger values of $\tilde{\alpha}$, or less curved field-space manifolds. This can be traced back to the dependence of the Hubble scale on the field-space curvature, which scales as $H \propto \sqrt{\tilde{\alpha}}$. Hence in the first e-fold, or within the first Hubble-time after inflation, lower values of $\tilde{\alpha}$ will result in a larger number of tachyonic bursts and hence a larger overall amplification. Furthermore, a larger Hubble term for larger values of $\tilde{\alpha}$ will result in a faster red-shifting of the background field amplitude $\delta(t)$, resulting in a faster suppression of the parametric resonance, in line with Fig. 4.8.

[7] In the units of Appendix 4C and Ref. [160], this corresponds to $k_{\rm max} \simeq \frac{1}{\sqrt{\alpha}}M^2/M_{\rm Pl}$, leading to $k_{\rm max} \simeq 33M^2/M_{\rm Pl}$ for $\alpha = 10^{-3}$ and $k_{\rm max} \simeq 100M^2/M_{\rm Pl}$ for $\alpha = 10^{-4}$. This is consistent with Figure 5 of Ref. [160].

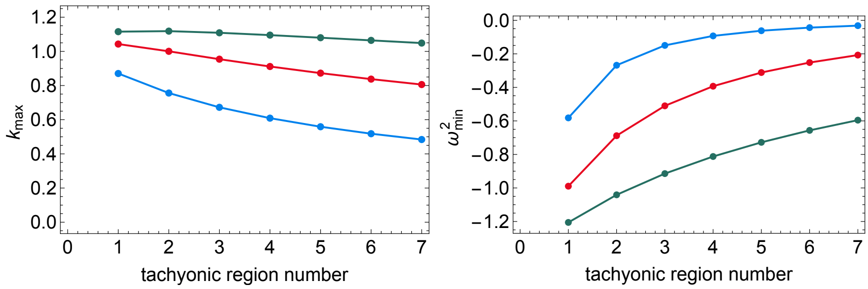

Figure 4.9: *Left:* The dependence of the maximum excited wavenumber $k_{\rm max}$ on the number of tachyonic regions for $n = 3/2$ and $\tilde{\alpha} = 10^{-2}, 10^{-3}, 10^{-4}$ (blue, red and green respectively). *Right:* The minimum (maximally negative) value of the effective frequency-squared of χ fluctuations $\omega^2_{\rm min}$ as a function of the number of tachyonic regions for the same parameters and color-coding.

4.3.3 WKB results

We use the WKB analysis as described in Ref. [306], in order to make analytical progress in computing the amplification of the $\delta\chi$ modes during tachyonic preheating. In contrast to Refs. [307–309], where tachyonic preheating lasted for a few inflaton oscillations at most, in the present case, multiple inflaton oscillations might be required, in order to siphon enough energy from the inflaton into radiation modes. However, given the fact that the Hubble time is much larger than the period of oscillations, preheating will still be almost instantaneous in terms of the number of e-folds. Based on $\omega/H_{\rm end} \sim 1/\sqrt{\tilde{\alpha}}$, we can estimate the number of background oscillations occurring during the first e-fold of preheating to be $N_{\rm osc.} \sim 0.2/\sqrt{\tilde{\alpha}}$.

We neglect the effect of the expansion of the Universe, hence taking $H = 0$. This is an increasingly good approximation for smaller values of $\tilde{\alpha}$, since $H_{\rm end} \sim \sqrt{\tilde{\alpha}}$. Furthermore, the static universe WKB analysis will provide a useful comparison to the Floquet analysis of Section 4.3.4. The equation of motion for the fluctuations in the χ field becomes[8]

$$\partial_t^2 \chi_k + \omega_\chi^2(k,t)\,\chi_k = 0\,, \tag{4.47}$$

where

$$\omega_\chi(k,t)^2 = k^2 + m^2_{{\rm eff},\chi} = k^2 + m^2_{1,\chi} + m^2_{2,\chi}\,, \tag{4.48}$$

where the components of the effective mass are given in Eq. (4.33). Following Ref. [306], we write the WKB form of the mode-functions before,

[8]For the remainder of this work we denote the fluctuations of the χ field as χ_k rather than $\delta\chi_k$ for notational simplicity.

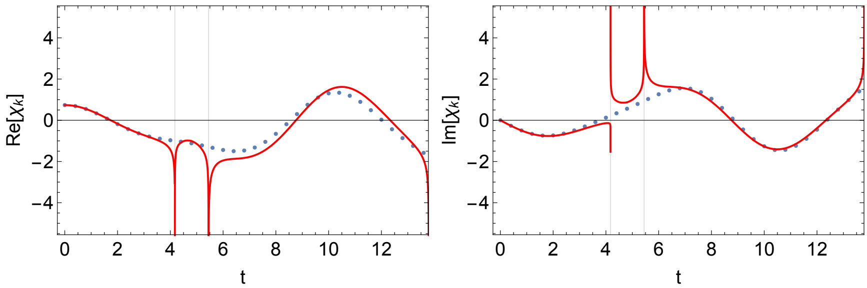

Figure 4.10: Comparison of the real (left) and imaginary (right) parts of the WKB solution (red line) and the numerical solution (blue dots) of the χ mode evolution in the static universe approximation around the first tachyonic amplification burst for $n = 3/2$, $\tilde{\alpha} = 10^{-3}$ and $k = 0.8\mu$. We see very good agreement, except in the vicinity of the points where $\omega^2 = 0$ and the WKB solution diverges.

during and after a tachyonic transition (regions I, II and III respectively).

$$\begin{aligned}
\chi_k^I &= \frac{\alpha^n}{\sqrt{2\omega_k(t)}} e^{-i\int \omega_k(t)dt} + \frac{\beta^n}{\sqrt{2\omega_k(t)}} e^{i\int \omega_k(t)dt} \\
\chi_k^{II} &= \frac{a^n}{\sqrt{2\Omega_k(t)}} e^{-\int \Omega_k(t)dt} + \frac{b^n}{\sqrt{2\Omega_k(t)}} e^{\int \Omega_k(t)dt} \\
\chi_k^{III} &= \frac{\alpha^{n+1}}{\sqrt{2\omega_k(t)}} e^{-i\int \omega_k(t)dt} + \frac{\beta^{n+1}}{\sqrt{2k}} e^{i\int \omega_k(t)dt}
\end{aligned} \tag{4.49}$$

where $\Omega_k^2(t) = -\omega_k^2(t)$. The amplification factor after the first tachyonic region for each mode k is

$$A_k = e^{\int_{t_-}^{t_+} \Omega_k(t)dt} \tag{4.50}$$

where $t_\pm$ are the points at which the effective frequency vanishes, $\omega_k^2(t_\pm) = \Omega_k^2(t_\pm) = 0$.

Fig. 4.10 shows the result of the numerical solution and the WKB result before, during and after the first tachyonic amplification phase. We see that the agreement is very good, hence we can use the expression of Eq. (4.50) to estimate the growth rate of fluctuations.

As shown in Eq. (4.49), following the first tachyonic burst all modes with wavenumbers $k \leqslant k_{\max}$ will be amplified. Subsequent background oscillations will cause destructive or constructive interference, leading to the formation of stability and instability bands, the latter exhibiting no exponential growth. In Ref. [306] it is shown that the amplitude of the

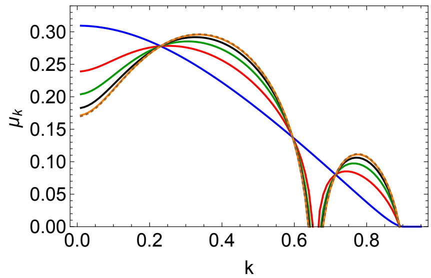

Figure 4.11: The Floquet exponent μ_k derived using the WKB approximation in Eq. (4.53). The Floquet exponent after $1, 2, 4, 10, 50, 100$ tachyonic regimes is shown (blue, red, green, black, orange and brown-dotted respectively).

wavefunction for a mode with wavenumber k after the j'th tachyonic burst is

$$|\beta_k^j|^2 = e^{2jA_k}(2\cos\Theta_k)^{2(j-1)} \,. \tag{4.51}$$

where Θ_k is the total phase accumulated between two consecutive tachyonic regimes. We can define an averaged growth rate as

$$\chi_k(t) \sim e^{\mu_k t} P(t) \,, \tag{4.52}$$

where $P(t)$ is a bounded (periodic) function and μ_k is the Floquet exponent, as we discuss in detail in Section 4.3.4. Since there are two tachyonic regimes for each background oscillation, the Floquet exponent μ_k is extracted from Eq. (4.51) as

$$\mu_k = \frac{2}{T}\frac{1}{2j}\log|\beta_k^j|^2 \,, \tag{4.53}$$

where T is the background period of oscillation. As shown in Fig. 4.11, the Floquet exponent extracted from Eqs. (4.51) and (4.53) depends on time, albeit mildly after the first few tachyonic bursts. However, there is a clear asymptotic regime that emerges after the background inflaton field has undergone multiple oscillations. The asymptotic value should be compared to the "true" Floquet exponent, which we compute in Section 4.3.4.

4.3.4 Floquet charts

Floquet theory is a powerful tool for studying parametric resonance in the static universe approximation. The algorithm for computing Floquet charts can be found in the literature (see for example Ref. [285]).

We may further understand properties of the Floquet charts by examining the Fourier structure of certain field-space quantities. In the rigid-spacetime limit, Eq. (4.47) for the isocurvature modes χ_k may be written in the suggestive form

$$\frac{d}{dt}\begin{pmatrix}\chi_k \\ \dot{\chi}_k\end{pmatrix} = \begin{pmatrix} 0 & 1 \\ -(k^2 + m^2_{\text{eff},\chi}) & 0\end{pmatrix}\begin{pmatrix}\chi_k \\ \dot{\chi}_k\end{pmatrix}, \tag{4.54}$$

again using $m^2_{\text{eff},\chi} = m^2_{1,\chi} + m^2_{2,\chi}$ in the rigid-spacetime limit. This equation is of the form

$$\dot{x}(t) = \mathcal{P}(t)\, x(t)\,, \tag{4.55}$$

where $\mathcal{P}(t)$ is a periodic matrix. The period of the background is T, but the period of $m^2_{\text{eff},\chi}$ is $T/2$, since it depends quadratically on the background field $\phi(t+T) = \phi(t)$ and its derivative $\dot{\phi}(t+T) = \dot{\phi}(t)$. In Ref. [302] a semi-analytic method was described for computing the edges of the instability bands at arbitrary high accuracy, by reducing the system to an algebraic matrix equation. The truncation of the resulting matrices determines the number of Floquet bands that can be accurately computed. In the present work we determine the edges of the instability bands after the computation of the full Floquet chart using *Mathematica*.

Fig. 4.12 shows the Floquet charts for $n = 3/2$ and $\tilde{\alpha} = 10^{-2}, 10^{-3}, 10^{-4}$. We can see that, when normalized appropriately with $\tilde{\alpha}$, the Floquet charts look similar, especially when it comes to the first two instability bands, which essentially control the entirety of the parametric resonance. The relation between Floquet charts for different values of α becomes even more evident, when we show a few contours of the first instability bands on the same plot. It is then obvious that for $\tilde{\alpha} \lesssim 10^{-3}$ the parametric resonance in the static universe approximation is identical, regardless of the exact value of the field-space curvature[9]. This is no surprise, since the WKB analysis of Section 4.3.3 predicted the scaling behavior of the parametric resonance strength for low values of $\tilde{\alpha}$. The Floquet chart of Fig. 4.12 can be considered a "master diagram", from which the Floquet chart for arbitrary values of $\tilde{\alpha} \lesssim 0.01$ can be easily read-off by using the appropriate scaling with $\tilde{\alpha}$.

Finally, Fig. 4.13 shows the comparison between the Floquet exponent computed using the algorithm described in Ref. [285] and using the WKB analysis. We see that the WKB analysis is able to capture the existence

[9]For $\tilde{\alpha} = 10^{-2}$ the edges of the first two instability bands follow the ones exhibited by $\tilde{\alpha} \ll 1$, while the low-k edge of the first band shows slightly larger Floquet exponents.

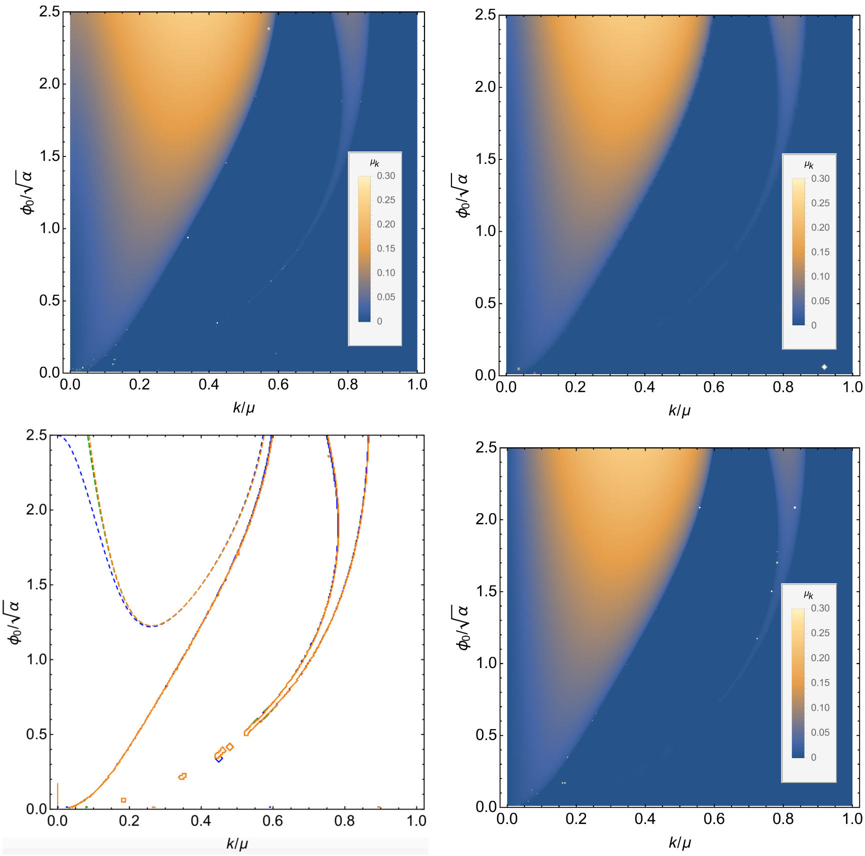

Figure 4.12: *Clockwise from the top:* The 3-D Floquet charts for $n = 3/2$ and $\tilde{\alpha} \equiv \alpha\, M_{\rm Pl}^{-2} = 10^{-2}, 10^{-3}, 10^{-4}$. *Bottom left panel:* The contour plots for $\mu_k = 0$ (solid lines) and $\mu_k = 0.1$ (dashed lines). The blue, green and orange curves are for $\tilde{\alpha} = 10^{-2}, 10^{-3}, 10^{-4}$ respectively.

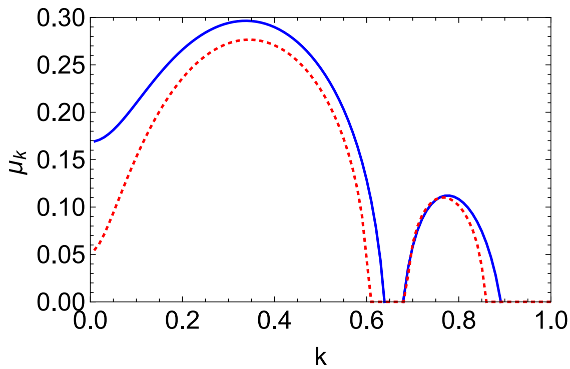

Figure 4.13: The (asymptotic) Floquet exponent computed using the WKB approximation (blue solid) and the Floquet exponent computed using the numerical algorithm described in Section 4.3.4 for $n = 3/2$ and $\tilde{\alpha} = 10^{-3}$. The agreement is very good, given the inherent limitations of the WKB approximation.

of the first two instability bands, even though the shape does not perfectly match the fully numerical solution.

4.3.5 Expanding Universe

There are two complications introduced by studying preheating in an expanding universe: the (slow) decay of the amplitude of the background oscillations due to the non-zero Hubble drag and the red-shifting of the physical wavenumber $k_{\text{phys}} = k_{\text{comoving}}/a$ due to the increasing scale-factor $a(t)$. Both effects are comparable, so they must be studied together. While a WKB analysis can be performed in an expanding universe [306], it must take into account the evolution of both k_{phys} and $\phi(t)$ numerically. Since we believe that it will not add significantly to building intuition on the model at hand, we will not pursue it here. Instead we numerically solve the equations of motion for the χ fluctuations, working in the linear regime as follows: The evolution for the background inflaton field and the Hubble rate are solved numerically using Eqs. (4.22) and (4.23). We subsequently compute the produced χ fluctuations driven by the background inflaton field. The back-reaction of the produced χ fluctuations on the inflaton field or the Hubble rate is ignored. This is a valid approximation until the energy density of the χ fluctuations becomes comparable to the background inflaton energy density. We briefly discuss back-reaction effects in Appendix 4D. We start our computations several e-folds before the end of inflation, in order for the effective mass to be positive for all modes, according to Fig. 4.5 and

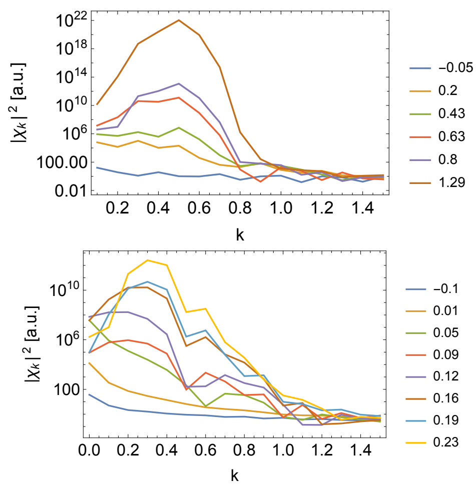

Figure 4.14: The spectra of the fluctuations in the χ field $|\chi_k|^2$ (in arbitrary units) as a function of the wavenumber k (in units of μ) at different times for $n = 3/2$ and $\tilde{\alpha} = 10^{-3}$ (left) and $\tilde{\alpha} = 10^{-4}$ (right). The comparison with Fig. 5 of Ref. [160] shows agreement in the initial stages, when the linear analysis is valid. The comparison is most easily done by considering the amplification occurring between the various time-points shown in the figures, both here and in Ref. [160]. Note that Ref. [160] uses a different normalization for k, as discussed in Appendix 4C. The linear analysis presented here cannot capture the re-scattering effects leading to the broadening of the χ spectrum at late times that was observed in Ref. [160]. The times corresponding to the various curves are shown in the legend of each panel, measured in e-folds after the end of inflation (negative values correspond to spectra during the last stages of inflation).

so that the WKB solutions of Eq. (4.39) provide accurate initial conditions for our code.

Fig. 4.14 shows the spectra of the fluctuations in the χ field at different times. We see that the band structure of the static universe Floquet charts of Section 4.3.4 has disappeared, essentially leaving behind a region of excited modes with comoving wavenumbers that satisfy $k \leqslant k_{\rm max} \approx \mu$. This occurs because each mode with a specific wavenumber k redshifts through the bands of Fig. 4.12, hence a mode with $k \leqslant k_{\rm max}$ will eventually redshift into the main instability band. Even though the exact band structure is erased, the WKB analysis can still capture very well the behavior after the first tachyonic burst. We see that the amplification factor computed in Eq. (4.50) matches very well with the actual amplification. For small values of $\tilde{\alpha}$, where the Hubble scale is much smaller than the frequency of background oscillations, Eq. (4.50) can provide useful intuition for the behavior of the χ fluctuations during the first few ϕ oscillations. Using Eq. (4.14) the maximum excited wavenumber can be immediately compared to the Hubble scale at the end of inflation to give

$$\frac{k_{\mathrm{max}}}{H_{\mathrm{end}}} \simeq \frac{2}{\tilde{\alpha}} \gg 1 \tag{4.56}$$

Hence tachyonic amplification occurs predominately for sub-horizon modes, meaning that they will behave like radiation after the end of preheating.

Fig. 4.15 shows the evolution of the energy density in the background inflaton field ϕ and the fluctuations of the χ field. Considering a finite amount of wavenumbers $k < k_{\mathrm{UV}}$ initialized at the Bunch Davies vacuum, we can compute their energy density at the end of inflation to be

$$\rho_\chi = \int \frac{d^3k}{(2\pi)^3} k^2 \frac{1}{2k} = \frac{1}{(2\pi)^2} \frac{k_{UV}^4}{4} \tag{4.57}$$

This corresponds to the red-dashed line of Fig. 4.15, where we took $k_{\mathrm{UV}} = 1.5\mu$. This is not a physical energy density, since these are vacuum modes. It is however useful as a check of our numerical calculation. Using different values of k_{UV} leads to different early time behavior, as shown from the green-dashed line in Fig. 4.15. As long as $k_{\mathrm{UV}} \geqslant k_{\mathrm{max}}$, the exact choice of k_{UV} becomes irrelevant once tachyonic resonance begins and all modes within $k < k_{\mathrm{max}}$ become exponentially amplified. Hence the blue and green-dashed curves of Fig. 4.15, corresponding to $k_{\mathrm{UV}} = 1.5\mu$ and $k_{\mathrm{UV}} = \mu$ respectively, become indistinguishable shortly after the end of inflation. In is interesting to note that we find for $n = 3/2$ and $\alpha = 10^{-4}$ that preheating will conclude at $N_{\mathrm{reh}} = 0.2$, where the energy density in χ fluctuations equals the energy density in the background field. This result agrees well with the findings of Fig. 4 of Ref. [160], where the results of a full lattice code are shown for the same model parameters.

4.4 Potential dependence

So far we have used the T-model potential of Eqs. (4.62) and (4.63) with $n = 3/2$ as a concrete example to study in detail both analytically and numerically. This potential has the added benefit of allowing for an easy comparison with the full lattice simulations presented in Ref. [160][10]. We

[10] After submission of the present manuscript, an updated version of Ref. [160] appeared. This includes results for two potential types, corresponding to $n = 3/2$ and $n = 1$, as well as two values of the field-space curvature parameter α. These match our results, as we describe in Section 4.5.

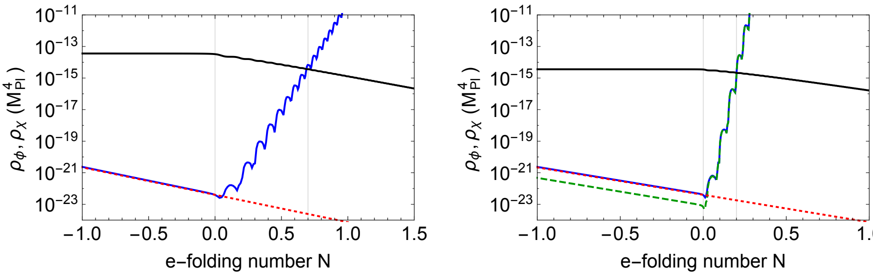

Figure 4.15: The energy density in the background inflaton field (black) and the χ fluctuations (blue) for $n = 3/2$ and $\tilde{\alpha} = 10^{-3}$ (left) and $\tilde{\alpha} = 10^{-4}$ (right). The red-dashed lines show the scaling a^{-4}, which is observed by the fluctuations before the onset of the tachyonic preheating regime. The green-dashed line on the right panel shows a calculation using a different range of UV modes, as explained further in the main text. $N = 0$ marks the end of inflation and we see that preheating concludes within a fraction of an e-fold in both cases.

now extend the analysis to arbitrary values of n, hence to the whole family of the generalized T-model potentials. The background dynamics is summarized in Figs. 4.1 and 4.6 through the dependence of $H_{\rm end}$, $\phi_{\rm end}$ and the period of oscillation T on $\tilde{\alpha}$ and n.

Fig. 4.16 shows the effective mass-squared for $\tilde{\alpha} = 10^{-3}$ and varying n as a function of time, both in the static universe approximation and using the full expanding universe background solution. The former will be used for computing the resonance structure. It is worth noting that the maximally negative value of $m^2_{\mathrm{eff},\chi}$ is larger in the expanding universe case, compared to the static universe one. This is due to the fact that we consider the initial conditions $\{\phi_0, \dot{\phi}_0\} = \{\phi_{\rm end}, 0\}$. In reality, the inflaton velocity is not zero at the end of inflation, hence the Ricci-driven component of the effective mass, which is proportional to $|\dot{\phi}|^2$ is underestimated in our static universe calculations. One important difference between the various values of n shown in Fig. 4.16 can be traced back to Eq. (4.46), which defines the potential contribution of the effective mass near the point $\phi(t) = 0$ or equivalently $\left|\dot{\phi}(t)\right| = \max$, where the Riemann contribution $m^2_{2,\chi}$ is maximized. For $n = 1$ the potential is locally quadratic, hence describing massive fields[11]. This leads to a non-zero positive contribution to the ef-

[11] A locally quadratic potential that becomes less steep at larger field values can also support oscillons. It was shown in Ref. [305] that oscillons can emerge during preheating in a single-field T-model for $n = 1$. Since oscillons are massive objects, a period of oscillon domination causes the universe to acquire an equation of state of $w = 0$, identical to that of a matter dominated era.

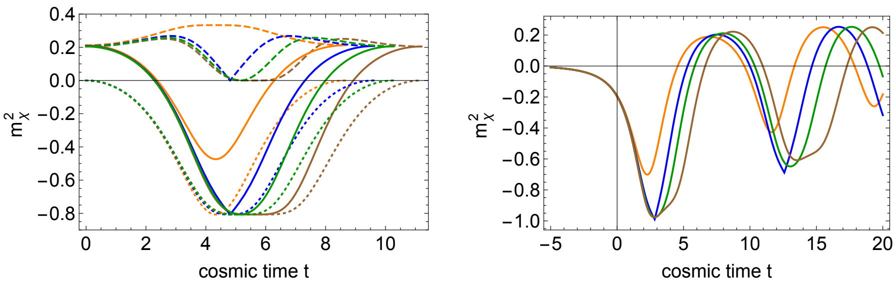

Figure 4.16: *Left:* The two main components of the effective mass squared for χ fluctuations: the potential contribution (dashed) and the field-space Ricci contribution (dotted), along with the sum (solid) for $\tilde{\alpha} = 10^{-3}$ and $n = 1, 3/2, 2, 3$ (orange, blue, green and brown respectively). The plot shows one period in the static universe approximation with $\phi_{\rm max} = \phi_{\rm end}$.
Right: The sum $m^2_{1,\chi} + m^2_{2,\chi}$ using the full expanding universe solution for the background field $\phi(t)$. Inflation is taken to end at $t = 0$.

fective mass-squared for all values of time and wavenumber, thus reducing the overall efficiency of tachyonic resonance, through reducing both A_k of Eq. (4.50) and $k_{\rm max}$. For $n \geqslant 3/2$, the potential contribution vanishes for $\phi(t) = 0$, hence the Riemann term completely determines the maximally negative value of $m^2_{{\rm eff},\chi}$. Furthermore, $\left|\dot{\phi}(t)\right|_{\rm max}$ is found to be almost identical for all values of n. The main difference for increasing the value of n is the increased duration of the regime where $m^2_{1,\phi} \approx 0$. Overall, for $n \geqslant 3/2$ the maximum excited wavenumber $k_{\rm max}$ is the same, while the amplification factor A_k grows, because each tachyonic burst lasts longer. This is shown in Fig. 4.17 using both the WKB approximation, as well as by computing the Floquet exponent numerically following Section 4.3.4. We see that for $n = 1$ the WKB approximation captures only the first instability band, while for $n \geqslant 3/2$ the first two instability bands are well described.

If one tries to plot the three dimensional Floquet diagrams using the field rescaling $\phi_0/\sqrt{\alpha}$, which was used in Fig. 4.12, no unifying pattern emerges. The proper scaling however is $\phi_0/\phi_{\rm end}$, since the comparison must begin at the background field value present at the end of inflation. Using this field rescaling, we can see in Fig. 4.18 and more clearly in Fig. 4.19 that the edges of the instability bands for $\phi_0 = \phi_{\rm end}$ are almost identical for $n \geqslant 3/2$ and significantly higher than the case of $n = 1$. Also, the overall Floquet exponents exhibited are larger for larger values of n, as expected from the behavior of the effective frequency-squared shown in Fig. 4.16.

Starting from Bunch-Davies initial conditions during inflation, specifically initializing our computations at $N_{\rm init} \simeq -4$, we evolved the fluctua-

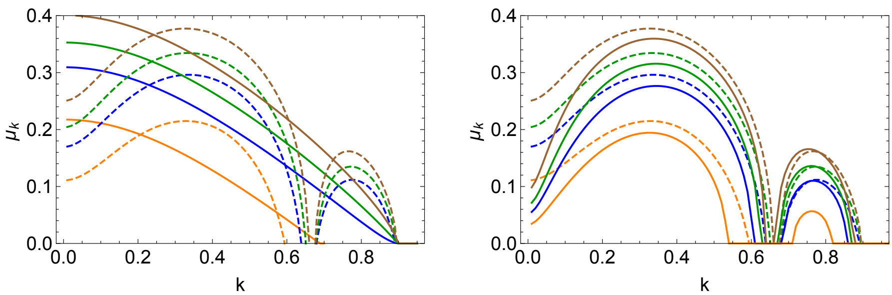

Figure 4.17: *Left:* The asymptotic Floquet exponent (dashed) and the Floquet exponent after the first tachyonic burst (solid) using the WKB approximation for $n = 1, 3/2, 2, 3$ (orange, blue, green and brown respectively). *Right:* The asymptotic Floquet exponent using the WKB method (dashed) and using the algorithm of Section 4.3.4 (solid). The agreement is remarkable given the limitations of the WKB approximation.

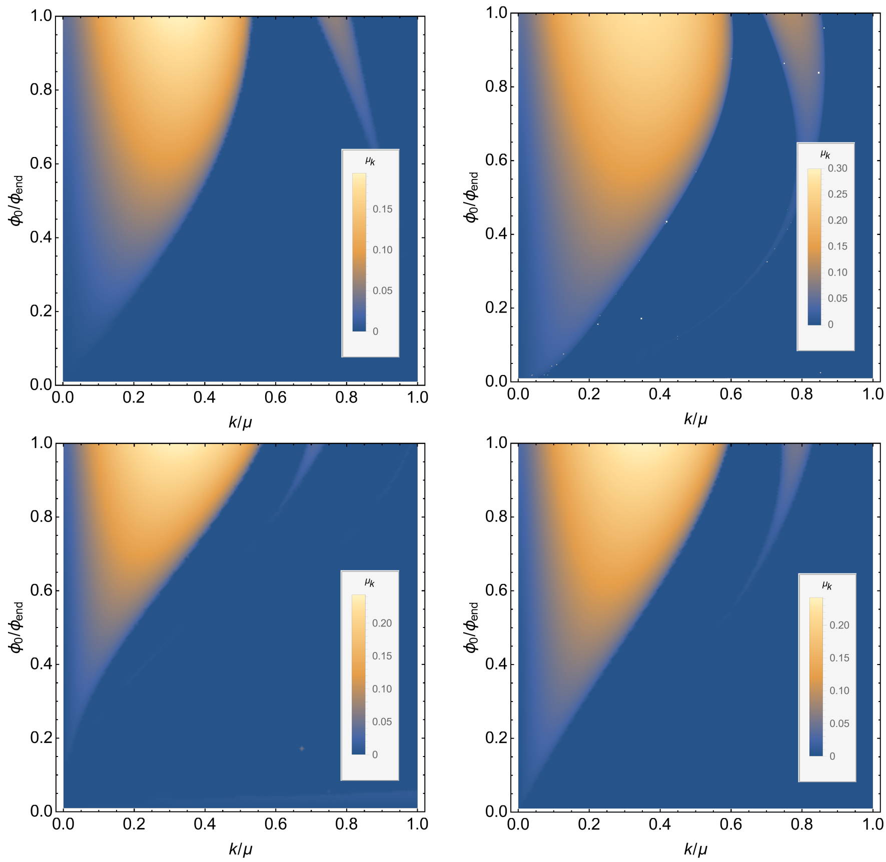

Figure 4.18: Clockwise from top left: The Floquet charts for $\alpha = 10^{-3}$ and $n = 1, 3/2, 2, 3$

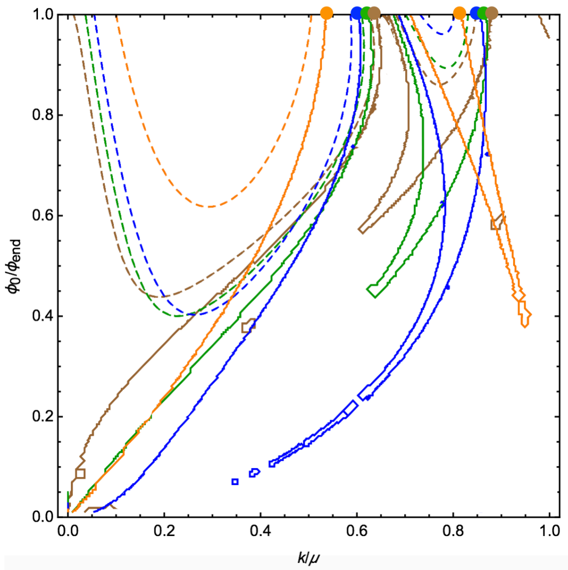

Figure 4.19: The contour plots for $\mu_k = 0$ (solid lines) and $\mu_k = 0.1$ (dashed lines) for $\tilde{\alpha} = 10^{-3}$ and $n = 1, 3/2, 2, 3$ (orange, blue, green and brown respectively). The colored dots on the top denote the right edges of the first and second instability bands. We can see that the edges of the bands for $n \geqslant 3/2$ are almost overlapping, while the range of excited wavenumbers for $n = 1$ is significantly smaller.

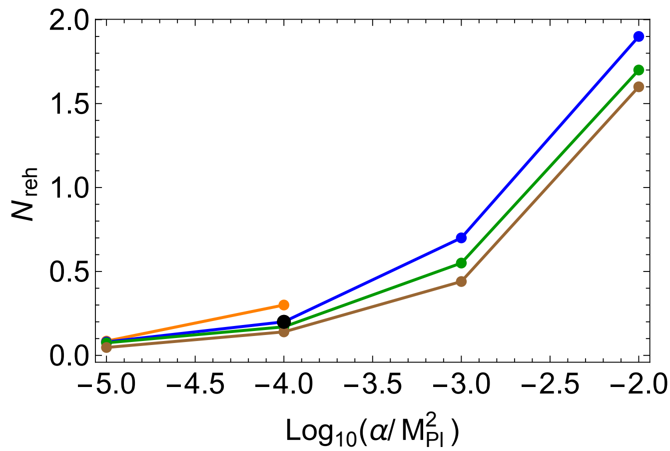

Figure 4.20: The time required (in e-folds) for the transfer of the entire inflaton energy density into modes of the χ field as a function of the field-space curvature parameter α for $n = 1, 3/2, 2, 3$ (orange, blue, green and brown respectively). The black point shows the parameters used in Ref. [160]. The linear no-backreaction approximation is used. We see that preheating is essentially instantaneous for $\alpha \lesssim 10^{-4} M_{\rm Pl}^2$.

tions in the χ field on the single-field ϕ background, taking into account the expansion of the universe and working in the linear regime, hence neglecting any mode-mode coupling and back-reaction effects. Fig. 4.20 shows the time needed for the complete transfer of energy from the χ background field to χ radiation modes[12]. For $n = 1$ and $\alpha \gtrsim 10^{-3} M_{\rm Pl}^2$ preheating did not complete through this channel. Overall we see faster preheating for larger values of n, hence steeper potentials. However the differences are diminishing for highly curved field-space manifolds, practically disappearing for $\alpha \lesssim 10^{-4} M_{\rm Pl}^2$, where preheating occurs almost instantaneously.

4.5 Summary and Discussion

In the present work we studied preheating in a two-field generalization of the T-model, which is part of the larger family of α-attractors, characterized by a field-space manifold of constant negative curvature. We focused on the production of non-inflaton particles, since inflaton self-resonance in the single-field T-model has been extensively studied (e.g. Ref. [305]), finding

[12] An updated version of Ref. [160] includes simulations for $\{\tilde{\alpha}, n\} = \{10^{-3}, 3/2\}, \{10^{-4}, 3/2\}, \{10^{-4}, 1\}$ exhibiting complete preheating at $N_{\rm reh} \approx 0.7, 0.15, 0.2$ respectively, which match the values shown in Fig. 4.20 for these parameter values.

reheating to complete within a few e-folds for $n \neq 1$ and oscillon formation leading to a prolonged matter-dominated phase for $n = 1$.

We examined the possibility of multi-field effects arising during inflation and found a strong single-field attractor along a straight background trajectory $\chi = 0$. In order for multi-field effects to produce observable signatures, like "ringing" patterns on the CMB, the initial conditions have to be extremely fine-tuned, which makes such an event unlikely. The strong single-field inflationary attractor ensures that preheating will also occur around a single-field background, at least during the initial stage, when back-reaction effects can be safely ignored. Different multi-field potentials on hyperbolic manifolds might support genuinely multi-field background trajectories, leading to significantly different preheating dynamics. This remains an intriguing possibility worth further study.

We found that most key preheating quantities rely crucially on the field-space curvature parameter α, in fact exhibiting simple scaling behaviors. The Hubble scale at the end of inflation scales as $H_{\rm end} \sim \sqrt{\alpha}$ and is largely independent of the potential steepness, a characteristic trait of α-attractors. However the period of background oscillations does not involve α, meaning that more background oscillations "fit" in the first e-fold after inflation for higher values of the field-space curvature (low values of α). The maximum amplified wavenumber is roughly constant for all values of α and potential steepness parameter n, with the exception of $n = 1$, where $k_{\rm max}$ is smaller by about 25%.

Since the frequency of background oscillations is much larger than the Hubble scale at the end of inflation, the static universe is an increasingly good approximation for larger values of the field-space curvature. This makes Floquet theory a useful tool for understanding preheating in the two-field T-model. We found that when plotting the Floquet charts for a specific value of the potential steepness parameter n using the wavenumber and the background field amplitude rescaled by $\sqrt{\alpha}$, all Floquet charts collapse into a single "master diagram" for small values of α.

This scaling behavior of the Floquet charts persists even for different potentials within the T-model. In the case of varying n the background field must be normalized by the field value at the end of inflation $\phi_{\rm end}$ in order for the Floquet chart scaling behavior to appear. As expected, the scaling between Floquet charts of different potentials is not exact, but similarities are enough to explain the similar preheating behavior shown in Fig. 4.20. There we see that preheating lasts longer for larger values of α and smaller values of n, while recovering the results of Ref. [160] for

$n = 3/2$ and $\tilde{\alpha} = 10^{-4} M_{\rm Pl}^2$, $n = 3/2$ and $\tilde{\alpha} = 10^{-3} M_{\rm Pl}^2$, as well as for $n = 1$ and $\tilde{\alpha} = 10^{-4} M_{\rm Pl}^2$.

While observing reheating is difficult due to the inherently small length scales involved, knowledge of the duration of reheating is essential to correctly match the CMB modes to the exact point during inflation when they left the horizon [161]. Expanding on the lattice simulations of Ref. [160] we showed that preheating in the two-field T-model is essentially instantaneous for highly curved field-space manifolds, regardless of the exact form of the potential. This reduces the uncertainty of the predictions of this class of models for the scalar spectral index n_s. Unfortunately the low values of α required for the onset of instantaneous preheating makes the observation of tensor modes in these models unlikely even with the CMB Stage 4 experiments, since the resulting tensor-to-scalar ratio is too small $r < 10^{-4}$.

The scaling behavior found in T-model preheating does not guarantee that similar effects will arise in other α-attractor models. Our results can be applied to study preheating in broader classes of multi-field inflationary models with hyperbolic field-space manifolds. We leave an exhaustive analysis for future work.

4.6 Appendix 4A: Generalization of the T-model

A simple generalization of the T-model [160, 301] is given by the superpotential

$$W_H = \sqrt{\alpha}\mu\, S\, F(Z) \tag{4.58}$$

and Kähler potential

$$K_H = \frac{-3\alpha}{2} \log\left[\frac{(1 - Z\bar{Z})^2}{(1 - Z^2)(1 - \bar{Z}^2)}\right] + S\bar{S}\,. \tag{4.59}$$

Using the relation between the Kähler potential and the superpotential

$$Z = \frac{T-1}{T+1} \tag{4.60}$$

and choosing

$$F(Z) = Z^n \tag{4.61}$$

we get

$$K_H = \frac{-3\alpha}{2} \log\left[\frac{(T + \bar{T})^2}{4T\bar{T}}\right] + S\bar{S} \tag{4.62}$$

and

$$W_H = \sqrt{\alpha}\mu S \left(\frac{T-1}{T+1}\right)^n . \tag{4.63}$$

as in Ref. [301]. The potential follows to be of the form

$$V = \alpha\mu^2 \left(Z\bar{Z}\right)^n \left(\frac{(1-Z^2)(1-\bar{Z}^2)}{(1-Z\bar{Z})^2}\right)^{3\alpha/2} . \tag{4.64}$$

One can use multiple field-space bases to describe these models. The choice

$$Z = \tanh\left(\frac{\phi + i\theta}{\sqrt{6\alpha}}\right) \tag{4.65}$$

was used in Ref. [301], leading to the kinetic term

$$\mathcal{L}_{kin} = \frac{1}{2}\mathcal{G}_{\phi\phi}\,\partial_\mu\phi\,\partial^\mu\phi + \frac{1}{2}\mathcal{G}_{\theta\theta}\,\partial_\mu\theta\,\partial^\mu\theta \tag{4.66}$$

with

$$\mathcal{G}_{\phi\phi} = \mathcal{G}_{\theta\theta} = \frac{1}{\cos^2\left(\sqrt{\frac{2}{3\alpha}}\theta\right)} \tag{4.67}$$

and the two-field potential

$$V(\phi,\theta) = \alpha\mu^2 \left(\frac{\cosh\left(\sqrt{\frac{2}{3\alpha}}\phi\right) - \cos\left(\sqrt{\frac{2}{3\alpha}}\theta\right)}{\cosh\left(\sqrt{\frac{2}{3\alpha}}\phi\right) + \cos\left(\sqrt{\frac{2}{3\alpha}}\theta\right)}\right)^n \left(\cos\left(\sqrt{\frac{2}{3\alpha}}\theta\right)\right)^{-3\alpha} . \tag{4.68}$$

We instead choose the basis used in Ref. [160], which can be derived from Eq. (4.65) by performing the transformation

$$\cos\left(\sqrt{\frac{2}{3\alpha}}\theta\right) = \frac{1}{\cosh\left(\sqrt{\frac{2}{3\alpha}}\chi\right)} . \tag{4.69}$$

This leads to the kinetic term (4.2)

$$\mathcal{L}_{kin} = \frac{1}{2}\partial_\mu\chi\partial^\mu\chi + \frac{1}{2}\cosh^2\left(\sqrt{\frac{2}{3\alpha}}\chi\right)\partial_\mu\phi\partial^\mu\phi\,, \tag{4.70}$$

and potential (4.3)

$$V(\phi,\chi) = \alpha\mu^2 \left(\frac{\cosh(\beta\phi)\cosh(\beta\chi) - 1}{\cosh(\beta\phi)\cosh(\beta\chi) + 1}\right)^n \left(\cosh(\beta\chi)\right)^{2/\beta^2} , \tag{4.71}$$

where $\beta = \sqrt{2/3\alpha}$.

This choice of the field-space basis allows an easier comparison between our work and Ref. [160] and simple equations of motion, both for the background as well as for the fluctuations. This comes at a price, namely the illusion that the two field-space directions are inherently different, one of them even being canonically normalized. However, as can be seen in Appendix 4B, this basis describes a field-space with a constant curvature at every point.

4.7 Appendix 4B: Field-Space quantities for hyperbolic space

The kinetic term for the two-field model at hand is written as

$$\mathcal{L} = \frac{1}{2}\mathcal{G}_{IJ}\partial_\mu\phi^I\partial^\mu\phi^J \,, \tag{4.72}$$

where $\{\phi^1, \phi^2\} \equiv \{\phi, \chi\}$. In the basis used the non-zero field-space quantities are

- The metric

$$\mathcal{G}_{\phi\phi} = e^{2b(\chi)} = e^{2\log(cosh(\beta\chi))} = cosh^2(\beta\chi)\,, \quad \mathcal{G}_{\chi\chi} = 1 \tag{4.73}$$

- The inverse metric

$$\mathcal{G}^{\phi\phi} = e^{-2b(\chi)} = e^{-2\log(cosh(\beta\chi))} = \mathrm{sech}^2(\beta\chi)\,, \quad \mathcal{G}^{\chi\chi} = 1 \tag{4.74}$$

- The Christoffel symbols

$$\Gamma^{\phi}_{\chi\phi} = \beta\tanh(\beta\chi)\,, \quad \Gamma^{\chi}_{\phi\phi} = -\frac{1}{2}\beta\sinh(2\beta\chi) \tag{4.75}$$

- The Riemann tensor

$$\mathcal{R}^{\phi}_{\chi\phi\chi} = -\beta^2\,, \quad \mathcal{R}^{\phi}_{\chi\chi\phi} = \beta^2\,, \quad \mathcal{R}^{\chi}_{\phi\phi\chi} = \beta^2\cosh^2(\beta\chi)\,, \quad \mathcal{R}^{\chi}_{\phi\chi\phi} = -\beta^2\cosh^2(\beta\chi) \tag{4.76}$$

- The Ricci tensor

$$\mathcal{R}_{\phi\phi} = -\beta^2\cosh^2(\beta\chi)\,, \quad \mathcal{R}_{\chi\chi} = -\beta^2 \tag{4.77}$$

- Finally, the Ricci scalar

$$\mathcal{R} = -2\beta^2 = -\frac{4}{3\alpha}\,, \tag{4.78}$$

where we used

$$\beta = \sqrt{\frac{2}{3\alpha}}\,. \tag{4.79}$$

4.8 Appendix 4C: Alternative time parametrization

For completeness and ease of comparison with Ref. [160] we present a different rescaling prescription. Specifically in Ref. [160] the field-space curvature is rescaled using the reduced Planck mass as $\alpha = M_{\rm Pl}^2\tilde{\alpha}$ and the equation of motion for the background field becomes

$$\ddot{\tilde{\phi}} + 3H\dot{\tilde{\phi}} + \left(\frac{M^2}{M_{\rm Pl}}\right)^2 \frac{\sqrt{6}n}{\sqrt{\tilde{\alpha}}}\mathrm{csch}\left(\frac{\sqrt{\frac{3}{2}}\tilde{\phi}}{\sqrt{\alpha}}\right)\tanh^{2n}\left(\frac{\sqrt{\frac{3}{2}}|\tilde{\phi}|}{2\sqrt{\alpha}}\right) = 0\,. \tag{4.80}$$

Time is then rescaled by $m \equiv M^2/M_{\rm Pl}$, leading to the equation

$$\frac{d^2\tilde{\phi}}{d(mt)^2} + 3\tilde{H}\frac{d\tilde{\phi}}{d(mt)} + \frac{\sqrt{6}n}{\sqrt{\tilde{\alpha}}}\mathrm{csch}\left(\frac{\sqrt{\frac{3}{2}}\tilde{\phi}}{\sqrt{\alpha}}\right)\tanh^{2n}\left(\frac{\sqrt{\frac{3}{2}}|\tilde{\phi}|}{2\sqrt{\alpha}}\right) = 0\,, \tag{4.81}$$

where $\tilde{H} = H/m$. The relevant plots, Floquet exponents and comoving wavenumbers in Ref. [160] are presented and measured in units of $M^2/M_{\rm Pl}$.

The Hubble scale is

$$\tilde{H}^2 = \frac{1}{3}\left[\frac{1}{2}\left(\frac{d\tilde{\phi}}{d(mt)}\right)^2 + \tanh^{2n}\left(\frac{|\tilde{\phi}|}{\sqrt{6\tilde{\alpha}}}\right)\right]\,.$$

The fluctuation equations with this definition of time become

$$\frac{d^2Q_\phi}{d(mt)^2} + 3\frac{H}{m}\frac{dQ_\phi}{d(mt)} + \left[\frac{(k/m)^2}{a^2} + \frac{V_{\phi\phi}}{m^2}\right]Q_\phi = 0\,, \tag{4.82}$$

$$\frac{d^2Q_\phi}{d(mt)^2} + 3\frac{H}{m}\frac{dQ_\phi}{d(mt)} + \left[\frac{(k/m)^2}{a^2} + \frac{V_{\phi\phi}}{m^2}\right]Q_\phi = 0 \tag{4.83}$$

with

$$\frac{V_{\phi\phi}}{m^2} = \frac{d^2}{d\tilde{\phi}^2}\left[\tanh^{2n}\left(\frac{|\tilde{\phi}|}{\sqrt{6\tilde{\alpha}}}\right)\right]\,. \tag{4.84}$$

The ratio of the two mass-scales that can be used to normalize time and wave-numbers is

$$\frac{m}{\mu} = \sqrt{\tilde{\alpha}}\,, \tag{4.85}$$

making the comparison of our linear results with the full lattice simulations of Ref. [160] straightforward.

4.9 Appendix 4D: Back-reaction

Since the present work is focused on extracting semi-analytical arguments, based on the WKB approximation, it is worth examining some back-reaction effects more closely. There are several sources of back-reaction and the only way to accurately describe their combined effects is through lattice simulations, as done for the system under study in Ref. [160]. On a qualitative level, we can distinguish various back-reaction effects:

- Mode-mode mixing: This refers to non-linear mixing between the modes $\delta\chi_k$ and usually leads to a power cascade towards the UV. Mode-mode mixing is required for thermalization and is outside of the scope of linear theory. Even in lattice simulations, proper study of thermalization processes usually requires even more UV modes than are usually available.

- Induced $\delta\phi$ fluctuations due to $\delta\chi$ modes scattering off the inflaton condensate ϕ.

- Siphoning energy off the inflaton condensate and acting as a extra drag term for the inflaton motion $\phi(t)$, thus suppressing background oscillations.

We will focus on estimating the last term, as it is the one that can damp the background motion and thus suppress tachyonic preheating[13].
The full equation of motion for the ϕ field is

$$\ddot{\phi} + \Gamma^{\phi}_{\chi\phi}\dot{\chi}\dot{\phi} + 3H\dot{\phi} + \mathcal{G}^{\phi\phi}V_{,\phi} = 0 \tag{4.86}$$

In order to estimate the terms arising from the back-reaction of the produced χ particles, we Taylor expand all terms involving χ and use a Hartree-type approximation to substitute all quadratic quantities with their average

[13]Thermalization can affect Bose enhancement by altering the produced $\delta\chi_k$ spectrum, but it typically operates close to or after the point of complete preheating. Since we only intend to estimate back-reaction effects, we will not discuss it further.

value

$$\chi^2 \quad \to \quad \langle\chi^2\rangle = \int \frac{d^3k}{(2\pi)^3}|\delta\chi_k|^2 \tag{4.87}$$

$$\chi\dot{\chi} \quad \to \quad \langle\chi\dot{\chi}\rangle = \int \frac{d^3k}{(2\pi)^3}\delta\chi_k \cdot \delta\dot{\chi}_k^* \,. \tag{4.88}$$

The background equation of motion for the inflaton ϕ thus becomes

$$\ddot{\phi} + 3H\dot{\phi} + \mathcal{G}^{\phi\phi}V_{,\phi} = -\beta^2\langle\chi\dot{\chi}\rangle\dot{\phi} + \Delta V\langle\chi^2\rangle V_{,\phi} \tag{4.89}$$

where ΔV arises from expanding $\mathcal{G}^{\phi\phi}$ and $V_{,\phi}$ around $\chi = 0$. The term in the equation of motion involving $\langle\chi\dot{\chi}\rangle$ arises from the Christoffel symbol and acts as an extra drag term, whereas ΔV can be thought of as an extra force. Fig. 4.21 shows the potential term $\mathcal{G}^{\phi\phi}V_{,\phi}$ along with the back-reaction contributions to the equations of motion for the case of $\tilde{\alpha} = 0.001$ and $n = 3/2$. We see that the back-reaction terms only become important close to the point of complete preheating, defined as $\rho_\phi = \rho_{\delta\chi}$. This means that during the last inflaton oscillation(s) before complete preheating is achieved, the background inflaton motion will be suppressed due to the produced modes. This has the potential of quenching the resonance and causing the stop of χ particle production. However tachyonic resonance is usually very robust, since –as we described using the WKB analysis– as long as the inflaton velocity is non-zero, the hyperbolic metric will lead to a tachyonic instability of $\delta\chi_k$. A careful numerical investigation of tachyonic resonance, albeit in another context, can be found in Ref. [308], where lattice results were compared to linear calculations, like the ones presented here. It was shown that for the case where the linear calculations pointed to complete tachyonic preheating after a few inflaton oscillations, lattice simulations led to very similar results. The lattice simulations of Ref. [160] indeed point to a decay of the inflaton condensate and complete preheating, but an evolution of $\phi(t)$ identical to the back-reaction-free case up until very close to that point. Hence linear analysis can successfully capture the initial growth of $\delta\chi$ fluctuations and provide strong indications for parameter choices that allow for complete preheating.

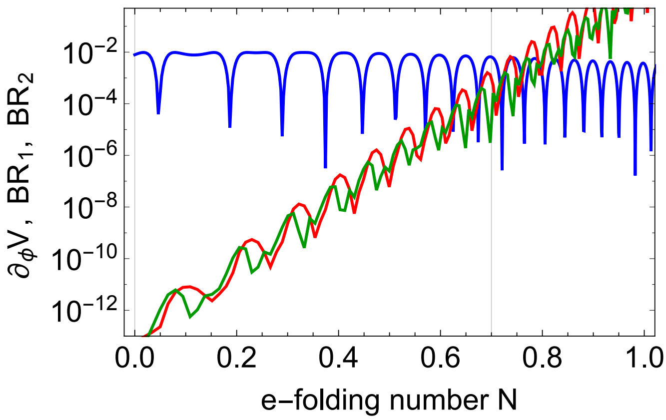

Figure 4.21: The magnitude of the inflaton potential term $|V_{,\phi}|$ (blue) and the two back-reaction terms $BR_1 \equiv |\beta^2 \langle \chi \dot{\chi} \rangle \dot{\phi}|$ (green) and $BR_2 \equiv \Delta V \langle \chi^2 \rangle |V_{,\phi}|$ (red) for $\tilde{\alpha} = 0.001$ and $n = 3/2$. The vertical line at $N = 0.7$ corresponds to the time of complete preheating, according to Fig. 4.15. We see that back-reaction effects only become important close to the point of complete preheating and they do not affect the early time dynamics, as expected.

5 Preheating with asymmetric multi-field potentials

Abstract: We analyze and compare the multi-field dynamics during inflation and preheating in symmetric and asymmetric models of α-attractors, characterized by a hyperbolic field-space manifold. We show that the generalized (asymmetric) E- and (symmetric) T-models exhibit identical two-field dynamics during inflation for a wide range of initial conditions. The resulting motion can be decomposed in two approximately single-field segments connected by a sharp turn in field-space. The details of preheating can nevertheless be different. For the T-model one main mass-scale dominates the evolution of fluctuations of the spectator field, whereas for the E-model, a competing mass-scale emerges due to the steepness of the potential away from the inflationary plateau, leading to different contributions to parametric resonance for small and large wave-numbers. Our linear multi-field analysis of fluctuations indicates that for highly curved manifolds, both the E- and T-models preheat almost instantaneously. For massless fields this is always due to efficient tachyonic amplification of the spectator field, making single-field results inaccurate. Interestingly, there is a parameter window corresponding to $r = \mathcal{O}(10^{-5})$ and massive fields, where the preheating behavior is qualitatively and quantitatively different for symmetric and asymmetric potentials. In that case, the E-model can completely preheat due to self-resonance for values of the curvature where preheating in the T-model is inefficient. This provides a first distinguishing feature between models that otherwise behave identically, both at the single-field and multi-field level. Finally, we discuss how one can describe multi-field preheating on a hyperbolic manifold by identifying the relevant mass-scales that control the growth of inflaton and spectator fluctuations, which can be applied to any α-attractor model and beyond.

Keywords: inflation, reheating, asymmetry.

Based on:
O. Iarygina, E. I. Sfakianakis, D. G. Wang and A. Achúcarro
Multi-field inflation and preheating in asymmetric α-attractors.
[arXiv:2005.00528].

5.1 Introduction

Our understanding of the early universe is largely based on two observationally constrained phases: inflation and big-bang nucleosynthesis (BBN). Inflation remains the leading framework for physics of the very early universe because it provides an elegant solution for the horizon and flatness problems [27, 28] as well as a mechanism to seed quantum fluctuations which is in excellent agreement with the latest observational tests [53] for a wide range of models. At the same time, BBN is based on the detailed information about nuclear reactions and provides predictions for the light-element abundances [310]. So far the theoretical predictions of BBN match observations to very high accuracy. On the other hand, the reheating process that provides an exit from inflation and transition to the thermal state of the universe, which is required for BBN, is far less explored or constrained. The duration of reheating determines the moment of transition to the radiation dominated era, hence it can affect BBN and shift the time at which CMB-relevant scales left the horizon during inflation, thereby altering inflationary predictions. Therefore, a detailed knowledge of the reheating physics is crucial in the era of precision cosmology, in order to reduce theoretical uncertainties and provide a smooth link between the theory and present (or future) observational data.

Since the energy scale of the early universe is expected to be very high (over or close to $E^{1/4} \sim 10^{16}$Gev), the universe may be populated with multiple scalar fields which could participate in inflation and affect the relevant dynamics. Therefore, despite the simplicity of single-field models, there is strong motivation to study multi-field effects and their predictions. Recent work has revealed an abundance of models with strong turns in the inflationary trajectory [59–62, 65, 67, 68, 70, 311–313]. Multi field models of this sort have been shown to possess strong dynamical single-field attractors, which are of a different nature compared to usual single-field inflation. In fact these novel attractors lead to large turn-rate, possibly seeding large non-Gaussianity. Given the theoretical motivation and the multi-field "surprises" that have been revealed to occur during inflation in some cases, it is essential to extend inflationary models to include multiple fields. In particular, focusing on two-fields can provide a breadth of novel phenomena, while allowing us to build intuition and easily visualize the dynamics.

Due to the huge number of inflationary models, it is hardly possible to state universal (model independent) physical predictions for the various observables. In the last few years a broad class of inflationary theories have been discovered, that can be grouped under the name of "cosmological attractors". This includes conformal attractors [49, 314], universal attractors with non-minimal coupling to gravity [154, 315] and α-attractors [50, 66, 243–245]. This class of models brings together a lot of well-known inflationary models such as the Starobinsky model [251], the GL model [316, 317], and Higgs inflation [156, 318]. All of the models have different setups, yet give very close cosmological predictions for the important observables. It is thus important that we clarify the twofold meaning of the term "attractor" in the context of inflation. For most multi-field models, the term attractor is used to describe a specific trajectory in field space, toward which the inflationary evolution will flow, regardless of the initial conditions within a certain basin of attraction. For the "cosmological attractors" [49, 50, 154, 156, 243–245, 251, 314–318], the term is not mainly used to describe a dynamical attractor in field space, but denotes the fact that in some parameter regime, the observables will "flow" to a specific value, which is then largely insensitive to the exact parameter values. In particular for the scalar spectral index n_s and the tensor-to-scalar ratio r, α-attractors and related models give

$$n_s = 1 - \frac{2}{N_*}, \quad r = \frac{12\alpha}{N_*^2}, \tag{5.1}$$

where N_* is the time in e-folds before the end of inflation, where modes first exit the horizon during inflation and α is a dimensionless parameter that –in some models– encodes the field-space curvature[1]. For $N_* \gtrsim 55$, the cosmological attractor predictions lead to very good agreement with the observational data. These models can be further used to link inflation to the dark energy (cosmological constant) problem [319] and aspects of supersymmetry breaking [320]. Frequent use of the term "α-attractors" is made to describe single-field systems with plateau potentials, usually of the form $V \propto \left|1 - e^{-\phi/\Lambda}\right|^{2n}$ or $V \propto |\tanh(\phi/\Lambda)|^{2n}$, leading to the predictions of

[1] It is interesting to note, that two-field α-attractors with $\alpha = \mathcal{O}(1)$ can lead to the predictions of Eq. (5.1) without possessing a dynamical single-field attractor [61].

Eq. (5.1). However the flattening of the potential is merely a by-product of a more general feature of α-attractors: hyperbolic field-space manifolds. As we further demonstrate in the present work, the presence of a second field is crucial for the full dynamics of α-attractors during preheating and must be considered to properly extract the predictions of these models, making the single field analysis generally insufficient.

It is worth mentioning that, despite α-attractor models being in a great agreement with the Planck 2018 data, there is still the strong inverse dependence on N_* in Eq. (5.1). Therefore, the uncertainties from the duration of reheating are becoming increasingly important as more data are being gathered. In particular, the latest *Planck* release [53] has shown a slight tension (depending on the exact data sets that are being combined) between the measured value of n_s and the α-attractor predictions for $N_* \simeq 50$.

In this paper we focus specifically on α-attractor models, which are characterized by a hyperbolic field-space geometry with the constant negative curvature determined by the parameter α. There have been several constructions of α-attractor models, but two of the earliest ones, which are still considered the prototypical workhorses, are T- and E-models. In the single-field limit, they represent potentials that are respectively symmetric and antisymmetric around the minimum. By construction, α-attractors are two-field models, since they are constructed by specific choices of the superpotential and Kähler potential in $\mathcal{N} = 1$ supergravity models of a complex scalar field, corresponding to an axion-dilaton system (see Appendix 5A). The effects of two-field dynamics in T-model preheating has received attention recently using both numerical [160] and semi-analytical techniques [158]. Here, we complement our analysis of the symmetric two-field T-model, by examining a class of generalized E-model potentials [321], in which the inflaton potential is asymmetric with respect to the origin, which is also the global minimum of the potential. We explore differences and similarities in the inflationary dynamics, the duration and the underlying mechanism of preheating for symmetric and asymmetric potentials.

We find interesting two-field dynamics during inflation, leading to a single-field attractor in which the second field (spectator) is stabilized at its minimum. Interestingly, the similarities of the T- and E-model during inflation go beyond the existence of a strong single-field attractor with a large basin of attraction. In fact, we show that the full two-field dynamics of the two models is identical, up to slow-roll corrections. Given the existence of a strong single field attractor, we have analyzed the excitation of fluctuations in the inflaton and spectator field, the latter driven by a tachyonic instability due to the negatively curved field-space manifold. By analyzing the preheating efficiency of the E-model, we find qualitative differences with similar studies of the related T-model. In particular, the parametric resonance of inflaton fluctuations is significantly more enhanced in the E-model, as compared to the T-model. Furthermore, for $10^{-4} \lesssim \alpha \lesssim 10^{-3}$, preheating is efficient for the E-model, but not the T-model. This presents the first example of a difference between these two α-attractor models and can lead to different predictions for CMB observables.

This work is organized as follows. In Section 5.2 we introduce a generalization of the E-model, with an inflaton ϕ and spectator field χ, and study the background motion with a detailed comparison to the T-model. We find that during inflation, the approach to the single-field attractor of the E- and T-models is identical, up to slow-roll corrections. In order to assess the strength of the single-field attractor and treat the two fields on the same footing, regardless of the intricacies of the specific parametrization on the curved field-space manifold, we evaluated the background evolution with initial conditions chosen to lie on several iso-potential surfaces. The resulting motion can be viewed as approximately single-field trajectories joined by a sharp tun in field-space, followed by a brief period of transient oscillations. Section 5.3 provides an overview of the fluctuation analysis for the case of multiple fields. We focus on the parametric excitation of χ fluctuations –since the corresponding parametric resonance for ϕ fluctuations has been studied in the literature and is weaker for most parameters of interest– and extensively study separate contributions to the effective frequency that affect particle production. In Section 5.4 we use Floquet theory to study particle production and invoke the various mass-scales to explain the differences between the T- and E-model results. We numerically compute the transfer of energy to radiative degrees of freedom in the linear approximation, neglecting mode-mode coupling and backreaction. We focus on the $n = 1$ case, where the system close to the minimum is described as consisting of interacting massive particles, and compare the preheating efficency of the T- and E-model. In Section 5.5 we conclude and provide an outlook for further studies.

5.2 Model and inflationary dynamics

Having studied the preheating behaviour of the generalized two-field T-model in Chapter 4, we move to the corresponding generalization of the E-model. The T- and E- model can be viewed as the prototypical examples of symmetric and asymmetric α-attractors. Analyzing them can help us build the toolbox and intuition needed to analyze any current or future α-attractor scenario that possesses a late-time single-field attractor. As before, we consider a model consisting of two interacting scalar fields on a hyperbolic manifold of constant negative curvature. The specific supergravity construction can be found in Appendix 5A, leading to the two field Lagrangian

$$\mathcal{L} = -\frac{1}{2}\left(\partial_\mu\chi\partial^\mu\chi + e^{2b(\chi)}\partial_\mu\phi\partial^\mu\phi\right) - V(\phi,\chi)\,, \tag{5.2}$$

where $b(\chi) = \log\left(\cosh(\beta\chi)\right)$ and $\beta = \sqrt{2/3\alpha}$. But now the corresponding two-field potential is

$$V(\phi,\chi) = \alpha\mu^2\left(1 - \frac{2e^{-\beta\phi}}{\cosh\left(\beta\chi\right)} + e^{-2\beta\phi}\right)^n \left(\cosh(\beta\chi)\right)^{2/\beta^2}\,. \tag{5.3}$$

For $\chi = 0$ the potential becomes

$$V(\phi,0) = \alpha\mu^2\left[\left(1 - e^{-\beta\phi(t)}\right)^2\right]^n\,, \tag{5.4}$$

which is a simple one-parameter family of the single-field E-model described in Ref. [321].

The background equations of motion for $\phi(t)$ at $\chi(t) = 0$ are

$$\ddot{\phi} + 3H\dot{\phi} + 2\sqrt{\frac{2}{3}}\frac{\sqrt{\alpha}n\left[\left(e^{-\beta\phi}-1\right)^2\right]^n}{e^{\beta\phi}-1} = 0 \tag{5.5a}$$

$$3H^2 = \frac{1}{2}\left(\frac{d\phi}{dt}\right)^2 + \alpha\left[\left(1 - e^{-\beta\phi}\right)^2\right]^n = 0 \tag{5.5b}$$

where we rescaled the field ϕ by $M_{\rm Pl}$, time t by μ and the curvature parameter α by $M_{\rm Pl}^2$, as in Chapter 4. We lift tildes for rescaled quantities (which were used in Chapter 4) for the simplicity of notation. Hence with these conventions the Hubble scale is measured in units of μ. The same is true for the comoving wavenumbers, as we will see in Section 5.3.

5.2.1 Single-field background motion

Eqs. (5.5) can be simplified during slow-roll inflation, for $\phi \gg \sqrt{\alpha}$

$$3H\dot{\phi} + \frac{2\sqrt{2}}{\sqrt{3}}\sqrt{\alpha}\,ne^{-\beta\phi} \simeq 0\,,\quad 3H^2 \simeq \frac{\alpha}{M_{\rm Pl}^2}\mu^2 \tag{5.6}$$

where we explicitly wrote the dimensions of the various quantities in the equation of the Hubble scale. These equations are almost identical to the ones that govern the inflationary behaviour of the T-model discussed in Chapter 4, and can be solved analogously

$$\dot{\phi} \simeq -\frac{2\sqrt{2}n}{3} e^{-\beta\phi} , \quad N = \frac{3\alpha}{4n} e^{\beta\phi} . \tag{5.7}$$

One may notice a factor of 2 difference in comparison to the case of the T-model. This leads to the slow-roll quantities

$$\epsilon \equiv -\frac{\dot{H}}{H^2} \simeq \frac{3\alpha}{4N^2} , \quad \eta \equiv \frac{\dot{\epsilon}}{\epsilon H} \simeq \frac{2}{N} \tag{5.8}$$

and in turn to the tensor-to-scalar ratio

$$r = 16\epsilon = \frac{12\alpha}{N^2} . \tag{5.9}$$

As expected, the results for the slow-roll parameters and Hubble scale during single-field inflation are identical for the generalized T- and E-models. Following the breakdown of the slow-roll analysis close to $\epsilon = 1$, inflation can be shown to end at $\phi_{\rm end} = \mathcal{O}(1)\sqrt{\alpha}$ and the corresponding Hubble scale to be $H^2_{\rm end} \sim \mathcal{O}(1)\alpha\,\mu^2$. From the amplitude of the scalar power spectrum

$$A_s = \frac{H^2}{8\pi M^2_{\rm Pl}\epsilon} \simeq 2 \times 10^{-9} \tag{5.10}$$

we extract the mass-scale $\mu \simeq 6 \times 10^{-6} M_{\rm Pl}$ for $N = 55$ e-folds. Note that this scale is the same for the T model described in Chapter 4.

Comparison with the T model, which has a potential

$$V_T(\phi, \chi = 0) = \alpha\mu^2 \left[\tanh^2\left(\frac{\beta\phi}{2}\right)\right]^n \tag{5.11}$$

leads to the same functions of $\epsilon(N)$ and $\eta(N)$, but a slightly different function of $\phi(N)$. In particular

$$\phi_T(N) \simeq \phi(N) + \frac{\log(2)}{\beta} \tag{5.12}$$

where ϕ_T and ϕ correspond to the slow-roll expressions for the T- and E-model respectively, for the same parameters α and n. Fig. 5.1 shows that Eq. (5.12) holds very well, even for relating $\phi_{\rm end}$ between the T- and E-models. Furthermore, the Hubble scale at the end of inflation scales as

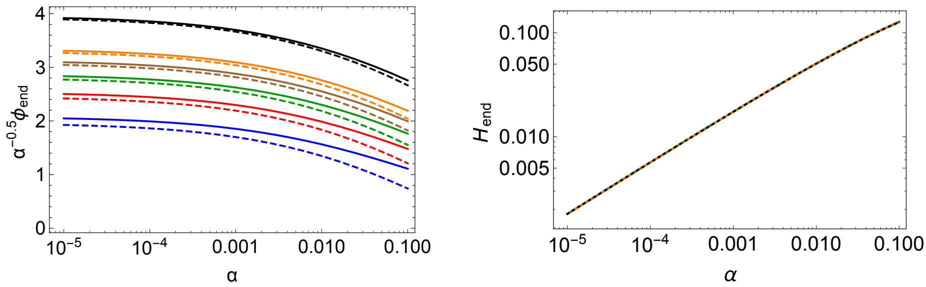

Figure 5.1: *Left:* The rescaled value of the inflaton field at the end of inflation $\phi_{\rm end}/\sqrt{\alpha}$ as a function of α for $n = 1, 1.5, 2, 2.5, 3, 5$ (blue, red, green, brown, orange and black respectively). The solid curves correspond to the E-model potential of Eq. (5.4), while the dotted ones correspond to $\phi_{\rm end}$ for the T-model potential of Eq. (5.11) shifted vertically by $\log(2)/\beta$ according to Eq. (5.12). We see that the values of $\phi_{\rm end}$ are similar for the T- and E-models and scale as $\phi_{\rm end} \propto \sqrt{\alpha}$ for small α. *Right:* The rescaled Hubble scale at the end of inflation $H_{\rm end}/\sqrt{\alpha}$ for the same parameters and color-coding. The upper / lower curves correspond to the T- and E-model respectively. The parameter α is measured in units of $M_{\rm Pl}^2$, while ϕ is measured in units of $M_{\rm Pl}$ and the Hubble scale is measured in units of μ.

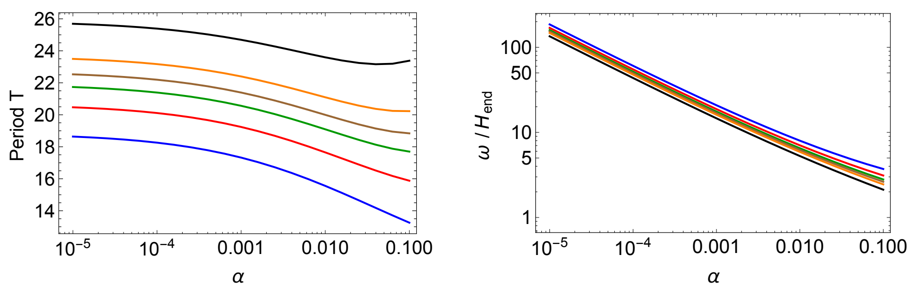

Figure 5.2: *Left:* The period of background oscillations of the inflaton field (in units of μ^{-1}) for $H = 0$ and $\phi_{\rm max} = \phi_{\rm end}$ as a function of α for $n = 1, 1.5, 2, 2.5, 3, 5$ (blue, red, green, brown, orange and black respectively). The solid curves correspond to the period of the E-model, while the dotted ones correspond to the period of the T-model divided by 2. We see that the period of the T-model is twice that of the E-model to a high degree of accuracy. Both frequencies are largely insensitive to changes in α. *Right:* The frequency of background oscillations $\omega = 2\pi/T$ divided by the Hubble scale at the end of inflation, rescaled by $\sqrt{\alpha}$. The solid / dotted curves correspond to the E- and T-model respectively and the color-coding is the same. It is evident that for small values of α, the hierarchy between the background oscillation frequency and the Hubble scale grows as $1/\sqrt{\alpha}$.

$H_{\text{end}} \sim 0.5\sqrt{\alpha}$ in units of μ. The scaling is similar for the E- and T-models, with slightly different pre-factors, as shown in Fig. 5.1.

After inflation, the background field undergoes oscillations with a decaying amplitude, due to Hubble friction. In order to define a characteristic period of oscillations, we neglect Hubble friction and set the field to its value at the end of inflation, as given in Fig. 5.1. The results are shown in Fig. 5.2, where both the period of oscillations T as well as the scale hierarchy ω/H_{end} is shown. We see a strong hierarchy between the frequency of background oscillations and the Hubble scale, which gets stronger for smaller values of α (higher field-space curvature), scaling as $\omega \propto H_{\text{end}}/\sqrt{\alpha}$. This means that for small α the Hubble scale can be neglected, to a good approximation, as it takes a large number of background oscillations for any considerable red-shifting to occur. We also see that the hierarchy between the oscillation frequency and the Hubble scale is somewhat stronger for the T-model, hence we expect more damping of the background motion per oscillation for the E-model. In order to understand the relation between the period of the two models $T_T \simeq 2T_E$ that can be immediately extracted from Fig. (5.1) we take a closer look at the single-field potential of the two models and compute one characteristic evolution for $\alpha = 10^{-3}$ and $n = 1$.

The T-model potential is symmetric with respect to the origin, while the E-model potential is highly asymmetric, consisting of a flat plateau on one side (akin to the T-model) and a steep potential "wall" on the other side. One thus expects that the background motion will be equally asymmetric, spending much more time near the plateau ($\phi > 0$) and far less time near the steep potential wall ($\phi < 0$). This is indeed the case as shown in Fig. 5.3. Given that the plateau behaviour is similar between the T- and E-models, one would expect that the T-model period would be larger, almost double that of the E-model. If one considers the difference in ϕ_{end}, the fact that the T-model starts "higher up on the plateau" at the end of inflation, the relation $T_T \simeq 2T_E$ ends up being an excellent description of the relation between the background motion of the two models.

A simple measure of the asymmetry of the background motion of the E-model seen in Fig. 5.3 can be analytically captured, by computing the ratio of the period for the positive and negative half-cycle. By neglecting the effect of Hubble friction on the background motion, the relation of the two maximum field values $\phi_\pm$ (ϕ_+ being the maximally positive value and ϕ_- the maximally negative value) are given by

$$1 - e^{-\beta\phi_+} = -1 + e^{-\beta\phi_-} \,. \tag{5.13}$$

This is independent of the parameter n and is derived through simple con-

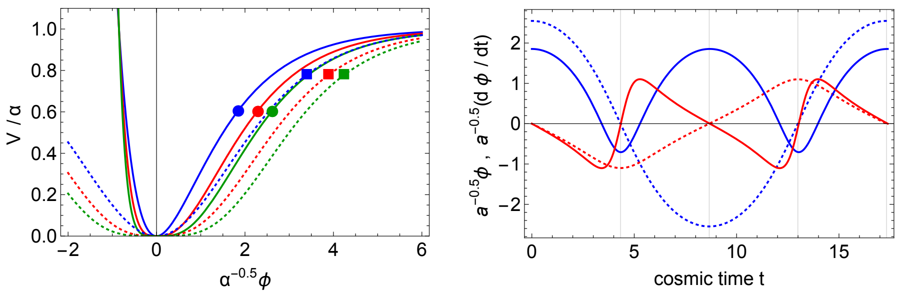

Figure 5.3: *Left:* The single field potential rescaled by α for $n = 1, 1.5, 2$ (blue, red and green respectively). The solid curves correspond to the E-model, while the dotted ones correspond to the T-model. The dots / squares show $\phi_{\rm end}$ for the E- and T-model respectively for $\alpha = 10^{-3}$. *Right:* The rescaled background motion ($\phi/\sqrt{\alpha}$ in blue and $\dot{\phi}/\sqrt{\alpha}$ in red) for $n = 1$ and $\alpha = 10^{-3}$ for the E- and T-models (solid / dotted), by neglecting the Hubble friction term.

servation of energy for $\dot{\phi}_\pm = 0$. We see that the effect of α is trivially given through the rescaling of $\phi_\pm$ by $\sqrt{\alpha}$. Fig. 5.4 shows that Eq. (5.13) accurately captures the behaviour of the system for a wide range of parameters. The half-period is then computed as

$$T_\pm = \pm \int_0^{\phi_\pm} \frac{1}{\sqrt{2(V_{\max} - V)}} d\phi \,. \tag{5.14}$$

Fig. 5.4 shows the ratio T_-/T_+ for different values of $\phi_+/\sqrt{\alpha}$. As expected, the ratio approaches unity for small field values, since the field only probes the first (symmetric) term in a Taylor expansion $V \propto |\phi|^n$. For large field-values the asymmetry of the background motion can be very pronounced. Furthermore, the effect of n on the period ratio is not important.

As an interesting remark, we must note that the first oscillation is larger in amplitude than what one would naively compute by using $\phi_+ = \phi_{\rm end}$. By including the kinetic energy at the end of inflation, Eq. (5.13) becomes

$$\frac{3}{2}\left(1 - e^{-\beta\phi_{\rm end}}\right) = -1 + e^{-\beta\phi_-} \tag{5.15}$$

for the first half-oscillation. This is especially important for low values of α, where the Hubble scale is much smaller than the frequency of oscillation, hence the Hubble damping per oscillation is negligible (at least initially).

In light of the difference between the background trajectories of the E- and T-model and the highly asymmetric nature of the former, it is interesting to examine the spectral content of $\phi(t)$ in both cases as a function of the

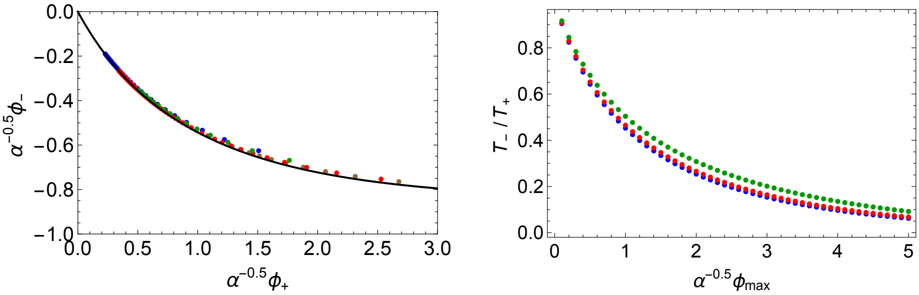

Figure 5.4: *Left:* The relation of ϕ_+ to ϕ_- for $\{\alpha, n\} = \{10^{-3}, 1\}, \{10^{-4}, 1\}, \{10^{-3}, 3/2\}, \{10^{-3}, 5\}$ (blue, red, green and black respectively). The black solid curve shows the analytic result of Eq. (5.13). *Right:* The ratio of the negative to positive half-period as a function of the rescaled field amplitude for $n = 1, 3/2, 5$ (blue, red and green respectively).

parameters n and α. By neglecting the Hubble drag term, the background evolution of the inflaton field is a periodic function, and thus can be written as a Fourier series

$$\phi(t) = a_0 + \sum_{\lambda=1}^{\infty} a_\lambda \cos\left(\frac{2\pi\lambda}{T}t\right) + \sum_{\lambda=1}^{\infty} b_\lambda \sin\left(\frac{2\pi\lambda}{T}t\right) \tag{5.16}$$

with the Fourier coefficients

$$a_0 = \frac{2}{T}\int_0^T \phi(t)dt\,, \quad a_\lambda = \frac{2}{T}\int_0^T \phi(t)\cos\left(\frac{2\pi\lambda}{T}t\right)dt\,, \quad b_\lambda = 0 \tag{5.17}$$

We compute the background motion in the static universe approximation ($H = 0$) by setting the initial conditions $\{\phi, \dot{\phi}\} = \{\phi_{\text{end}}, 0\}$ at $t = 0$, where ϕ_{end} is the field value at the end of inflation, and numerically solving the Minkowski-space background equation of motion. In this context the coefficients of the sinusoidal terms $\{b_\lambda\}$ vanish identically for both the E- and T-model, while the Fourier series for the T-model consists of only odd terms: $\{\alpha_\lambda\}$ with $\bmod(\lambda, 2) = 1$. Fig. 5.5 shows the richer spectral content of the E-model as opposed to the T-model.

5.2.2 Multi-field effects during inflation

Similarly to the generalized T-model [158, 160, 321], the generalized E-model exhibits a single valley along $\chi = 0$, as shown in Fig. 5.6. Analogously to Chapter 4, we find that by starting away from the ϕ axis, inflation will

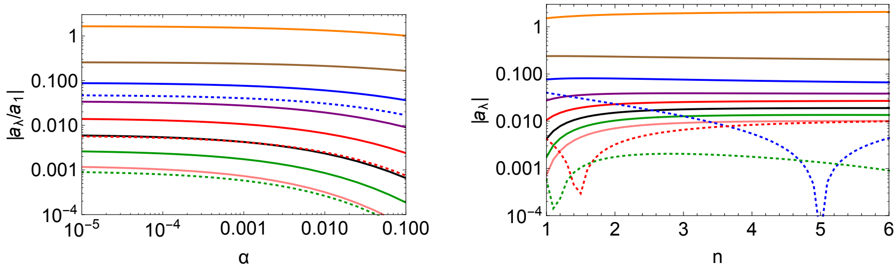

Figure 5.5: *Left:* The magnitude of the normalized Fourier coefficients $|a_\lambda/a_1|$ for $\lambda = 0, 2, 3, 4, 5, 6, 7, 8$ (orange, brown, blue, purple, red, black, green and pink respectively) for the E-model (solid) and the T-model (dotted) as a function of α with $n = 1$. *Right:* $|a_\lambda|$ with the same color-coding as a function of n with $\alpha = 10^{-3}$. Both panels show that the background motion of the E-model has a richer harmonic structure than that of the T-model. For the T-model $a_n \neq 0$ for $n = 3, 5, 7$ as explained in the main text.

proceed along a single-field trajectory with ϕ being effectively constant until $\chi = 0$. After that, inflation will proceed along the valley of the potential, as shown in Fig. 5.6. By using the single-field slow-roll equations of motion, we can express the field ϕ as a function of the e-folding number $N_{\mathrm{sf},\phi}$ on a single-field trajectory along ϕ

$$V(N_{\mathrm{sf},\phi}, \chi) = \alpha\mu^2 \left[1 - \frac{2}{\cosh(\beta\chi)}\frac{3\alpha}{4nN_{\mathrm{sf},\phi}} + \left(\frac{3\alpha}{4nN_{\mathrm{sf},\phi}}\right)^2\right]^n \cosh^{2/\beta^2}(\beta\chi) \tag{5.18}$$

By dropping the field value in favor of the e-folding number, we gain a more intuitive understanding of the size of each term. Before proceeding, we must stress that $N_{\mathrm{sf},\phi}$ is the e-folding number of a single field trajectory with $\chi = 0$, not the full multi-field trajectory, and it is only used as a substitute for the field ϕ. As Fig. 5.6 shows, the sharp turn in field-space means that the substitution of ϕ by $N_{\mathrm{sf},\phi}$ has physical relevance beyond its mathematical convenience. It corresponds to the duration of inflation that will take place after the sharp turn at $\chi = 0$. By considering large values of $N_{\mathrm{sf},\phi}$, such that we get a large number of e-folds (55 or more) along a single field trajectory along ϕ, we can keep the lowest order term in $N_{\mathrm{sf},\phi}$, which leads to

$$V(N_{\mathrm{sf},\phi}, \chi) = \alpha\mu^2 \cosh^{2/\beta^2}(\beta\chi) \left[1 - \frac{3\alpha}{2N_{\mathrm{sf},\phi}}\mathrm{sech}(\beta\chi) + \mathcal{O}\left(\frac{\alpha^2}{N^2_{\mathrm{sf},\phi}}\right)\right]. \tag{5.19}$$

The next to leading order term $\mathcal{O}\left(\alpha^2/N_{\mathrm{sf},\phi}^2\right)$ can be dropped if

$$\beta\chi < \log\left(\frac{16nN_{\mathrm{sf},\phi}}{3\alpha}\right) . \tag{5.20}$$

We must note again that Eq. (5.19) represents a series expansion in $1/N_{\mathrm{sf},\phi}$ and holds for every value of χ, within the limits of Eq. (5.20). By applying the same procedure to the two-field generalized T-model that was studied in Chapter 4, we arrive at the exact same series expansion, up to and including the term that is $\mathcal{O}\left(N_{\mathrm{sf},\phi}^{-1}\right)$. The two potentials are different at the level of the $\mathcal{O}\left(\alpha^2/N_{\mathrm{sf},\phi}^2\right)$ term. This clearly shows that the two potentials are not only equivalent during inflation at the single-field level, leading to the same predictions for n_s and r, but that their two-field behaviour is also identical, up to slow-roll corrections, since the potential along the χ direction is the same up to $\mathcal{O}(N^{-2}) = \mathcal{O}(\epsilon)$ terms. The equivalence becomes increasingly better for smaller values of α. Hence the approach to the $\chi = 0$ attractor, which was examined in Chapter 4 for a wide range of initial conditions, as well as the behaviour along the attractor, will be practically indistinguishable between the two models. We must note that the above analysis does not provide any guarantee that this equivalence will persist during preheating, since it has been obtained by using the slow roll analysis during the early (CMB-relevant) stages of inflation.

Both the above analysis and the more extended multi-field analysis shown in Chapter 4, was performed in the $\{\phi, \chi\}$ basis. However, for curved field-space manifolds, the magnitude of a field value does not always correspond to the physically relevant parameter. For that, we can look for intuitive criteria to check the strength of the single-field attractor and the two-stage structure of the inflationary trajectory shown in Fig. 5.6. One such criterion for testing the strength of the late-time single field attractor arises as we vary the field values on equi-potential surfaces $V(\phi, \chi) = \mathrm{const}$.

Given the fact that we know the behaviour and observables of the system, once it reaches the single field attractor at $\chi(t) \simeq 0$, we examine the duration of inflation and the position of the sharp transition between the two single-field regimes as we fix the initial energy $V(\phi_0, \chi_0)$ for $\dot\phi_0 = \dot\chi_0 = 0$. We start by fixing the potential energy of the initial conditions, which corresponds to the left panel of Fig. 5.7. The initial potential energy is taken to be $V(\phi_0, \chi_0)$. We see that the lines are equidistant to each other before the turn of the trajectory happens. The total number of e-folds and the number of e-folds before the turn are sensitive to the change of initial values

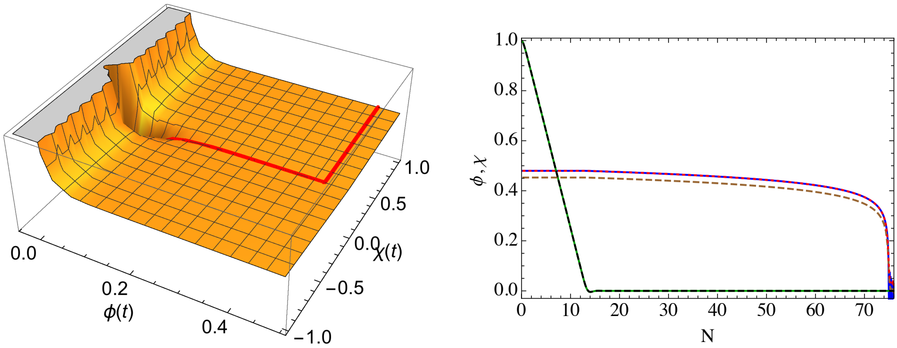

Figure 5.6: *Left:* The three-dimensional plot of the E-model potential $V(\phi,\chi)$ given in Eq. (5.3) for $n = 3/2$ and $\alpha = 0.001$ along with a characteristic trajectory computed by choosing the initial conditions $\phi_0 = \frac{1}{\beta}\log\left(\frac{4nN}{3\alpha}\right)$ and $\chi_0 = 1$. *Right:* The evolution of ϕ (blue), χ (green) for the same parameters. The brown-dashed and black-dashed curves correspond to the T model with the same parameters and the initial conditions chosen as $\chi_0 = 1$ and $\phi_0 = \frac{1}{\beta}\log\left(\frac{8nN}{3\alpha}\right)$. The red-dashed curve is ϕ for the T-model shifted vertically by $\log(2)/\beta$, following Eq. (5.12). All field values are measured in units of $M_{\rm Pl}$. It is worth noting that the blue-solid and red-dashed curves are indistinguishable, as are the green-solid and black-dashed ones. This demonstrates the identical multi-field behavior of the T- and E-models during inflation, that is derived in the main text.

of ϕ_0 and χ_0. From the right panel of the Fig. 5.7 we see that to get 60 e-folds of inflation we must have $\phi_0 \gtrsim 1.1$. With the increase of χ_0 the number of e-folds before the turn increases as well. For the equi-potential choice of initial conditions the subtraction from the duration of inflation the position of the turn, i.e. $N_{\rm end} - N_{\rm turn}$, is the same for all parameters ϕ_0, χ_0.

Intruiging phenomenology can arise if one puts the evolution of $\chi(t)$ into the observable range, i.e. let it evolve at least 30 e-folds before the turn. To make it happen for $\alpha = 0.01$ we have to artificially tune χ_0 to be $\chi_0 \approx 10$, at the same time keeping $\phi_0 = \mathcal{O}(1)$, however for $\alpha = 0.001$ both ϕ_0 and χ_0 can be of the same order $\mathcal{O}(1)$. Using the two-field potential of Eq. (5.3), we can compute the slow-roll quantities during the initial phase of inflation along $\phi \simeq$ const. We use the fact that the field trajectory proceeds with almost zero turn-rate, hence the projection vectors align with the coordinate system, $\hat{\sigma}^\phi \simeq 0$. This greatly simplifies the calculations (we use the notation of Ref. [266]), since the motion occurs along χ, which is a canonically normalized field. The slow roll quantities along the adiabatic direction are

$$\epsilon = -\frac{\dot{H}}{H^2} \simeq \frac{M_{\rm Pl}^2}{2}\left(\frac{V_\chi}{V}\right)^2 , \quad \eta_{\sigma\sigma} \simeq M_{\rm Pl}^2 \frac{\mathcal{M}_{\sigma\sigma}}{V} \tag{5.21}$$

where the adiabatic effective mass along the χ direction is

$$\mathcal{M}_{\sigma\sigma} \simeq \mathcal{G}^{\chi\chi}(\mathcal{D}_\chi \mathcal{D}_\chi V) = V_{\chi\chi} \tag{5.22}$$

It is straighforward to compute the above quantities. Interestingly they both asymptote to a fixed value for $\{\phi, \chi\} \gtrsim \mathcal{O}(1)$, which reads

$$\epsilon \simeq 3\alpha \, , \;\; \eta_{\sigma\sigma} \simeq 2\epsilon \simeq 6\alpha \tag{5.23}$$

This result is insensitive to the exact value of α and n and it is identical for the E- and T-model. The orthogonal direction, which in this case is the ϕ direction, controls the evolution of the isocurvature modes. It is straightforward to check that the isocurvature effective mass in this case is larger than the Hubble scale, hence the isocurvature modes decay. The curvature perturbation is thus controlled by the χ fluctations that exit the horizon during this stage, which acquire a spectral tilt

$$n_s = 1 - 6\epsilon + 2\eta_{\sigma\sigma} \simeq 1 - 6\alpha. \tag{5.24}$$

This can be made compatible with the *Planck* data. However, the tensor to scalar ratio $r = 16\epsilon \simeq 48\alpha$ is too large, $r > 0.1$, for values of α that provide the correct scalar spectral index. These results use the asymptotic values of ϵ and $\eta_{\sigma\sigma}$ and a region of (almost) zero turn rate $|\omega| \ll H$. The existence of a non-zero turn rate during this first stage of inflation can lower the tensor-to-scalar ratio (see e.g. Ref. [263]). A full calculation of the power spectrum during the transition between the two (almost) single field trajectories requires a more thorough investigation, possibly focusing on a different parameter range than the ones associated with efficient preheating ($\alpha \ll 1$).

A full analysis of the initial condition dependence that defines the observables of the two-stage inflationary phase and the corresponding observational viability of two-stage α-attractor inflation is beyond the scope of the present work. However Fig. 5.7 shows that if one wants to extract information about the probability distribution of the inflationary trajectory and the resulting spectral observables, one would need to choose a prior distribution for the initial values of the fields (and corresponding velocities). Our intuitive choice for choosing initial conditions through iso-potential lines,

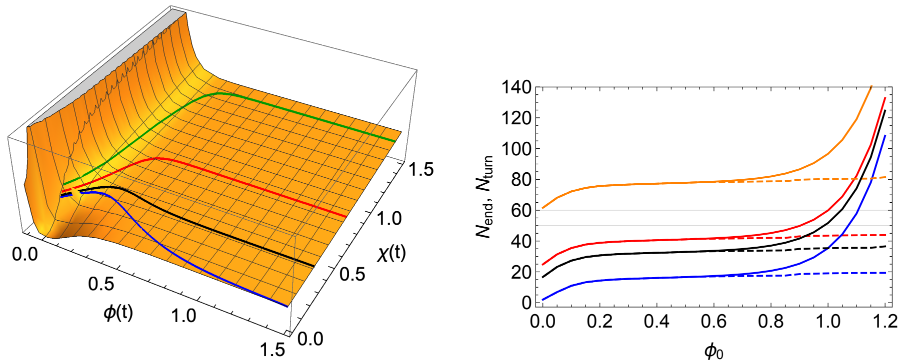

Figure 5.7: *Left:* The initial value lines for constant potential for ϕ_0=1.5 and χ_0=1.4 (green), χ_0=0.7 (red), χ_0=0.3 (black), χ_0=0 (blue) (from top curves to bottom) for $n = 3/2$ and $\alpha = 0.01$.
Right: The total number of e-folds (solid lines) and the number of e-folds before the sharp turn (dashed lines) starting from the beginning of inflation for ϕ_0=1.2 and χ_0=19 (orange), χ_0=10 (red), χ_0=8 (black), χ_0=4 (blue), (from top curves to bottom) for $n = 3/2$ and $\alpha = 0.01$. The two horizontal thin lines correspond to 50 and 60 e-folds, hence the range between them corresponds to the time, during which the CMB-relevant modes left the horizon. All field values are measured in units of $M_{\rm Pl}$.

shows that the choice of prior distribution is likely to affect the outcome (see e.g. Ref. [322]). Even though the single field attractor is strong enough to suppress multi-field signatures, the size of the part of parameter space that would showcase them is non-trivial to compute.

5.3 Fluctuations

In principle, the analysis of fluctuations in models of inflation that involve multiple fields on a curved manifold requires the use of a covariant formalism. This has been developed for preheating in Ref. [136] and extensively used in Refs. [302–304] for studying preheating in multi-field inflation with non-minimal couplings to gravity. Similarly as in Chapter 4, our current parametrization of the hyperbolic field-space manifold makes the equations for the gauge-invariant perturbations

$$Q^I \equiv \delta\phi^I + \frac{\dot{\phi}^I}{H}\psi \tag{5.25}$$

particularly simple along the single-field attractor $\chi = 0$. Their equations of motion were discussed in Introduction as well as in Chapter 4, therefore we will not repeat the analysis here.

By rescaling the perturbations as $Q^I(x^\mu) \to X^I(x^\mu)/a(t)$ and working in terms of conformal time, $d\eta = dt/a(t)$, we write the second order action in a form that resembles Minkowski space

$$S_2^{(X)} = \int d^3x d\eta \left[-\frac{1}{2}\eta^{\mu\nu}\delta_{IJ}\partial_\mu X^I \partial_\nu X^J - \frac{1}{2}\mathbb{M}_{IJ} X^I X^J \right] , \tag{5.26}$$

where

$$\mathbb{M}_{IJ} = a^2 \left(\mathcal{M}_{IJ} - \frac{1}{6}\delta_{IJ} R \right) . \tag{5.27}$$

This makes quantization straightforward, by promoting the fields X^I to operators $\hat{X}^I$ and expanding $\hat{X}^\phi$ and $\hat{X}^\chi$ in sets of creation and annihilation operators and associated mode functions

$$\hat{X}^I = \int \frac{d^3k}{(2\pi)^{3/2}} \left[u^I(k,\eta)\hat{a}^I e^{ik\cdot x} + u^{I*}(k,\eta)\hat{a}^{I\dagger} e^{-ik\cdot x} \right] . \tag{5.28}$$

Since the modes decouple on a single-field background with vanishing turn-rate, the equations of motion are

$$\begin{aligned} \partial_\eta^2 v_k + \Omega_\phi^2(k,\eta) v_k \simeq 0 \,, \quad \Omega_\phi^2(k,\eta) = k^2 + a^2 m_{\text{eff},\phi}^2 \,, \\ \partial_\eta^2 z_k + \Omega_\chi^2(k,\eta) z_k \simeq 0 \,, \quad \Omega_\chi^2(k,\eta) = k^2 + a^2 m_{\text{eff},\chi}^2 \,, \end{aligned} \tag{5.29}$$

where we defined $u^\phi \equiv v$ and $u^\chi \equiv z$. For completeness, we provide again the definitions for components of the effective masses. The effective masses of the two types of fluctuations, along the background motion and perpendicular to it, consist in principle of four distinct contributions [136]:

$$m_{\text{eff},\phi}^2 \equiv m_{1,\phi}^2 + m_{2,\phi}^2 + m_{3,\phi}^2 + m_{4,\phi}^2 \tag{5.30}$$

$$m_{\text{eff},\chi}^2 \equiv m_{1,\chi}^2 + m_{2,\chi}^2 + m_{3,\chi}^2 + m_{4,\chi}^2 \tag{5.31}$$

each of them corresponding to a different source. Full expressions for arbitrary $\mathcal{G}_{IJ}$ can be found for example in Ref. [136]. However using the fact that $\chi = 0$ and $\mathcal{G}_{IJ} = \mathbb{I}$ along the single field attractor at background level the effective mass components become simple:

- The components $m_{2,I}^2$ are written as

$$m_{1,\phi}^2 = V_{\phi\phi} \,, \quad m_{1,\chi}^2 = V_{\chi\chi} \tag{5.32}$$

corresponding to the local curvature of the potential.

- The component $m_{2,\phi}^2$ vanishes identically, while

$$m_{2,\chi}^2 = \frac{1}{2} R \dot{\phi}^2 \tag{5.33}$$

arises from the field-space curvature and has no analogue in flat field-space models.

- The component $m_{3,\phi}^2$ encodes the effects of the coupled metric perturbations and is written as

$$m_{3,\phi}^2 = -\frac{1}{M_{\rm Pl}^2 a^3} \mathcal{D}_t \left(\frac{a^3}{H} \dot{\phi}^2 \right) . \tag{5.34}$$

Since the metric perturbations are only related to the adiabatic perturbations and cannot affect the isocurvature modes, the term $m_{3,\chi}^2$ vanishes identically[2]. Furthermore, this contribution is subdominant for these models and parameter range of interest, as discussed in Refs. [158, 160].

- Finally the terms

$$m_{4,\phi}^2 = m_{4,\chi}^2 = -\frac{1}{6} R \,, \tag{5.35}$$

where $R = 6(2-\epsilon)H^2$ is the space-time Ricci scalar, arise from our choice of mode-functions in a curved space-time.

It is straightforward to check that the potential components of the effective masses scale as $m_{1,I}^2 \sim \mu^2$, as does the field-space curvature component $\mu_{2,\chi}^2$. The coupled metric perturbations component is subdominant for $\alpha \ll 1$, since $m_{3,\phi}^2 \sim \mu^2 \sqrt{\alpha}$ (see Chapter 4). Finally, the term that encodes the space-time curvature is even smaller, scaling as $m_{4,I}^2 \sim \mu^2 \alpha$. This is reminiscent of another family of plateau models, ξ-attractors, which produce similar CMB spectra to α-attractors [136, 154, 254].

Before we proceed with preheating calculations, we must revisit the claims made in Sections. 5.2.2 about the existence and stability of a single-field attractor along $\chi = 0$. The analysis made so far relies on background quantities. However, it has been shown that negatively curved manifolds

[2]During inflation, the adiabatic modes are fluctuations along the background trajectory and the isocurvature modes are fluctuations perpendicular to it. Due to the existence of a single-field attractor $\chi = 0$, the adiabatic and isocurvature modes can be simply matched to $\delta\phi$ and $\delta\chi$ respectively.

can lead to unstable fluctuations during inflation and a subsequent destabilization of the inflationary trajectory. After the system has settled into the attractor at $\chi = 0$, the effective super-horizon mass of χ fluctuations is given by

$$m^2_{\chi,\text{eff}} = V_{\chi\chi}(\chi = 0) + \frac{1}{2}R\dot{\phi}^2$$
$$= 2\alpha e^{-2\beta\phi}\left(e^{-2\beta\phi}\left(e^{\beta\phi}-1\right)^2\right)^{n-1}\left(e^{\beta\phi}\left(e^{\beta\phi}+\beta^2 n-2\right)+1\right) - \frac{2}{3\alpha}\dot{\phi}^2. \tag{5.36}$$

By using the slow-roll equations of motion this becomes

$$m^2_{\chi,\text{eff}} \simeq \left(2 + \frac{1}{N}\right)\alpha \tag{5.37}$$

for small α and large N. This means that until close to the end of inflation, where the slow-roll expressions break down, the χ fluctuations exhibit a positive effective mass and are suppressed. The E-model is thus safe from "geometric destabilization" effects during the inflationary stage along $\chi = 0$ [54, 55], even for highly curved field-space manifolds. This arises because the potential also depends on the curvature parameter α. We verified this claim by numerically evaluating Eq. (5.3) for various choices of n and α.

We define the energy density in each mode as

$$\rho_{\delta\phi}(k,\eta) = \frac{1}{2a^4}\left(|\partial_\eta v_k(\eta)|^2 + \Omega^2_\phi(k,\eta)|v_k(\eta)|^2\right) \tag{5.38}$$
$$\rho_{\delta\chi}(k,\eta) = \frac{1}{2a^4}\left(|\partial_\eta z_k(\eta)|^2 + \Omega^2_\chi(k,\eta)|z_k(\eta)|^2\right) \tag{5.39}$$

where we ignored interaction terms, since we are working in the linear approximation. The expressions can be easily written in cosmic rather than conformal time.

We focus primarily on the parametric excitation of $\delta\chi$ modes, since the analysis of single field parametric resonance can be found in the literature (see e.g. Refs. [323, 324]). For field-space manifolds with $\alpha \gtrsim \mathcal{O}(10^{-3})$ the corresponding instability factors are much smaller for $\delta\phi$ as compared to $\delta\chi$, with the exception of the E-model for $n = 1$. Furthermore, the analysis of ϕ fluctuations is in principle identical, with the exception that the curvature term is missing from the effective mass. We provide further results for the growth of ϕ and χ fluctuations in Section 5.4.3.

5.3.1 Effective frequency

Before we proceed to construct the Floquet charts and numerically compute the evolution of χ fluctuations, we focus on the effective mass ω_χ^2 and its dependence on the parameters n and α. This will guide our intuition about the system, so that we can recognize the interesting parameter regimes and important factors that will ultimately determine the preheating efficiency.

We start with the Riemann component $m_{2,\chi}^2$, which does not depend strongly on the potential and field-space parameters n and α

$$\frac{1}{2}\mathcal{R}\dot{\phi}^2 \sim -\mathcal{O}(1) \tag{5.40}$$

similarly to the behaviour found in the context of the T-model in Chapter 4. This scaling can be simply understood as follows: the field-space curvature is $\mathcal{R} = -\frac{4}{3\alpha}$. At the same time, the time derivative $\dot{\phi}^2$ has its maximum value at the minimum of the potential $\phi = 0$. Following the analysis of Section 5.2, we see that the field amplitude scales as $\phi \sim \phi_{\rm end} \sim \sqrt{\alpha}$, while the relevant oscillation time scale T is essentially independent of α for sufficiently small α. These scalings have been numerically verified in Figs. 5.1 and 5.2 respectively and lead to $\dot{\phi}^2 \sim \alpha \sim \mathcal{R}^{-1}$. The $\mathcal{O}(1)$ amplitude of the Riemann term in Eq. (5.40) has been numerically evaluated and is maximized close to unity for several parameter choices, especially for $\alpha \ll 1$.

We next move to the component $m_{1,\chi}^2$ of the effective χ mass, which is due to the potential. This can be written for small α as

$$V_{\chi\chi}(\chi = 0) \simeq \frac{4}{3} n e^{-\beta\phi} \left(\left(1 - e^{-\beta\phi}\right)^2 \right)^{n-1} . \tag{5.41}$$

For $n = 1$, this term is simplified as $V_{\chi\chi}^{n=1}(\chi = 0) \simeq \frac{4}{3} e^{-\beta\phi}$ and oscillates between two extremum values at $\phi = \phi_\pm$ (shown in Fig. 5.4), while having a constant, time-independent value of $4/3$ when the inflaton field crosses the origin $\phi = 0$. The maximum of $V_{\chi\chi}^{n=1}$ can be easily computed using Eq. (5.15)

$$V_{\chi\chi}^{n=1}\Big|_{\max,(1)} \simeq \frac{2}{3}\left(5 - 3e^{-\beta\phi_{\rm end}}\right) , \tag{5.42}$$

where we neglected the effect of the Hubble drag. This is an increasingly good approximation for small values of α. The behaviour of the $\delta\chi$ effective mass is shown in Fig. 5.8 for $n = 1$ and several values of $\alpha \ll 1$. It is

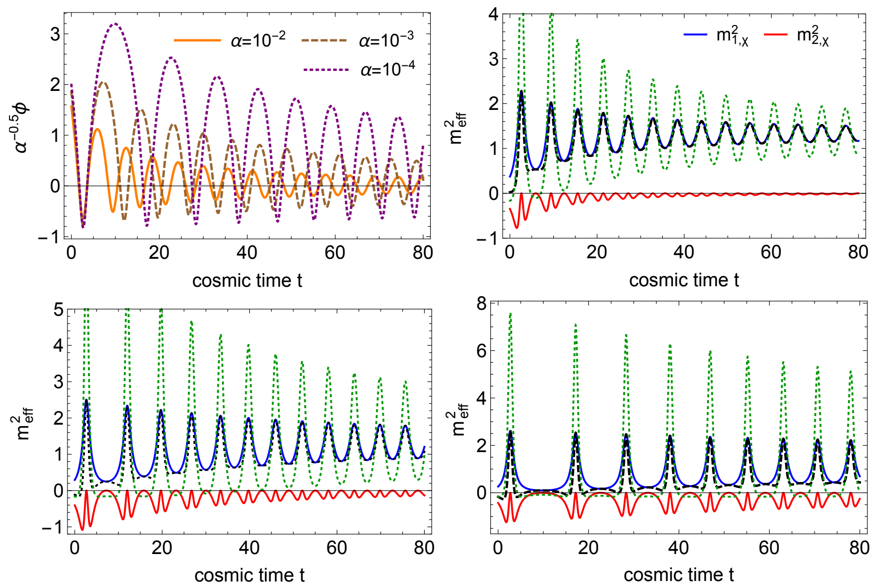

Figure 5.8: *Top left:* The rescaled background amplitude of ϕ (in units of $M_{\rm Pl}$) for $n = 1$ and $\alpha = 10^{-2}, 10^{-3}, 10^{-4}$ (orange, brown-dashed and purple-dotted respectively). *Top right & bottom panels:* The effective mass (in units of μ^2) of the ϕ and χ fluctuations (green-dotted and black-dashed) along with the components of m_χ^2 for the same parameters. The effective mass components $m_{3,\phi}^2$ and $m_{4,\{\phi,\chi\}}^2$ are not shown, because they are subdominant for $\alpha \ll 1$.

simple to see that the Riemann term red-shifts as a^{-2} , while the potential derivative oscillation amplitude red-shifts as a^{-1}. This follows trivially from $\Delta V_{\chi\chi} \sim (1 - e^{-\beta\phi}) \sim \sqrt{V}$, where $\Delta V_{\chi\chi}$ is the amplitude of the oscillation of $V_{\chi\chi}$ shown in Fig. 5.8, while from the equipartition theorem $\dot{\phi}^2 \sim V$. Hence, both the wave-number contribution k^2/a^2, as well as the Riemann contribution become subdominant after the first e-fold, which lasts for more oscillations for smaller values of α. Using Eq. (5.42) and the results $\phi_{\rm end} \lesssim 2\sqrt{\alpha}$, shown in Fig. 5.1, we arrive at $V_{\chi\chi}^{n=1}\big|_{\max,(1)} \lesssim 2.9$. This simple approximation is able to capture the exact (numerical) result shown in Fig. 5.8.

E-model potentials with larger values of the potential parameter n can be analyzed in a similar way. By Taylor-expanding the potential around its global minimum at $\phi = \chi = 0$, it is straightforward to see that $V_{\chi\chi} \propto \phi^2\chi^{2(n-1)}/\alpha^{n-1}$ for $n > 1$. Thus all χ derivatives of the potential vanish for $\phi = 0$, contrary to the case of $n = 1$. Simply put, potentials with $n > 1$ describe massless fields in the small-amplitude regime.

The component of the effective χ mass that is due to the potential can be written for small α, similarly to the $n = 1$ case, as

$$V_{\chi\chi}(\chi = 0) \simeq \frac{4}{3} n e^{-\beta\phi} \left(\left(1 - e^{-\beta\phi}\right)^2 \right)^{n-1} \tag{5.43}$$

The height of the first "spike" can be computed using Eq. (5.15)

$$V_{\chi\chi}^{n>1}\Big|_{\max,(1)} = \left(\frac{3}{2}\right)^{2n-3} \left(5 - 3e^{-\beta\phi_{\text{end}}}\right) \left(1 - e^{-\beta\phi_{\text{end}}}\right)^{2(n-1)} . \tag{5.44}$$

Fig. 5.9 shows the evolution of the effective frequency and its two main components, the potential and Riemann terms, for $n = 3/2$ and $n = 2$. An interesting feature of this model is the evolution of the height of the first spike, which scales approximately as

$$V_{\chi\chi}^{\max}(\chi = 0) \sim \left(\frac{1}{a}\right)^{\min(n,4)} . \tag{5.45}$$

Simply put, for $n < 2$ the wavenumber contribution to the effective frequency k^2/a^2 becomes less important after the first few oscillations, while for $n > 2$ it comes to dominate over the potential at late times, for sufficiently large wave-numbers. For the marginal case of $n = 2$ the relative size of the wave-number and potential terms remains roughly constant.

By examining the general form of $m^2_{\text{eff},\chi}$ for $n = 1$, shown in Fig. 5.8, we see that the negative part of the effective mass $m^2_{2,\chi}$ is largely cancelled by the positive contribution of $m^2_{1,\chi}$ (not affected by neglecting the subdominant term $m^2_{4,\chi}$). It means that the tachyonic resonance in the E-model is completely damped for $n = 1$ and preheating can only proceed by parametric resonance alone. Parametric resonance in the simple case of the Mathieu equation $\ddot{u}(t) + [A + 2q\cos(2t)]u(t)$ is largely controlled by the relative size of A and q and is suppressed for $A \gg q$. Fig. 5.8 shows that while the offset A remains constant, the oscillation amplitude q is damped, hence we expect parametric resonance to quickly shut off, at least for $\alpha = \mathcal{O}(0.01)$. For smaller values of α the effective mass exhibits a highly oscillatory behaviour, where the amplitude of the oscillation is almost equal to the constant offset of $m^2_{\text{eff},\chi}$. Furthermore, the anharmonic behaviour of the background (see Fig. 5.5) is mirrored in the anharmonic effective mass, particularly in the dominant component $V_{\chi\chi}$, where we see a "spike" appearing at the points where ϕ is maximally negative. This can lead to a violation of the adiabaticity condition $\left|\dot{\omega}/\omega^2\right| \ll 1$.

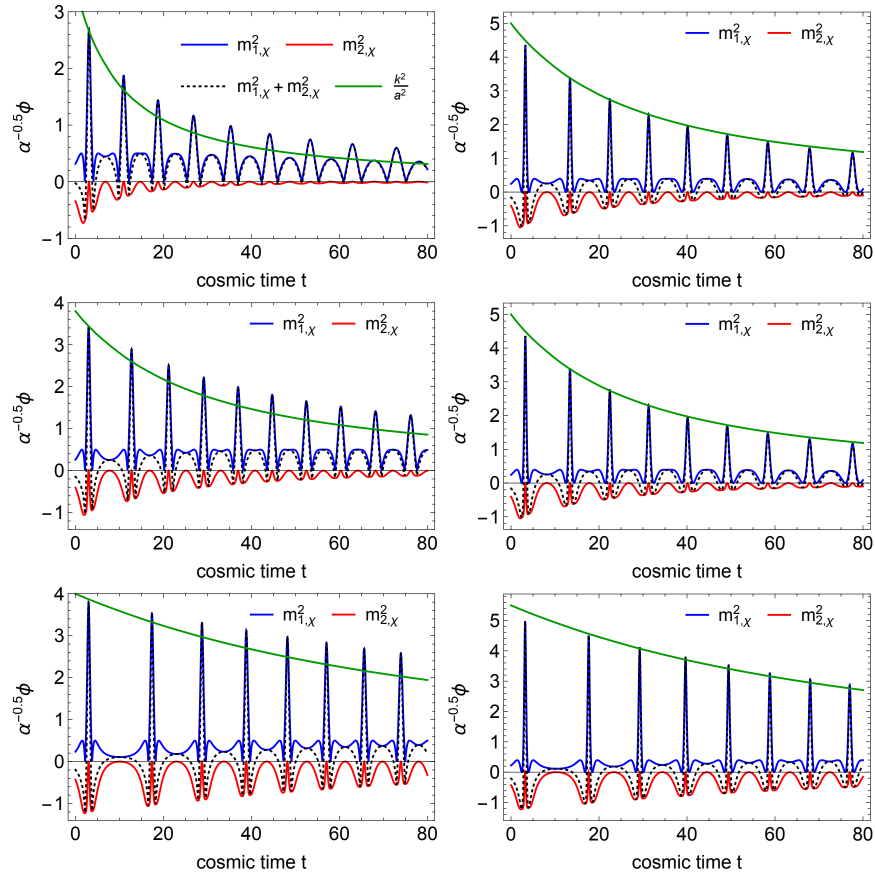

Figure 5.9: Effective frequency $\omega^2_\chi(k,t)$ for $n = 3/2, 2$ (left and right respectively) and $\alpha = 10^{-2}, 10^{-3}, 10^{-4}$ (top to bottom). The effective frequency is measured in units of $\mu^2 \simeq 3.6 \cdot 10^{-11} M^2_{\rm Pl}$. We see that for $n = 3/2$ the effect of the wavenumber term k^2/a^2 becomes progressively less important compared to the potential spike, which is not the case for $n = 2$, where the two terms red-shift in tandem.

The phenomenon of a spike in the effective frequency of fluctuations driving the adiabaticity violation was observed in preheating of multi-field models with non-minimal coupling to gravity [136, 302, 303, 325, 326], including but not limited to Higgs inflation [304, 326]. In that context, the field-space curvature is non-uniform: the manifold is asymptotically flat at large field values and the Ricci scalar exhibits a large positive spike at the origin[3]. In order to properly define an adiabaticity parameter and use a WKB-type analysis, the frequency of the fluctuations $\delta\chi$ must be (much) greater than the frequency of the background oscillations; simply put, $\delta\chi$ must oscillate multiple times between the "spikes" shown in Figs. 5.8 and 5.9. We have shown using both analytical and numerical arguments (see Fig. 5.2) that the background frequency is $\omega_{\rm bg} \equiv 2\pi/T \sim 0.5$, with a mild dependence on the parameters α and n. While the maximum value of $m_{{\rm eff},\chi}$ is larger than $\omega_{\rm bg}$, the averaged value over one period is not, in fact $\langle m_{{\rm eff},\chi}\rangle_T \sim \omega_{\rm bg}$. Thus, in order to properly use the adiabaticity condition as a criterion for preheating, we should restrict ourselves to cases where the wave-number contribution k^2/a^2 is non-negligible. For now, let us consider cases where $k \gtrsim \mu$ (we choose to measure k in units of μ, as in Chapter 4).

Fig. 5.10 shows the evolution of the adiabaticity condition for $n = 1$ and $k = 0.5\mu$, where we see adiabaticity violation for only a few oscillations at $\alpha \leqslant 10^{-3}$. If we consider larger wave-numbers, $k \simeq \mu$, we find $\left|\dot\omega/\omega^2\right| < 1$ for $n = 1$. The situation is however different for $n \geqslant 3/2$, where we find instances of $\dot\omega/\omega^2 > 1$ for $k \geqslant \mu$. Fig. 5.10 shows the evolution of the peaks in the adiabaticity parameter, occurring around the maximally negative value of $\phi(t)$. For $n = 2$ we see that the adiabaticity parameter is violated (for $\alpha \leqslant 10^{-2}$) initially, but $\left|\dot\omega/\omega^2\right|$ decreases with time. The situation is reversed for $n = 3/2$, where we see that the adiabaticity parameter grows with time. Finally, the value of $\left|\dot\omega/\omega^2\right|$ grows with decreasing α for all values of n that we examined, signifying a common trend.

Before we conclude this section, it is important to distinguish two different types of sharp features in the effective frequency of fluctuations. The field-space induced spikes that were found in non-minimally coupled models [136, 302–304, 325, 326] arise when the fields pass through the origin and have their maximal velocity. They can lead to significant adiabaticity violation over a large range of wave-numbers and thus can drive very efficient

[3]This description corresponds to the analysis performed in the Einstein frame as in Refs. [136, 302, 303]. The analysis of these models in the Jordan frame was performed in Ref. [326], where the adiabaticity violation was a result of a spike in the background field velocity as it crossed the origin.

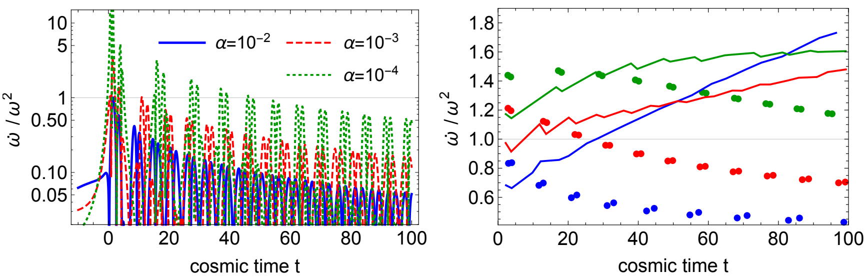

Figure 5.10: *Left:* The adiabaticity condition $|\dot{\omega}/\omega^2|$ for $n = 1$ and $\alpha = 10^{-2}, 10^{-3}, 10^{-4}$ (blue solid, red dashed and green dotted respectively) and $k = 0.5\mu$. *Right:* The peaks of the adiabaticity condition $|\dot{\omega}/\omega^2|$ for $n = 3/2$ (solid curves) and $n = 2$ (dots) for $\alpha = 10^{-2}, 10^{-3}, 10^{-4}$ (blue, red and green respectively) and $k = 1.5\mu$.

particle production. Contrary to this, Ref. [327] found sharp features in a model of unitarized Higgs inflation (mixed Higgs-Starobinsky inflation). This feature however arises from a sharp potential barrier and is thus similar to the feature found in the E-model and completely different than the sharp feature found in "regular" Higgs inflation preheating [304]. The potential-driven spike in the effective frequency leads to typically weaker preheating than the field-space-driven one, at least for the models mentioned here. It would be interesting to perform an EFT-type analysis for preheating models with sharp features, but this goes beyond the scope of our present analysis and is left for future work.

5.4 Mass-scales and Preheating

Due to the construction of the E-model, which arises by defining the Kähler potential and superpotential for a complex field Z, the ϕ and χ dependence of the potential are related to each other. The second derivative of the potential with respect to χ, which is one of the two main components in the effective mass-squared $m^2_{\text{eff},\chi}$, can be related to the potential value itself as

$$\left.\frac{V_{\chi\chi}}{V}\right|_{\chi=0} = 2 + \frac{n}{3\alpha \sinh^2\left(\frac{\beta\phi}{2}\right)} . \tag{5.46}$$

This diverges at $\phi = 0$ for all values of α and n, which is easy to understand by Taylor expanding the two terms for $\chi = 0$ as $V(\chi = 0) \simeq \frac{2^n}{3^n a^{n-1}}\phi^{2n} + \mathcal{O}(\phi^{2n+1})$ and $V_{\chi\chi}(\chi = 0) \simeq \frac{2^{n+1}n}{3^n a^{n-1}}\phi^{2n-2} + \mathcal{O}(\phi^{2n-1})$. We see that for all values of n the potential V vanishes faster than the derivative $V_{\chi\chi}$ for

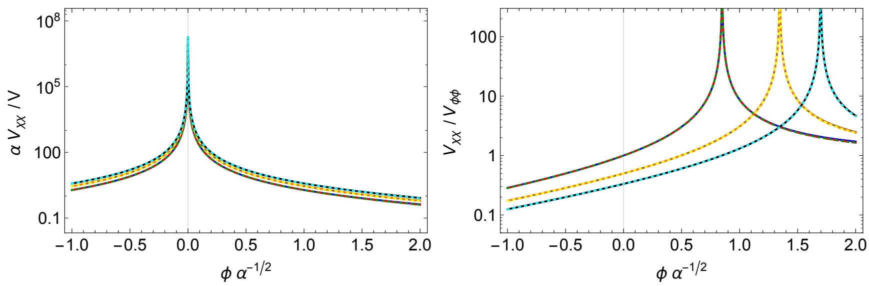

Figure 5.11: *Left:* The ratio $V_{\chi\chi}/V$ multiplied by the factor α as a function of the rescaled inflaton field for $n = 1, 3/2, 2$ and $\alpha = 10^{-2}, 10^{-3}, 10^{-4}$. The color-coding is as follows: $\{n,\alpha\} = \{1, 10^{-2}\}, \{1, 10^{-3}\}, \{1, 10^{-4}\}$: blue, red-dashed, green-dotted, $\{n,\alpha\} = \{3/2, 10^{-2}\}, \{3/2, 10^{-3}\}, \{3/2, 10^{-4}\}$: brown, orange-dashed, yellow-dotted, $\{n,\alpha\} = \{2, 10^{-2}\}, \{2, 10^{-3}\}, \{2, 10^{-4}\}$: black, purple-dashed, cyan-dotted. We see that for field values relevant for preheating the α dependence is canceled out when multiplying by α and the n dependence is weak. *Right:* The ratio $V_{\chi\chi}/V_{\phi\phi}$ for the same parameters and color-coding. In both panels, the three curves corresponding to the same value of n and different values of α are indistinguishable.

$\chi = 0$ and $\phi \to 0$. For asymptotically large values of ϕ the ratio becomes constant and equal to 2. However for $\phi = \mathcal{O}(1)\sqrt{\alpha}$, which is the relevant parameter range for preheating, the ratio is $V_{\chi\chi}/V = \mathcal{O}(1) \times \alpha^{-1}$, where the proportionality factor depends on n and ϕ.

Furthermore, the ϕ and χ mass-scales are also related to each other as

$$\left.\frac{V_{\chi\chi}}{V_{\phi\phi}}\right|_{\chi=0} = -\frac{\left(e^{\beta\phi}-1\right)^2\left(6\alpha + n\,\mathrm{csch}^2\left(\frac{\beta\phi}{2}\right)\right)}{4n\left(e^{\beta\phi}-2n\right)} \simeq -\frac{\left(e^{\beta\phi}-1\right)^2\mathrm{csch}^2\left(\frac{\beta\phi}{2}\right)}{4\left(e^{\beta\phi}-2n\right)}\,, \tag{5.47}$$

where the last equation holds for $\alpha \ll 1$. We see that $V_{\phi\phi}$ changes sign, since the potential is concave during inflation. For (large) negative values of ϕ the scaling of the ratio $V_{\chi\chi}/V_{\phi\phi}$ simplifies as $V_{\chi\chi}/V_{\phi\phi} \sim e^{\sqrt{2}\phi/\sqrt{3\alpha}}/(2n)$. The full behavior is shown in Fig. 5.11.

Finally, Fig. 5.12 shows the potential close to the origin for each of the fields $V(\phi, \chi = 0)$ and $V(\phi = 0, \chi)$ for $n = 1$. We see that the mass of the ϕ and χ particles is equal. This can have important phenomenological consequences, since the inability of the particles to decay into each other opens the way for the emergence of composite oscillons, comprised of both fields [328]. Oscillons appear when the potential of a scalar field is shallower than quadratic away from the origin. Intuitively, this makes the frequency of large oscillations smaller than the mass of the particle, creating a potential barrier that keeps the particles bound inside the oscillon. Two-field oscillons are more complicated and only a few examples have been found in the literature (see e.g. Refs. [328–331]. A feature of two-field systems exhibiting oscillons must be the inability of the scalar field comprising the oscillon to decay into lighter fields. In the α-attractor case it is reasonable to expect that, since the two fields have the same mass, decays and scatterings will be kinematically suppressed, possibly leading to long-lived oscillons. The study of oscillons in α-attractors is beyond the scope of the present work. One further interesting observation can be made when one compares the mass of particles in the E- and T-model. In the latter case, the small field excitations of the $n = 1$ potential have a mass of $\mu/\sqrt{3}$, half of the E-model case. This leads to a simple criterion for tachyonic resonance in α-attractors. The maximally negative contribution to the effective mass of the χ fluctuations is related to the Hubble scale at the end of inflation through energy conservation (neglecting Hubble drag after inflation)

$$\frac{1}{2}\mathcal{R}\dot{\phi}^2 = 3\mathcal{R}M_{\rm Pl}^2H^2 \simeq -\mu^2 \tag{5.48}$$

Fig. 5.1 shows that the Hubble scale at the end of inflation differs by about 10% for the E- and T-models for small values of α, regardless of the potential steepness n. In the EFT language, α-attractors in the small α regime show a strong hierarchy of scales, where the Hubble scale is almost constant and much smaller than the background oscillation frequency [332]. Fig. 5.12 shows the potential contribution to the effective mass for the E- and T-model. We see that while the tachyonic contribution is similar in the two models, the potential contribution is larger for the E-model. Thus, a quick calculation of the energy density at the end of inflation and the mass of the spectator field in any α-attractor model can provide a strong indication for the efficiency of tachyonic preheating. The case of asymmetric α-attractors is slightly more involved, because of the introduction of one further mass-scale, in which case one must check the possibility of non-adiabatic behavior due to it, as discussed in Section 5.3.1.

5.4.1 Floquet charts

In order to compare the efficiency of particle production (mode amplification) during preheating, we will use Floquet theory, by working in the static universe approximation, where the inflaton field oscillates periodically without Hubble friction. We use the algorithm described in Ref. [118]. The equation of motion for the χ_k modes (similarly for the ϕ_k ones) for $H = 0$

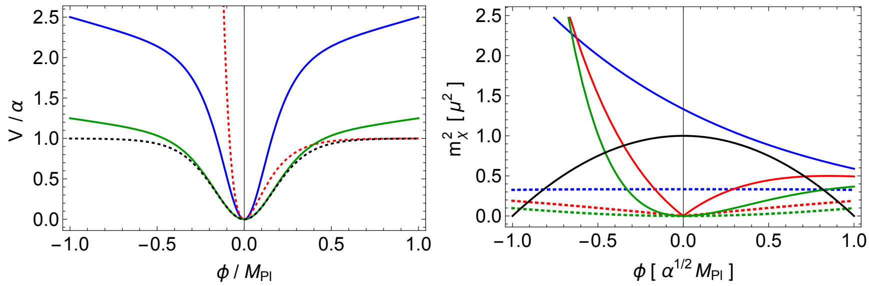

Figure 5.12: *Left:* The field $V(\phi, \chi = 0)$ (dotted) and $V(\phi = 0, \chi)$ (solid) for the massive case $n = 1$ of the E- and T-models (red/blue and black/green respectively). We see that in each model the ϕ and χ masses are equal to each other. However the masses of the fields in the T-model are larger than the ones in the E-model. *Right:* The potential contribution to the $\delta\chi$ effective mass for the E- and T- model (solid and dotted curves respectively) for $n = 1, 3/2, 2$ (blue,red green) and $\alpha \ll 1$. The black line shows an estimate of the tachyonic field-space contribution. We see that in the E-model for $n = 1$, the potential term can dominate over the tachyonic field-space curvature term, consistent with the behavior shown in Fig. 5.8.

and $a(t) = 1$ is written as

$$\frac{d}{dt}\begin{pmatrix}\chi_k \\ \dot{\chi}_k\end{pmatrix} = \begin{pmatrix}0 & 1 \\ -(k^2 + m^2_{\text{eff},\chi}) & 0\end{pmatrix}\begin{pmatrix}\chi_k \\ \dot{\chi}_k\end{pmatrix}, \tag{5.49}$$

where $m^2_{\text{eff},\chi} = m^2_{1,\chi} + m^2_{2,\chi}$. This equation is of the form

$$\dot{x}(t) = \mathcal{P}(t)\, x(t)\,, \tag{5.50}$$

where $\mathcal{P}(t)$ is a periodic matrix. The solutions are of the form

$$\chi_k(t) = e^{\mu_k t} g_1(t) + e^{-\mu_k t} g_2(t) \tag{5.51}$$

where g_1, g_2 are periodic functions and μ_k is the Floquet exponent. If μ_k has a non-zero real component, one of the two solutions will be exponentially growing, signaling an instability and efficient amplification for this specific wavenumber.

Figure 5.13 shows the Floquet charts for the generalized E-model for the case of $n = 3/2$. We see that, when properly rescaled, the Floquet charts for different values of $\alpha \ll 1$ are similar to each other. However, unlike the case of the T-model in Chapter 4, the Floquet charts do not exactly reach a "master diagram" for $10^{-2} \leqslant \alpha \leqslant 10^{-4}$. This can be traced back to the existence of two mass-scales: the field-space curvature and the steep

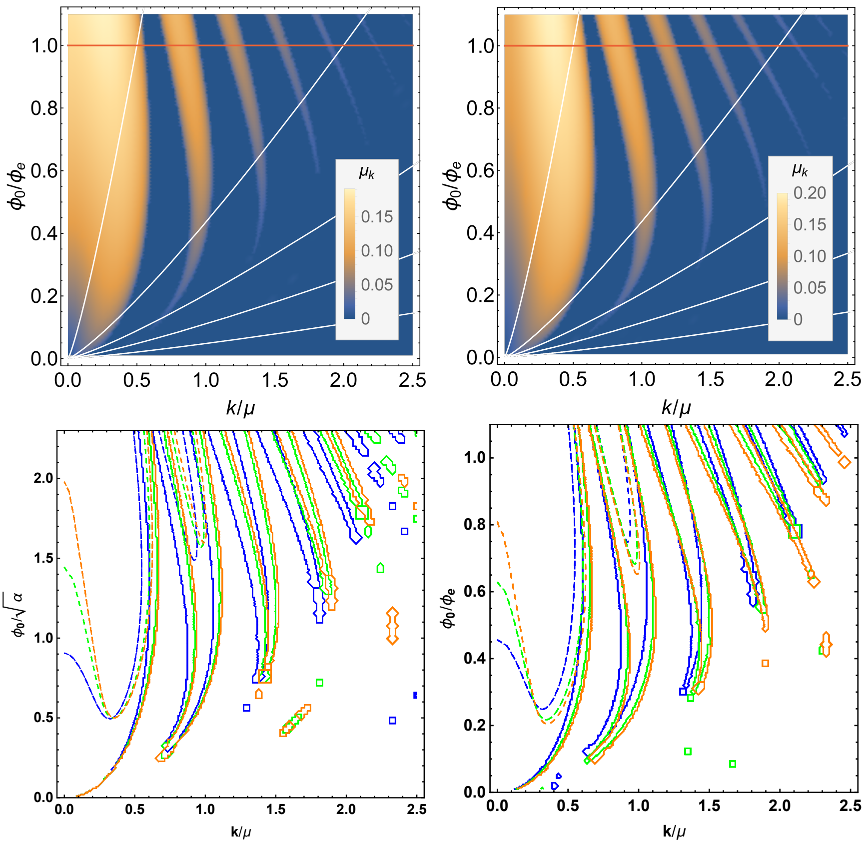

Figure 5.13: *Upper row:* The 3-D Floquet charts for $n = 3/2$ and $\alpha = 10^{-2}, 10^{-4}$ (left and right panels respectively). *Bottom row:* The contour plots for $\mu_k = 0$ (solid lines) and $\mu_k = 0.1$ (dashed lines) in units of μ. The background field oscillation amplitude ϕ_0 is rescaled either by $\sqrt{\alpha}$ (left) or by the field value at the end of inflation $\phi_{\rm end}$ [which is denoted here as ϕ_e] (right). The blue, green and orange curves are for $\alpha = 10^{-2}, 10^{-3}, 10^{-4}$ respectively. We see that, when properly rescaled, the Floquet charts asymptote to a "master diagram" for $\alpha \ll 1$.

potential at maximum negative ϕ. While the former does not scale with α for $\alpha \ll 1$, the latter does in a non-trivial way, albeit weakly, as shown in Fig. 5.8. Furthermore, the existence of multiple instability bands, unlike in the T-model case, can be an indication of the richer spectral content of the background field.

By constructing the Floquet diagram using the field amplitude ϕ_0 rescaled by the field value at the end of inflation $\phi_{\rm end}$ rather than $\sqrt{\alpha}$, the approach to a master diagram becomes better, especially for the higher k instability bands. This is due to the high sensitivity of $V_{\chi\chi}^{\rm max}$ on ϕ_0, as shown in Fig. 5.9. Furthermore, the value of $V_{\chi\chi}^{\rm max}$ mostly affects the higher instability bands, as we will discuss in Section 5.4.2.

Fig. 5.14 shows the Floquet charts for the cases of $n = 1$ and $n = 2$, which correspond to a locally quadratic and quartic potential near the origin. The Floquet charts for $n = 3/2$ and $n = 2$ are visually similar exhibiting multiple, non-trivial, instability bands in the range $k \lesssim 2.5\mu$. However, the Floquet chart for $n = 1$ has a completely distinct structure. The reason behind this discrepancy is that, as shown in Section 5.3.1, the structure of the effective mass of χ fluctuations is different for $n = 1$ as compared to $n \geqslant 3/2$. For $n = 1$ the tachyonic contribution of the field-space is entirely negated by the potential contribution. For $n \geqslant 3/2$ both the negative field space contribution and the positive potential term are visible. As we will show, the field-space effects are present for $n \geqslant 3/2$, especially for $k \lesssim \mu$, hence the dominant instability bands are similar amongst those models. This is different from the generalized T-model case discussed in Chapter 4, where the Floquet charts for all values of n show instability bands of similar shape and position, albeit not identical ones, exhibiting smaller Floquet exponent μ_k for $n = 1$.

5.4.2 Parametric resonance and competing mass-scales

As a way to encode the structure of preheating in the generalized E-model and make our results easily transferrable to other models, we examine the different mass-scales (and corresponding time-scales) that arise for the background motion and χ fluctuations.

The Hubble scale at the end of inflation $H_{\rm end}$ is proportional to the mass-scale μ and is defined by the requirement that the density fluctuations encoded in the CMB have the proper amplitude. It enters the calculation, by normalizing the amplitude of the Bunch-Davies vacuum, compared to the background energy density, hence it shows how much fluctuations must grow to dominate over the background energy density and lead to complete

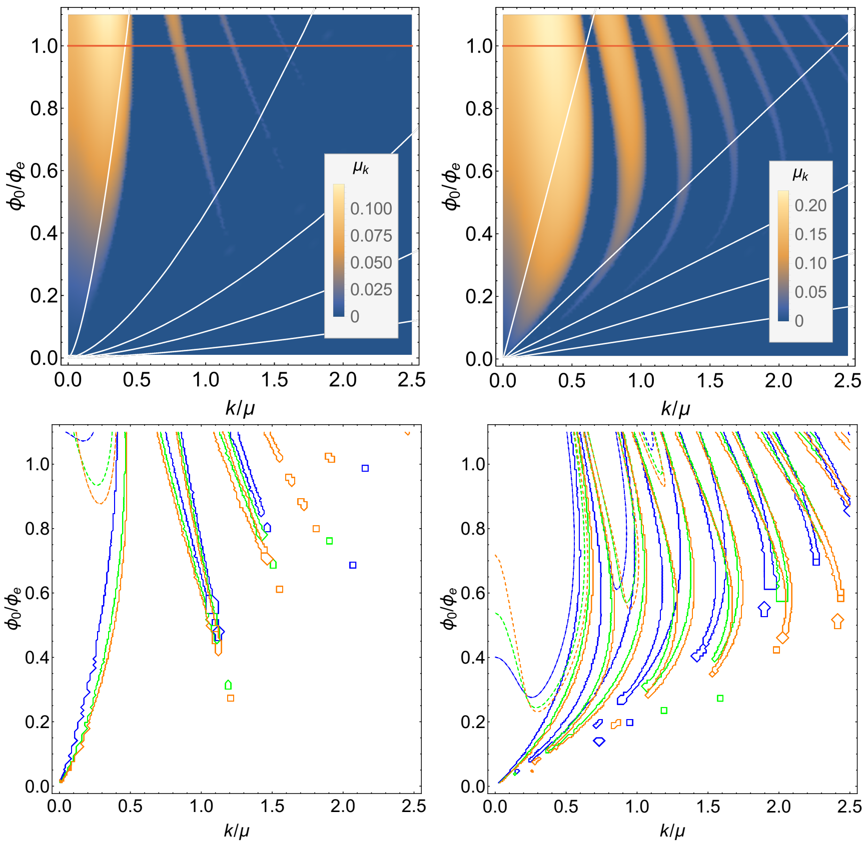

Figure 5.14: *Left column:* The 3-D Floquet charts for $n = 1$ (upper panel) and $\alpha = 10^{-4}$. The contour plots for $\mu_k = 0$(solid lines) and $\mu_k = 0.1$ (dashed lines) for $n = 1$ with the field amplitude rescaled by the field value at the end of inflation ϕ_e (bottom panel). The blue, green and orange curves are for $\alpha = 10^{-2}, 10^{-3}, 10^{-4}$ respectively. *Right column:* The same quantities for $n = 2$. We see the significantly suppressed parametric resonance for $n = 1$, both in the number of instability bands, as well as in the width and magnitude of the main instability band.

preheating. Furthermore, the Hubble scale controls the red-shifting of the mode wavenumbers and the amplitude of the inflaton condensate.

The background frequency $\omega_{\rm bg}$ controls the period of background oscillations. This is related to the local curvature of the potential near the origin $V_{\phi\phi}(\phi = 0, \chi = 0)$. In simple polynomial models of inflation, for example quadratic inflation, these two time-scales, the Hubble scale and the background frequency, are connected. However in plateau models, like α-attractors, a large hierarchy can exist between them (Fig. 5.2). The potential exhibits more mass-scales, including the local curvature of the spectator field potential $V_{\chi\chi}(\phi = 0, \chi = 0)$ and the average frequency of the χ fluctuations $\langle\omega_\chi\rangle$ over one background period. The former defines the mass of χ particles, while the latter is related to the existence of broad or narrow resonance.

The field-space curvature $\mathcal{R} \propto \alpha^{-1}$ enters the effective frequency of χ fluctuations through the combination $\frac{1}{2}\mathcal{R}\dot{\phi}^2$. This drives the efficient tachyonic resonance. For both the T- and E-model, this combination peaks close to -1, when the background field crosses the origin.

Finally, the maximum value of the potential curvature $V_{\phi\phi}^{(\rm max)}$, as well as the width of the "spike" measured as $\Delta\phi$ or Δt, control the higher harmonic content of the background motion. Due to the structure of the E-model potential, $V_{\phi\phi}^{(\rm max)}$ is also related to the spike in the effective frequency of the χ fluctuations, $V_{\chi\chi}^{(\rm max)}$.

Having seen that the field-space contribution is similar for the E- and T-models and also similar among different parameter choices n and $\alpha \ll 1$, we turn our attention to disentangling the potential and background contributions to the parametric resonance. For that we construct the Floquet diagrams for $\delta\chi$ by neglecting the field-space contribution. Fig. 5.15 shows the Floquet exponents for $n = 3/2$ and $n = 2$. We see that the exponents arising from the full $\delta\chi$ effective mass and those that are computed by considering only the potential and wavenumber contributions are very similar for $k > \mu$ and differ greatly for $k \lesssim \mu$, where the full system shows much more efficient particle production than the potential-only contribution.

We can thus conclude that the high-k resonance bands are mostly controlled by the potential. By contrast, the resonance structure differs greatly for $k \lesssim \mu$. This is due to the fact that the tachyonic part strongly enhances modes with $k \lesssim \mu$, as shown extensively for the T-model in Chapter 4, while it plays a subdominant role for large wavenumbers.

The existence for the multiple resonance bands for the E-model and not the T-model (see Chapter 4) is rooted in the existence of another mass-scale

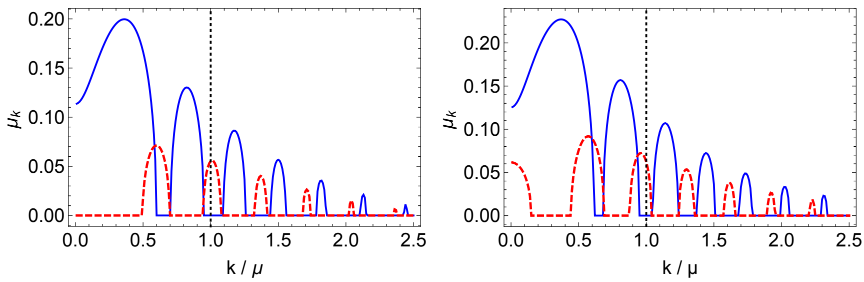

Figure 5.15: The Floquet exponent μ_k for $\alpha = 10^{-4}$, $\phi = \phi_{\text{end}}$ and $n = 3/2, 2$ (left and right respectively). The blue curves correspond to the full Floquet exponent, while the red-dashed one correspond to the Floquet exponent computed by neglecting the field-space contribution. The Floquet exponents are measured in units of μ^{-1}. The vertical dotted lines distinguish the regimes $k < \mu$ and $k > \mu$. The regime $k < \mu$ is controlled by the Ricci term in the effective mass, since the large field-space induced instability is absent in the case of the potential-only calculation. The regime $k > \mu$ is populated by multiple instability bands in both cases, with minor differences in position and height. We can thus deduce that parametric resonance in this regime is dominated by the effects of the potential term.

in the problem $V_{\phi\phi}^{\max} \propto V_{\chi\chi}^{\max}$, which leads the inflaton field and the effective mass of the χ fluctuations to acquire a large number of higher harmonics.

Before proceeding to compute particle production in an expanding universe, we wish to make a general comment in order to clear a common misconception in the literature. Frequent use of the term "α-attractors" is made to describe single-field systems with flat potentials of the form $V = V_0 \left|1 - e^{-\phi/\Lambda}\right|^{2n}$ or $V = V_0 \left|\tanh(\phi/\Lambda)\right|^{2n}$. However the flattening of the potential is merely a by-product of a more general feature of α-attractors: the existence of a hyperbolic field-space manifolds. As we have demonstrated in the present work and in Chapter 4, along with similar work by other authors, the presence of a second field is crucial for the full dynamics of α-attractors during preheating. The full two-field dynamics must be considered in order to properly extract the predictions of these models.

5.4.3 Expanding Universe

Having extensively analyzed the parametric resonance structure of the generalized two-field E-model for any value of the potential steepness parameter n and the field space curvature parameter α, we now incorporate the effects of the non-zero expansion rate of the universe during preheating. While there are semi-analytic methods to incorporate the effects of the expansion in parametric resonance studies, using either Floquet theory or the WKB approximation (see e.g. Refs. [160, 306, 309]), we will not rely on them, since they do not provide anything further in this case, in terms of intuitive understanding, to the static universe analysis. We will instead numerically compute the evolution of fluctuations, taking into account the expansion of the universe and the red-shifting of the amplitude of the background inflaton oscillations. We will however neglect the back-reaction of the fluctuations onto the inflaton condensate and the non-linear mode-mode coupling of the fluctuations.

Our present study can be used as a strong indication for the parameter values that can lead to complete preheating, as well as elucidating the differences between the T- and E-models. Ultimately, the question of complete preheating and subsequent thermalization will have to be decided using lattice simulations, such as the ones presented in Ref. [160] for the T-model and in Ref. [325] for the related family of ξ-attractors. In the case of the generalized two-field T-model, our semi-analytical results were shown to agree with the full lattice computation for a broad range of parameters, while at the same time elucidating the underlying physics and demonstrating the scaling properties of the Floquet charts [158, 160]. In the present work, we show that single-field simulations are unable to capture the most important time-scales, which are controlled by the tachyonic growth of the spectator field in both the E- and T-models of α-attractors. Section 5.4 suggests that this effect will carry over to other models with negatively curved field-space manifolds

Fig. 5.16 shows the growth of ϕ and χ fluctuations for the T- and E-models with n=1. This can be thought of as the physically “generic” case, since it describes massive particles in the small field limit. We see that the behavior of the two models is qualitatively different. In the case of the E-model the ϕ resonance is stronger, leading to possibly complete preheating already at $\alpha = 10^{-3}$, where the χ resonance is vastly subdominant. The two become comparable at $\alpha \lesssim 10^{-3}$, where preheating can complete within less than an e-fold.

In the case of the T-model, the χ resonance is always stronger than the ϕ resonance for $n = 1$. We see that the T-model does not completely preheat for $\alpha = 10^{-3}$. In the case of efficient parametric resonance in the ϕ field (for $\alpha \lesssim 10^{-4}$), lattice simulations have shown the fragmentation of the inflaton condensate and the subsequent formation of localized structures (oscillons) [323]. It is interesting to consider whether tachyonic resonance into the χ field can deplete the inflaton condensate before it has time to fragment.

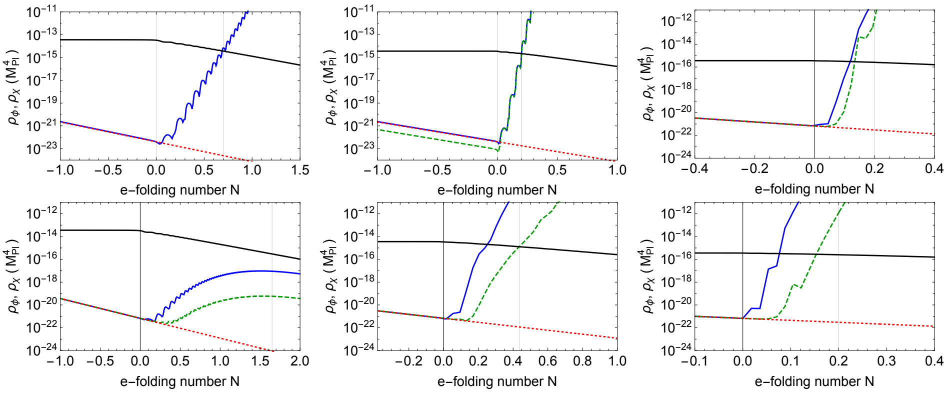

Figure 5.16: Energy density in ϕ and χ fluctuations (green-dashed and blue) and the background energy density of the inflaton (black) as a function of e-folds for the E-model (upper panels) and the T-model (lower panels) with $n = 1$ and $\alpha = 10^{-3}, 10^{-4}, 10^{-5}$ (left to right). We see efficient preheating for the E-model for $\alpha = 10^{-3}$, which is absent for the T-model. Furthermore, the E-model for $n = 1$ and $\alpha > 10^{-5}$ preheats predominately through inflaton self-resonance, while in the case of the T-model tachyonic amplification of the spectator field is always stronger than inflaton self-resonance.

Even in the case of a fragmented inflaton, one must consider the two possibilities: either resonance of the ϕ field to χ modes can proceed within the oscillons leading to the decay of the localized structures or composite oscillons consisting of both fields can form (see e.g. [328, 333]). Parametric resonance of scalar fields in localized structures, such as oscillons [334], Q-balls [335] or axion clumps [336], is similar to the homogenous field case with one important qualitative difference. If the Floquet exponent (computed by neglecting the spatial structure of the clump) is smaller than the time-scale on which the produced particles escape the clump, Bose enhancement is destroyed and the parametric resonance effectively shuts off [336]. In our case the maximum Floquet exponent is $\mu_k \sim \mu$, where $\mu = \mathcal{O}(10^{-6}) M_{\rm Pl}$. The size of the oscillons formed in single-field models with α-attractor-like potentials is $L = \mathcal{O}(\mu^{-1})$. The comparison between the homogeneous field Floquet exponent and the escape time $\mu_{\rm esc} \approx 1/(2L)$ shows that it is indeed possible for efficient production of χ particles to proceed within the oscillon, but a detailed calculation is needed to reach a definite conclusion, since non-trivial $\mathcal{O}(1)$ factors are involved in the calculation.

Fig. 5.17 shows the spectrum of produced ϕ and χ modes during the initial stages of preheating, before backreaction effects become important. We see that for $n = 1$ and $\alpha = 10^{-4}$ the parametric resonance of the ϕ

modes is stronger than that of the χ ones. This can be expected based on the results of Fig. 5.8, where we see that the two effective masses oscillate around $m^2 = 4\mu^2/3$, while the oscillation amplitude for the ϕ effective mass is larger, leading to a stronger resonance (see e.g. Ref. [118]). The similarity of the two effective masses for ϕ and χ fluctuations is a direct consequence of the E-model potential, which arises from a supergravity construction, where one specifies the potential of a complex scalar field, whose components are related to ϕ and χ, as shown in Appendix 5A. An interesting feature arises when we compare the χ spectrum for $n = 3/2$ and $n = 2$. For $n = 2$ the maximum excited wavenumber is set by the initial amplification and is found to be $k_{\rm max} \simeq 1.2\mu$. For $n = 3/2$ the value of $k_{\rm max}$ grows with time. This can be traced back to the behavior we saw in Fig. 5.10, where the adiabaticity violation for $n = 3/2$ was shown to grow with time, contrary to $n = 2$. This behavior is explained by using the results of Fig. 5.9, where it was demonstrated that the height of the effective mass spike –which controls the large k resonance– red-shifts slower than a^{-2} for $n = 3/2$, hence it becomes progressively more important compared to the wavenumber term k^2/a^2.

Finally, Fig. 5.18 provides a visual summary of the preheating efficiency for different models and parameter values. For the case of massive particles, $n = 1$, the T-model exhibits efficient preheating through the χ field for $\alpha \lesssim 10^{-4}$. On the other hand, parametric resonance in the E-model is more efficient, starting at $\alpha \approx 10^{-3}$, albeit through self-resonance of the ϕ field, since tachyonic production of χ modes is shut off due to the large positive mass term (see Fig. 5.8). For steeper potentials $n \geqslant 3/2$, self-resonance of the ϕ field becomes progressively more inefficient, while tachyonic resonance of χ modes becomes efficient already at $\alpha \approx 10^{-3}$ and is able to completely preheat the universe within 1.5 e-folds after the end of inflation, much faster than a naive single-field analysis would suggest.

Overall this means that α-attractors with $n = 1$ and $\alpha \gtrsim 10^{-3}$, equivalently a tensor to scalar ratio $r \gtrsim 10^{-6}$, can undergo a long matter-dominated expansion after the end of inflation and the decay of the inflaton condensate can proceed only through perturbative decays to other particles. Unfortunately, there is no concrete theoretical motivation for the size of such couplings, hence the transition to radiative degrees of freedom cannot be estimated. For potentials describing massless scalar fields, the decay of the condensate to radiative degrees of freedom can occur very quickly through tachyonic production of the spectator field χ, for both the E-model explored here and the T-model explored in Refs. [158, 160].

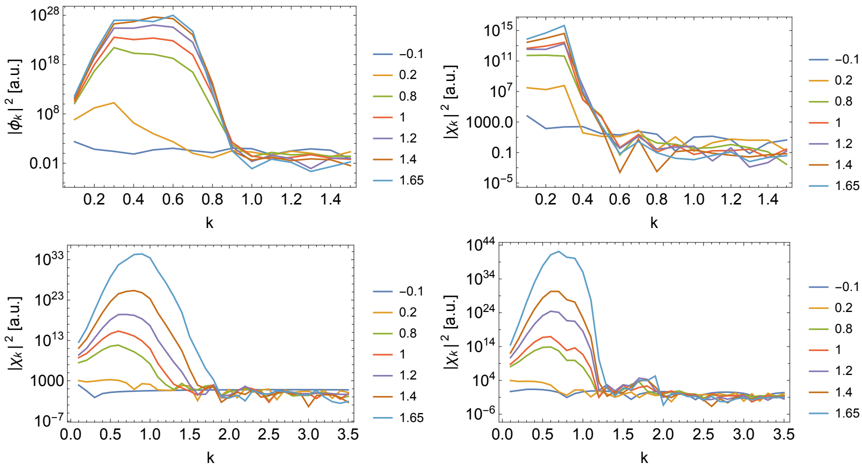

Figure 5.17: The spectra of the ϕ fluctuations $|\phi_k|^2$ and χ fluctuations $|\chi_k|^2$ (in arbitrary units) in the E-model as a function of the wavenumber k (in units of μ) at different times for $\{n, \alpha\} = \{1, 10^{-4}\}$ (upper panels) and $\{n, \alpha\} = \{3/2, 10^{-3}\}$, $\{n, \alpha\} = \{2, 10^{-3}\}$ (lover panels, left and right respectively). The times corresponding to the various curves are shown in the legend of each panel, measured in e-folds after the end of inflation (negative values correspond to spectra during the last stages of inflation). We see that for $n = 1$ the amplification of the ϕ (inflaton) modes is much stronger than that of the χ (spectator) modes. For $n = 3/2$ we see that at later times, the range of excited χ wavenumbers grows, while for $n = 2$ it remains constant at $k_{\max} \simeq \mu$. This is in agreement with the behavior of the effective mass shown in Fig. 5.9.

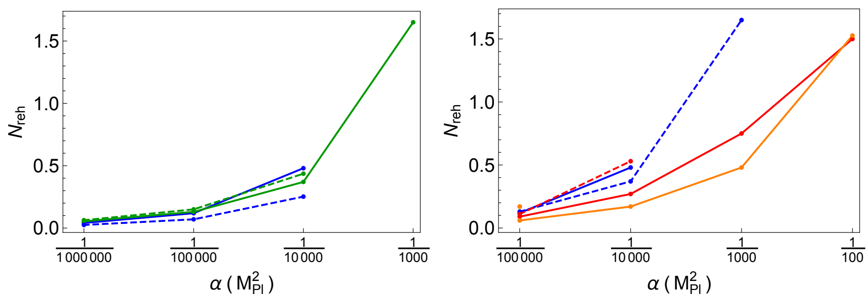

Figure 5.18: *Left:* The time of reheating for $n = 1$ through ϕ (green) and χ (blue) fluctuations for the T- and E-models (dashed and solid curves respectively) *Right:* The E-model behavior for $n = 1, 3/2, 6$ (blue, red, orange) and resonance through ϕ or χ modes (dashed and solid curves respectively). For $10^{-4} \lesssim \alpha \lesssim 10^{-3}$ the E-model preheats predominately through inflaton self-resonance, while the T-model does not completely preheat. For $n \geqslant 3/2$ the E-model preheats through amplification of the spectator field for $\alpha \lesssim 0.01$. For small values of $\alpha \lesssim 10^{-4}$ preheating is practically instantaneous (lasting less than one e-fold) for any potential parameter n.

5.4.4 Gravitational waves

It has been shown that efficient preheating leading to a turbulent fluid can lead to the production of gravitational waves. This can occur e.g. through coupling of the inflaton to gauge fields, as well as through inflaton decay through self-resonance. The latter case is similar to the current analysis of parametric resonance in α-attractors, where the spectator field is amplified. Using the "rule of thumb" estimates of Ref. [177], the frequency of GW's today is related to the Hubble scale at the time of generation and the dominant wavenumber of the source as

$$f \simeq 2.7 \cdot 10^{10} \frac{k_{\rm phys}}{\sqrt{M_{\rm Pl} H}} \, {\rm Hz}\,. \tag{5.52}$$

In most models, the physical wavenumber is proportional to the Hubble scale, thus reducing the Hubble scale reduces the frequency of the GW signal as $f \propto \sqrt{H}$. As has been extensively shown in the present work and in Refs. [158, 160], preheating in α-attractors occurs at a typical wavenumber $k \sim \mu$, while the Hubble scale scales as $M_{\rm Pl} H \sim \sqrt{\alpha}\mu$. Using these estimates, the peak GW frequency today becomes

$$f \sim \frac{10^7}{\alpha^{1/4}} \, {\rm Hz}\,, \tag{5.53}$$

where we used the value of $\mu \simeq 6 \times 10^{-6}\, M_{\rm Pl}$ required to produce the observed amplitude of density fluctuations. Thus, contrary to the common behavior of GW from preheating, reducing the Hubble scale through reducing α (increasing the field-space curvature) will actually increase the peak frequency of GW's, pushing them further away from the observable range of interferometers. It remains interesting to follow progress in detection strategies for Ultra High Frequency gravitational waves, as many early universe sources operate in this regime.

5.5 Summary and Discussion

In the present work we revisited the multi-field behavior of the generalized E-model, which consists of two-fields on a hyperbolic manifold. More highly curved manifolds lead to a lower Hubble scale and correspondingly to a smaller tensor to scalar ratio. We focus on the region $10^{-7} \lesssim r \lesssim 10^{-4}$, which is below the direct detection limits of the next generation CMB experiments. The potential of the inflaton field ϕ is asymmetric with respect to the global minimum at the origin. It exhibits a flat plateau where inflation is realized, leading to the usual Starobinsky-like predictions $n_s \sim N_*^{-1}$ and $r \sim N_*^{-2}$ and a sharp potential"wall", which the field probes after inflation and during preheating. By contrast, the potential of the spectator field χ is symmetric with respect to the minimum at $\chi = 0$. Several studies in the literature have examined the equivalence of the single-field behavior of the E- and T-models during inflation. Going beyond these studies we were able to show that the similarities of the T- and E-model extend beyond the single-field analysis. In fact, their multi-field behavior during inflation is identical up to slow-roll corrections. Previous analyses of the E- and T-models have established the existence of a single field attractor along the minimum of the spectator field [321]. In order to assess the possibility of multi-field effects beyond the single-field attractor, we examined the basin of attraction by choosing a wide variety of initial conditions along iso-potential surfaces. We showed that the global behavior of this system consists of two straight inflationary trajectories, each keeping one of the fields constant. While each of them can be made arbitrarily long by appropriate choice of initial field values, only the final trajectory, the single field attractor along $\chi = 0$ gives results that are in agreement with the CMB. It remains to be seen, if similar two-stage behavior appears in other realizations of α-attractors and if some well-motivated models exist where both stages can lead to predictions that are consistent with CMB measurements. Furthermore, the two straight trajectories are joined by a sharp turn and a brief period of oscillations around $\chi = 0$. An assessment of the observability of such a signal [337] at CMB or LSS scales is beyond the scope of this work and is left for future analysis.

Reheating is crucial for connecting inflationary predictions to CMB observables. Especially in the case of inflationary models that follow the predictions of the Starobinsky model, $n_s = 1 - 2/N_*$, the latest *Planck* results [53] are putting mild pressure on $N_* \simeq 50$, instead preferring a value closer to $N_* = 60$. Such models include the Starobinsky model, Higgs inflation and its generalizations of non-minimally coupled models [154–156] and of course α-attractors. These results and the anticipated improvement from next generation experiments, like LiteBird and CMB-S4, can significantly constrain the existence of a prolonged matter dominated expansion after inflation.

The preheating efficiency depends on the amplification of fluctuations of the inflaton and spectator fields, which is governed by their corresponding effective masses. The coupled metric perturbations component that contributes to the inflaton self-resonance is proportional to $\sqrt{\alpha}$ and becomes subdominant for $\alpha \ll 1$. The term that encodes the space-time curvature is even smaller, being proportional to α. The inflaton self-resonance is thus solely determined by the second derivative of the potential, while the resonance structure of the spectator field is determined by the interplay of the potential contribution and the field-space effects, which do not scale with α. Furthermore, the wavenumbers that are amplified due to parametric resonance of either the inflaton or spectator fields do not depend on α and scale as $k \lesssim \mathcal{O}(1)\mu$, where $\mu \simeq 6 \times 10^{-6}\, M_{\rm Pl}$ in order to produce the correct amplitude of density perturbations. By contrast the Hubble scale depends on α as $H \propto \mu\sqrt{\alpha}$. Hence for small α the dominant preheating dynamics is occurring at very sub-horizon (sub-Hubble) scales. This creates the apparent paradox that reducing the inflationary scale will lead to the frequency of GW's from preheating to increase as $f \propto \alpha^{-1/4} \propto H^{-1/2}$ rather than decrease, as in the usual case for low-scale inflation.

The preheating efficiency of the E-model is qualitatively different than that of the T-model [158, 160]. The parametric resonance of ϕ fluctuations is significantly more enhanced in the E-model, as compared to the T-model. This can be traced back to the inherent asymmetry of the E-model potential, which introduced a spike in the effective mass of the fluctuations and higher harmonic content in the background motion. For massive fields, the tachyonic component of the spectator effective mass in the E-model is canceled by the contribution of the potential term, hence tachyonic amplification is completely shut off. However the spike introduced by the potential term leads to efficient parametric resonance. However, a similar spike is present in the self-resonance of the inflaton field and is more pronounced than the one in the spectator effective mass. This leads to the E-model preheating predominately through self-resonance for massive fields ($n = 1$). Furthermore, preheating in the E-model is efficient for higher values of α than in the T-model ($\alpha \sim 10^{-3}$), leading to the first distinguishing feature between them.

For massless fields, or equivalently potentials that behave as $V(\phi, \chi) \propto \{|\phi|^{2n}, |\chi|^{2n}\}$ with $n \geqslant 3/2$ close to the minimum, the spectator field dominates the preheating behavior of the E-model, leading to fast preheating for $\alpha \lesssim 0.01$. For small wavenumbers ($k \lesssim \mu$), the χ modes grow tachyonically due to the effects of the negative field-space. For larger wavenumbers, the amplification is controlled by the potential spike, leading to parametric resonance and multiple instability bands. For highly curved manifolds $\alpha \lesssim 10^{-4}$, preheating concludes within less than an e-fold for any potential choice. The preheating dynamics of both the E- and T-model reinforce the need for notational clarity regarding α-attractors: a flat potential of the form $V \propto \left|1 - e^{-\phi/\Lambda}\right|^{2n}$ or $V \propto |\tanh(\phi/\Lambda)|^{2n}$ that is usually associated with α-attractors should not be regarded as their main characteristic. On the contrary, the hyperbolic manifold, from which the potential flatness originates, and their multi-field nature, should be taken into account to properly address the dynamics of α-attractor models. In anticipation of upcoming CMB and LSS data, that hope to further restrict the value of n_s and r, theoretical uncertainties must become small enough to allow for an accurate comparison between theory and observation. Single-field simulations are unable to capture the most important preheating time-scales, which are controlled by the tachyonic growth of the spectator field in both the E- and T-models of α-attractors. We must thus consider the full two-field dynamics in order to put α-attractor predictions to the test.

Using the T- and E-models as characteristic examples, we analyzed the various mass-scales that control the tachyonic growth of fluctuations, making a first step towards an Effective Field Theory description of preheating in hyperbolic manifolds [332]. The necessary presence of a spectator field, as required by the supergravity constructions of α-attractors, make it necessary to extend the single-field preheating results found in the literature [323] to examine the effects of efficient tachyonic preheating. Having provided a qualitative and quantitative understanding of the relevant time and mass-scales, we leave such two-field lattice simulations for future work.

5.6 Appendix 5A: Generalization of the E-model

For completeness, we describe here the $\mathcal{N} = 1$ Supergravity embedding of the two-field E-model [321] considered in the main text. Similarly as in Chapter 4 we consider the super-potential

$$W_H = \sqrt{\alpha}\mu\, S\, F(Z) \tag{5.54}$$

and Kähler potential

$$K_H = \frac{-3\alpha}{2} \log\left[\frac{(1 - Z\bar{Z})^2}{(1 - Z^2)(1 - \bar{Z}^2)}\right] + S\bar{S}\,. \tag{5.55}$$

Using the relation between the Kähler potential and the superpotential

$$Z = \frac{T - 1}{T + 1} \tag{5.56}$$

and choosing for the E-model

$$F(Z) = \left(\frac{2Z}{Z+1}\right)^n \tag{5.57}$$

we get

$$K_H = \frac{-3\alpha}{2} \log\left[\frac{(T+\bar{T})^2}{4T\bar{T}}\right] + S\bar{S} \tag{5.58}$$

and

$$W_H = \sqrt{\alpha}\mu S \left(\frac{T-1}{T}\right)^n . \tag{5.59}$$

as in Ref. [321]. The potential is of the form

$$V = \alpha\mu^2 4^n \left[\frac{(Z\bar{Z}-1)^2}{(Z^2-1)(\bar{Z}^2-1)}\right]^{-3\alpha/2} \left[\frac{Z\bar{Z}}{(1+Z)(1+\bar{Z})}\right]^2 . \tag{5.60}$$

With the same field-space basis as in Chapter 4, i.e. see (4.65) – (4.69), one may find the corresponding two-field potential

$$V(\phi,\chi) = \alpha\mu^2 \left(1 - \frac{2e^{-\beta\phi}}{\cosh(\beta\chi)} + e^{-2\beta\phi}\right)^n (\cosh(\beta\chi))^{2/\beta^2} , \tag{5.61}$$

where again $\beta = \sqrt{2/3\alpha}$. It is trivial to see that for $\chi = 0$ we recover the usual expression for the E-model

$$V(\phi,\chi) = \alpha\mu^2 \left(1 - e^{-\beta\phi}\right)^{2n} . \tag{5.62}$$

where the exponent is $2n$ instead of 2.

The expressions for the non-zero components of the field-space metric together with Christoffel symbols, Riemann and Ricci tensors are the same as in Chapter 4 and we do not duplicate them here.

Bibliography

[1] A. D. Linde, "Particle physics and inflationary cosmology," Contemp. Concepts Phys. **5**, 1-362 (1990)

[2] B. J. T. Jones, "A Brief History of Cosmology", Astronomical Society of the Pacific Conference Series, Vol. 126 (1997).

[3] D. Baumann, "Inflation," Contribution to: TASI 2009, 523-686, [arXiv:0907.5424 [hep-th]].

[4] D. Baumann, "Cosmology" Lecture notes, `http://cosmology.amsterdam/education/cosmology`

[5] A. Einstein, "The Foundation of the General Theory of Relativity," Annalen Phys. **49**, no.7, 769-822 (1916)

[6] A. Friedman, "On the Curvature of space," Z. Phys. **10**, 377-386 (1922)

[7] A. Friedmann, "On the Possibility of a world with constant negative curvature of space," Z. Phys. **21**, 326-332 (1924)

[8] G. Lemaitre, "A Homogeneous Universe of Constant Mass and Growing Radius Accounting for the Radial Velocity of Extragalactic Nebulae," Annales Soc. Sci. Bruxelles A **47**, 49-59 (1927)

[9] H. P. Robertson, "Kinematics and World-Structure," Astrophys. J. **82**, 284-301 (1935)

[10] A. G. Walker, "On Milne's theory of world-structure," Proceedings of the London Mathematical Society, vol. 42, p. 90–127, 1937.

[11] V. M. Slipher, "Nebulae," Proc. Am. Phil. Soc. **56**, 403-409 (1917)

[12] E. Hubble, "A relation between distance and radial velocity among extra-galactic nebulae," Proc. Nat. Acad. Sci. **15**, 168-173 (1929)

[13] E. Hubble and M. L. Humason, "The Velocity-Distance Relation among Extra-Galactic Nebulae," Astrophys. J. **74**, 43-80 (1931)

[14] R. A. Alpher, H. Bethe and G. Gamow, "The origin of chemical elements," Phys. Rev. **73**, 803-804 (1948)

[15] R. A. Alpher and R. Herman, "Evolution of the Universe," Nature **162**, no.4124, 774-775 (1948)

[16] A. A. Penzias and R. W. Wilson, "A Measurement of excess antenna temperature at 4080-Mc/s," Astrophys. J. **142**, 419-421 (1965)

[17] E. Lifshitz, " On the gravitational stability of the expanding universe," J. Phys. (USSR) **10**, no.2, 116 (1946)

[18] R. K. Sachs and A. M. Wolfe, "Perturbations of a cosmological model and angular variations of the microwave background," Astrophys. J. **147**, 73-90 (1967)

[19] J. C. Mather, E. S. Cheng, D. A. Cottingham, R. E. Eplee, D. J. Fixsen, T. Hewagama, R. B. Isaacman, K. A. Jesnsen, S. S. Meyer and P. D. Noerdlinger, *et al.* "Measurement of the Cosmic Microwave Background spectrum by the COBE FIRAS instrument," Astrophys. J. **420**, 439-444 (1994)

[20] G. F. Smoot, C. L. Bennett, A. Kogut, *et al.* "Structure in the COBE Differential Microwave Radiometer First-Year Maps" Astrophys. J. **396**, pp. L1–L5, 1992.

[21] R. H. Cyburt, B. D. Fields and K. A. Olive, "Primordial nucleosynthesis in light of WMAP," Phys. Lett. B **567**, 227-234 (2003) [arXiv:astro-ph/0302431 [astro-ph]].

[22] A. Coc, J. P. Uzan and E. Vangioni, "Standard Big-Bang Nucleosynthesis after Planck," [arXiv:1307.6955 [astro-ph.CO]].

[23] A. Coc, P. Petitjean, J. P. Uzan, E. Vangioni, P. Descouvemont, C. Iliadis and R. Longland, "New reaction rates for improved primordial D/H calculation and the cosmic evolution of deuterium," Phys. Rev. D **92**, no.12, 123526 (2015) [arXiv:1511.03843 [astro-ph.CO]].

[24] W. De Sitter, "On the relativity of inertia. remarks concerning Einstein's latest hypothesis", Proc. Kon. Ned. Acad. Wet **19** (1917), no. 2 1217–1225.

[25] W. De Sitter, "On the curvature of space", Proc. Kon. Ned. Acad. Wet, vol. 20, pp. 229–243, 1917.

[26] E. Gliner, "Algebraic Properties of the Energy-momentum Tensor and Vacuum-like States of Matter", Soviet Physics JETP, Vol. **22**, p.378, (1966).
E. Gliner, "Vacuum-like state of a medium and Friedmann cosmology", Docl.Akad.Nauk SSSR **192**, 771 (1970);
E. Gliner, I. Dymnikova, "Nonsingular Friedmann cosmology", Sov. Astron. Lett. **1**, 93 (1975).

[27] A. H. Guth, "The Inflationary Universe: A Possible Solution to the Horizon and Flatness Problems," Phys. Rev. D **23**, 347-356 (1981)

[28] A. D. Linde, "A New Inflationary Universe Scenario: A Possible Solution of the Horizon, Flatness, Homogeneity, Isotropy and Primordial Monopole Problems," Phys. Lett. B **108**, 389-393 (1982)

[29] A. Albrecht and P. J. Steinhardt, "Cosmology for Grand Unified Theories with Radiatively Induced Symmetry Breaking," Phys. Rev. Lett. **48**, 1220-1223 (1982)

[30] V. Mukhanov, "Physical Foundations of Cosmology," Oxford: Cambridge University Press, 2005.

[31] G. N. Remmen and S. M. Carroll, "Attractor Solutions in Scalar-Field Cosmology," Phys. Rev. D **88** (2013), 083518 [arXiv:1309.2611 [gr-qc]].

[32] R. Brandenberger, Int. J. Mod. Phys. D **26** (2016) no.01, 1740002 [arXiv:1601.01918 [hep-th]].

[33] C. Gordon, D. Wands, B. A. Bassett and R. Maartens, "Adiabatic and entropy perturbations from inflation," Phys. Rev. D **63**, 023506 (2000) [arXiv:astro-ph/0009131 [astro-ph]].

[34] S. Groot Nibbelink and B. J. W. van Tent, [arXiv:hep-ph/0011325 [hep-ph]].

[35] S. Groot Nibbelink and B. J. W. van Tent, "Scalar perturbations during multiple field slow-roll inflation," Class. Quant. Grav. **19**, 613-640 (2002) [arXiv:hep-ph/0107272 [hep-ph]].

[36] A. Achucarro, J. O. Gong, S. Hardeman, G. A. Palma and S. P. Patil, "Features of heavy physics in the CMB power spectrum," JCAP **01**, 030 (2011) [arXiv:1010.3693 [hep-ph]].

[37] J. O. Gong and T. Tanaka, "A covariant approach to general field space metric in multi-field inflation," JCAP **03**, 015 (2011) [erratum: JCAP **02**, E01 (2012)] [arXiv:1101.4809 [astro-ph.CO]].

[38] G. A. Palma, S. Sypsas and C. Zenteno, "Seeding primordial black holes in multifield inflation," Phys. Rev. Lett. **125**, no.12, 121301 (2020) [arXiv:2004.06106 [astro-ph.CO]].

[39] J. Fumagalli, S. Renaux-Petel and L. T. Witkowski, "Oscillations in the stochastic gravitational wave background from sharp features and particle production during inflation," [arXiv:2012.02761 [astro-ph.CO]].

[40] J. Fumagalli, S. Renaux-Petel and L. T. Witkowski, "Resonant features in the stochastic gravitational wave background," [arXiv:2105.06481 [astro-ph.CO]].

[41] A. Achúcarro and G. A. Palma, "The string swampland constraints require multi-field inflation," JCAP **02**, 041 (2019) [arXiv:1807.04390 [hep-th]].

[42] A. Hetz and G. A. Palma, "Sound Speed of Primordial Fluctuations in Supergravity Inflation," Phys. Rev. Lett. **117**, no.10, 101301 (2016) [arXiv:1601.05457 [hep-th]].

[43] C. Vafa, "The String landscape and the swampland," [arXiv:hep-th/0509212 [hep-th]].

[44] T. D. Brennan, F. Carta and C. Vafa, "The String Landscape, the Swampland, and the Missing Corner," PoS **TASI2017** (2017), 015 [arXiv:1711.00864 [hep-th]].

[45] E. Palti, "The Swampland: Introduction and Review," Fortsch. Phys. **67** (2019) no.6, 1900037 [arXiv:1903.06239 [hep-th]].

[46] C. Corianò and P. H. Frampton, "Swampland Conjectures and Cosmological Expansion," [arXiv:2010.02939 [hep-th]].

[47] M. van Beest, J. Calderón-Infante, D. Mirfendereski and I. Valenzuela, "Lectures on the Swampland Program in String Compactifications," [arXiv:2102.01111 [hep-th]].

[48] G. Obied, H. Ooguri, L. Spodyneiko and C. Vafa, "De Sitter Space and the Swampland," [arXiv:1806.08362 [hep-th]].

[49] R. Kallosh and A. Linde, “Universality Class in Conformal Inflation,” JCAP **07** (2013), 002 [arXiv:1306.5220 [hep-th]].

[50] R. Kallosh, A. Linde and D. Roest, “Superconformal Inflationary α-Attractors,” JHEP **1311**, 198 (2013) doi:10.1007/JHEP11(2013)198 [arXiv:1311.0472 [hep-th]]. R. Kallosh, A. Linde and D. Roest, “Large field inflation and double α-attractors,” JHEP **1408**, 052 (2014) doi:10.1007/JHEP08(2014)052 [arXiv:1405.3646 [hep-th]].

[51] S. Ferrara, R. Kallosh, A. Linde and M. Porrati,“Minimal Supergravity Models of Inflation,” Phys. Rev. D **88** (2013) no.8, 085038 [arXiv:1307.7696 [hep-th]]; R. Kallosh and A. Linde, “Non-minimal inflationary attractors,” JCAP 1310 (2013): 033, arXiv:1307.7938 [hep-th]; R. Kallosh and A. Linde, “Multi-field conformal cosmological attractors,” JCAP 1312 (2013): 006, arXiv:1309.2015 [hep-th]; R. Kallosh and A. Linde, “Planck, LHC, and α-attractors,” Phys. Rev. D 91 (2015): 083528, arXiv:1502.07733 [astro-ph.CO]; J. J. M. Carrasco, R. Kallosh, and A. Linde, “Cosmological attractors and initial conditions for inflation,” arXiv:1506.00936 [hep-th].

[52] J. J. M. Carrasco, R. Kallosh, A. Linde and D. Roest, “Hyperbolic geometry of cosmological attractors,” Phys. Rev. D **92** (2015) no.4, 041301 doi:10.1103/PhysRevD.92.041301 [arXiv:1504.05557 [hep-th]].

[53] Y. Akrami *et al.* [Planck], “Planck 2018 results. X. Constraints on inflation,” Astron. Astrophys. **641**, A10 (2020), [arXiv:1807.06211 [astro-ph.CO]].

[54] S. Renaux-Petel and K. Turzyński, “Geometrical Destabilization of Inflation,” Phys. Rev. Lett. **117** (2016) no.14, 141301 [arXiv:1510.01281 [astro-ph.CO]].

[55] S. Renaux-Petel, K. Turzyński and V. Vennin, “Geometrical destabilization, premature end of inflation and Bayesian model selection,” JCAP **11** (2017), 006 [arXiv:1706.01835 [astro-ph.CO]].

[56] S. Garcia-Saenz and S. Renaux-Petel, “Flattened non-Gaussianities from the effective field theory of inflation with imaginary speed of sound,” JCAP **11** (2018), 005 [arXiv:1805.12563 [hep-th]].

[57] O. Grocholski, M. Kalinowski, M. Kolanowski, S. Renaux-Petel, K. Turzyński and V. Vennin, “On backreaction effects in geometrical destabilisation of inflation,” JCAP **05** (2019), 008 [arXiv:1901.10468 [astro-ph.CO]].

[58] M. Cicoli, V. Guidetti and F. G. Pedro, “Geometrical Destabilisation of Ultra-Light Axions in String Inflation,” JCAP **05** (2019), 046 [arXiv:1903.01497 [hep-th]].

[59] A. R. Brown, “Hyperbolic Inflation,” Phys. Rev. Lett. **121** (2018) no.25, 251601 [arXiv:1705.03023 [hep-th]].

[60] S. Mizuno and S. Mukohyama, “Primordial perturbations from inflation with a hyperbolic field-space,” Phys. Rev. D **96** (2017) no.10, 103533 [arXiv:1707.05125 [hep-th]].

[61] A. Achúcarro, R. Kallosh, A. Linde, D. G. Wang and Y. Welling, “Univer-

sality of multi-field α-attractors," JCAP **04** (2018), 028 [arXiv:1711.09478 [hep-th]].

[62] T. Bjorkmo and M. C. D. Marsh, "Hyperinflation generalised: from its attractor mechanism to its tension with the 'swampland conditions'," JHEP **04** (2019), 172 [arXiv:1901.08603 [hep-th]].

[63] J. Fumagalli, S. Garcia-Saenz, L. Pinol, S. Renaux-Petel and J. Ronayne, "Hyper-Non-Gaussianities in Inflation with Strongly Nongeodesic Motion," Phys. Rev. Lett. **123** (2019) no.20, 201302 [arXiv:1902.03221 [hep-th]].

[64] T. Bjorkmo, R. Z. Ferreira and M. C. D. Marsh, "Mild Non-Gaussianities under Perturbative Control from Rapid-Turn Inflation Models," JCAP **12** (2019), 036 [arXiv:1908.11316 [hep-th]].

[65] P. Christodoulidis, D. Roest and E. I. Sfakianakis, "Angular inflation in multi-field α-attractors," JCAP **11** (2019), 002 [arXiv:1803.09841 [hep-th]].

[66] A. Linde, D. G. Wang, Y. Welling, Y. Yamada and A. Achúcarro, "Hypernatural inflation," JCAP **07** (2018), 035 [arXiv:1803.09911 [hep-th]].

[67] P. Christodoulidis, D. Roest and E. I. Sfakianakis, "Attractors, Bifurcations and Curvature in Multi-field Inflation," JCAP **08** (2020), 006 [arXiv:1903.03513 [gr-qc]].

[68] P. Christodoulidis, D. Roest and E. I. Sfakianakis, "Scaling attractors in multi-field inflation," JCAP **12** (2019), 059 [arXiv:1903.06116 [hep-th]].

[69] A. Achúcarro, V. Atal, C. Germani and G. A. Palma, "Cumulative effects in inflation with ultra-light entropy modes," JCAP **02** (2017), 013 [arXiv:1607.08609 [astro-ph.CO]].

[70] A. Achúcarro, E. J. Copeland, O. Iarygina, G. A. Palma, D. G. Wang and Y. Welling, "Shift-symmetric orbital inflation: Single field or multifield?," Phys. Rev. D **102** (2020) no.2, 021302 [arXiv:1901.03657 [astro-ph.CO]].

[71] A. Achúcarro, G. A. Palma, D. G. Wang and Y. Welling, "Origin of ultra-light fields during inflation and their suppressed non-Gaussianity," JCAP **10** (2020), 018 [arXiv:1908.06956 [hep-th]].

[72] A. Achúcarro and Y. Welling, "Orbital Inflation: inflating along an angular isometry of field space," [arXiv:1907.02020 [hep-th]].

[73] Y. Welling, "Simple, exact model of quasisingle field inflation," Phys. Rev. D **101** (2020) no.6, 063535 [arXiv:1907.02951 [astro-ph.CO]].

[74] A. Maleknejad and M. M. Sheikh-Jabbari, "Gauge-flation: Inflation From Non-Abelian Gauge Fields," Phys. Lett. B **723**, 224-228 (2013) [arXiv:1102.1513 [hep-ph]].

[75] A. Maleknejad and M. M. Sheikh-Jabbari, "Non-Abelian Gauge Field Inflation," Phys. Rev. D **84**, 043515 (2011) [arXiv:1102.1932 [hep-ph]].

[76] A. Maleknejad, M. M. Sheikh-Jabbari and J. Soda, "Gauge Fields and Inflation," Phys. Rept. **528**, 161-261 (2013) [arXiv:1212.2921 [hep-th]].

[77] J. Cervero and L. Jacobs, "Classical Yang-Mills Fields in a Robertson-walker Universe," Phys. Lett. B **78**, 427-429 (1978)

[78] M. Henneaux, "REMARKS ON SPACE-TIME SYMMETRIES AND NON-

ABELIAN GAUGE FIELDS," J. Math. Phys. **23**, 830-833 (1982)

[79] P. V. Moniz, J. M. Mourao and P. M. Sa, "The Dynamics of a flat Friedmann-Robertson-Walker inflationary model in the presence of gauge fields," Class. Quant. Grav. **10**, 517-534 (1993)

[80] D. V. Galtsov and M. S. Volkov, "Yang-Mills cosmology: Cold matter for a hot universe," Phys. Lett. B **256**, 17-21 (1991)

[81] K. Bamba, S. Nojiri and S. D. Odintsov, "Inflationary cosmology and the late-time accelerated expansion of the universe in non-minimal Yang-Mills-F(R) gravity and non-minimal vector-F(R) gravity," Phys. Rev. D **77**, 123532 (2008) [arXiv:0803.3384 [hep-th]].

[82] D. V. Gal'tsov, "Non-Abelian condensates as alternative for dark energy," [arXiv:0901.0115 [gr-qc]].

[83] D. V. Gal'tsov and E. A. Davydov, "Cosmological models with Yang-Mills fields," Proc. Steklov Inst. Math. **272**, no.1, 119-140 (2011) [arXiv:1012.2861 [gr-qc]].

[84] D. V. Gal'tsov and E. A. Davydov, "Yang-Mills condensates in cosmology," Int. J. Mod. Phys. Conf. Ser. **14**, 316-325 (2012) [arXiv:1112.2943 [hep-th]].

[85] A. Maleknejad, M. M. Sheikh-Jabbari and J. Soda, JCAP **01**, 016 (2012) [arXiv:1109.5573 [hep-th]].

[86] O. Iarygina and E. I. Sfakianakis, "Gravitational waves from spectator Gauge-flation," [arXiv:2105.06972 [hep-th]].

[87] J. M. Bardeen, "Gauge Invariant Cosmological Perturbations," Phys. Rev. D **22** (1980), 1882-1905

[88] H. Kodama and M. Sasaki, "Cosmological Perturbation Theory," Prog. Theor. Phys. Suppl. **78** (1984), 1-166

[89] M. Sasaki, "Large Scale Quantum Fluctuations in the Inflationary Universe," Prog. Theor. Phys. **76** (1986), 1036

[90] V. F. Mukhanov, "Quantum Theory of Gauge Invariant Cosmological Perturbations," Sov. Phys. JETP **67** (1988), 1297-1302

[91] V. F. Mukhanov, H. A. Feldman and R. H. Brandenberger, "Theory of cosmological perturbations. Part 1. Classical perturbations. Part 2. Quantum theory of perturbations. Part 3. Extensions," Phys. Rept. **215** (1992), 203-333

[92] E. Bertschinger, "Cosmological dynamics: Course 1," [arXiv:astro-ph/9503125 [astro-ph]].

[93] B. A. Bassett, S. Tsujikawa and D. Wands, "Inflation dynamics and reheating," Rev. Mod. Phys. **78** (2006), 537-589 [arXiv:astro-ph/0507632 [astro-ph]].

[94] K. A. Malik and D. Wands, "Cosmological perturbations," Phys. Rept. **475** (2009), 1-51 [arXiv:0809.4944 [astro-ph]].

[95] S. Cremonini, Z. Lalak and K. Turzynski, "Strongly Coupled Perturbations in Two-Field Inflationary Models," JCAP **03** (2011), 016 [arXiv:1010.3021 [hep-th]].

[96] A. J. Tolley and M. Wyman, "The Gelaton Scenario: Equilateral non-Gaussianity from multi-field dynamics," Phys. Rev. D **81** (2010), 043502 [arXiv:0910.1853 [hep-th]].

[97] A. Achucarro, J. O. Gong, S. Hardeman, G. A. Palma and S. P. Patil, "Effective theories of single field inflation when heavy fields matter," JHEP **05** (2012), 066 [arXiv:1201.6342 [hep-th]].

[98] S. Pi and M. Sasaki, "Curvature Perturbation Spectrum in Two-field Inflation with a Turning Trajectory," JCAP **10** (2012), 051 [arXiv:1205.0161 [hep-th]].

[99] X. Chen and Y. Wang, "Quasi-Single Field Inflation and Non-Gaussianities," JCAP **04** (2010), 027 [arXiv:0911.3380 [hep-th]].

[100] X. Chen and Y. Wang, "Large non-Gaussianities with Intermediate Shapes from Quasi-Single Field Inflation," Phys. Rev. D **81** (2010), 063511 [arXiv:0909.0496 [astro-ph.CO]].

[101] N. Arkani-Hamed and J. Maldacena, "Cosmological Collider Physics," [arXiv:1503.08043 [hep-th]].

[102] D. H. Lyth and D. Wands, Phys. Lett. B **524** (2002), 5-14 doi:10.1016/S0370-2693(01)01366-1 [arXiv:hep-ph/0110002 [hep-ph]].

[103] D. H. Lyth, C. Ungarelli and D. Wands, Phys. Rev. D **67** (2003), 023503 doi:10.1103/PhysRevD.67.023503 [arXiv:astro-ph/0208055 [astro-ph]].

[104] B. P. Abbott *et al.* [LIGO Scientific and Virgo], "Observation of Gravitational Waves from a Binary Black Hole Merger," Phys. Rev. Lett. **116**, no.6, 061102 (2016) [arXiv:1602.03837 [gr-qc]].

[105] B. P. Abbott *et al.* [LIGO Scientific and Virgo], "Binary Black Hole Mergers in the first Advanced LIGO Observing Run," Phys. Rev. X **6**, no.4, 041015 (2016) [erratum: Phys. Rev. X **8**, no.3, 039903 (2018)] [arXiv:1606.04856 [gr-qc]].

[106] B. P. Abbott *et al.* [LIGO Scientific and Virgo], "GW151226: Observation of Gravitational Waves from a 22-Solar-Mass Binary Black Hole Coalescence," Phys. Rev. Lett. **116**, no.24, 241103 (2016) [arXiv:1606.04855 [gr-qc]].

[107] B. P. Abbott *et al.* [LIGO Scientific and VIRGO], Phys. Rev. Lett. **118**, no.22, 221101 (2017) [erratum: Phys. Rev. Lett. **121**, no.12, 129901 (2018)] [arXiv:1706.01812 [gr-qc]].

[108] B. P. Abbott *et al.* [LIGO Scientific and Virgo], Astrophys. J. Lett. **851**, L35 (2017) [arXiv:1711.05578 [astro-ph.HE]].

[109] B. P. Abbott *et al.* [LIGO Scientific and Virgo], Phys. Rev. Lett. **119**, no.14, 141101 (2017) [arXiv:1709.09660 [gr-qc]].

[110] N. Bartolo, C. Caprini, V. Domcke, D. G. Figueroa, J. Garcia-Bellido, M. C. Guzzetti, M. Liguori, S. Matarrese, M. Peloso and A. Petiteau, *et al.* "Science with the space-based interferometer LISA. IV: Probing inflation with gravitational waves," JCAP **12**, 026 (2016) [arXiv:1610.06481 [astro-ph.CO]].

[111] N. Bartolo, V. Domcke, D. G. Figueroa, J. García-Bellido, M. Peloso,

M. Pieroni, A. Ricciardone, M. Sakellariadou, L. Sorbo and G. Tasinato, "Probing non-Gaussian Stochastic Gravitational Wave Backgrounds with LISA," JCAP **11**, 034 (2018) [arXiv:1806.02819 [astro-ph.CO]].

[112] V. Corbin and N. J. Cornish, "Detecting the cosmic gravitational wave background with the big bang observer," Class. Quant. Grav. **23**, 2435-2446 (2006) [arXiv:gr-qc/0512039 [gr-qc]].

[113] S. Kawamura, M. Ando, N. Seto, S. Sato, T. Nakamura, K. Tsubono, N. Kanda, T. Tanaka, J. Yokoyama and I. Funaki, *et al.* "The Japanese space gravitational wave antenna: DECIGO," Class. Quant. Grav. **28**, 094011 (2011)

[114] A. G. A. Brown *et al.* [Gaia], "Gaia Data Release 2: Summary of the contents and survey properties," Astron. Astrophys. **616** (2018), A1 [arXiv:1804.09365 [astro-ph.GA]].

[115] C. J. Moore, D. P. Mihaylov, A. Lasenby and G. Gilmore, Phys. Rev. Lett. **119** (2017) no.26, 261102 [arXiv:1707.06239 [astro-ph.IM]].

[116] A. Vallenari, "The future of astrometry in space," Frontiers in Astronomy and Space Sciences 5 (2018) 11. `https://www.frontiersin.org/article/10.3389/fspas.2018.00011`.

[117] J. Garcia-Bellido, H. Murayama and G. White, "Exploring the Early Universe with Gaia and THEIA," [arXiv:2104.04778 [hep-ph]].

[118] M. A. Amin, M. P. Hertzberg, D. I. Kaiser and J. Karouby, "Nonperturbative Dynamics Of Reheating After Inflation: A Review," Int. J. Mod. Phys. D **24**, 1530003 (2014) [arXiv:1410.3808 [hep-ph]].

[119] C. Caprini and D. G. Figueroa, "Cosmological Backgrounds of Gravitational Waves," Class. Quant. Grav. **35** (2018) no.16, 163001 [arXiv:1801.04268 [astro-ph.CO]].

[120] S. Kuroyanagi, T. Chiba and T. Takahashi, "Probing the Universe through the Stochastic Gravitational Wave Background," JCAP **11** (2018), 038 [arXiv:1807.00786 [astro-ph.CO]].

[121] J. Kovac, E. M. Leitch, C. Pryke, J. E. Carlstrom, N. W. Halverson and W. L. Holzapfel, "Detection of polarization in the cosmic microwave background using DASI," Nature **420**, 772-787 (2002) [arXiv:astro-ph/0209478 [astro-ph]].

[122] `https://cmb-s4.org`

[123] `http://litebird.jp/eng/`

[124] J. Chluba, A. Kogut, S. P. Patil, M. H. Abitbol, N. Aghanim, Y. Ali-Haïmoud, M. A. Amin, J. Aumont, N. Bartolo and K. Basu, *et al.* "Spectral Distortions of the CMB as a Probe of Inflation, Recombination, Structure Formation and Particle Physics: Astro2020 Science White Paper," Bull. Am. Astron. Soc. **51** (2019) no.3, 184 [arXiv:1903.04218 [astro-ph.CO]].

[125] E. J. Copeland, A. R. Liddle, D. H. Lyth, E. D. Stewart and D. Wands, "False vacuum inflation with Einstein gravity," Phys. Rev. D **49** (1994), 6410-6433 [arXiv:astro-ph/9401011 [astro-ph]].

[126] D. Baumann and L. McAllister, "Inflation and String Theory," Cambridge Monographs on Mathematical Physics. Cambridge University Press, 2015. [arXiv:1404.2601 [hep-th]].

[127] K. Freese, J. A. Frieman and A. V. Olinto, "Natural inflation with pseudo - Nambu-Goldstone bosons," Phys. Rev. Lett. **65** (1990), 3233-3236

[128] A. Linde, "On the problem of initial conditions for inflation," Found. Phys. **48** (2018) no.10, 1246-1260 [arXiv:1710.04278 [hep-th]].

[129] A. Borde and A. Vilenkin, "Eternal inflation and the initial singularity," Phys. Rev. Lett. **72** (1994), 3305-3309 [arXiv:gr-qc/9312022 [gr-qc]].

[130] A. Borde and A. Vilenkin, "Singularities in inflationary cosmology: A Review," Int. J. Mod. Phys. D **5** (1996), 813-824 [arXiv:gr-qc/9612036 [gr-qc]].

[131] A. Borde, A. H. Guth and A. Vilenkin, "Inflationary space-times are incompletein past directions," Phys. Rev. Lett. **90** (2003), 151301 [arXiv:gr-qc/0110012 [gr-qc]].

[132] R. Brandenberger and P. Peter, "Bouncing Cosmologies: Progress and Problems," Found. Phys. **47** (2017) no.6, 797-850 [arXiv:1603.05834 [hep-th]].

[133] L. Kofman, A. D. Linde and A. A. Starobinsky, "Towards the theory of reheating after inflation," Phys. Rev. D **56** (1997), 3258-3295 [arXiv:hep-ph/9704452 [hep-ph]].

[134] J. Garcia-Bellido, Lecture notes "Inflation and reheating", `https://physique.cuso.ch/fileadmin/physique/document/LectureNotes_Inflation_JGB.pdf`

[135] K. D. Lozanov, "Lectures on Reheating after Inflation," [arXiv:1907.04402 [astro-ph.CO]].

[136] M. P. DeCross, D. I. Kaiser, A. Prabhu, C. Prescod-Weinstein and E. I. Sfakianakis, "Preheating after Multifield Inflation with Nonminimal Couplings, I: Covariant Formalism and Attractor Behavior," Phys. Rev. D **97** (2018) no.2, 023526 [arXiv:1510.08553 [astro-ph.CO]].

[137] A. D. Dolgov and A. D. Linde, "Baryon Asymmetry in Inflationary Universe," Phys. Lett. B **116** (1982), 329

[138] L. F. Abbott, E. Farhi and M. B. Wise, "Particle Production in the New Inflationary Cosmology," Phys. Lett. B **117** (1982), 29

[139] A. Albrecht, P. J. Steinhardt, M. S. Turner and F. Wilczek, "Reheating an Inflationary Universe," Phys. Rev. Lett. **48** (1982), 1437

[140] D. V. Nanopoulos, K. A. Olive and M. Srednicki, "After Primordial Inflation," Phys. Lett. B **127** (1983), 30-34

[141] M. Morikawa and M. Sasaki, "Entropy Production in the Inflationary Universe," Prog. Theor. Phys. **72** (1984), 782

[142] A. Hosoya and M. a. Sakagami, "Time Development of Higgs Field at Finite Temperature," Phys. Rev. D **29** (1984), 2228

[143] M. S. Turner, Phys. Rev. D **28** (1983), 1243 doi:10.1103/PhysRevD.28.1243

[144] J. H. Traschen and R. H. Brandenberger, "Particle Production During Out-of-equilibrium Phase Transitions," Phys. Rev. D **42** (1990), 2491-2504

[145] A. D. Dolgov and D. P. Kirilova, "ON PARTICLE CREATION BY A TIME DEPENDENT SCALAR FIELD," Sov. J. Nucl. Phys. **51** (1990), 172-177 JINR-E2-89-321.

[146] Y. Shtanov, J. H. Traschen and R. H. Brandenberger, "Universe reheating after inflation," Phys. Rev. D **51** (1995), 5438-5455 [arXiv:hep-ph/9407247 [hep-ph]].

[147] L. Kofman, A. D. Linde and A. A. Starobinsky, "Reheating after inflation," Phys. Rev. Lett. **73** (1994), 3195-3198 [arXiv:hep-th/9405187 [hep-th]].

[148] L. A. Kofman, "The Origin of matter in the universe: Reheating after inflation," [arXiv:astro-ph/9605155 [astro-ph]].

[149] P. B. Greene, L. Kofman, A. D. Linde and A. A. Starobinsky, "Structure of resonance in preheating after inflation," Phys. Rev. D **56**, 6175 (1997) [hep-ph/9705347].

[150] S. Y. Khlebnikov and I. I. Tkachev, "Resonant decay of Bose condensates," Phys. Rev. Lett. **79** (1997), 1607-1610 [arXiv:hep-ph/9610477 [hep-ph]].

[151] W. Magnus and S. Winkler, "Hill's Equation", Dover Books on Mathematics Series. Dover Publications, 2004.

[152] N. W. Mac Lachlan, "Theory and Application of Mathieu functions", Dover, New York, (1961).

[153] D. I. Kaiser, E. A. Mazenc and E. I. Sfakianakis, "Primordial Bispectrum from Multifield Inflation with Nonminimal Couplings," Phys. Rev. D **87** (2013), 064004 [arXiv:1210.7487 [astro-ph.CO]].

[154] D. I. Kaiser and E. I. Sfakianakis, "Multifield inflation after Planck: The case for nonminimal couplings," Phys. Rev. Lett. 112 (2014): 011302, arXiv:1304.0363 [astro-ph.CO].

[155] R. Kallosh, A. Linde, and D. Roest, "Universal attractor for inflation at strong coupling," Phys. Rev. Lett. 112 (2014): 011303, arXiv:1310.3950 [hep-th].

[156] F. L. Bezrukov and M. Shaposhnikov, "The Standard Model Higgs boson as the inflaton," Phys. Lett. B **659**, 703 (2008) [arXiv:0710.3755 [hep-th]].

[157] R. N. Greenwood, D. I. Kaiser, and E. I. Sfakianakis, "Multifield dynamics of Higgs inflation," Phys. Rev. D87 (2013): 044038, arXiv:1210.8190 [hep-ph].

[158] O. Iarygina, E. I. Sfakianakis, D. G. Wang and A. Achucarro, "Universality and scaling in multi-field α-attractor preheating," JCAP **06** (2019), 027 [arXiv:1810.02804 [astro-ph.CO]].

[159] O. Iarygina, E. I. Sfakianakis, D. G. Wang and A. Achúcarro, "Multi-field inflation and preheating in asymmetric α-attractors," [arXiv:2005.00528 [astro-ph.CO]].

[160] T. Krajewski, K. Turzyński and M. Wieczorek, "On preheating in α-attractor models of inflation," Eur. Phys. J. C **79**, no.8, 654 (2019) [arXiv:1801.01786 [astro-ph.CO]].

[161] A. R. Liddle and S. M. Leach, "How long before the end of inflation were observable perturbations produced?," Phys. Rev. D **68** (2003), 103503

[arXiv:astro-ph/0305263 [astro-ph]].

[162] J. Martin and C. Ringeval, "First CMB Constraints on the Inflationary Reheating Temperature," Phys. Rev. D **82** (2010), 023511 [arXiv:1004.5525 [astro-ph.CO]].

[163] P. A. R. Ade *et al.* [Planck], "Planck 2013 results. XXII. Constraints on inflation," Astron. Astrophys. **571** (2014), A22 [arXiv:1303.5082 [astro-ph.CO]].

[164] S. Y. Khlebnikov and I. I. Tkachev, "Relic gravitational waves produced after preheating," Phys. Rev. D **56** (1997), 653-660 [arXiv:hep-ph/9701423 [hep-ph]].

[165] A. Ashoorioon, B. Fung, R. B. Mann, M. Oltean and M. M. Sheikh-Jabbari, "Gravitational Waves from Preheating in M-flation," JCAP **03** (2014), 020 [arXiv:1312.2284 [hep-th]].

[166] R. Easther and E. A. Lim, "Stochastic gravitational wave production after inflation," JCAP **04** (2006), 010 [arXiv:astro-ph/0601617 [astro-ph]].

[167] R. Easther, J. T. Giblin, Jr. and E. A. Lim, "Gravitational Wave Production At The End Of Inflation," Phys. Rev. Lett. **99** (2007), 221301 [arXiv:astro-ph/0612294 [astro-ph]].

[168] J. F. Dufaux, A. Bergman, G. N. Felder, L. Kofman and J. P. Uzan, "Theory and Numerics of Gravitational Waves from Preheating after Inflation," Phys. Rev. D **76** (2007), 123517 [arXiv:0707.0875 [astro-ph]].

[169] J. Garcia-Bellido, D. G. Figueroa and A. Sastre, "A Gravitational Wave Background from Reheating after Hybrid Inflation," Phys. Rev. D **77** (2008), 043517 [arXiv:0707.0839 [hep-ph]].

[170] J. Garcia-Bellido and D. G. Figueroa, "A stochastic background of gravitational waves from hybrid preheating," Phys. Rev. Lett. **98** (2007), 061302 [arXiv:astro-ph/0701014 [astro-ph]].

[171] J. F. Dufaux, G. Felder, L. Kofman and O. Navros, "Gravity Waves from Tachyonic Preheating after Hybrid Inflation," JCAP **03** (2009), 001 [arXiv:0812.2917 [astro-ph]].

[172] J. T. Giblin, Jr, L. R. Price and X. Siemens, "Gravitational Radiation from Preheating with Many Fields," JCAP **08** (2010), 012 [arXiv:1006.0935 [astro-ph.CO]].

[173] D. G. Figueroa, J. Garcia-Bellido and A. Rajantie, "On the Transverse-Traceless Projection in Lattice Simulations of Gravitational Wave Production," JCAP **11** (2011), 015 [arXiv:1110.0337 [astro-ph.CO]].

[174] L. Bethke, D. G. Figueroa and A. Rajantie, "On the Anisotropy of the Gravitational Wave Background from Massless Preheating," JCAP **06** (2014), 047 [arXiv:1309.1148 [astro-ph.CO]].

[175] D. G. Figueroa and T. Meriniemi, "Stochastic Background of Gravitational Waves from Fermions – Theory and Applications," JHEP **10** (2013), 101 [arXiv:1306.6911 [astro-ph.CO]].

[176] D. G. Figueroa, "A gravitational wave background from the decay of the standard model Higgs after inflation," JHEP **11** (2014), 145 [arXiv:1402.1345

[astro-ph.CO]].
[177] J. T. Giblin and E. Thrane, Phys. Rev. D **90** (2014) no.10, 107502 doi:10.1103/PhysRevD.90.107502 [arXiv:1410.4779 [gr-qc]].
[178] L. Canetti, M. Drewes and M. Shaposhnikov, "Matter and Antimatter in the Universe," New J. Phys. **14** (2012), 095012 [arXiv:1204.4186 [hep-ph]].
[179] A. D. Sakharov, "Violation of CP Invariance, C asymmetry, and baryon asymmetry of the universe," Pisma Zh. Eksp. Teor. Fiz. **5** (1967), 32-35
[180] M. P. Hertzberg and J. Karouby, "Generating the Observed Baryon Asymmetry from the Inflaton Field," Phys. Rev. D **89** (2014) no.6, 063523 [arXiv:1309.0010 [hep-ph]].
[181] M. P. Hertzberg and J. Karouby, "Baryogenesis from the Inflaton Field," Phys. Lett. B **737** (2014), 34-38 [arXiv:1309.0007 [hep-ph]].
[182] A. Dolgov and K. Freese, "Calculation of particle production by Nambu Goldstone bosons with application to inflation reheating and baryogenesis," Phys. Rev. D **51** (1995), 2693-2702 [arXiv:hep-ph/9410346 [hep-ph]].
[183] A. Dolgov, K. Freese, R. Rangarajan and M. Srednicki, "Baryogenesis during reheating in natural inflation and comments on spontaneous baryogenesis," Phys. Rev. D **56** (1997), 6155-6165 [arXiv:hep-ph/9610405 [hep-ph]].
[184] J. Garcia-Bellido, D. Y. Grigoriev, A. Kusenko and M. E. Shaposhnikov, "Nonequilibrium electroweak baryogenesis from preheating after inflation," Phys. Rev. D **60** (1999), 123504 [arXiv:hep-ph/9902449 [hep-ph]].
[185] S. Davidson, M. Losada and A. Riotto, "A New perspective on baryogenesis," Phys. Rev. Lett. **84** (2000), 4284-4287 [arXiv:hep-ph/0001301 [hep-ph]].
[186] A. Megevand, "Effect of reheating on electroweak baryogenesis," Phys. Rev. D **64** (2001), 027303 [arXiv:hep-ph/0011019 [hep-ph]].
[187] A. Tranberg and J. Smit, "Baryon asymmetry from electroweak tachyonic preheating," JHEP **11** (2003), 016 [arXiv:hep-ph/0310342 [hep-ph]].
[188] A. Tranberg and J. Smit, "Simulations of cold electroweak baryogenesis: Dependence on Higgs mass and strength of CP-violation," JHEP **08** (2006), 012 [arXiv:hep-ph/0604263 [hep-ph]].
[189] T. Hiramatsu, E. I. Sfakianakis and M. Yamaguchi, "Gravitational wave spectra from oscillon formation after inflation," JHEP **03** (2021), 021 [arXiv:2011.12201 [hep-ph]].
[190] A. Arvanitaki, S. Dimopoulos, M. Galanis, L. Lehner, J. O. Thompson and K. Van Tilburg, "Large-misalignment mechanism for the formation of compact axion structures: Signatures from the QCD axion to fuzzy dark matter," Phys. Rev. D **101** (2020) no.8, 083014 [arXiv:1909.11665 [astro-ph.CO]].
[191] A. Diaz-Gil, J. Garcia-Bellido, M. Garcia Perez and A. Gonzalez-Arroyo, "Magnetic field production during preheating at the electroweak scale," Phys. Rev. Lett. **100** (2008), 241301 [arXiv:0712.4263 [hep-ph]].
[192] A. Diaz-Gil, J. Garcia-Bellido, M. Garcia Perez and A. Gonzalez-Arroyo, "Primordial magnetic fields from preheating at the electroweak scale," JHEP **07** (2008), 043 [arXiv:0805.4159 [hep-ph]].

[193] A. Kandus, K. E. Kunze and C. G. Tsagas, “Primordial magnetogenesis,” Phys. Rept. **505** (2011), 1-58 [arXiv:1007.3891 [astro-ph.CO]].

[194] T. Markkanen, S. Nurmi, S. Rasanen and V. Vennin, “Narrowing the window of inflationary magnetogenesis,” JCAP **06** (2017), 035 [arXiv:1704.01343 [astro-ph.CO]].

[195] T. Kobayashi and S. Mukohyama, “Effects of Light Fields During Inflation,” Phys. Rev. D **81**, 103504 (2010) [arXiv:1003.0076 [astro-ph.CO]].

[196] S. Renaux-Petel and K. Turzynski, “On reaching the adiabatic limit in multi-field inflation,” JCAP **06**, 010 (2015), [arXiv:1405.6195 [astro-ph.CO]].

[197] S. Cremonini, Z. Lalak and K. Turzynski, “On Non-Canonical Kinetic Terms and the Tilt of the Power Spectrum,” Phys. Rev. D **82**, 047301 (2010), [arXiv:1005.4347 [hep-th]].

[198] C. van de Bruck and M. Robinson, “Power Spectra beyond the Slow Roll Approximation in Theories with Non-Canonical Kinetic Terms,” JCAP **08**, 024 (2014), [arXiv:1404.7806 [astro-ph.CO]].

[199] A. A. Starobinsky, “Multicomponent de Sitter (Inflationary) Stages and the Generation of Perturbations,” JETP Lett. **42**, 152-155 (1985)

[200] D. S. Salopek and J. R. Bond, “Nonlinear evolution of long wavelength metric fluctuations in inflationary models,” Phys. Rev. D **42**, 3936-3962 (1990)

[201] M. Sasaki and E. D. Stewart, “A General analytic formula for the spectral index of the density perturbations produced during inflation,” Prog. Theor. Phys. **95**, 71-78 (1996), [arXiv:astro-ph/9507001 [astro-ph]].

[202] M. Sasaki and T. Tanaka, “Superhorizon scale dynamics of multiscalar inflation,” Prog. Theor. Phys. **99**, 763-782 (1998), [arXiv:gr-qc/9801017 [gr-qc]].

[203] H. C. Lee, M. Sasaki, E. D. Stewart, T. Tanaka and S. Yokoyama, “A New delta N formalism for multi-component inflation,” JCAP **10**, 004 (2005), [arXiv:astro-ph/0506262 [astro-ph]].

[204] A. G. Muslimov, “On the Scalar Field Dynamics in a Spatially Flat Friedman Universe,” Class. Quant. Grav. **7**, 231-237 (1990)

[205] J. E. Lidsey, “The Scalar field as dynamical variable in inflation,” Phys. Lett. B **273**, 42-46 (1991)

[206] E. J. Copeland, E. W. Kolb, A. R. Liddle and J. E. Lidsey, “Reconstructing the inflation potential, in principle and in practice,” Phys. Rev. D **48**, 2529-2547 (1993), [arXiv:hep-ph/9303288 [hep-ph]].

[207] X. Chen, G. A. Palma, W. Riquelme, B. Scheihing Hitschfeld and S. Sypsas, Phys. Rev. D **98**, no.8, 083528 (2018), [arXiv:1804.07315 [hep-th]].

[208] P. A. R. Ade *et al.* [Planck], “Planck 2015 results. XVII. Constraints on primordial non-Gaussianity,” Astron. Astrophys. **594**, A17 (2016), [arXiv:1502.01592 [astro-ph.CO]].

[209] D. H. Lyth and Y. Rodriguez, “The Inflationary prediction for primordial non-Gaussianity,” Phys. Rev. Lett. **95**, 121302 (2005), [arXiv:astro-ph/0504045 [astro-ph]].

[210] C. T. Byrnes, K. Y. Choi and L. M. H. Hall, “Conditions for large

non-Gaussianity in two-field slow-roll inflation," JCAP **10**, 008 (2008) [arXiv:0807.1101 [astro-ph]].

[211] C. T. Byrnes and G. Tasinato, "Non-Gaussianity beyond slow roll in multi-field inflation," JCAP **08**, 016 (2009) [arXiv:0906.0767 [astro-ph.CO]].

[212] C. T. Byrnes and K. Y. Choi, "Review of local non-Gaussianity from multi-field inflation," Adv. Astron. **2010**, 724525 (2010) [arXiv:1002.3110 [astro-ph.CO]].

[213] M. Dias, J. Frazer and M. c. D. Marsh, "Seven Lessons from Manyfield Inflation in Random Potentials," JCAP **01**, 036 (2018), [arXiv:1706.03774 [astro-ph.CO]].

[214] T. Bjorkmo and M. C. D. Marsh, "Manyfield Inflation in Random Potentials," JCAP **02**, 037 (2018), [arXiv:1709.10076 [astro-ph.CO]].

[215] S. C. Hotinli, J. Frazer, A. H. Jaffe, J. Meyers, L. C. Price and E. R. M. Tarrant, "Effect of reheating on predictions following multiple-field inflation," Phys. Rev. D **97**, no.2, 023511 (2018) [arXiv:1710.08913 [astro-ph.CO]].

[216] D. Seery and J. E. Lidsey, "Primordial non-Gaussianities from multiple-field inflation," JCAP **09**, 011 (2005), [arXiv:astro-ph/0506056 [astro-ph]].

[217] J. M. Maldacena, "Non-Gaussian features of primordial fluctuations in single field inflationary models," JHEP **05**, 013 (2003) [arXiv:astro-ph/0210603 [astro-ph]].

[218] P. Creminelli and M. Zaldarriaga, "Single field consistency relation for the 3-point function," JCAP **10**, 006 (2004), [arXiv:astro-ph/0407059 [astro-ph]].

[219] P. Agrawal, G. Obied, P. J. Steinhardt and C. Vafa, "On the Cosmological Implications of the String Swampland," Phys. Lett. B **784**, 271-276 (2018) [arXiv:1806.09718 [hep-th]].

[220] N. Aghanim *et al.* [Planck], "Planck 2018 results. VI. Cosmological parameters," Astron. Astrophys. **641**, A6 (2020) [arXiv:1807.06209 [astro-ph.CO]].

[221] K. Abazajian *et al.* [CMB-S4], "CMB-S4: Forecasting Constraints on Primordial Gravitational Waves," [arXiv:2008.12619 [astro-ph.CO]].

[222] P. Campeti, E. Komatsu, D. Poletti and C. Baccigalupi, "Measuring the spectrum of primordial gravitational waves with CMB, PTA and Laser Interferometers," JCAP **01**, 012 (2021) [arXiv:2007.04241 [astro-ph.CO]].

[223] P. Adshead and M. Wyman, "Chromo-Natural Inflation: Natural inflation on a steep potential with classical non-Abelian gauge fields," Phys. Rev. Lett. **108**, 261302 (2012) [arXiv:1202.2366 [hep-th]].

[224] P. Adshead and M. Wyman, "Gauge-flation trajectories in Chromo-Natural Inflation," Phys. Rev. D **86**, 043530 (2012) [arXiv:1203.2264 [hep-th]].

[225] M. M. Sheikh-Jabbari, "Gauge-flation Vs Chromo-Natural Inflation," Phys. Lett. B **717**, 6-9 (2012) [arXiv:1203.2265 [hep-th]].

[226] A. Maleknejad and M. Zarei, "Slow-roll trajectories in Chromo-Natural and Gauge-flation Models, an exhaustive analysis," Phys. Rev. D **88**, 043509 (2013) [arXiv:1212.6760 [hep-th]].

[227] R. Namba, E. Dimastrogiovanni and M. Peloso, "Gauge-flation confronted

with Planck," JCAP **11**, 045 (2013) [arXiv:1308.1366 [astro-ph.CO]].

[228] E. Dimastrogiovanni and M. Peloso, "Stability analysis of chromo-natural inflation and possible evasion of Lyth's bound," Phys. Rev. D **87**, no.10, 103501 (2013) [arXiv:1212.5184 [astro-ph.CO]].

[229] P. Adshead, E. Martinec and M. Wyman, "Perturbations in Chromo-Natural Inflation," JHEP **09**, 087 (2013) [arXiv:1305.2930 [hep-th]].

[230] P. Adshead, E. Martinec and M. Wyman, "Gauge fields and inflation: Chiral gravitational waves, fluctuations, and the Lyth bound," Phys. Rev. D **88**, no.2, 021302 (2013) [arXiv:1301.2598 [hep-th]].

[231] P. Adshead, E. Martinec, E. I. Sfakianakis and M. Wyman, "Higgsed Chromo-Natural Inflation," JHEP **12**, 137 (2016) [arXiv:1609.04025 [hep-th]].

[232] P. Adshead and E. I. Sfakianakis, "Higgsed Gauge-flation," JHEP **08**, 130 (2017) [arXiv:1705.03024 [hep-th]].

[233] E. Dimastrogiovanni, M. Fasiello and T. Fujita, "Primordial Gravitational Waves from Axion-Gauge Fields Dynamics," JCAP **01** (2017), 019 [arXiv:1608.04216 [astro-ph.CO]].

[234] Y. Watanabe and E. Komatsu, "Gravitational Wave from Axion-SU(2) Gauge Fields: Effective Field Theory for Kinetically Driven Inflation," [arXiv:2004.04350 [hep-th]].

[235] A. Agrawal, T. Fujita and E. Komatsu, "Tensor Non-Gaussianity from Axion-Gauge-Fields Dynamics : Parameter Search," JCAP **06**, 027 (2018) [arXiv:1802.09284 [astro-ph.CO]].

[236] L. Mirzagholi, E. Komatsu, K. D. Lozanov and Y. Watanabe, "Effects of Gravitational Chern-Simons during Axion-SU(2) Inflation," JCAP **06**, 024 (2020) [arXiv:2003.05931 [gr-qc]].

[237] T. Fujita, R. Namba and Y. Tada, "Does the detection of primordial gravitational waves exclude low energy inflation?," Phys. Lett. B **778**, 17-21 (2018) [arXiv:1705.01533 [astro-ph.CO]].

[238] B. Thorne, T. Fujita, M. Hazumi, N. Katayama, E. Komatsu and M. Shiraishi, "Finding the chiral gravitational wave background of an axion-SU(2) inflationary model using CMB observations and laser interferometers," Phys. Rev. D **97**, no.4, 043506 (2018) [arXiv:1707.03240 [astro-ph.CO]].

[239] T. Fujita, E. I. Sfakianakis and M. Shiraishi, "Tensor Spectra Templates for Axion-Gauge Fields Dynamics during Inflation," JCAP **05**, 057 (2019) [arXiv:1812.03667 [astro-ph.CO]].

[240] A. Papageorgiou, M. Peloso and C. Unal, "Nonlinear perturbations from the coupling of the inflaton to a non-Abelian gauge field, with a focus on Chromo-Natural Inflation," JCAP **09**, 030 (2018) [arXiv:1806.08313 [astro-ph.CO]].

[241] A. Papageorgiou, M. Peloso and C. Unal, "Nonlinear perturbations from axion-gauge fields dynamics during inflation," JCAP **07**, 004 (2019) [arXiv:1904.01488 [astro-ph.CO]].

[242] A. Maleknejad and E. Komatsu, "Production and Backreaction of Spin-2 Particles of $SU(2)$ Gauge Field during Inflation," JHEP **05**, 174 (2019) [arXiv:1808.09076 [hep-ph]].

[243] S. Ferrara, R. Kallosh, A. Linde and M. Porrati, "Minimal Supergravity Models of Inflation," Phys. Rev. D **88**, no. 8, 085038 (2013) [arXiv:1307.7696 [hep-th]]. S. Ferrara, P. FrÃ© and A. S. Sorin, "On the Topology of the Inflaton Field in Minimal Supergravity Models," JHEP **1404**, 095 (2014) [arXiv:1311.5059 [hep-th]]. S. Ferrara, P. Fre and A. S. Sorin, "On the Gauged KÃ¤hler Isometry in Minimal Supergravity Models of Inflation," Fortsch. Phys. **62**, 277 (2014) [arXiv:1401.1201 [hep-th]].

[244] S. Cecotti and R. Kallosh, "Cosmological Attractor Models and Higher Curvature Supergravity," JHEP **1405**, 114 (2014) [arXiv:1403.2932 [hep-th]].

[245] R. Kallosh and A. Linde, "Planck, LHC, and α-attractors," Phys. Rev. D **91**, 083528 (2015) [arXiv:1502.07733 [astro-ph.CO]].

[246] A. Maleknejad, "Axion Inflation with an SU(2) Gauge Field: Detectable Chiral Gravity Waves," JHEP **07**, 104 (2016) [arXiv:1604.03327 [hep-ph]].

[247] R. R. Caldwell and C. Devulder, "Axion Gauge Field Inflation and Gravitational Leptogenesis: A Lower Bound on B Modes from the Matter-Antimatter Asymmetry of the Universe," Phys. Rev. D **97**, no.2, 023532 (2018) [arXiv:1706.03765 [astro-ph.CO]].

[248] P. Adshead, A. J. Long and E. I. Sfakianakis, "Gravitational Leptogenesis, Reheating, and Models of Neutrino Mass," Phys. Rev. D **97**, no.4, 043511 (2018) [arXiv:1711.04800 [hep-ph]].

[249] A. Maleknejad, "SU(2)$_R$ and its Axion in Cosmology: A common Origin for Inflation, Cold Sterile Neutrinos, and Baryogenesis," [arXiv:2012.11516 [hep-ph]].

[250] A. Maleknejad, "Chiral Anomaly in SU(2)$_R$-Axion Inflation and the New Prediction for Particle Cosmology," [arXiv:2103.14611 [hep-ph]].

[251] A. A. Starobinsky, "A New Type of Isotropic Cosmological Models Without Singularity," Phys. Lett. B **91**, 99 (1980) [Phys. Lett. **91B**, 99 (1980)].

[252] L. Jarv, A. Racioppi and T. Tenkanen, "Palatini side of inflationary attractors," Phys. Rev. D **97**, no. 8, 083513 (2018) [arXiv:1712.08471 [gr-qc]].

[253] P. Carrilho, D. Mulryne, J. Ronayne and T. Tenkanen, "Attractor Behaviour in Multifield Inflation," JCAP **1806**, no. 06, 032 (2018) [arXiv:1804.10489 [astro-ph.CO]].

[254] M. Galante, R. Kallosh, A. Linde and D. Roest, "Unity of Cosmological Inflation Attractors," Phys. Rev. Lett. **114**, no. 14, 141302 (2015) doi:10.1103/PhysRevLett.114.141302 [arXiv:1412.3797 [hep-th]].

[255] D. H. Lyth and A. Riotto, "Particle physics models of inflation and the cosmological density perturbation," Phys. Rept. 314 (1999): 1, arXiv:hep-ph/9807278.

[256] D. Wands, "Multiple field inflation," Lect. Notes Phys. 738 (2008): 275, arXiv:astro-ph/0702187.

[257] A. Mazumdar and J. Rocher, "Particle physics models of inflation and curvaton scenarios," Phys. Rept. **497**, 85 (2011), arXiv:1001.0993 [hep-ph].

[258] V. Vennin, K. Koyama, and D. Wands, "Encylopedia Curvatonis," JCAP 1511 (2015): 008, arXiv:1507.07575 [astro-ph.CO].

[259] J.-O. Gong, "Multi-field inflation and cosmological perturbations," Int. J. Mod. Phys. D **26**, 1740003 (2017), arXiv:1606.06971 [astro-ph.CO].

[260] C. Gordon, D. Wands, B. A. Bassett and R. Maartens, "Adiabatic and entropy perturbations from inflation," Phys. Rev. D **63**, 023506 (2001) [astro-ph/0009131]; S. Groot Nibbelink and B. J. W. van Tent, "Density perturbations arising from multiple field slow roll inflation," hep-ph/0011325 ; S. Groot Nibbelink and B. J. W. van Tent, "Scalar perturbations during multiple field slow-roll inflation," Class. Quant. Grav. **19**, 613 (2002) [hep-ph/0107272].

[261] C. M. Peterson and M. Tegmark, "Testing multifield inflation: A geometric approach," Phys. Rev. D **87**, no. 10, 103507 (2013) [arXiv:1111.0927 [astro-ph.CO]] ; C. M. Peterson and M. Tegmark, "Testing Two-Field Inflation," Phys. Rev. D **83**, 023522 (2011) [arXiv:1005.4056 [astro-ph.CO]] ; C. M. Peterson and M. Tegmark, "Non-Gaussianity in Two-Field Inflation," Phys. Rev. D **84**, 023520 (2011) [arXiv:1011.6675 [astro-ph.CO]].

[262] A. Achucarro, J. O. Gong, S. Hardeman, G. A. Palma and S. P. Patil, "Effective theories of single field inflation when heavy fields matter," JHEP **1205** (2012) 066 doi:10.1007/JHEP05(2012)066 [arXiv:1201.6342 [hep-th]].

[263] A. Achucarro, V. Atal, S. Cespedes, J. O. Gong, G. A. Palma and S. P. Patil, "Heavy fields, reduced speeds of sound and decoupling during inflation," Phys. Rev. D **86** (2012) 121301 doi:10.1103/PhysRevD.86.121301 [arXiv:1205.0710 [hep-th]].

[264] Z. Lalak, D. Langlois, S. Pokorski and K. Turzynski, "Curvature and isocurvature perturbations in two-field inflation," JCAP **0707**, 014 (2007) [arXiv:0704.0212 [hep-th]].

[265] Y. Welling, "Multiple Field Inflation and Signatures of Heavy Physics in the CMB," arXiv:1502.04369 [gr-qc].

[266] D. I. Kaiser, E. A. Mazenc, and E. I. Sfakianakis, "Primordial bispectrum from multifield inflation with nonminimal couplings," Phys. Rev. D87 (2013): 064004, arXiv:1210.7487 [astro-ph.CO].

[267] K. Schutz, E. I. Sfakianakis, and D. I. Kaiser, "Multifield inflation after Planck: Isocurvature modes from nonminimal couplings," Phys. Rev. D89 (2014): 064044, arXiv:1310.8285 [astro-ph.CO].

[268] M. Cicoli, V. Guidetti, F. G. Pedro and G. P. Vacca, "A geometrical instability for ultra-light fields during inflation?," arXiv:1807.03818 [hep-th].

[269] M. Dias, J. Frazer, A. Retolaza, M. Scalisi and A. Westphal, "Pole N-flation," arXiv:1805.02659 [hep-th].

[270] N. Bartolo, D. M. Bianco, R. Jimenez, S. Matarrese and L. Verde, "Supergravity, α-attractors and primordial non-Gaussianity," JCAP **1810**, no. 10,

017 (2018) [arXiv:1805.04269 [astro-ph.CO]].

[271] K. I. Maeda, S. Mizuno and R. Tozuka, "α-attractor-type Double Inflation," arXiv:1810.06914 [hep-th].

[272] A. H. Guth and D. I. Kaiser, "Inflationary cosmology: Exploring the universe from the smallest to the largest scales," Science **307**, 884 (2005), arXiv:astro-ph/0502328 [astro-ph].

[273] B. A. Bassett, S. Tsujikawa, and D. Wands, "Inflation dynamics and reheating," Rev. Mod. Phys. **78**, 537 (2006), arXiv:astro-ph/0507632.

[274] D. H. Lyth and A. R. Liddle, *The Primordial Density Perturbation: Cosmology, Inflation, and the Origin of Structure* (New York: Cambridge University Press, 2009).

[275] D. Baumann, "TASI Lectures on inflation," arXiv:0907.5424 [hep-th].

[276] J. Martin, C. Ringeval, and V. Vennin, "Encyclopedia inflationaris," Phys. Dark Univ. **5-6**, 75 (2014), arXiv:1303.3787 [astro-ph.CO].

[277] A. H. Guth, D. I. Kaiser, and Y. Nomura, "Infltationary paradigm after Planck 2013," Phys. Lett. B **733**, 112 (2014), arXiv:1312.7619 [astro-ph.CO].

[278] A. D. Linde, "Inflationary cosmology after Planck 2013," arXiv:1402.0526 [hep-th].

[279] J. Martin, "The observational status of cosmic inflation after Planck," arXiv:1502.05733 [astro-ph.CO].

[280] G. Steigman, "Primordial nucleosynthesis in the precision cosmology era," Ann. Rev. Nucl. Part. Sci. **57**, 463 (2007), arXiv:0712.1100 [astro-ph].

[281] B. D. Fields, P. Molaro, and S. Sarkar, "Big-bang nucleosynthesis," Chin. Phys. C **38**, 339 (2014), arXiv:1412.1408 [astro-ph.CO].

[282] R. H. Cyburt, B. D. Fields, K. A. Olive, and T.-H. Yeh, "Big bang nucleosynthesis: 2015," Rev. Mod. Phys. **88**, 015004 (2016), arXiv:1505.01076 [astro-ph.CO].

[283] R. Allahverdi, R. Brandenberger, F.-Y. Cyr-Racine, and A. Mazumdar, "Reheating in inflationary cosmology: Theory and applications," Ann. Rev. Nucl. Part. Sci. **60**, 27 (2010), arXiv:1001.2600 [hep-th].

[284] A. V. Frolov, "Non-linear dynamics and primordial curvature perturbations from preheating," Class. Quant. Grav. **27**, 124006 (2010), arXiv:1004.3559 [gr-qc].

[285] M. A. Amin, M. P. Hertzberg, D. I. Kaiser, and J. Karouby, "Nonperturbative dynamics of reheating after inflation: A review," Int. J. Mod. Phys. D **24**, 1530003 (2015), arXiv:1410.3808 [hep-ph].

[286] M. A. Amin and D. Baumann, "From wires to cosmology," JCAP 02 (2016): 045, arXiv1512.02637 [astro-ph.CO].

[287] P. Adshead, R. Easther, J. Pritchard, and A. Loeb, "Inflation and the scale dependent spectral index: Prospects and strategies," JCAP 1102 (2011): 021, arXiv:1007.3748 [astro-ph.CO].

[288] L. Dai, M. Kamionkowski, and J. Wang, "Reheating constraints to inflationary models," Phys. Rev. Lett. **113**, 041302 (2014), arXiv:1404.6704 [astro-

ph.CO].

[289] P. Creminelli, D. L. Nacir, M. Simonovi, G. Trevisan, and M. Zaldarriaga, "φ^2 inflation at its endpoint," Phys. Rev. D **90**, 083513 (2014), arXiv:1405.6264 [astro-ph.CO].

[290] J. Martin, C. Ringeval, and V. Vennin, "Observing the inflationary reheating," Phys. Rev. Lett. **114**, 081303 (2015), arXiv:1410.7958 [astro-ph.CO].

[291] J.-O. Gong, G. Leung, and S. Pi, "Probing reheating with primordial spectrum," JCAP 05 (2015): 027, arXiv:1501.03604 [hep-ph].

[292] R.-G. Cai, Z.-K. Guo, and S.-J. Wang, "Reheating phase diagram for single-field slow-roll inflationary models," Phys. Rev. D **92**, 063506 (2015), arXiv:1501.07743 [gr-qc].

[293] J. L. Cook, E. Dimastrogiovanni, D. A. Easson, and L. M. Krauss, "Reheating predictions in single field inflation," JCAP 04 (2015): 004, arXiv:1502.04673 [astro-ph.CO].

[294] V. Domcke and J. Heisig, "Constraints on the reheating temperature from sizable tensor modes," Phys. Rev. D **92**, 103515 (2015), arXiv:1504.00345 [astro-ph.CO].

[295] A. Taruya and Y. Nambu, "Cosmological perturbation with two scalar fields in reheating after inflation," Phys. Lett. B 428 (1998): 37, arXiv:gr-qc/9709035.

[296] F. Finelli and R. Brandenberger, "Parametric amplification of metric fluctuations during reheating in two field models," Phys. Rev. D 62 (2000): 083502, arXiv:hep-ph/0003172.

[297] S. Tsujikawa and B. A. Bassett, "A new twist to preheating," Phys. Rev. D 62 (2000): 043510, arXiv:hep-ph/0003068; S. Tsujikawa and B. A. Bassett, "When can preheating affect the CMB?," Phys. Lett. B 536 (2002): 9, arXiv:astro-ph/0204031.

[298] A. Chambers and A. Rajantie, "Lattice calculation of non-Gaussianity from preheating," Phys. Rev. Lett. 100 (2008): 041302, arXiv:0710.4133 [astro-ph].

[299] J. R. Bond, A. V. Frolov, Z. Huang, and L. Kofman, "Non-Gaussian spikes from chaotic billiards in inflation preheating," Phys. Rev. Lett. 103 (2009): 071301, arXiv:0903.3407 [astro-ph].

[300] G. Leung, E. R. M. Tarrant, C. T. Byrnes and E. J. Copeland, "Reheating, multifield inflation and the fate of the primordial observables," JCAP 1209 (2012): 008, arXiv:1206.5196 [astro-ph.CO].

[301] J. J. M. Carrasco, R. Kallosh and A. Linde, "Cosmological Attractors and Initial Conditions for Inflation," Phys. Rev. D **92**, no. 6, 063519 (2015) doi:10.1103/PhysRevD.92.063519 [arXiv:1506.00936 [hep-th]].

[302] M. P. DeCross, D. I. Kaiser, A. Prabhu, C. Prescod-Weinstein and E. I. Sfakianakis, "Preheating after multifield inflation with nonminimal couplings, II: Resonance Structure," arXiv:1610.08868 [astro-ph.CO].

[303] M. P. DeCross, D. I. Kaiser, A. Prabhu, C. Prescod-Weinstein and

E. I. Sfakianakis, "Preheating after multifield inflation with nonminimal couplings, III: Dynamical spacetime results," arXiv:1610.08916 [astro-ph.CO].

[304] E. I. Sfakianakis and J. van de Vis, "Preheating after Higgs Inflation: Self-Resonance and Gauge boson production," arXiv:1810.01304 [hep-ph].

[305] K. D. Lozanov and M. A. Amin, "Equation of State and Duration to Radiation Domination after Inflation," Phys. Rev. Lett. **119**, no. 6, 061301 (2017) [arXiv:1608.01213 [astro-ph.CO]] ; K. D. Lozanov and M. A. Amin, "Self-resonance after inflation: oscillons, transients and radiation domination," Phys. Rev. D **97**, no. 2, 023533 (2018) [arXiv:1710.06851 [astro-ph.CO]].

[306] J. F. Dufaux, G. N. Felder, L. Kofman, M. Peloso and D. Podolsky, "Preheating with trilinear interactions: Tachyonic resonance," JCAP **0607**, 006 (2006) [hep-ph/0602144].

[307] K. Freese, E. I. Sfakianakis, P. Stengel and L. Visinelli, "The Higgs Boson can delay Reheating after Inflation," JCAP **1805**, no. 05, 067 (2018) [arXiv:1712.03791 [hep-ph]].

[308] P. Adshead, J. T. Giblin, T. R. Scully and E. I. Sfakianakis, "Magnetogenesis from axion inflation," JCAP **1610**, 039 (2016) [arXiv:1606.08474 [astro-ph.CO]].

[309] P. Adshead, J. T. Giblin, T. R. Scully and E. I. Sfakianakis, "Gauge-preheating and the end of axion inflation," JCAP **1512**, no. 12, 034 (2015) [arXiv:1502.06506 [astro-ph.CO]].

[310] G. Steigman, "Primordial Nucleosynthesis in the Precision Cosmology Era," Ann. Rev. Nucl. Part. Sci. **57**, 463 (2007) doi:10.1146/annurev.nucl.56.080805.140437 [arXiv:0712.1100 [astro-ph]].

[311] T. Bjorkmo, "The rapid-turn inflationary attractor," arXiv:1902.10529 [hep-th].

[312] R. Bravo, G. A. Palma and S. Riquelme, "A Tip for Landscape Riders: Multi-Field Inflation Can Fulfill the Swampland Distance Conjecture," JCAP **02**, 004 (2020) [arXiv:1906.05772 [hep-th]].

[313] S. Garcia-Saenz, S. Renaux-Petel and J. Ronayne, "Primordial fluctuations and non-Gaussianities in sidetracked inflation," JCAP **1807**, no. 07, 057 (2018) [arXiv:1804.11279 [astro-ph.CO]].

[314] R. Kallosh and A. Linde, "Multi-field Conformal Cosmological Attractors," JCAP **1312**, 006 (2013) doi:10.1088/1475-7516/2013/12/006 [arXiv:1309.2015 [hep-th]].

[315] R. Kallosh, A. Linde and D. Roest, "Universal Attractor for Inflation at Strong Coupling," Phys. Rev. Lett. **112** (2014) no.1, 011303 doi:10.1103/PhysRevLett.112.011303 [arXiv:1310.3950 [hep-th]].

[316] A. S. Goncharov and A. D. Linde, "Chaotic Inflation Of The Universe In Supergravity," Sov. Phys. JETP **59**, 930 (1984) [Zh. Eksp. Teor. Fiz. **86**, 1594 (1984)]. A. B. Goncharov and A. D. Linde, "Chaotic Inflation in Supergravity," Phys. Lett. **139B**, 27 (1984). doi:10.1016/0370-2693(84)90027-3

[317] A. Linde, "Does the first chaotic inflation model in supergravity provide the

best fit to the Planck data?," JCAP **1502**, 030 (2015) doi:10.1088/1475-7516/2015/02/030 [arXiv:1412.7111 [hep-th]].

[318] D. S. Salopek, J. R. Bond and J. M. Bardeen, "Designing Density Fluctuation Spectra in Inflation," Phys. Rev. D **40**, 1753 (1989).

[319] Y. Akrami, R. Kallosh, A. Linde and V. Vardanyan, "Dark energy, α-attractors, and large-scale structure surveys," JCAP **1806**, no. 06, 041 (2018)

[320] S. Ferrara, R. Kallosh and A. Linde, "Cosmology with Nilpotent Superfields," JHEP **1410**, 143 (2014) doi:10.1007/JHEP10(2014)143 [arXiv:1408.4096 [hep-th]]. J. J. M. Carrasco, R. Kallosh and A. Linde, JHEP **1510**, 147 (2015) doi:10.1007/JHEP10(2015)147 [arXiv:1506.01708 [hep-th]].

[321] J. J. M. Carrasco, R. Kallosh and A. Linde, "Cosmological Attractors and Initial Conditions for Inflation," Phys. Rev. D **92**, no. 6, 063519 (2015) doi:10.1103/PhysRevD.92.063519 [arXiv:1506.00936 [hep-th]].

[322] P. Christodoulidis, D. Roest and R. Rosati, "Many-field Inflation: Universality or Prior Dependence?," arXiv:1907.08095 [astro-ph.CO].

[323] K. D. Lozanov and M. A. Amin, "Self-resonance after inflation: oscillons, transients and radiation domination," Phys. Rev. D **97**, no. 2, 023533 (2018) [arXiv:1710.06851 [astro-ph.CO]].

[324] K. Turzyński and M. Wieczorek, "Floquet analysis of self-resonance in single-field models of inflation," Phys. Lett. B **790**, 294 (2019) [arXiv:1808.00835 [astro-ph.CO]].

[325] R. Nguyen, J. van de Vis, E. I. Sfakianakis, J. T. Giblin and D. I. Kaiser, "Nonlinear Dynamics of Preheating after Multifield Inflation with Nonminimal Couplings," arXiv:1905.12562 [hep-ph].

[326] Y. Ema, R. Jinno, K. Mukaida and K. Nakayama, "Violent Preheating in Inflation with Nonminimal Coupling," JCAP **1702**, no. 02, 045 (2017) [arXiv:1609.05209 [hep-ph]].

[327] M. He, R. Jinno, K. Kamada, S. C. Park, A. A. Starobinsky and J. Yokoyama, "On the violent preheating in the mixed Higgs-R^2 inflationary model," Phys. Lett. B **791**, 36 (2019) [arXiv:1812.10099 [hep-ph]].

[328] E. I. Sfakianakis, "Analysis of Oscillons in the SU(2) Gauged Higgs Model," arXiv:1210.7568 [hep-ph].

[329] N. Graham, "An Electroweak oscillon," Phys. Rev. Lett. **98**, 101801 (2007) Erratum: [Phys. Rev. Lett. **98**, 189904 (2007)] [hep-th/0610267].

[330] N. Graham, "Numerical Simulation of an Electroweak Oscillon," Phys. Rev. D **76**, 085017 (2007) [arXiv:0706.4125 [hep-th]].

[331] E. Farhi, N. Graham, V. Khemani, R. Markov and R. Rosales, "An Oscillon in the SU(2) gauged Higgs model," Phys. Rev. D **72**, 101701 (2005) [hep-th/0505273].

[332] O. Ozsoy, J. T. Giblin, E. Nesbit, G. Sengor and S. Watson, "Toward an Effective Field Theory Approach to Reheating," Phys. Rev. D **96**, no. 12, 123524 (2017) [arXiv:1701.01455 [hep-th]].

[333] M. Gleiser, N. Graham and N. Stamatopoulos, "Generation of Coherent Structures After Cosmic Inflation," Phys. Rev. D **83**, 096010 (2011) [arXiv:1103.1911 [hep-th]].

[334] M. P. Hertzberg, Phys. Rev. D **82**, 045022 (2010) doi:10.1103/PhysRevD.82.045022 [arXiv:1003.3459 [hep-th]].

[335] M. Kawasaki and M. Yamada, "Decay rates of Gaussian-type I-balls and Bose-enhancement effects in 3+1 dimensions," JCAP **1402**, 001 (2014) [arXiv:1311.0985 [hep-ph]].

[336] M. P. Hertzberg and E. D. Schiappacasse, "Dark Matter Axion Clump Resonance of Photons," JCAP **1811**, 004 (2018) [arXiv:1805.00430 [hep-ph]].

[337] M. Konieczka, R. H. Ribeiro and K. Turzynski, "The effects of a fast-turning trajectory in multiple-field inflation," JCAP **1407**, 030 (2014) [arXiv:1401.6163 [astro-ph.CO]].

Summary

From a time of ancient gods, warlords and kings people were curious about the origin of our Universe. Nowadays, with the theoretical and experimental tools of modern cosmology the scientific community is breaking the boundaries of the previously unsolved questions, pushing forward our understanding of the Universe. From the myths that our world is located on the backs of four elephants, who are standing themselves on a turtle, humanity has arrived at the era of precision cosmology that allows us to talk about previously philosophical questions in scientific terms with further confirmation or falsification by observational experiments.

Our current understanding is that about 13.77 billion years ago the Universe began from a dense and hot state, that expanded and continues to expand today. The leading paradigm in the physics of the early universe is called cosmological inflation. It describes the earliest stage of the Universe's expansion that happened about 10^{-36} seconds after the moment we call the "Big Bang". Quantum fluctuations produced during inflation serve as the source for the density inhomogeneities that became stars, galaxies, clusters of galaxies and, in turn, formed the large scale structure. To connect the inflationary era with the Universe we observe nowadays, the energy that drives inflation must be transferred to elementary particles and to radiation. This process is called reheating. When particles settle into thermal equilibrium, the formation of chemical elements starts, which is followed by the rest of cosmic evolution.

This thesis is dedicated to the exploration of *the primordial dark ages*: unknown physics during the inflationary and reheating eras that has not been *directly* probed by observations. We focus on novel effects in inflation and reheating in multi-dimensional field spaces, with the aim to provide new connections to astrophysical observables and reduce theoretical uncertainties, in order to properly test inflationary models and understand the physics of the early universe. In particular, the unknown expansion

history of the universe during the reheating era connects the cosmic microwave background observations to inflationary physics. The cosmic microwave background is the oldest light in the universe that was emitted about 380.000 years after the beginning of the universe's evolution and provides us a snapshot of the primordial universe. In addition to that, both the inflationary and reheating eras generate various signatures to be seen in upcoming experiments, for instance, via gravitational waves and cosmic microwave background polarization.

The first part of the thesis studies inflation with multiple scalar fields as well as covers the physics of gauge fields during the inflationary era. Gauge fields are unavoidable components of any successful field theory. They describe fundamental forces of nature and explain the dynamics of elementary particles. On the other hand, the studies of multi-field inflation are motivated by high energy completions of low energy field theories. Since energies in the primordial universe are extremely high, it is natural to assume that multiple fields may participate in inflationary dynamics.

In Chapter 2 we present a new class of inflationary models that is called "shift-symmetric orbital inflation". The field that drives inflation in this case orbits along an angular direction with a constant arbitrary radius. In this model the extra degree of freedom is responsible for the primordial observables at the end of inflation. Nevertheless, it governs single-field-like predictions that are favoured by observations. We explicitly prove the neutral stability of the attractor solution.

Chapter 3 is dedicated to the study of the predictions for the amplitude and tensor tilt of chiral gravitational waves produced by a non-Abelian gauge field sector that is realised as a spectator for a standard scalar single-field inflation. We find a maximum allowed value for the gravitational wave enhancement with respect to the standard vacuum predictions, that could be potentially distinguishable in future cosmic microwave background polarization experiments.

The second part of the thesis explores reheating in multi-field models of inflation with curved field-space geometries. A knowledge of the physics of the reheating era is crucial since its efficiency and duration significantly influences the cosmic microwave background predictions and may affect primordial nucleosynthesis.

Chapter 4 studies preheating in one broad family of multi-field models of inflation that is called α-attractors. We show analytically a simple scaling behaviour that allows for an easy estimate of the reheating efficiency for large values of the field-space curvature.

Chapter 5 investigates and compares the dynamics during inflation and reheating for the multi-field α-attractor model with prototype potentials that are symmetric and asymmetric around the minimum. We explicitly show the significance of the asymmetry and its influence on the reheating efficiency.

The aim of this thesis is to shed light on the primordial dark ages of cosmology, push forward their frontier and motivate further development. We live in an exciting time of precision measurements in modern cosmology that may disclose previously unknown physics of the early universe. However, a correct interpretation of the observations significantly relies on theoretical understanding of the early universe physics. Below we outline a few directions that require a deep investigation in the coming years.

- *Gravitational wave* experiments opened a new window for probing the physics of the early Universe via the stochastic gravitational wave background. It is important to deeply understand their production mechanisms in order to correctly interpret the measurements of the upcoming experiments.

- *Features in the primordial power spectrum* are exciting signatures from both the inflationary and reheating eras that may be potentially visible in the cosmic microwave background and large scale structure spectra. This subject requires a thorough analytical understanding and future research.

- *An effective theory of reheating* is essential for the correct understanding of the cosmic microwave background predictions. In turn, predictions for inflationary models strongly depend on the physics of the reheating era. Hence, the development of the effective field theory of reheating for curved field-space manifolds is an important goal for theoretical physics. Special attention would require incorporating the non-linear effects and systematic analytical studies of stable long-lived spatially localized structures such as oscillons, especially in the general multi-field set-ups.

In order to keep the motivation for further exciting explorations it is good to remember:

"The cosmos is within us. We are made of star-stuff.
We are a way for the universe to know itself."

Carl Sagan

Samenvatting

Sinds de tijd van de oude goden, krijgsheren en koningen zijn mensen nieuwsgierig over de oorsprong van onze heelal. Vandaag de dag, doorbreekt de wetenschappelijke gemeenschap de grenzen van de voorheen onopgeloste vragen en bevordert ons begrip van het universum met behulp van de theoretische en experimentele hulpmiddelen van de moderne kosmologie. Uit de mythe, dat onze wereld op de ruggen van vier olifanten ligt, die zelf op een schildpad staan, is de mensheid aangekomen in het tijdperk van precisie- kosmologie die het mogelijk maakt om eerdere filosofische vragen in wetenschappelijke termen te bespreken ter bevestiging of verwerping door observaties en experimenten.

Ons huidige begrip is dat ongeveer 13.77 miljard jaar geleden het universum begon in een dichte en hete toestand, die uitdijde en vandaag de dag nog steeds uitdijt. Het leidende paradigma in de fysica van het vroege heelal wordt kosmologische inflatie genoemd. Het beschrijft het vroegste stadium van de uitdijing van het heelal, ongeveer 10^{-36} seconden na het moment dat we de “Oerknal” noemen. Kwantum fluctuaties die tijdens inflatie worden geproduceerd, dienen als de bron voor de dichtheidsinhomogeniteiten die sterren, sterrenstelsels, en clusters van sterrenstelsels werden en op hun beurt de grootschalige structuur vormen. Om het inflatie tijdperk te verbinden met het heelal dat we tegenwoordig waarnemen, moet de energie die de inflatie aandrijft, worden omgevormd naar elementaire deeltjes en naar straling. Dit proces wordt heropwarmen genoemd. Wanneer deeltjes in thermisch evenwicht komen, begint de vorming van chemische elementen, gevolgd door de rest van de kosmische evolutie.

Dit proefschrift is gewijd aan de verkenning van *de primordiale donkere tijd*: onbekende fysica tijdens de inflatie- en heropwarmingsperioden die niet direct door waarnemingen zijn onderzocht. We richten ons op nieuwe effecten in inflatie en voorverwarming in multidimensionale veldruimten, met het doel om nieuwe verbanden te leggen met astrofysische waarnemingen en de theoretische onzekerheden te verminderen, om inflatie modellen goed te kunnen testen en de fysica van het vroege heelal te begrijpen. In het bijzonder verbindt de onbekende uitdij-geschiedenis van het heelal tijdens het heropwarmtijdperk de waarnemingen van de kosmische achtergrond-waarnemingen met de inflatiefysica. De kosmische microgolf achtergrond is het oudste licht in het heelal, dat werd uitgezonden ongeveer 380.000 jaar na het begin van de evolutie van het heelal en biedt ons een momentopname van het oer-universum. Bovendien genereren zowel het inflatie- als het heropwarmingstijdperk diverse afdrukken die in toekomstige experimenten te zien zullen zijn, bijvoorbeeld via zwaartekrachtgolven en polarisatie van de kosmische microgolf-achtergrond straling.

Het eerste deel van het proefschrift bestudeert inflatie met meervoudige scalaire velden en behandelt de fysica van ijkvelden tijdens het inflatie-tijdperk. Ijkvelden zijn onvermijdelijke componenten van elke successvolle veldentheorie. Zij beschrijven fundamentele natuurkrachten en verklaren de dynamica van elementaire deeltjes. Anderzijds zijn de studies van de multi-veldinflatie gemotiveerd door hoge energie vervollediging van lage energie veld theorieën. Aangezien de energieën in het oer-universum extreem hoog zijn, is het natuurlijk om aan te nemen dat meerdere velden kunnen deelnemen aan de inflatiedynamica.

In Hoofdstuk 2 presenteren we een nieuwe klasse van inflatiemodellen die we “shift-symmetric orbital inflation” noemen. Het veld dat de inflatie aandrijft, draait in dit geval langs een cirkel met een constante willekeurige straal. In dit model is de extra vrijheidsgraad verantwoordelijk voor de primordiale waarnemingen aan het eind van de inflatie. Niettemin geeft het enkel-veldachtige voorspellingen die door waarnemingen worden gesteund. We bewijzen expliciet de neutrale stabiliteit van de attractoroplossing.

Hoofdstuk 3 is gewijd aan voorspellingen voor de amplitude en kanteling van het spectrum van chirale gravitatiegolven geproduceerd door een niet-Abelse ijkveldsector die wordt gerealiseerd als een spectator voor een standaard scalaire één-velds inflatie. We vinden een maximaal toegestane waarde voor de verhoging van de gravitatie golf ten opzichte van de standaard vacuüm voorspellingen, die potentieel onderscheidbaar zou kunnen zijn in toekomstige kosmische microgolf polarisatie-experimenten.

Het tweede deel van het proefschrift onderzoekt de heropwarming in multi-veld modellen van inflatie met gekromde veld-ruimte geometrieën. Kennis van de fysica van het heropwarmingstijdperk is cruciaal, omdat de efficiëntie en duur ervan de voorspellingen van de kosmische microgolfachtergrond aanzienlijk beïnvloedt en de primordiale nucleosynthese kunnen beïnvloeden.

Hoofdstuk 4 bestudeert heropwarming in een brede familie van multiveldmodellen van inflatie, α-attractoren genoemd. We tonen analytisch een eenvoudig schalingsgedrag dat een eenvoudige schatting mogelijk maakt van de heropwarmingsefficiëntie voor grote waarden van de veld-ruimte kromming.

Hoofdstuk 5 onderzoekt en vergelijkt de dynamica tijdens inflatie en heropwarming voor het multiveld α-attractormodel met prototype potentialen die symmetrisch en asymmetrisch zijn rond het minimum. We tonen expliciet de betekenis van de asymmetrie en de invloed ervan op het heropwarmingsrendement.

Het doel van dit proefschrift is om licht te werpen op de primordïale donkere tijden van de kosmologie, hun grenzen te verleggen en verdere ontwikkeling te motiveren. We leven in een opwindende tijd van precisiemetingen in de moderne kosmologie die tot nu toe onbekende fysica van het vroege heelal aan het licht kunnen brengen. Een juiste interpretatie van de waarnemingen is echter sterk afhankelijk van theoretisch begrip van de fysica van het vroege heelal. Hieronder schetsen wij enkele richtingen die in de komende jaren diepgaand onderzoek vereisen.

- *Zwaartekrachtsgolfexperimenten* openden een nieuw venster voor het onderzoeken van de fysica van het vroege heelal via de stochastische zwaartekrachtgolf achtergrond. Het is belangrijk om hun productie mechanismen goed te begrijpen om de metingen van de komende experimenten correct te interpreteren.

- *Kenmerken in het primordïale vermogensspectrum* zijn opwindende kenmerken van zowel het inflatie- als het opwarmende tijdperk die mogelijk zichtbaar zijn in de kosmische microgolfachtergrond en in het grootschalige structuur spectrum. Dit onderwerp vereist een grondig analytisch inzicht en toekomstig onderzoerk.

- *Een effectieve theorie van opwarmen* is essentieel voor het juiste begrip van de voorspellingen van de kosmische achtergrondstraling. Op hun beurt zijn voorspellingen voor inflatiemodellen sterk afhankelijk van de fysica van het opwarmtijdperk. Daarom is de ontwikkeling van de effectieve veldtheorie van heropwarming voor gekromde veldruimtes een belangrijk doel voor de theoretische fysica. Speciale aandacht zou moeten gaan naar het incorporeren van de niet-lineaire effecten en systematische analytische studies van stabiele langlevende ruimtelijk gelokaliseerde structuren zoals oscillons, vooral in situaties met meerdere velden.

Om de motivatie voor verdere spannende verkenningen vast te houden, is het goed om de volgende afspraak te onthouden:

"De cosmos is in ons. We zijn gemaakt van sterrenstof.
We zijn een manier voor het universum om zichzelf te leren kennen."

Carl Sagan

List of publications

- O. Iarygina and E. I. Sfakianakis, *"Gravitational waves from spectator Gauge-flation,"* [arXiv:2105.06972 [hep-th]].
- O. Iarygina, E. I. Sfakianakis, D. G. Wang and A. Achúcarro, *"Multi-field inflation and preheating in asymmetric α-attractors,"* [arXiv:2005.00528 [astro-ph.CO]].
- A. Achúcarro, E. J. Copeland, O. Iarygina, G. A. Palma, D. G. Wang and Y. Welling, *"Shift-symmetric orbital inflation: Single field or multifield?,"* Phys. Rev. D **102** (2020) no.2, 021302.
- O. Iarygina, E. I. Sfakianakis, D. G. Wang and A. Achúcarro, *"Universality and scaling in multi-field α-attractor preheating,"* JCAP **06** (2019), 027.

Curriculum Vitae

I was born on the 7th of June in 1992 in Kyiv, Ukraine. In 2009 I graduated with honours from the school No. 58 and became a student at the Faculty of Physics at Taras Shevchenko National University of Kyiv. I studied there from 2009 till 2015 and obtained my bachelor and master degrees in physics.

In 2014 I received the DAAD study scholarship and did my second master study within a two year master program in theoretical and mathematical physics, that was jointly run by the physics and mathematics departments of Ludwig-Maximilians-Universität München and Technische Universität München. My master project was done at the Arnold Sommerfeld Center for Theoretical Physics under the supervision of Prof. Gia Dvali.

From October 2016 I am a PhD student at the Lorentz Institute for Theoretical Physics in the theoretical cosmology group of Prof. Ana Achúcarro. During my PhD studies I was a teaching assistant for the courses "Theoretical Cosmology", "Quantum Field Theory", "Physics of Machine Learning", "Advanced Topics in Modern Cosmology".

After my PhD I will be a postdoctoral researcher at the Nordic Institute for Theoretical Physics (Nordita) in Stockholm, Sweden.

Acknowledgements

Ana, it is hard to express in words how much I am grateful to you. You were my support at every bifurcation point on my PhD trajectory. Your scientific supervision gave me so many insights. I highly appreciate all the time you dedicated to our discussions. After our conversations my world still turns upside down. Personally and psychologically, your wisdom and experience gave me the strength to go through these not so easy 5 years. I could not even dream of a better supervisor. Thank you so much for all your guidance and help.

Evangelos, I would like to thank you for being my co-supervisor and collaborator. You helped me a lot to integrate back into research after the pauses I had and to feel myself comfortable with asking and tackling challenging scientific questions.

I am very grateful to Ed Copeland, Gonzalo Palma, Dong-Gang Wang and Yvette Welling for being my collaborators. It was a great pleasure to work with you. Thank you for all the insights and inspiration I got from our discussions.

Further, I would like to thank Jan Aarts, Fedor Bezrukov, Ed Copeland, Azadeh Maleknejad, Koenraad Schalm and Stanislav Vilchinskiy for reading the manuscript of my thesis. Lisanne Janssen, thank you very much for the help with the Dutch translation of the summary. Moreover, I would like to thank Koen Kuijken and Koenraad Schalm for valuable comments on the Dutch summary.

In addition, I would like to thank all my colleagues at the Lorentz Institute for an amazing working environment you create. Special thank you to Yashar Akrami, Kyrylo Bondarenko, Omar Contigiani, Alice Garoffolo, Guadalupe Cañas-Herrera, Matteo Martinelli, Andrii Magalich, Georgios Papadomanolakis, Simone Peirone, Fabrizio Renzi and Valeri Vardanyan. Thank you, Koenraad Schalm and Alessandra Silvestri, I enjoyed a lot being a teaching assistant for your courses. Next, I would like to thank

Fran Ouwerkerk for taking care of all the administrative formalities.

I would like to say a special thank you to Alexey Boyarsky. Your open-mindedness and willingness to help have always inspired me. Discussions with you have highly influenced my view on contemporary science.

Thank you very much my friends outside science for being beside me during all this time. Especially I would like to thank Hanna Sheredeko and Artem Pichak for your support during challenging times.

I would never have gotten to this point without the support of my family. Mama, thank you for your unconditional love and kindness. It was always a strong foundation for me. Papa, thank you for the freedom and trust. It taught me to be independent and persistent. Thank you my brother Oleksandr, uncle Vyacheslav, grandfather Mykhailo, grandmothers Natalia and Eugenia for being the people to look up to. Each of you has highly influenced me and helped to become a person who I am now. Dear family, this thesis is dedicated to you.

Lisanne, thank you so much for being with us and taking care of the children while I was working on this thesis.

Ivan, it would be impossible to complete this work without you. Thank you for continuous support, encouragement and for being enthusiastic about our forthcoming life journeys. Mykhailo and Lev, thank you for the love, joy and precious moments we are sharing every day. You are my inspiration.